Thèse de doctorat

Spécialité : Océanographie Physique

présentée par

Nicolas Rascle

Impact des vagues sur la circulation océanique

---

soutenue le 18 Septembre 2007 devant le jury composé de :

M. Xavier Carton	Président du jury	UBO, Brest
M. Vladimir Kudryavtsev	Rapporteur	NIERSC, Saint-Pétersbourg
M. Agustin Sanchez-Arcilla	Rapporteur	UPC, Barcelone
M. Philippe Bonneton	Examinateur	U. Bordeaux 1, Talence
M. Bertrand Chapron	Examinateur	IFREMER, Plouzané
M. Rodrigo Pedreros	Examinateur	BRGM, Orléans
M. Fabrice Ardhuin	Directeur de thèse	SHOM, Brest

Remerciements

Comme il est d'usage, quelques mots pour remercier tous ceux qui m'ont aidé à réaliser cette thèse depuis mon arrivée à Brest en 2004.

Ma thèse a été financée par une bourse CNRS/DGA.

Et puis je tiens à remercier tout d'abord Fabrice Ardhuin pour sa disponibilité, sa patience, ses encouragements et son enthousiasme débordant, et ses autres qualités humaines qui en font un directeur de thèse exceptionnel.

Merci à Rudy Magne pour son recul et ses conseils avisés sur la thèse (et sur la vie aussi au passage !).

Au CMO, merci à Stéphanie Louazel, Nadine Paugam, Alain Serpette, Yves Morel de Toulouse.

Merci au LPO de la fac pour son accueil en son sein depuis 2006, et les conseils techniques glanés à droite à gauche auprès de Gildas Cambon (et bon courage pour la fin), Steven Herbette, Bruno Blanke, Xavier Carton, Guillaume Roullet.

Merci à Patrick Marchesiello et à Phillipe Estrade pour leur coup de main pour démarrer avec ROMS.

Merci à Romain Bourdallé-Badie de Mercator à Toulouse, pour son temps passé sur notre projet.

Enfin merci à Bertrand Chapron pour son suivi de ma thèse avec Fabrice, pour ses conseils, remarques et autres divagations.

Acknowledgements

Thanks to my thesis reviewers, Vladimir Kudryavtsev and Agustin Sanchez-Arcilla, for the time they spent on my manuscript this summer.

Thanks to each member of my thesis jury, for their time and for their kind commentaries.

Thanks also to Jim McWilliams for his review of my thesis plan in the middle of my PhD.

Contents

Table of contents

Introduction générale

Le contexte : L'hydrodynamique côtière et de surface

Avant de parler de vagues et de circulation océanique, je souhaiterais introduire le contexte générale de cette étude. L'étude de la circulation océanique, et de l'océan en général, est au carrefour de nombreux enjeux, et il semble opportun d'en dresser une liste rapide pour avoir une idée des applications pratiques de la présente recherche.

À l'échelle du globe, la circulation océanique intéresse particulièrement pour son impact sur le climat. À l'échelle côtière, les intérêts sont plus divers, depuis la connaissance et la prévision des mouvements des masses d'eau pour application à la biologie, à la biogéochimie, l'halieuthique, à la défense sous-marine, jusqu'au suivi des pollutions et au sauvetage en mer. Enfin à l'échelle littorale, l'hydrodynamique de l'océan est étudiée principalement pour ses applications à l'érosion des cotes, au transport sédimentaire.

Pour beaucoup d'applications parmi celles citées ci-dessus, un des pré-requis est de posséder un modèle de l'océan qui représente correctement les transports particulaires près de la surface (suivi des pollutions, sauvetage en mer, étude des dérives de larves en halieuthique), qui représente correctement le mélange des couches de surface océaniques , avec les cycles diurnes et saisonniers (études climatiques, biogéochimie), et qui représente correctement la circulation aux abords immédiats des plages, dans la zone de déferlement des vagues et au-delà, sur le plateau interne (érosion des plages, transport des sédiments, suivi des polluants rejetés de la côte). En fait une grande partie des activités de recherche océanographiques nécessitent une bonne connaissance de l'hydrodynamique près de la surface et près de la côte, et ce n'est pas surprenant puisque l'essentiel des activités humaines et animales s'y concentrent.

Voila ce qui constitue la motivation pour étudier l'hydrodynamique de cette partie de l'océan, et plus précisément l'impact des vagues sur celle-ci.

Problématique : L'impact des vagues

Les vagues jouent un rôle prépondérant dans la dynamique de l'océan au niveau littoral. Par exemple, des vagues d'incidence oblique gênèrent des courants le long des plages, et ces courants sont généralement plus importants que les courants crées par le vent, la marée ou les courants du large. Les modèles hydrodynamiques littoraux intègrent donc les vagues comme un forçage essentiel.

Au contraire, dans les modèles côtiers d'océan, à des échelles de grandeur de l'ordre d'une baie, d'une région ou d'un bassin océanique, l'océan évolue uniquement en réponse au vent, à la marée et aux différents forçages sur la température et sur la salinité. Les vagues, et plus généralement l'état de mer, ne sont pas pris en compte. Hors de la zone de déferlement bathymétrique, les vagues sont ainsi largement ignorées.

Pourtant, l'énergie cinétique turbulente (TKE) produite par le déferlement des vagues est supérieure, au moins d'un ordre de grandeur, à la production de TKE par le cisaillement du courant d'Ekman (Terray et al., 1996). De même, la pseudo-quantité de mouvement des vagues, intégrée verticalement (c.à.d. le transport de Stokes des vagues) est de l'ordre de grandeur du transport d'Ekman correspondant au vent qui les a créées : McWilliams and Restrepo (1999), ainsi que Polton et al. (2005), ont donné une première estimation de ce transport de Stokes à 40% du transport d'Ekman aux moyennes latitudes. Cependant, une analyse plus réaliste tenant compte du fait que les vagues sont rarement complètement développées par vent fort serait certainement plus proche de 10%. En surface, la dérive de Stokes des vagues de vent a été estimée par Kenyon (1969) à plus de 3% de la vitesse du vent à 10 m, une vitesse comparable à la dérive due au vent des particules d'eau à la surface. Enfin, le transfert de la quantité de mouvement du vent vers l'océan passe généralement à plus de 80% par les vagues, alors que 20% ou moins sont dus aux frottements visqueux à la surface (Donelan, 1998; Banner and Peirson, 1998).

Ces diverses observations et analyses ont amené à reconsidérer l'importance des vagues dans la description de l'océan, y compris loin de la côte. En particulier pour des problématiques liées aux dérives près de la surface ou liées au mélange près de la surface, les vagues doivent jouer un rôle important, compte tenu des ordres de grandeurs précédents.

Également il apparaît un fossé entre la description littorale, avec vagues, et la description côtière, sans vagues, de l'océan. Pourtant, la zone intermédiaire, au-delà de la zone de déferlement des vagues et que nous nommerons pré-littorale comme Denamiel (2006), est d'importance cruciale en terme de transports de sédiment, de matériel biologique ou chimique, puisque c'est dans cette zone que se retrouvent tous

les matériels issus de la zone littorale. Une description cohérente des courants induits par les vagues, depuis la plage jusqu'au large, au même titre que les courants induits par les autres forçages tels le vent ou la marée, est ainsi nécessaire pour modéliser cette zone pré-littorale.

Plan de l'exposé

Parce que l'impact général des vagues sur l'hydrodynamique est à cheval sur différents champs d'investigations, depuis la clôture turbulente et le mélange vertical jusqu'à la circulation littorale, la bibliographie n'a pas été, comme il est d'usage habituellement, regroupée dans une partie spécifique. Au contraire, chacune des différentes parties traite de sa bibliographie spécifique.

Notre exposé s'articule en 3 parties.

Les aspects généraux seront rappelés dans un chapitre préliminaire. J'y ferai notamment une description simple des vagues et du transport de masse qui leur est associé. La séparation du champ de vitesse en une partie vagues et une partie courant moyen y sera présentée, ainsi que la force de Stokes-Coriolis. Ces deux notions reviendront de façon récurrente tout au long de ce travail.

Ensuite une première partie traitera plus précisément de l'effet des vagues sur l'hydrodynamique loin de la côte. L'étude sera alors à une dimension verticale et s'attachera à décrire de façon cohérente les courants d'Ekman et la dérive près de la surface sous l'effet des vagues. On y abordera également les problèmes de mélange induit par les vagues et de clôture turbulente, et ses conséquences sur les profils de vitesse près de la surface.

Une deuxième partie reviendra sur le mélange lié aux vagues, mais cette fois sur son impact sur la profondeur de la couche de mélange. Les modèles et les paramètres pour prendre en compte ce mélange induit par les vagues seront discutés, ainsi que l'impact sur la formation et l'érosion des thermoclines.

Enfin une troisième partie présentera une description de la circulation induite par les vagues depuis la zone de déferlement jusqu'au plateau continental. Les aspects liés à la non-uniformité du champ de vagues, connus par exemple sous le terme "tensions de radiation", seront abordés. L'analyse séparée des vagues et des courants, ainsi que ses conséquences sur la compréhension des courants de la zone infra-littorale, sera abordée.

General introduction in english

The context: The hydrodynamics near the coast and near the surface

Before discussing the waves and their impact on the ocean circulation, I would like to introduce the general context of this study. The study of the oceanic circulation, and more generally the study of the ocean, might benefit to many activities and a short review might be helpful to understand the possible applications of the present thesis.

At global scale, the ocean circulation is under particular interest for its impact on the climate. But at coastal scale, the motivations are more diverse, from the understanding and forecasting of the water mass transport for applications to biology, biochemistry, halieutic, submarine defense, to pollutants monitoring and search and rescue. Also at nearshore scale, the ocean hydrodynamics is mainly studied for applications to coastal erosion or sedimentary transport.

For many of the applications cited above, one necessary step is to build an ocean model which correctly describes the transports of particles close to the surface (pollutants monitoring, search and rescue, drift of larvae), which correctly describes the mixing in the upper ocean with the resolution of the diurnal and seasonal cycle (climatic studies, biochemistry), and which correctly represents the circulation in the vicinity of the shore, in the surf-zone and beyond in the inner-shelf zone (coastal erosion, sedimentary transport, monitoring of the pollutants rejected from the coast). Actually a large part of the ocean research activities need an accurate understanding of the near-surface and nearshore hydrodynamics, and this is not surprising since most animal and human activities concentrate in those areas.

This sets up a motivation to study the hydrodynamics of this part of the ocean, and more precisely to study the impact of waves on it.

The issue: The impact of waves

Waves play a dominant role in the ocean dynamics close to the shore. For instance, obliquely incident waves create alongshore currents, and those currents are generally larger than the currents created by the wind, the tides or the off-shore currents. Therefore nearshore hydrodynamics models use the waves as an essential forcing.

On the contrary in the coastal models, at the scale of a bay, of a region or of an ocean, the ocean evolves only in response to the wind, the tide and the different forcings of the temperature and the salinity. Waves, and more generally the sea state, are then largely ignored outside of the surf-zone.

Nevertheless, the turbulent kinetic energy (TKE) produced by the wave breaking is at least an order of magnitude larger than the TKE produced by the shear of the Ekman currents (Terray et al., 1996). Also the vertically-integrated waves pseudo-momentum (i.e. the Stokes transport of the waves) is of the order of the Ekman transport corresponding to the wind which created those waves. McWilliams and Restrepo (1999) and Polton et al. (2005) gave a first estimation of this Stokes transport around 40% of the Ekman transport at mid-latitude. We note however that a more realistic estimation would be close to 10% given that the waves are seldom fully-developed under strong winds. At the surface, the Stokes drift was estimated by Kenyon (1969) to be more than 3% of the wind speed at 10 m, a velocity of the same order as the drift velocity of particles at the surface. Finally, the momentum from the wind transfers to the ocean generally through the wave field at 80%, whereas only 20% or less are due to the viscous friction at the surface (Donelan, 1998; Banner and Peirson, 1998).

All those observations have lead us to reconsider the importance of waves in the description of the ocean, even far from the coast. In particular for studies of near-surface drift or near-surface mixing, waves might play an important role given the previously listed orders of magnitude.

Also there is a gap between the nearshore descriptions (with waves) and the coastal descriptions (without waves) of the ocean. Yet the intermediate zone, the inner-shelf zone, is of crucial importance in terms of sedimentary transport, chemical or biological transport, since all the materials coming from the surf-zone finally end up there. A coherent description of wave-induced currents, from the shore to the open ocean, as well as the currents induced by the other forcings, is a necessary step to build a model of that inner-shelf zone.

Contents

As the general impact of waves on the hydrodynamics deals with many different topics, ranging from the turbulent closure and vertical mixing to the nearshore circulation, the bibliography has not been, as it is conventionally done, gathered in a specific part. On the contrary, each part deals with its specific bibliography.

The thesis is split into three parts.

The general concepts will be recalled in a preliminary chapter. I will made a simple description of the waves and of the associated mass transport. The separation of the velocity field into a wave part and a mean flow part will be presented, as well as the Stokes-Coriolis force. Those concepts will appear all along the thesis.

Then a first part will deal more precisely with the effects of waves on the dynamics in the open ocean. The study incorporates only one (vertical) dimension and will try to describe in a coherent manner the Ekman currents and the drift close to the surface in the presence of waves. Also the vertical mixing due to the waves will be parameterized with an appropriate turbulence closure. Its impact on the velocity profiles close to the surface will be discussed.

A second part will also focus on the wave-induced mixing, but more precisely on its impact on the mixed layer depth. Models and parameters to include the wave-induced mixing will be discussed, as well as the impact on the thermocline formation and erosion.

Finally, a third part be devoted to the description of the wave-induced circulation from the surf-zone to the shelf. Aspects linked to horizontally non-uniform wave fields, for instance known as radiation stress effects, will be discussed. The separated analysis of waves and currents, as well as its consequence on the understanding of the inner-shelf currents, will be discussed.

Chapter 1

General concepts

This chapter aims to introduce general concepts used in this study. We first recall the typical length and time scales of the waves, and the implications for the wave modelling. Then we introduce the Stokes drift of the waves and we discuss on a simple example the two major difficulties which appear for the modelling of waves and currents. The first difficulty is the motion of the free surface, for which a special averaging is needed. The second difficulty comes from the quite different physics of the mean flow and of the waves Stokes drift, for which a separation of waves and mean flow is needed to obtain suitable parameterizations. Finally, emphasis is made on the fact that the mean flow dynamics is different than the total drift dynamics, for instance with the appearance of the Stokes-Coriolis force for an horizontally uniform case.

1.1 Lengths and time scales

The present thesis investigates the role of the waves on the 3D dynamics of the upper ocean, and also on the 3D dynamics of the nearshore and costal oceans.

We recall here that the waves, i.e. short gravity waves at the surface, have typical wavelengths of 100 m, heights of 1 m and periods of 10 s. Those scales are rather small compared to the typical length and time scales of the ocean circulation, but it should be noted that the large scale variations of the wave field are much larger than the scale of a single wave and are comparable to those ocean circulation scales.

The variety of oceanic phenomenons influenced by waves is large, the typical horizontal scales spanning the range from hundreds of kilometers for large scale variations of the wave field to a meter for the energy containing eddies of the wave-stirred turbulent surface layer, and even less for the microscale breaking of the smallest waves.

Because of the limited numerical resources and because one also needs to analyze the physical features, it is customary for the purpose of ocean circulation to consider horizontal length scale smaller than a hundred of meters horizontally and one meter vertically as subgrid phenomenons. The present study will keep in mind these typical scales and try to find adapted descriptions and parameterizations, of small scale wave-induced turbulence for instance.

Also, we focus in the present thesis on wave-driven currents with time variations slower than the wave period. We therefore use a spectral approach, without resolving the phase of the waves, following the method employed in most of the wave prediction systems which simulate the generation, the propagation and the dissipation of the waves. In this kind of description, the sea state is considered as a sum of monochromatic waves, spread over a frequency-directional energy spectrum (e.g Komen et al., 1994).

1.2 Waves, Stokes drift, averaging

Let us take a monochromatic wave propagating in the x direction, in deep water and without current. The equations of motion, valid for $z < \eta$, are (e.g. Mei, 1989)

$$\left\{ \begin{array}{rcl} \eta & = & a\cos(\omega t - kx) \\ u & = & a\omega\cos(\omega t - kx)\exp(kz) \\ w & = & a\omega\sin(\omega t - kx)\exp(kz), \end{array} \right. \tag{1.1}$$

where a is the amplitude, ω the radian frequency, k the wavenumber, η the surface elevation and u, w the horizontal and vertical components of the wave motion. Note that the previous expressions, as well as most formulae in this chapter, are valid in the limit of small wave slope $ka \ll 1$. For simplicity, I will not discuss further the order of each approximations.

Now let us average in time this velocity, defining the time average $\overline{u} = \frac{1}{T}\int_0^T u dt$ over a wave period T. Assuming $u = 0$ for $z \geq \eta$, we get

$$\left\{ \begin{array}{rcll} \overline{u} & \simeq & \frac{a\omega}{\pi}\sqrt{1-\frac{z^2}{a}} & \text{for} \quad -a < z < a, \\ \overline{u} & = & 0 & \text{for} \quad z < -a. \end{array} \right. \tag{1.2}$$

In that Eulerian description, the Stokes drift, i.e. the time-averaged mass transport, is concentrate between the crests and the troughs of the waves (fig. 1.1, upper panel).

However the Lagrangian mean speed of a particle moving with the wave is

$$\begin{aligned} \overline{u}^L &= \overline{u(x(t),z(t),t)} \\ &= \overline{\frac{\partial u}{\partial x}x(t) + \frac{\partial u}{\partial z}z(t)}, \end{aligned} \tag{1.3}$$

where $(x(t), z(t))$ are the coordinates of the particle. The correlation between the displacement and the non-uniform velocity field yields a residual motion of the fluid particles. In other words, the orbits of the particles are not closed. The residual drift is the Stokes drift and is equal to

$$U_s = a^2 \omega k \exp(2kz), \tag{1.4}$$

where the vertical coordinates z represents this time the mean position of a particle of water.

This simple example illustrates the complications which appear due to the moving surface, even for linear waves, and the necessity of a careful averaging close to the surface. The choice of coordinates to describe both wave-induced motion and mean current is of great importance and must be discussed here.

Most field measurements are time averages made at almost fixed locations. Therefore the Eulerian description is traditionally used for oceanic circulation, and has been chosen in many studies on wave-driven mean flows. In the Eulerian description, the interface is distributed between the crest $z = a$ and the trough $z = -a$. When considering the mean fields, it is usually assumed that they can be analytically extended between the trough and the mean surface $z = \overline{\eta} = 0$. For example, the vertical integral of the velocity is defined as

$$T_m = \int_{-h}^{\overline{\eta}} u dz. \tag{1.5}$$

In the same time, the wave mass transport of the waves is either assumed to be a surface mass transport (Hasselmann, 1971; Stive and Wind, 1986; Newberger and Allen, 2007*b*) equal to

$$M^w = \overline{\int_{\overline{\eta}}^{\eta} u dz}, \tag{1.6}$$

or to be distributed according to the Lagrangian Stokes drift profile (McWilliams et al., 2004). Clearly, the Eulerian averaging procedure presents some oddities in its surface representation. The analytical extension of the fields is made whereas the phase relations between the field and the surface is of great importance. For

the example of the velocity, it leads to the wave Stokes drift. Although Eulerian averaging might give correct representation of the Stokes drift with a careful analysis (e.g. McWilliams et al., 2004), a not so detailed analysis might miss the full vertical distribution of the Lagrangian motion (Hasselmann, 1971; Stive and Wind, 1986; Newberger and Allen, 2007*b*).

For this reason, many authors have chosen to use a change of coordinates to make a proper averaging of the waves (e.g. Jenkins, 1986). The most simple one was recently proposed by Mellor (2003). It is simply the use of a particular σ-coordinate system, the one following the fluid vertical motion (to lowest order in the wave slope), to bring the particles back to their fixed vertical mean location and then to average in time the velocity (fig. 1.1, middle panel). For the case of the wave motion discussed above, the mean velocity obtained by this method is in agreement with the Lagrangian description of the Stokes drift. More complicated but along the same idea, Andrews and McIntyre (1978*a*) introduced the Generalized Lagrangian Mean (GLM). In that case, the particles are also horizontally displaced back to their mean position during a wave period (fig. 1.1, lower panel). The complexity of the mapping of Andrews and McIntyre (1978*a*) is compensated by the simplicity of exact phase-averaged equations.

1.3 Wave / Mean flow separation

A key point of the present work is the separation between the wave part and the mean flow. If we go back to the monochromatic waves of the previous section, once a proper wave-averaging procedure is applied (Mellor (2003) or GLM), one gets a mean Lagrangian velocity equal to the Stokes drift of the waves. Now adding a barotropic current brings no difficulties. One gets then a mean Lagrangian velocity equal to the Stokes drift of the waves plus the mean current. The mean current is then similar to the Eulerian mean current below the troughs.

On that simple example of monochromatic waves over a mean barotropic current, we can notice that the Lagrangian flow is vertically sheared because it includes the residual Lagrangian drift due to the wave motion, i.e. the waves Stokes drift. However, applying on the shear of that residual drift a vertical mixing term equal to the vertical mixing we would applied on a comparably sheared mean current would be physically meaningless. In fact the turbulence does not act similarly on the current and on the waves residual Stokes drift. In addition, the Stokes drift propagates with the waves group speed, whereas the mean current is advected at the much smaller current velocity. This leads us a central idea of this thesis, the separation of the mean flow and of the wave part. By separating them, and by

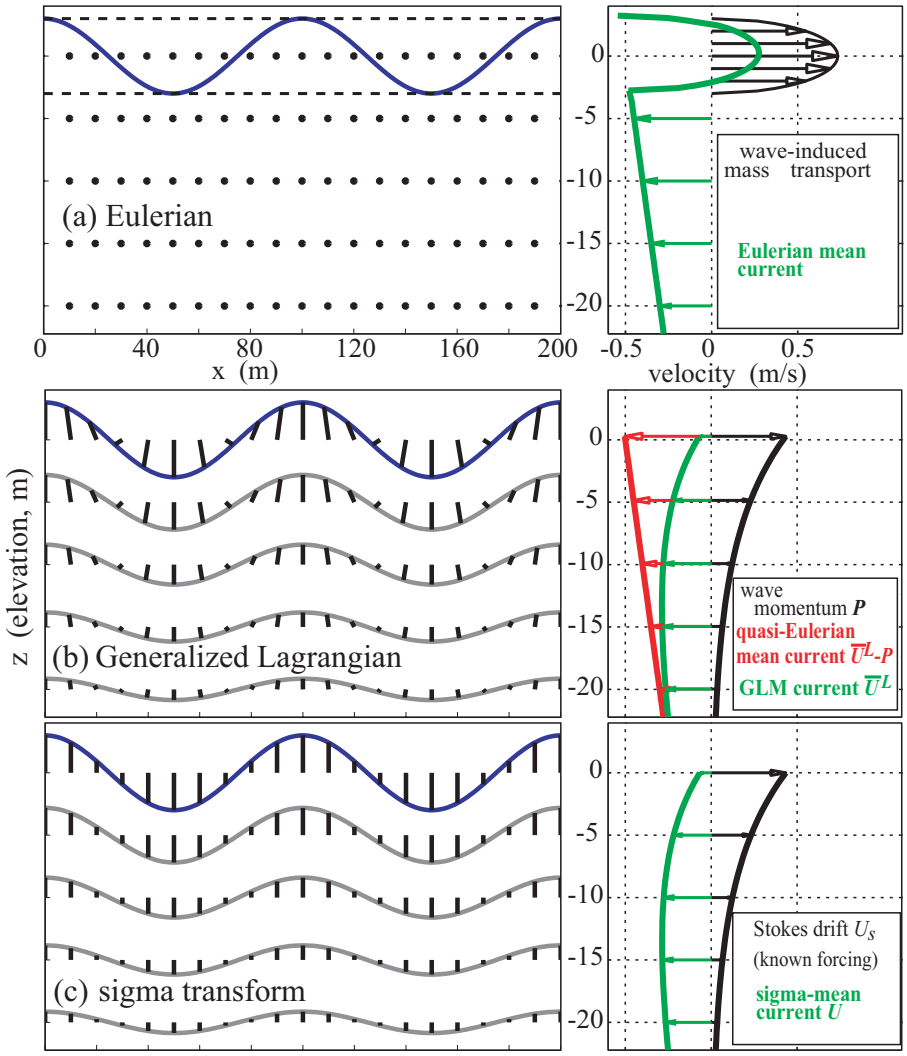

Figure 1.1: This figure was taken from Ardhuin et al. (2007*b*). Averaging procedures (left) and examples of resulting velocity profiles (right) in the case of (a) Eulerian averages (e.g. Rivero and Arcilla, 1995; McWilliams et al., 2004), (b) the Generalized Lagrangian Mean (Andrews and McIntyre, 1978*a*), and (c) sigma transform (Mellor, 2003; Ardhuin et al., 2007*c*). The thick black bars connect the fixed points $\mathbf{x}$ where the average field is evaluated, to the displaced points $\mathbf{x}+\xi$ where the instantaneous field is evaluated. For averages in moving coordinates the points $\mathbf{x}+\xi$ at a given vertical level ξ are along the gray lines. The drift velocity is the sum of the (quasi-Eulerian) current and the wave-induced mass transport. In the present illustration an Airy wave of amplitude 3 m and wavelength 100 m in 30 m depth, is superimposed on a hypothetical current of velocity $u(z) = -0.5 - 0.01z$ m/s for all $z < \eta(\mathbf{x})$. The current profile is not represented in (c) since it is not directly given in Mellor's theory, although it can obviously be obtained by taking the difference of the other two profiles.

parameterizing them separately because they are physically different, one can expect significant improvement of the modelling of combined waves and current.

That waves / mean flow separation is easy with a depth-uniform mean current,

as mentioned above. But the discussion is strongly complicated if we introduce a vertically varying current. Both averaging of Mellor (2003) and the GLM give the Lagrangian motion $\overline{u}^L$. That Lagrangian motion can be separated into a residual wave motion P and a mean flow $\widehat{u}$.

$$\overline{u}^L = P + \widehat{u}. \tag{1.7}$$

It should be noted that the mean flow is described in quasi-Eulerian coordinates. It is different from the Eulerian mean (at a fixed location).

Related to this, the residual wave part

$$P = \overline{\frac{\partial u^l}{\partial x} x^l(t) + \frac{\partial u^l}{\partial z} z^l(t)} \tag{1.8}$$

has been called the wave pseudo-momentum (see McIntyre, 1981, for a full discussion). Here u^l is the perturbation of the velocity field from the Lagrangian mean, and x^l, z^l is the displacement. P might be different from the Stokes drift defined as the Lagrangian motion $\overline{u}^L$ minus the Eulerian mean $\overline{u}$.

Also, in the case of vertically varying current, the residual motion P of the waves is different than the residual motion without current, because the vertical shear of the mean current can add to the vertical shear of the wave motion, modifying the correlation between the velocity and the displacement in formula 1.3. For simplicity, the rest of the thesis will ignore this distinction except in part III.

A more detailed description of the GLM separation of waves and mean flow has been made in Ardhuin et al. (2007*b*).

1.4 The Stokes-Coriolis effect

There is a mass transport associated with the wave motion. According to the linear wave theory, the vertical integral of the Stokes drift of a monochromatic wave (equ. 1.4) is

$$\begin{aligned} M^w &= \int_{-H}^{0} U_s dz \\ &= \frac{a^2 \omega}{2}. \end{aligned} \tag{1.9}$$

For large swells (i.e. waves not related to the local wind), this transport can be of the order of the Ekman transport of a moderate wind at mid-latitude, as noted by McWilliams and Restrepo (1999) and Polton et al. (2005).

However it was outlined by Ursell (1950) that in an inviscid ocean, horizontally

uniform, in infinite depth, and in a rotation frame, irrotational waves cannot have a steady net mass transport. This paradox was resolved by Hasselmann (1970), introducing a force called later the Stokes-Coriolis force or Hasselmann force. Xu and Bowen (1994) made apparent the physical meaning of this force. They made a simple calculation of the impact of the Earth rotation on the wave dynamics and showed that there is slight tilting of the orbits of the particles under passing waves. As a consequence there is an associated supplementary flux of momentum to the mean flow, equivalent to a force equal to fU_s and oriented to the right of the wave propagation. In other words, the Coriolis force acts on the wave pseudo-momentum, but the corresponding flux of momentum is released from the wave part to the mean flow as a the body force. This force drives a vertically integrated transport opposed to the Stokes transport of the waves.

Now examining the vertical distribution of the wave mass transport and of the Stokes-Coriolis force, two typical length scales appears, the Stokes scale $\delta_s = 1/2k$ and the Ekman scale δ_e (equal to $\sqrt{2K_z/f}$ if the vertical viscosity K_z is supposed uniform). As showed by Polton et al. (2005), if $\delta_s \gg \delta_e$, then $\widehat{u} = -P$ so that the mean flow totally compensates the Stokes drift of the waves (fig. 1.2, upper panel). This might be the case for a long swell, as studied in Part III. However the Stokes drift of a spectrum of wind waves is strongly surface trapped so that, in the presence of a strong vertical mixing, $\delta_s \ll \delta_e$ and the mean flow driven by the Stokes-Coriolis force cannot compensate the Stokes drift of the waves close to the surface (fig. 1.2, lower panel). Then the net wave-induced drift is approximately equal to the Stokes drift, which can be significant as shown in Part I.

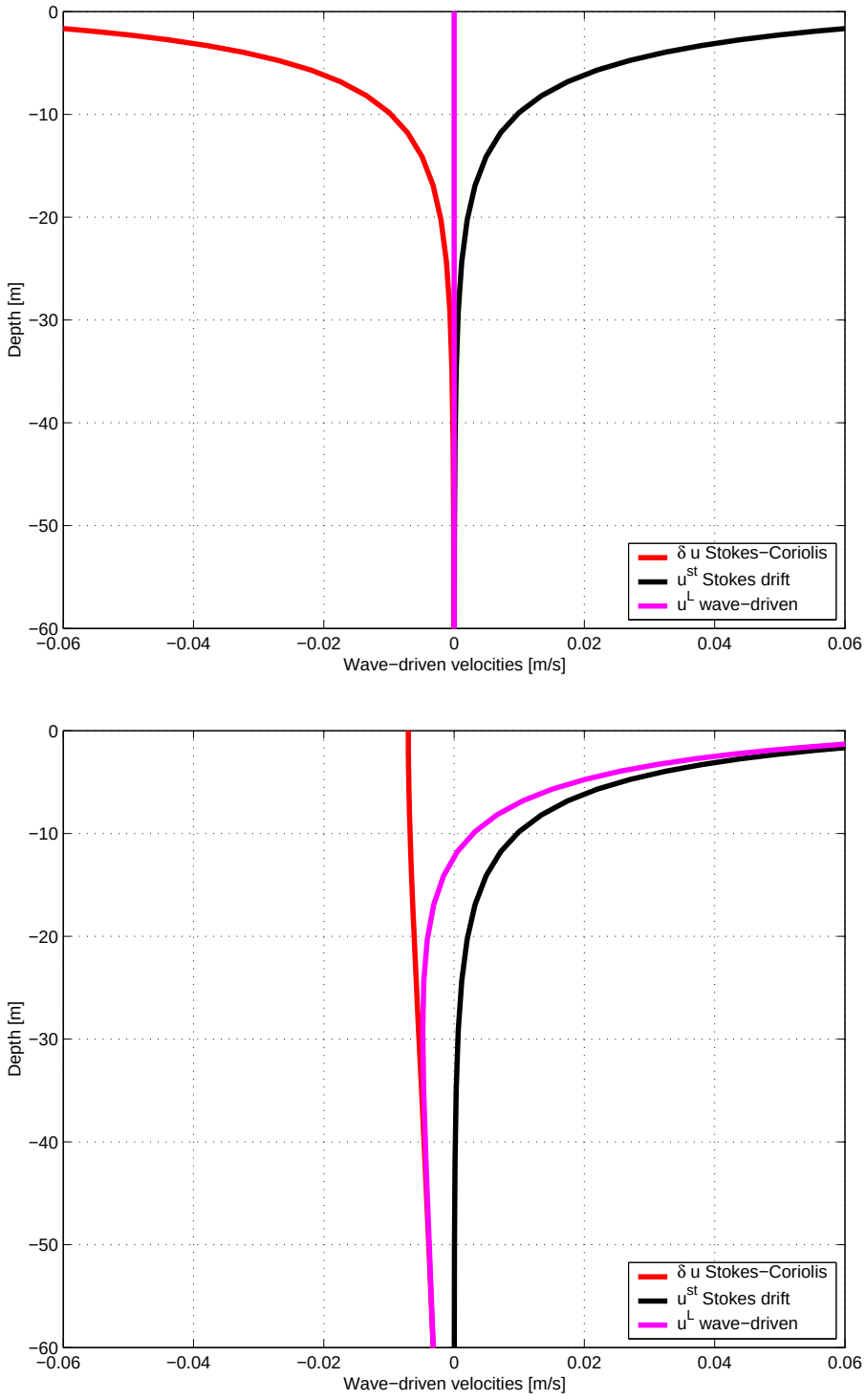

Figure 1.2: Vertical profiles of the Stokes drift, of the mean flow component in the waves direction and of the resulting Lagrangian drift. The Stokes drift is calculated with the wind waves assumed to be fully-developed with a wind speed of 10 ms^{-1}, the mean flow shown is driven by the Stokes-Coriolis force only (no wind stress). The upper panel has no vertical mixing whereas the lower panel incorporates a vertical mixing. In the case of no vertical mixing, the mean flow compensates the Stokes drift at each depth whereas it does not when the vertical mixing is included. The reader is referred for further details to the chapter 2 and to the fig. 2.10.

Part I

Impact of waves on the near-surface dynamics of the open ocean. One-dimensional study.

One-Dimensional study: Introduction

We start with the study of the impact of waves on the near surface off-shore dynamics, in its most simple description : a wind sea without any horizontal variations of the wind, waves or stratification.

First, the Stokes drift of the waves of a wind sea is evaluated. Previous evaluations were made using the spectrum of Pierson and Moskowitz (1964) by Kenyon (1969), Lewis and Belcher (2004) and Polton et al. (2005), leading to surface values of the Stokes drift around 3% of the wind speed at 10m. However the high frequency range of the spectrum, i.e. the small waves, makes a large contribution to the Stokes drift at the surface (see figure 4.1). Therefore we used a more realistic spectrum, the one of Kudryavtsev et al. (1999), were the high frequency range was carefully designed for applications to remote sensing. It leads to values of the surface Stokes drift much smaller, around 1.2% of the wind speed at most.

Secondly, the mean flow driven by the wind, i.e. the Ekman current, is evaluated using recent observations (e.g. Agrawal et al., 1992) and models (e.g. Craig and Banner, 1994; Noh, 1996) of the strong near surface mixing, attributed to breaking waves, in moderate and strong winds. Essentially, these models use a TKE calculation with a surface flux of TKE and use a mixing length with a prescribed large value at the surface. The consequent Ekman current is quite weak at the surface in the presence of wave breaking.

The impact of the Stokes-Coriolis force on the mean current is also estimated. This impact is quite weak given that the wind stress is always much larger than the equivalent Stokes-Coriolis stress of the corresponding wind waves.

The surface drift, which is the sum of the Stokes drift of the waves and the mean current, appears then mainly due to the Stokes drift of the waves, raising the question of direct parameterization from the wind speed, a common engineering practice (see Spaulding, 1999).

Finally, available observations of surface currents are discussed in the light of the present physical description. Essentially, observations are separated into Lagrangian

observations with drifters and observations of mean currents with current meters. Most of the data are useless for a detailed investigation because of no clear separation between mean flow and wave part (e.g. Schudlich and Price, 1998), or because of no available informations on waves (e.g. Churchill and Csanady, 1983). Previously used observations, namely, observations of mean current shears very close to the surface during SMILE (Santala, 1991) and of mean Ekman spirals during LOTUS3 (Lewis and Belcher, 2004; Polton et al., 2005) are reanalyzed to find evidence of the exposed physics.

The chapter 2 treats the case of an uniform ocean without stratification. The basics of this physical description are outlined and briefly compared to observations. The chapter 3 adds the stratification, comments on its effect on the net wave-induced drift, and makes a more rigorous comparison with the observations.

Chapter 2

One-Dimensional description: Part 1: without stratification

This chapter is written as an independent paper :

Drift and mixing under the ocean surface. A coherent one-dimensional description with application to unstratified conditions

Nicolas Rascle[(1)], Fabrice Ardhuin[(1)], Eugene A. Terray[(2)]

Published in Journal of Geophysical Research
March 2006

[(1)] *Centre Militaire d'Océanographie, SHOM, BREST, France*
[(2)] *Dept. of Applied Ocean Physics and Engineering, Woods Hole Oceanographic Institution, Woods Hole, Massachusetts, USA*

Abstract

Waves have many effects on near surface dynamics : breaking waves enhance mixing, waves are associated with a Lagrangian mean drift (the Stokes drift), waves act on the mean flow by creating Langmuir circulations, and also a return flow opposite to the Stokes drift, and, last but not least, waves modify the atmospheric surface roughness. A realistic ocean model is proposed to embrace all these aspects, focusing on near surface mixing and surface drift associated with the wind and generated waves. The model is based on the Generalized Lagrangian Mean that separates the momentum into a wave pseudo-momentum and a quasi-Eulerian momentum. A wave spectrum with a reasonable high-frequency range is used to compute the Stokes drift. A turbulent closure scheme based on a single evolution equation for the turbulent kinetic energy includes the mixing due to breaking wave effects and wave-turbulence interactions. The roughness length of the closure scheme is adjusted using observations of turbulent kinetic energy near the surface. The model is applied to unstratified and horizontally uniform conditions, showing good agreement with observations of strongly mixed quasi-Eulerian currents near the surface, when waves are developed. Model results suggest that a strong surface shear persists in the drift current, due to the Stokes drift contribution. In the present model the surface drift only reaches 1.5% of the wind speed. It is argued that stratification and the properties of drifting objects may lead to a supplementary drift as large as 1% of the wind speed.

2.1 Introduction

The ocean surface is where the vast majority of marine activities take place, and different dynamical descriptions have been invoked to describe the 100 m that straddle both sides of the air-sea interface. Different solutions have been developed for applications such as wave forecasting for safety at sea [e.g. *Komen et al.*, 1994], forecasting of drift for search and rescue or pollution mitigation [e.g. *Youssef and Spaulding* 1993], or modelling of the general ocean circulation with applications to climate studies [e.g. *Semtner*, 1995; *Bleck*, 2002].

Unfortunately, these descriptions of the upper ocean are often incoherent, not always based on first principles, and may not give parameters compatible available measurements that could constrain numerical forecasting models. Work for each of the three applications listed above have often focused on one key parameter, the significant wave height H_s, the surface drift current $U_{\varsigma=0}$, or the mixed layer temperature T_s. The advent of the Global Ocean Observing System (GOOS), and

efforts towards operational modelling of the ocean on global and regional scales, are good opportunities for finally achieving a common description of the ocean interface that would involve all the relevant dynamic processes : geostrophic currents, ocean waves, tides, internal waves, and known turbulent structures such as wind rolls in the atmospheric boundary layer, and both breaking waves and Langmuir circulations in the ocean mixed layer [*Ardhuin et al.*, 2005]. Many good fundamental contributions have studied one or two of these processes, including joint effects of wave motion and mean currents [e.g. *Weber*, 1981; *Jenkins*, 1987], wave breaking and Langmuir circulations effects on upper ocean mixing [*Agrawal et al.*, 1992; *Craig and Banner*, 1994; *Thorpe et al.*, 2003; *Mellor and Blumberg*, 2004].

A recent convergence of different approaches to the upper ocean dynamics shows a clear inconsistency. Mellor and Blumberg (2004) demonstrated that a parameterization for the strong mixing due to wave breaking, previously observed by Agrawal et al. (1992) and others, leads to improved hindcasts of mixed layer depth and temperature of the classic dataset from the Gulf of Alaska station Papa. This strong mixing also leads to a rather uniform Eulerian current profile, which has to be small, because the depth-integrated transport is the known Ekman transport. Mellor and Blumberg (2004) find surface currents less than 0.6% of the wind speed. Such a value of the Eulerian current may be larger than the quasi-Eulerian current observed by Santala and Terray (1992), but it is paradoxically small for experts in the forecasting of surface drift, for whom it is well established that the drift velocity is often close to 2 or 3% of the wind speed at 10 meters, U_{10} [*Spaulding*, 1999]. Both a strong mixing and a strong velocity shear at the surface should be obtained when surface waves are accounted for in a consistent way, including both wave breaking and wave-induced Stokes drift.

The goal of the present paper is to evaluate how well a simple but coherent model of the upper ocean performs in terms of drift velocities, Eulerian velocities, eddy viscosities and turbulent dissipation. Since waves are clearly an important part of the oceanic mixed layer, we shall also explore which wave parameters are important and how the mixed layer is modified. In particular the effect of the Hasselmann force [*Hasselmann*, 1970] that was reported to be significant by Lewis and Belcher (2004) is re-examined with a realistic parameterization of near-surface mixing. The present paper focuses on conditions that are statistically stationary and homogenous in the horizontal dimensions. The wave forcing and resulting wave properties are described in section 2. These drive a model for turbulent and mean Eulerian properties, as described in section 3. That model is based on the approximation, to second order in the wave slope, of the Generalized Lagrangian Mean (GLM2, see Andrews and McIntyre (1978*a*), and Groeneweg (1999)) applied to the Reynolds-Averaged

Navier-Stokes (RANS) equations. This GLM2-RANS formalism can be obtained by subtracting the wave pseudo-momentum from the total momentum equation given by Mellor (2003), and valid for horizontally-uniform conditions. This step, as well as a derivation from the equations of Andrews and McIntyre (1978*a*), is described by Ardhuin (2005). The numerical calculations use the computer code by Craig and Banner (1994), extended to account for wave effects specific to our GML2-RANS equations. In section 4, the various effects of the waves on the turbulent, Eulerian and Lagrangian properties are compared to observations of turbulent kinetic energy dissipation, quasi-Eulerian and Lagrangian velocities. Conclusions follow in section 5.

2.2 Wave dynamics

2.2.1 Spectral wave evolution

Ocean surface waves, generated by the wind, have a large influence on air-sea fluxes. In particular, waves are generally believed to absorb more than 50% the wind-to-ocean momentum flux τ^a [*Donelan*, 1998;*Banner and Peirson*, 1998]. This large fraction of the wind stress τ^a is the wave-induced stress τ^{in}. However, only a small fraction of τ^{in}, possibly up to 5%, is radiated in the wave field momentum flux, the vast majority is continuously lost by waves as they dissipate, essentially due to wave breaking [*Donelan*, 1998; *Janssen et al.*, 2004; *Ardhuin et al.*, 2004]. Another effect of interest to coastal oceanographers is that for a given wind speed, τ^a can be increased by as much as a factor three in coastal areas, due to the different nature of the wave field [e.g. *Drennan et al.* 2003; *Lange et al.* 2004].

Because ocean waves are generated by the wind, many authors have sought a direct parameterization of wave effects from the wind field. However, waves are not uniquely defined by the local wind speed and direction, in particular in coastal areas and marginal seas (like the Mediterranean sea), where wave development is limited by the fetch, but also in the tropics and mid-latitudes where a large part of the wave energy is due to long period waves (swell) that have propagated from distant storms, sometimes half-way round the Earth [*Snodgrass et al.* 1966]. In general, one needs to take into account the wave dynamics that are, on these large scales, statistically well defined by the directional wave spectrum $E(k,\theta)$, that distributes over wavenumbers k and directions θ the wave energy $E^w = \rho_w g \int E(k,\theta) \mathrm{d}k\mathrm{d}\theta$. The evolution of the spectrum is generally modelled using the energy balance equation

[*Gelci et al.*, 1957],

$$\frac{\mathrm{d}}{\mathrm{d}t}E(k,\theta) = S^{\mathrm{in}}(k,\theta) + S^{\mathrm{nl}}(k,\theta) + S^{\mathrm{ds}}(k,\theta) + S^{\mathrm{bot}}(k,\theta), \tag{2.1}$$

where the Lagrangian time derivative includes propagation effects, and S^{in}, S^{nl}, S^{ds}, S^{bot} are 'source terms' (either positive for true sources or negative for actual sinks) that represent the energy given to the spectral component (k,θ) by the atmosphere, the other wave components, the ocean turbulence in the water column and surface boundary layer, and the bottom boundary layer and sediments, respectively. This equation is easily extended to take into account varying currents [*Komen et al.* 1994; *White* 1999]. Each energy source terms can be converted in a momentum source term [e.g. *Phillips* 1977],

$$\tau^i = \rho_w g \int \frac{S^i(k,\theta)}{C}\mathrm{d}k\mathrm{d}\theta, \tag{2.2}$$

where C is the wave intrinsic phase speed. Of particular interest will be τ^{in} and $-\tau^{ds}$, the momentum fluxes, per unit surface of the ocean, input to waves from the wind, and delivered to the mean flow by the waves, respectively.

2.2.2 The Stokes drift

It is also well known that waves possess a pseudo-momentum that is equal to the mass transport velocity or Stokes drift $\mathbf{U}_s$ [e.g. *McIntyre* 1981]. This drift arises as the wave-induced orbits of particles are not exactly closed. From an Eulerian point of view this drift is zero everywhere below the wave troughs, and the wave-induced mass transport occurs between the deepest troughs and the highest crests. However, such an Eulerian view 'diffuses' the air-sea interface over a vertical distance of the order of the significant wave height H_s, which is not practical for investigating the surface gradient of any quantity. We shall thus prefer the Lagrangian point of view [e.g. *Andrews and McIntyre*, 1976], that yields, correct to second order in the wave slope, the following expression [*Kenyon*, 1969] for deep-water waves,

$$\begin{aligned}\mathbf{U}_s(z) &= 2\int_0^{2\pi}\int_0^{\infty}\mathbf{u}_\theta k\sigma e^{2kz}E(k,\theta)\mathrm{d}k\mathrm{d}\theta \\ &= \tfrac{2}{g}\int_0^{2\pi}\int_0^{\infty}\mathbf{u}_\theta \sigma^3 e^{2kz}E(k,\theta)\mathrm{d}k\mathrm{d}\theta.\end{aligned} \tag{2.3}$$

That expression uses the intrinsic wave radian frequency, as given by the deep water dispersion relation for linear gravity waves, $\sigma = \sqrt{gk}$, g is the acceleration of gravity, and $\mathbf{u}_\theta = (\cos\theta, \sin\theta)$ is the unit vector in the direction of propagation. The origin of the vertical coordinate z is at the mean water level.

$\mathbf{U}_s$ is clearly much smaller than the orbital wave velocity, by a factor ε that is the wave slope, typically less than 0.1. $\mathbf{U}_s$ is also strongly sheared at the surface because the contribution of each wave component decays exponentially over its Stokes depth $1/(2k)$, and the high-wavenumber components give a significant contribution to $\mathbf{U}_s$, but near the surface only (figure 1). Using a spectral shape proposed by Kudryavtsev et al. (1999), a wind of $U_{10} = 10$ m s^{-1} yields a surface drift of $\mathbf{U}_s(z = 0) = 0.11$ m s^{-1}, when only wave components with $2\pi/k > 5$ m are included , whereas all components up to $2\pi/k = 0.1$ m yield up to 0.13 m s^{-1}. The comparison with a monochromatic component shows the differences between wind sea and swell contributions : the swell-induced Stokes drift at the surface is typically less than 30% of the drift associated with a wind sea of same peak period and significant wave height. A large swell and a wind sea due to a weak wind can then produce surface Stokes drifts of the same order.

The Stokes transport

$$\mathbf{M}^w = \int_{-H}^{0} \mathbf{U}_s \mathrm{d}z = \int_0^{2\pi} \int_0^{\infty} \mathbf{u}_\theta \sigma E(k,\theta) \mathrm{d}k\mathrm{d}\theta \tag{2.4}$$

is slightly less influenced by the short (and slower) waves. Nevertheless the short waves contribute relatively more to $\mathbf{M}^w$ than to the wave energy, as the contribution of each spectral component to $\mathbf{M}^w$ is its surface elevation variance divided by the intrinsic phase speed.

2.2.3 Practical calculation of wave parameters

Because short waves are important, with $\mathbf{U}_s(z = 0)$ and $\mathbf{M}^w$ proportional to the third and first moments of the frequency spectrum, respectively, a numerical estimation of $\mathbf{U}_s$ based on (2.3) should use a wave spectrum that is well defined in that range. For general applications using numerical wave models such as WAM [*WAMDI Group*, 1988], the explicitly resolved spectrum can be carefully extended by a high-frequency tail. In the present study, we use the family of spectra proposed for remote-sensing applications by Kudryavtsev et al. (1999), and governed by the two main parameters that are the wind speed and the stage of wave development. These spectra have been carefully designed to reproduce both the long wave spectrum, with a spectral shape similar to that of Donelan et al. (1985), and the short wave spectrum with, in particular, a second moment of the wavenumber spectrum (or fourth moment of the frequency spectrum) that is well constrained by the optical measurements of the mean sea surface slope by Cox and Munk (1954). One can thus assume that the intermediate third moment that is the Stokes drift is well

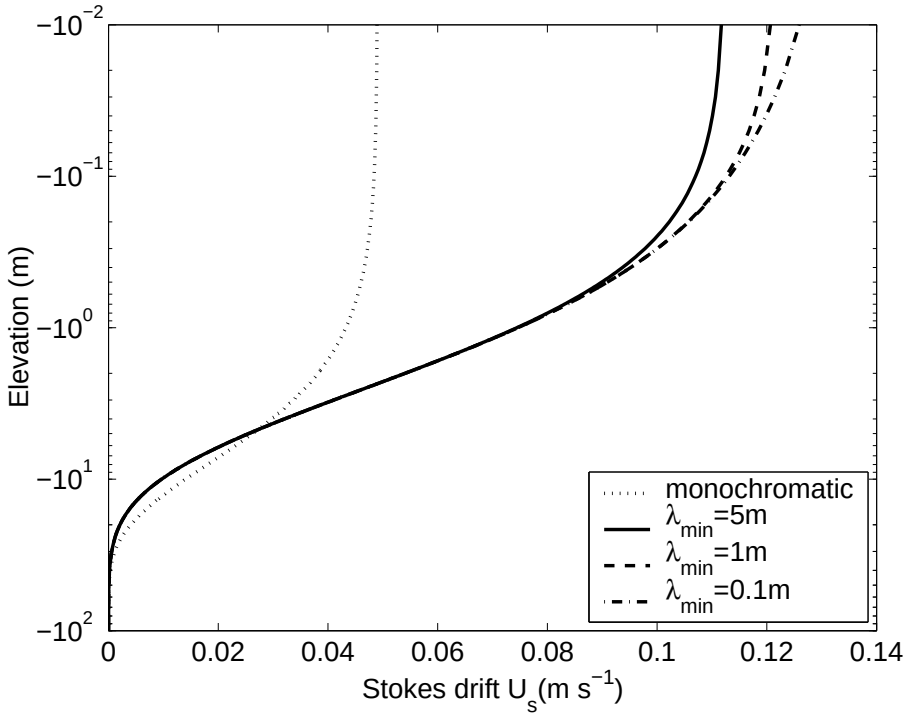

Figure 2.1: Stokes drift profile for a wind speed $U_{10} = 10$ m s^{-1} and a fetch larger than 1000 km (fully developed sea), based on the KMC spectrum [Kudryavtsev et al. (1999)] , and the integral (2.3). Different profiles are shown that only include wavelengths longer than a minimum value λ_{min}. For comparison, the drift due to a single wave component is also indicated. That single component has same peak wavelength and surface elevation variance (period $Tp = 8$s, $H_s = 2.8$m) as the wave spectrum.

represented by this model.

These spectra yield values of $\mathbf{U}_s(z=0)$ that can be larger than typical mean Eulerian currents, with a transport $\mathbf{M}^w$ of the order of the Ekman (1905) transport at mid-latitudes, except for short fetches or weak winds (figure 2). For fully developed waves, $\mathbf{U}_s(z=0) = 0.0125\mathrm{U}_{10}$ is consistent with recent observations of the drift of near-surface clouds of bubbles by Smith (manuscript submitted to JPO, 2005). In

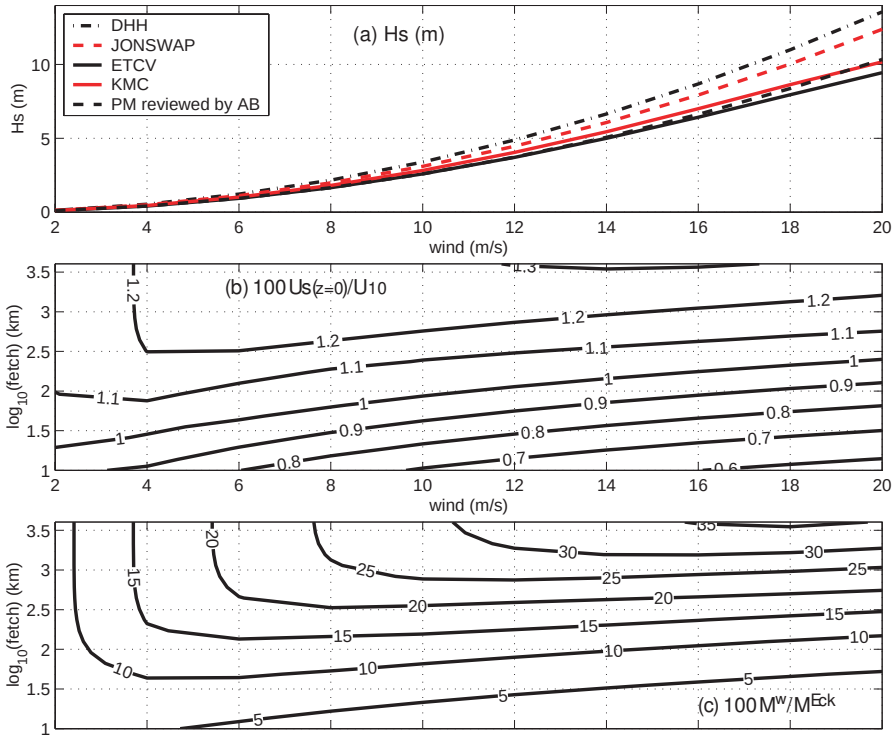

Figure 2.2: (a). Significant wave height at full development given by several parameterizations of the wave spectrum $E(k,\theta)$: PM is Pierson and Moskowitz (1964), AB is Alves and Banner (2003), DHH is Donelan et al. (1985), JONSWAP is Hasselmann et al. (1973), ETCV is Elfouhaily et al. (1997), and KMC is Kudryavtsev et al. (1999). For DHH and JONSWAP, full development is obtained by setting the peak frequency f_p to $0.123g/U_{10}$. (b) Surface Stokes drift as a function of fetch and wind speed U_{10} for the KMC spectrum, expressed as a percentage of U_{10}. (c) Magnitude of the vertically-integrated Stokes mass transport $\mathbf{M}^w$ as a function of fetch and U_{10}, expressed as a percentage of the corresponding Ekman (1905) transport u_*^2/f at mid-latitudes, with $f = 10^{-4}$.

the following calculations, the wind speed at 10 m height U_{10} is taken to be in the direction $\theta = 0$. The friction velocity $u_\star$ is determined from U_{10} using Charnock's expression [1955],

$$U_{10} = \frac{u_{a\star}}{\kappa} \log\left(\frac{z}{z_{a0}}\right), \tag{2.5}$$

with

$$z_{a0} = 0.018\, u_{a\star}^2/g, \tag{2.6}$$

where $z = 10$ m, $\tau^a = \rho_w u_\star^2 = \rho_a u_{a\star}^2$ is the wind stress, ρ_w and ρ_a are the densities of water and air. However it is well established that the sea-state and the wind speed are coupled, because of the dependance of the wind profile on the roughness of the sea [e.g. *Janssen*, 2004]. Donelan (1998) gives a parameterization of z_{a0} that uses the wave age c_p/U_{10} (where c_p is the phase speed at the peak of the wave frequency spectrum) and the significant wave height H_s,

$$z_{a0}/H_s = 1.67 * 10^{-4} \left(U_{10}/c_p\right)^{2.6}. \tag{2.7}$$

This effect will be evaluated in section 2.4.3.

2.3 Wave-averaged mixed layer equations

Oceanic motions are separated in three components, mean flow, waves and turbulence. Turbulence is separated from other motions by a an average over flow realizations for given wave phases. The mean flow and wave motions are then averaged with a Lagrangian mean so that the mean momentum is separated into a mean flow and a wave part. The vertical mean wave momentum is zero while the horizontal total mean momentum $\rho_w \mathbf{U}$ is split in a quasi-Eulerian mean $\rho_w \widehat{\mathbf{u}}$ and a Stokes drift,

$$\mathbf{U} = \widehat{\mathbf{u}} + \mathbf{U}_s. \tag{2.8}$$

This separation comes naturally with the definition of the Generalized Lagrangian Mean [*Andrews and McIntyre*, 1978]. Please note that $\mathbf{U}$ and $\mathbf{U}_s$ are $\overline{\mathbf{U}}^{\mathbf{L}}$ and $\mathbf{p}$ in their notations and are evaluated at a slightly displaced vertical position [*McIntyre*, 1988]. In measurements, this separation may be difficult to achieve [e.g. *Santala and Terray*, 1992; *Hristov et al.*, 1998]. Although the Stokes drift $\mathbf{U}_s$ corresponds to the wave-induced drift that arises from the correlations of wave-induced displacements and wave-induced velocity gradients, as defined by Phillips (1977), the quasi-Eulerian velocity $\widehat{\mathbf{u}}$ is more difficult to interpret. $\widehat{\mathbf{u}}$ is the mean velocity of a water particle $\mathbf{U}$, minus $\mathbf{U}_s$, but it is not easily related to Eulerian mean velocities. Another interesting velocity, in particular in remote-sensing applications, is the mean of the velocity at a point that is fixed horizontally but moves up and down with the surface elevation ζ. That mean surface velocity is $\widehat{u(\zeta)} = \widehat{\mathbf{u}}(\widehat{\zeta}) + \mathbf{U}_s(\widehat{\zeta})/2$, at second order in the wave slope.

If waves do not interact with the mean flow, $\widehat{\mathbf{u}}$ is the mean flow velocity in the limit of vanishingly small wave amplitudes. However, waves do generally interact with the mean flow.

2.3.1 The influence of waves on the mean flow

We will use now the equations established in Ardhuin et al. (2004*b*), which are an extension of *Mellor's* [2003] equations, valid for horizontally-uniform conditions. These are essentially a generalization in three dimensions of the equations of Garrett (1976), also discussed in Ardhuin et al. (2004*a*). These equations are also equivalent to the Generalized Lagrangian Mean equations as given by Groeneweg and Klopman (1998), neglecting the modulations of turbulent properties on the scale of the wave phase [*Ardhuin*, 2005]. Following Ekman (1905) we assume that the wave, velocity, and turbulent properties are uniform horizontally. In this case, the horizontal momentum conservation simplifies as

$$\frac{\partial \widehat{\mathbf{u}}}{\partial t} = -f\mathbf{e}_z \times (\widehat{\mathbf{u}} + \mathbf{U}_s) + \frac{\partial}{\partial z}\overline{\widehat{\mathbf{u}}'\widehat{w}'} - \mathbf{T}^{ds}(z), \tag{2.9}$$

with the following boundary conditions, defining our vertical coordinate so that the mean sea level is at $z = \widehat{\zeta} = 0$,

$$\overline{\widehat{\mathbf{u}}'\widehat{w}'}\Big|_{z=0} = \frac{\tau^a}{\rho_w} - \frac{\tau^{in}}{\rho_w} \tag{2.10}$$

and

$$\mathbf{u}|_{z=-H} = 0. \tag{2.11}$$

Here $\mathbf{T}^{ds}$ is a vertical distribution of τ_{ds}, so that $\tau_{ds} = \rho_w \int_{-H}^{0} T^{ds} dz$.

The influence of the wave motion on the quasi-Eulerian flow appears with the Hasselmann force $-f\mathbf{e}_z \times \mathbf{U}_s$ [*Hasselmann*, 1970], that combines the Coriolis parameter and the Stokes drift [e.g. *Xu and Bowen*, 1994], and in the momentum transfer from wind to the mean flow. One part of the momentum from the wind goes directly to the mean flow via the surface shear stress $\rho_w \left.\overline{\widehat{\mathbf{u}}'\widehat{w}'}\right|_{z=0}$. It is the direct mean viscous drag of air on water. The other part τ^{in} goes to the wave field, it is the form drag of wind over water plus the wave-induced modulations of the viscous stresses [*Longuet-Higgins*, 1969]. Then the wave field is also dissipated, releasing its momentum to the mean flow. This is the force $-\mathbf{T}^{ds}(z)$. This latter force is constituted by viscous dissipation (the virtual wave stress is part of it), interactions of waves with the turbulence [e.g. *Teixeira and Belcher*, 2002], and wave breaking [*Melville et al.*, 2002].

Observations of wave growth with fetch shows that the momentum retained by the wave field is around 5% of the momentum input (see section 2.2.1). This leads to the good approximation $\tau^{ds} \simeq -\tau^{in}$. Furthermore, supposing that the momentum is released by the wave field at the surface (i.e. $T^{ds} = \tau^{ds}\delta(z)/\rho_w$), equations for

the mean flow appear now with their usual form ($T^{ds} = 0$ and $\tau^{in} = 0$ in eq.2.9 and 2.10), except for the Hasselmann force.

2.3.2 Turbulent closure

Eq.2.9 involves the divergence of the Reynolds stresses $\overline{\widehat{\mathbf{u}}'\widehat{w}'}$ that should now be computed or parameterized. We will use the turbulent closure model of Craig and Banner (1994). It is a "level 2.5" turbulent closure scheme adapted from Mellor and Yamada (1982), with the dissipation of surface waves taken into account by introducing a near-surface injection of turbulent kinetic energy (TKE).

The Reynolds stress is assumed to be linearly related to the shear : $\overline{\widehat{\mathbf{u}}'\widehat{w}'} = K_z \partial \mathbf{u}/\partial z$, with the eddy viscosity $K_z = lqS_m$, where $b = q^2/2$ is the TKE per unit mass, and l the mixing length. The later is parameterized as

$$l = \kappa(z_0 - z), \tag{2.12}$$

where $\kappa = 0.4$ is the von Kármán's constant and z_0 is a roughness length.

The bottom has almost no effect on the near surface dynamics, provided that the depth is substantially greater than the Stokes depth (see section 2.2.2) and the Ekman scale, which is $u_*/4f$ because the turbulent viscosity varies nearly linearly with depth [*Craig and Banner*, 1994]. Therefore, the bottom boundary layer of Craig and Banner (1994) is not described here.

The equation for the evolution of TKE is :

$$\begin{aligned} \frac{\partial b}{\partial t} &= \underbrace{\frac{\partial}{\partial z}\left(lqS_q \frac{\partial b}{\partial z}\right)}_{a} + \underbrace{lqS_m \left(\left(\frac{\partial \widehat{u}}{\partial z}\right)^2 + \left(\frac{\partial \widehat{v}}{\partial z}\right)^2\right)}_{b} \\ &\quad - \underbrace{\frac{q^3}{Bl}}_{c} - \underbrace{\varphi^{ds}(z)}_{d}, \end{aligned} \tag{2.13}$$

where S_m, S_q and B are model constants for which the appropriate values are 0.39, 0.2 and 16.6. $\widehat{u}$ and $\widehat{v}$ are the components of the quasi-Eulerian velocity $\widehat{\mathbf{u}}$.

The TKE evolution comes from a transport term(a), a production term by the shear of the mean flow (b), a dissipation term (c) and a wave-induced source term (d). The transport term is parameterized by the eddy diffusivity lqS_q.

The conversion of wave kinetic and potential energy into TKE is the non-viscous

wave "dissipation" Φ_{oc} (per unit mass and unit surface) of the wave field,

$$\Phi_{oc} = g \int S^{ds}(k,\theta) dk d\theta. \tag{2.14}$$

S^{ds} is distributed over depth as

$$\int_{-H}^{0} \varphi^{ds}(z) dz = \Phi_{oc}. \tag{2.15}$$

Alternatively [*Craig and Banner*, 1994], Φ_{oc} may be prescribed as a surface flux of TKE and parameterized by $\Phi_{oc} = \alpha u_*^3$ with $\alpha \simeq 100$, consistent with the known loss of energy from the waves. How the prescription as a surface flux modifies the TKE profiles will be studied in section 2.4.1. The consequences of neglecting the variations of α with the wave age (from 50 for young waves and fully-developed waves to 150 otherwise) will be dealt with in section 2.4.3. The boundary condition for the TKE is then :

$$lqS_q \frac{\partial b}{\partial z}\bigg|_{z=0} = \alpha u_*^3, \tag{2.16}$$

which closes the model.

We will now focus our attention on the steady state solutions, when wind- and wave-induced inertial oscillations are damped. The sea state is again modelled by *Kudryavtsev et al.*'s [1999] spectrum. It is assumed that the wave field is locally uniform even if the sea is not fully developed. In other words, the gradients of the radiation stresses are supposed much smaller than the leading terms in the momentum balance that are the Coriolis force, the Hasselmann force and the vertical mixing (see Ardhuin et al. (2004*a*) for a discussion of the impact of the radiation stress tensor in fetch limited conditions).

2.4 Model results and validation

2.4.1 Calibration of the model with observed profiles of TKE dissipation

Two parameters remain unknown in this model : the roughness length z_0 and the scale α of the surface flux of TKE. α may practically come from a wave model, and is therefore supposed to be known [e.g. *Janssen et al.*, 2004]. z_0 is determined from measurements of TKE dissipation near the surface.

In terms of TKE, the surface layer can be divided in a "production layer" and a "diffusion layer" [*Craig and Banner*, 1994]. In the deeper layer, the TKE equation is dominated by shear production and dissipation. Closer to the surface, the TKE

balance is between diffusion from the surface flux and dissipation. One important modification brought by the present model to the one of Craig and Banner is the addition of the Stokes-Coriolis effect (the Hasselmann force). This effect modifies the Eulerian velocities over the whole water column (see section 2.4.2). But in the diffusion layer, the TKE production due to the shear of the mean flow has no importance. Therefore, the TKE is expected to remain unchanged near the surface by the addition of the Stokes-Coriolis term. The Numerical model results confirm this expectation, with relative changes in the magnitude of q less than 2% near the surface.

As a result, we can rely on previous works without the Stokes-Coriolis effect, providing a parameterization of z_0 based on measurements of TKE dissipation ϵ in the diffusion layer. Terray et al. (1996) proposed a scaling of the roughness length with the significant wave height H_s. It comes from the physical hypothesis that the surface mixing is proportional to the height of the breaking waves, which can be evaluated by H_s. Other scalings of z_0, linked to the wind speed or to the friction velocity are reported to fail [e.g. *Soloviev and Lukas*, 2003] because of no explicit dependance on the wave development. Terray et al. (2000) used the model of Craig and Banner (1994) to fit z_0 using dissipation data from several field experiments, with various stages of wave development [*Drennan et al.*, 1996]. They found $z_0 = 1.6H_s$. As was pointed out by the authors, the model does not fit very well the data at depths of the order of H_s. Therefore they proposed a modified length scale which seems to fit better the observations. However, if we attempt a Lagrangian interpretation of their Eulerian measurements, there is water between their uppermost data points and the surface where TKE dissipation also occurs. Even if we suppose that ϵ decays linearly from $2\Phi_{oc}/H_s$ at $z = -H_s$ to Φ_{oc}/H_s at $z = 0$, the vertically integrated dissipation rate in the figure 1 in Terray et al. (2000), between the surface and $-H_s$, is greater than the wave input flux Φ_{oc} of TKE. This cannot be explained by the production of TKE by the shear of the mean flow, which is negligible near the surface. Besides, a decrease of ϵ between $z = -H_s$ and the surface is not supported by the Lagrangian averaged data of Soloviev and Lukas (2003). The data and the modified mixing length of Terray et al. (2000) are not compatible, unless evidence is shown of very small dissipation rate between $z = -H_s$ and the surface. Therefore we do not take the modified form of the mixing length, as did Mellor and Blumberg (2004), and stick to (2.12). Soloviev and Lukas (2003) also used measurements of dissipation to estimate z_0, and found $z_0 = 0.6H_s$. However the contribution of swell to the significant wave height was not evaluated, which may have lead to an underestimation of the ratio z_0/H_s.

As the TKE equilibrium near the surface is between injection, dissipation and diffusion, one may wonder if a better representation of injection may not improve the model. The external source of TKE is the dissipation S^{ds} of the wave field, which is, in the case of a wind-sea, due to breaking S^{break} and wave-turbulence interactions S^{turb}. The viscous dissipation, which is negligible, does not constitute a source of TKE. The separation between breaking and turbulence effects is not simple, but these two effects probably yield different depths of TKE injection, which can modify the profiles of TKE and of TKE dissipation.

Teixeira and Belcher (2002) used rapid distorsion theory to derive an expression for the production of TKE due to interactions between turbulence and high frequency waves,

$$\varphi^{turb}(z) = \overline{\widehat{\mathbf{u}}'\widehat{w}'}\,\partial\mathbf{U_s}/\partial z. \tag{2.17}$$

Using Lagrangian average of the Reynolds-average Navier-Stokes equations, Ardhuin and Jenkins (2006) extended this expression to low frequency waves with the assumption that the turbulent fluxes are not correlated with the wave phases. The same expression was used in different studies of Langmuir circulations [e.g. *McWilliams et al.*, 1997], this time derived from the equations of Craik and Leibovich (1976). The resulting profile of TKE injection follows the profile of $\partial \mathrm{U}_s/\partial z$ since the momentum flux is often more uniform than U_s over the Stokes depth, which is typically smaller than the Ekman depth. The use of a spectral distribution of waves leads to a profile of $\partial \mathrm{U}_s/\partial z$ much more sheared at the surface than the profile of U_s, whereas the use of a monochromatic wave would strongly over-estimate the depth of injection of TKE (see fig.2.3). It follows from this calculation that

$$\Phi_{oc}^{turb} \simeq \overline{\widehat{u}'\widehat{w}'}\,\mathrm{U}_s(z=0) \simeq 10 \times u_*^3, \tag{2.18}$$

which is around 10% of $\Phi_{oc} = \alpha u_*^3$. That means that the dissipation of the waves by interactions with turbulence is only 10% of the total waves dissipation. However the correlations between wave groups and enhanced breaking [*Banner et al.*, 2000] may lead to a greater fraction of the total dissipation.

In the case of dissipation by breaking, an injection over a certain depth linked to the wavelength of the breaking wave may be more realistic. Sullivan et al. (2004) proposed a profile for the injection of momentum by a breaking wave, based on the laboratory data of Melville et al. (2002). That profile can be approximated, after

integration over time and horizontal dimensions of their breaker, by

$$f(z) = 4.227\left(1+\frac{5z}{\lambda}\right)^2 exp\left(-5\left(\frac{5z}{\lambda}\right)^2\right). \tag{2.19}$$

With this expression, most of momentum of breaking waves is released between the surface and a depth of $\lambda/5$, where λ is the wavelength of the breaking wave. We will suppose that, for a given wavelength, the injection of TKE and momentum follow the same depth profiles. To determine which waves are breaking, we will determine the spectral distribution of dissipation as in Donelan (1998), by supposing that the predominant terms in eq.2.1 are the input and the dissipation,

$$S^{in} + S^{ds} = 0, \tag{2.20}$$

which is formally valid only at the peak of the wave spectrum. Then the spectral distribution of dissipation can be obtained from S^{in}. The formulation of Makin and Kudryavtsev (1999) is, neglecting the sheltering effect [*Hara and Belcher*, 2002],

$$S^{in} = \int \beta(k,\theta)E(k,\theta)dkd\theta, \tag{2.21}$$

with

$$\beta = 32\frac{\rho_a}{\rho_w}\left(1-1.3\left(\frac{c}{U_{10}}\right)^5\right)\left(\frac{u_*}{c}\right)^2 cos(\theta)|cos(\theta)|. \tag{2.22}$$

Using (2.19)-(2.22) provides an estimation of $\varphi^{break}(z)$.

The appropriate surface boundary condition is now a zero flux of TKE, $lqS_q\partial b/\partial z = 0$. Figure 2.3 shows the profiles of φ^{ds} assuming that the dissipation of wave field comes entirely from breaking ($\varphi^{ds} = \varphi^{break}$) or entirely from wave-turbulence interactions ($\varphi^{ds} = \varphi^{turb}$). Both profiles are concentrated near the surface, much more so than the Stokes drift. A realistic case would be that wave dissipation comes from both phenomena with a ratio of the order of 20% for the wave-turbulence interactions ($\varphi^{ds} = 0.8\varphi^{break} + 0.2\varphi^{turb}$). Resulting profiles of dissipation are shown in fig.2.4, as well as profiles of dissipation with surface flux of TKE and different values of the roughness length.

As expected, in the extreme case of total dissipation due to wave-turbulence interactions, the TKE penetrates deeper which leads to more uniform dissipation profiles. The effect of depth injection is comparable to an increase of the roughness length. This is also true for the momentum, when the surface source is distributed over depth (not shown). The roughness length, which is fitted to measurements of dissipation, is supposed to take this effect into account. It can be seen from fig.2.4

that a surface roughness at least of the order of H_s is needed, even if all the TKE is deeply injected with the profile of $\partial \mathrm{U}_s/\partial z$.

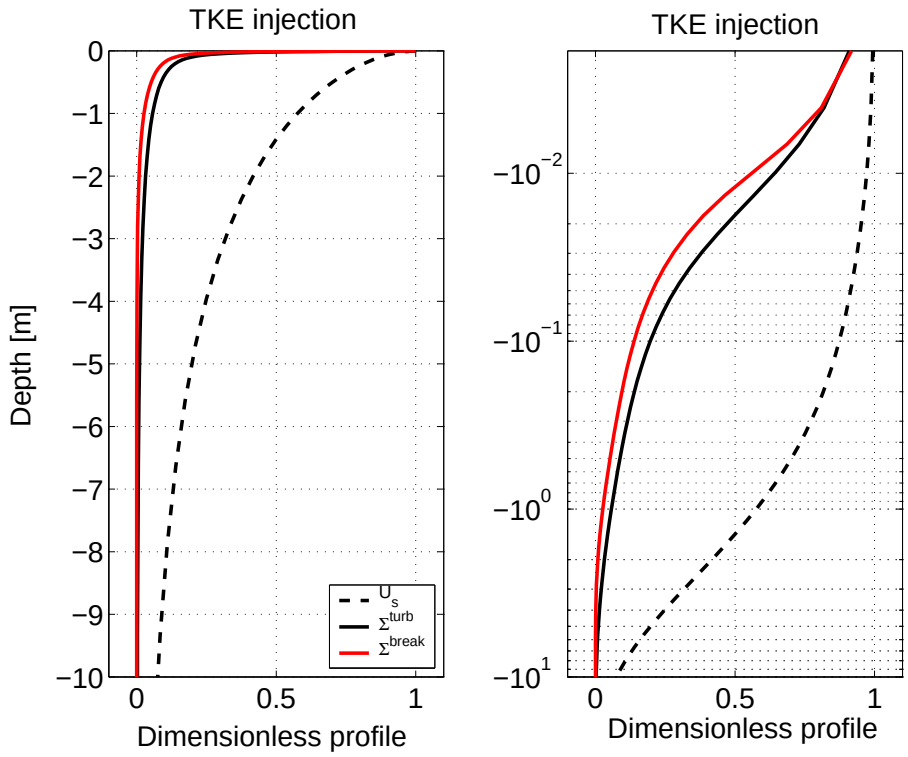

Figure 2.3: Profiles of normalized injection of TKE by wave breaking $\varphi^{break}(z)/\varphi^{break}(z=0)$, and by interactions with turbulence $\varphi^{turb}(z)/\varphi^{turb}(z=0)$, in the case of fully developed waves with a wind of $U_{10} = 10$ m s^{-1}. Also shown is the profile of the Stokes drift $\mathrm{U}_s(z)/\mathrm{U}_s(z=0)$.

2.4.2 Eulerian hodographs and shears

The most obvious effect of waves on the mean flow is the enhancement of mixing. This effect gets stronger as waves become developed, because the roughness length is proportional to the wave height. Fig.2.5 shows the expected difference between a young sea (wave age $C_p/U_{10} = 0.46$) and a fully-developed sea ($C_p/U_{10} = 1.25$).

Another effect, in appearance less important, comes from the Stokes-Coriolis term. We can compute this effect by subtracting the results of the quasi-Eulerian current $\widehat{\mathbf{u}}'$ from model without the Hasselmann force to the results of the full model $\widehat{\mathbf{u}}$. This net contribution $\delta\mathbf{u} = \widehat{\mathbf{u}} - \widehat{\mathbf{u}}'$ of the Hasselmann force for the quasi-Eulerian velocity is shown on figure 2.6. Polton et al. (2005) made detailed analysis of the impact of this Stokes-Coriolis term on the profile of $\widehat{\mathbf{u}}$, with constant and linearly varying eddy viscosities. They showed that the detailed profile of the Stokes drift does not matter as soon as the Ekman depth is much larger than the Stokes depth.

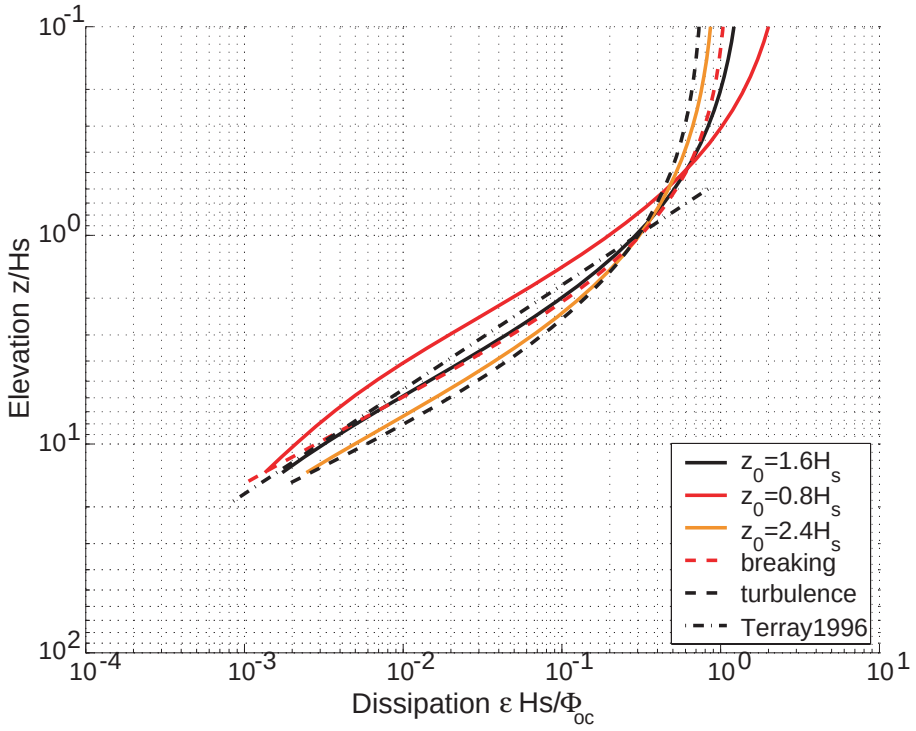

Figure 2.4: Normalized dissipation as a function of normalized depth, using the scaling of Terray et al. (2000), $\Phi_{oc} = \alpha u_*^3$ is the surface flux of TKE. Curves correspond to different values of the roughness length z_0. The effect of injection of TKE over depth is also shown, with $\varphi(z) = \varphi^{break}(z)$, following the profile of Sullivan et al. (2004), and with $\varphi(z) = \varphi^{turb}(z)$, following the profile of $\partial \mathrm{U}_s/\partial z$. Also shown is the result of Terray et al. (1996).

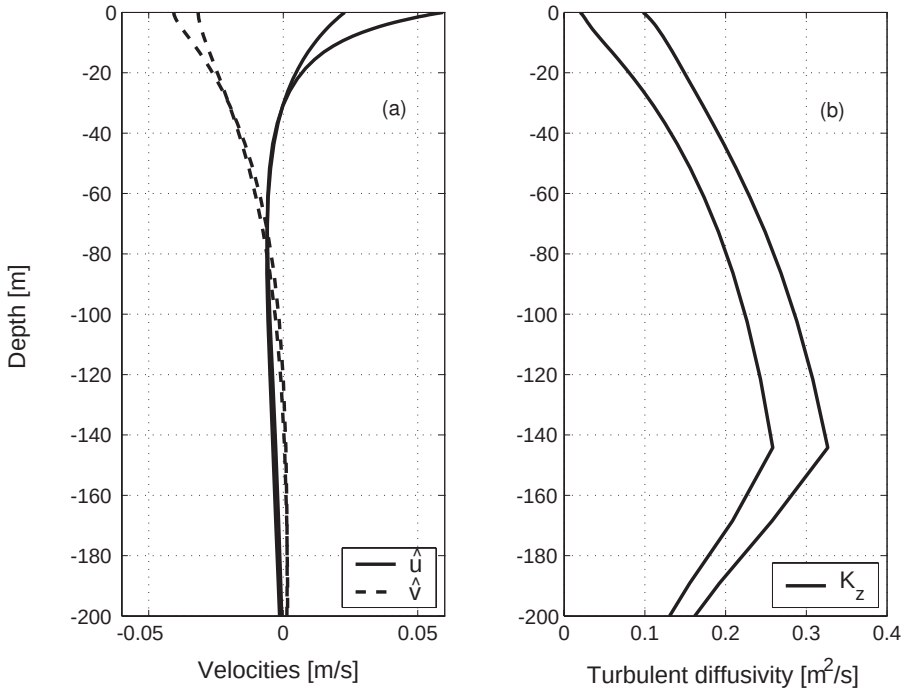

Figure 2.5: Evolution of profiles with an increasing fetch (wave heights from 0.6 m at 10 km offshore to the fully-developed value 2.5 m). (a) Quasi-Eulerian velocity profiles become more uniform. (b) Turbulent viscosity increases. The wind is set to $U_{10} = 10\text{ms}^{-1}$, and the water depth is 300m.

In this case, they showed that the contribution of the Hasselmann force is similar to the addition of a surface stress to the right of the wind, with a magnitude related to the Stokes transport $\mathbf{M}^w$. This is also true in our model since we are considering an unstratified water column (large Ekman depth) and a wind sea (small Stokes depth). Using a full spectrum to compute the Stokes drift is not important when looking at the Stokes-Coriolis effect on the quasi-Eulerian velocity $\widehat{\mathbf{u}}$. Eulerian velocities spiral in an Ekman fashion, and vanish at a depth given by the Ekman depth $u^*/4f$. The Hasselmann force has thus an influence much deeper than the Stokes drift [*Xu and Bowen*, 1994]. Because the transport induced by this Stokes-Coriolis term is equal to the Stokes transport [*Hasselmann*, 1970], an estimation of the importance of this effect is the ratio of the Stokes transport to the Ekman transport (fig.2.2), which can be more than 30% for mid-latitudes.

Substantial modifications at the surface (20%) and over the whole water column (30% at 100m) are found in the case of a developed sea (fig.2.6).

Lewis and Belcher (2004), and also Polton et al. (2005), studied the impact of the Stokes-Coriolis term on the Eulerian Ekman spiral, with an unstratified water column and with an eddy viscosity that varies linearly with depth. They reported that this Stokes-Coriolis term could explain the tendency of the spiral to be shifted

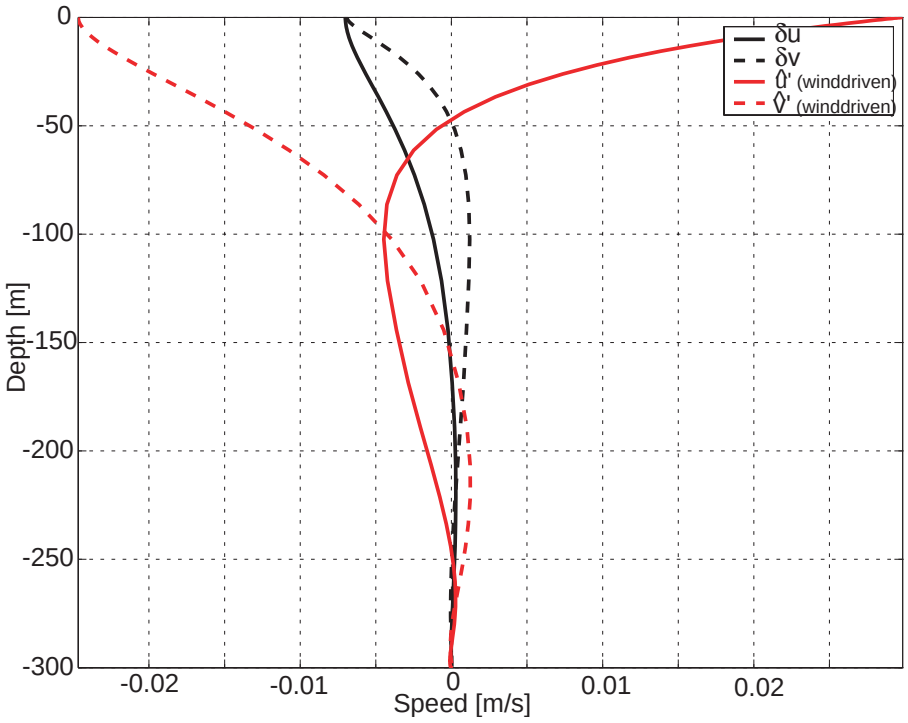

Figure 2.6: Quasi-Eulerian velocities driven by the wind stress ($\widehat{\mathbf{u}}'$) and driven by the Hasselmann force ($\delta\mathbf{u} = \widehat{\mathbf{u}} - \widehat{\mathbf{u}}'$). Velocities are computed respectively from the model without the Hasselmann force and from the full model minus the model without the Hasselmann force. The wind is set to $U_{10} = 10\text{ms}^{-1}$ and sea is developed (fetch > 1000km).

in the direction opposite to the wind, as observed in some field experiments, such as LOTUS3 [*Price and Sundermeyer*, 1999]. We must notice that they took small values of z_0, of the order of 1cm. Such values are commonly used in order to fit surface drift observations (see section 2.4.3) with the Eulerian surface current (around 3% of the wind speed U_{10}, e.g. $q = 0.03$ in table 3 of Lewis and Belcher (2004)). The present model was used to simulate conditions observed during the LOTUS3 experiment. The model mixing K_z is enhanced by breaking ($z_0 \simeq 2.5$m), which leads to quasi-Eulerian currents near the surface much reduced compared to Polton et al. (2005) (less than 1% of the wind speed U_{10}, fig.2.7). Polton et al. (2005) reported minors changes of velocity in the bulk Ekman layer to the values of z_0. But they used $z_0 \simeq 1$cm, which is two orders of magnitude below the values of the present model. Also it is the near-surface dynamics, within the first 10m, that is of interest here and it is quite sensitive to values of z_0 larger than 1m, as pointed out by *Craig and Banner* [1994, section 5], due to a very large increase in K_z. Therefore the good agreement found by Lewis and Belcher (2004) and by Polton et al. (2005) for the two uppermost current-meters ($z = -5$ and $z = -10$ m, figure 7) is not obtained with the present model. The value of the crosswind component of the model's velocity is only 50% of the observed value at $z = -5$ m. If the sub-surface deflection of the quasi-Eulerian velocity due to the Stokes-Coriolis effect is still significant, the vertical profiles and velocity spiral are more different from the observations than with the models of Lewis and Belcher (2004) and Polton et al. (2005). This misfit may be explained by the stratification : the mixed layer was only 10 to 25m thick during LOTUS3 [*Price and Sundermeyer*, 1999], with a strong diurnal cycling.

Terray et al. (2000) compared results of the Craig and Banner model (without the Stokes-Coriolis term) to quasi-Eulerian velocity profiles and shears, obtained with a wave-follower much closer the surface [*Santala and Terray*, 1992]. The addition of the Stokes-Coriolis term does not substantially modify the shear, but the magnitude of the currents is modified. However the field data used in Terray et al. (2000) was obtained with relatively young waves ($C_p/U_{10} \simeq 0.74$), so that currents driven by the Hasselmann force are one order of magnitude smaller than currents driven by the wind. Therefore this dataset is not ideal for highlighting the Stokes-Coriolis effect (fig.2.8). A dataset with fully-developed waves would have been more useful for that purpose. Moreover, the water column was stratified below 20m depth. Therefore the present comparison of their data and the model remains qualitative. However roughness length one order of magnitude smaller than H_s is clearly not compatible with this dataset.

McWilliams et al. (1997) used Large Eddy Simulations (LES) to study the impacts of Langmuir circulations (LCs) on the mixed layer in a weakly stratified

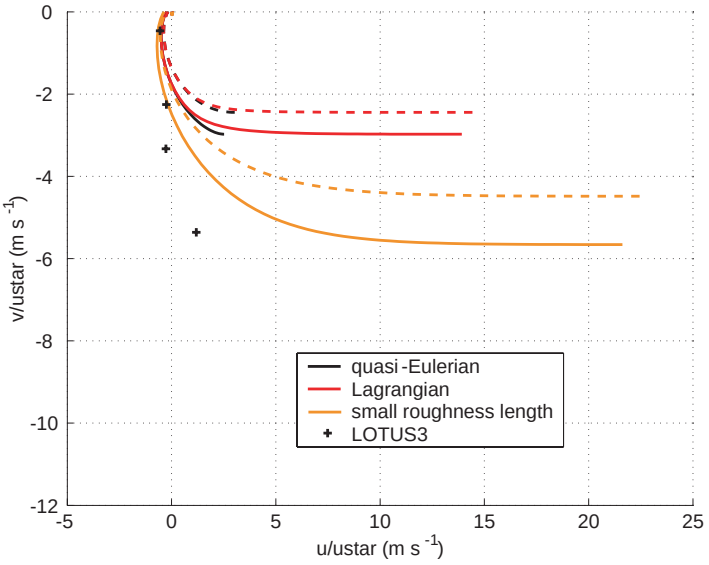

Figure 2.7: Hodographs of quasi-Eulerian and Lagrangian velocity. Curves are for $u_* = 8.3 \times 10^{-3}\text{ms}^{-1}$ and a fully developed sea ($H_s = 1.6$ m). Also shown is the mean profile from LOTUS3 [*Price and Sundermeyer*, 1999] at 5, 10, 15 and 25m and, for comparison with Polton et al. (2005), the Eulerian current from the model with a small surface mixing (small roughness length z_0=1.6×10^{-3}m). Solid lines are model results with the Hasselmann force, dashed lines without.

case.They did not take surface wave breaking into account but they used an input of TKE, given by the shear of the Stokes drift (2.17). Some comparison can be made between our present model with a simple turbulent closure scheme and their LES results : in particular they computed the impact of the Hasselmann force on the Eulerian current (their fig. 2). We must notice that their Stokes transport (a monochromatic wave of $H = 2.3$m and $\lambda = 60$m) is 4 times larger than expected at full development (they use $U_{10} = 5\text{ms}^{-1}$). In their case, the Ekman transport and the Stokes transport are of the same order. Fig.2.9 shows the present model results using the same Stokes drift as in McWilliams et al. (1997) and a Stokes drift from developed waves with $U_{10} = 5\text{ms}^{-1}$. These results are similar to the LES experiment, except for the u component in the near surface region that is much more uniform in their case. In spite of a close agreement between their bulk eddy viscosity and our eddy viscosity, the mixing due to LCs is significantly different to the one of our simple model. Kantha and Clayson (2004) used an intermediatly complex turbulence closure model based on two equations for q^2 and $q^2 l$, and simulated the same LES experiment. As they noticed, their model also underestimate the near surface mixing of the Langmuir cells.

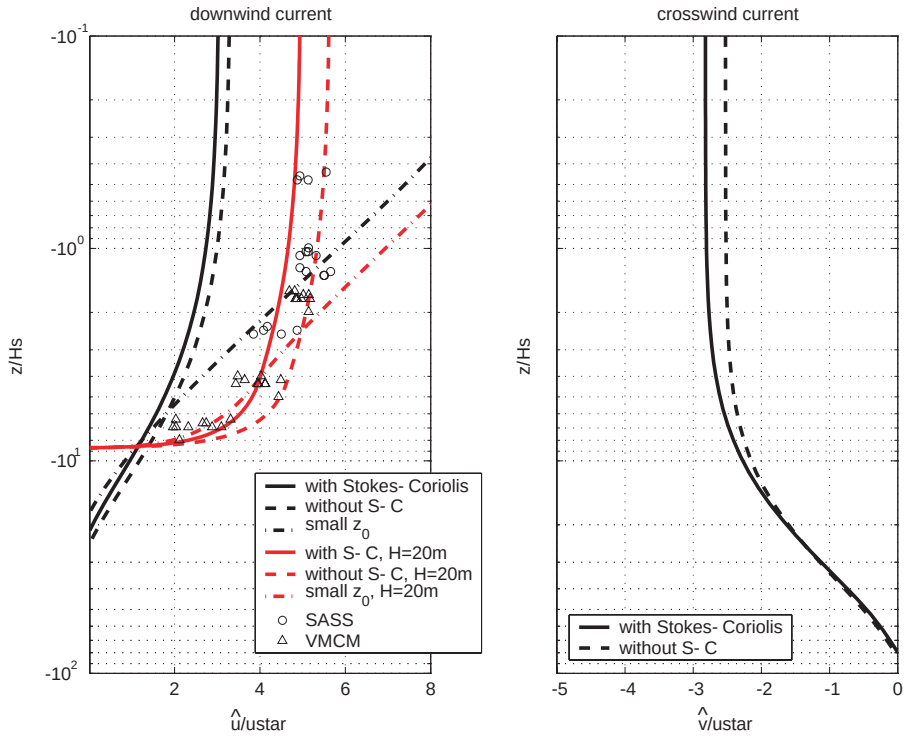

Figure 2.8: Downwind and crosswind quasi-Eulerian currents. Curves correspond to $U_{10} = 13.6$ m s^{-1} and a fetch of 100 km ($H_s = 2.3$ m). Solid and dashed lines show model results with and without the Hasselmann force, respectively. The data from the buoy (SASS) and the mooring (VMCM) of Terray et al. (2000) (their fig.3) are plotted with markers. As the water column was stratified during these measurements (thermocline at 20m depth), we also show for qualitative comparison for the downwind component the model results with a water depth of 20 m. Dashed-dotted lines are model results without the Hasselmann force and with a small roughness length $z_0 = 0.05 \times H_s$.

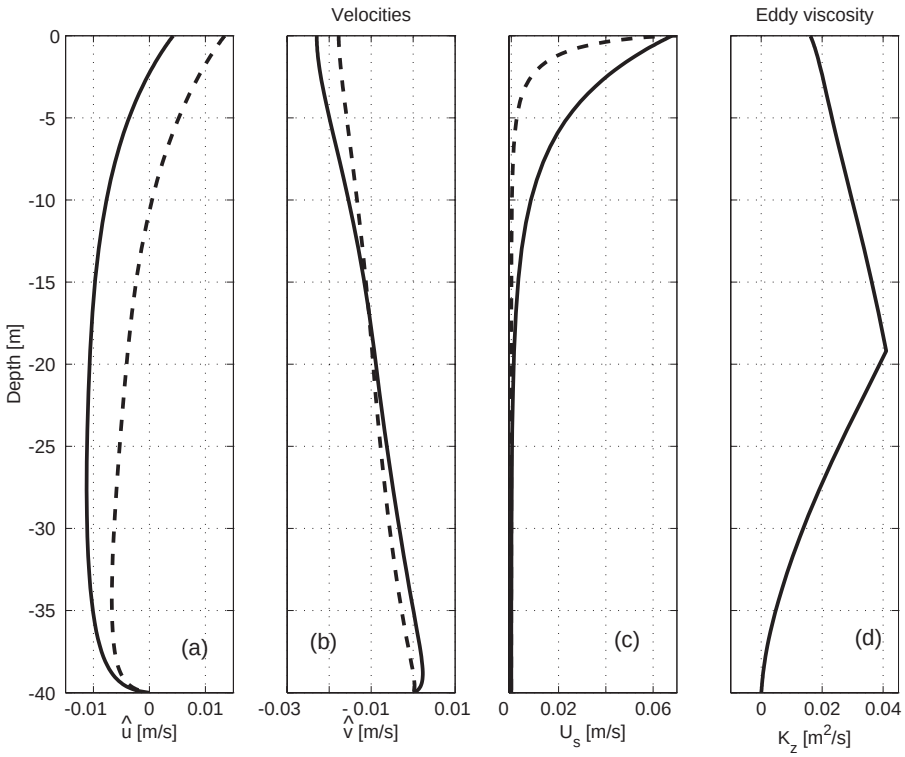

Figure 2.9: Profiles of quasi-Eulerian velocity components (a) $\widehat{u}$ and (b) $\widehat{v}$, (c) Stokes drift $\mathbf{U}_s$ and (d) eddy viscosity K_z. Curves are for $U_{10} = 5\text{m s}^{-1}$. Solid lines show results with the Stokes drift of a monochromatic wave as prescribed in McWilliams et al. (1997) and dashed lines show results for a fully-developed sea with this wind ($H_s = 0.9\text{m}$).

2.4.3 Lagrangian drift

The mean drift velocity $\mathbf{U}$ is the sum of the quasi-Eulerian flow $\widehat{\mathbf{u}}$, computed with the model described above, and the Stokes drift $\mathbf{U}_s$. Now considering the net wave-induced mass transport, the Stokes-Coriolis term is of prime importance. In terms of mass transport in the downwind direction, that term creates an Eulerian return flow which compensates the Stokes transport, leading to a zero wave-induced transport in steady conditions given by eq.2.9 [see also *Hasselmann*, 1970]. Because turbulence diffuses vertically the momentum source that is the Hasselmann force, the return flow is less sheared than the Stokes drift. Therefore the return flow does not compensate the Stokes drift near the surface, and overcompensates it below. Instead of quasi-Eulerian and Lagrangian , fig.2.10 shows a decomposition into quasi-Eulerian current driven by the wind $\widehat{\mathbf{u}}'$ and Stokes drift plus quasi-Eulerian current driven by the Hasselmann force $\mathbf{U}_s + \delta\mathbf{u} = \mathbf{U}_s + \widehat{\mathbf{u}} - \widehat{\mathbf{u}}'$.

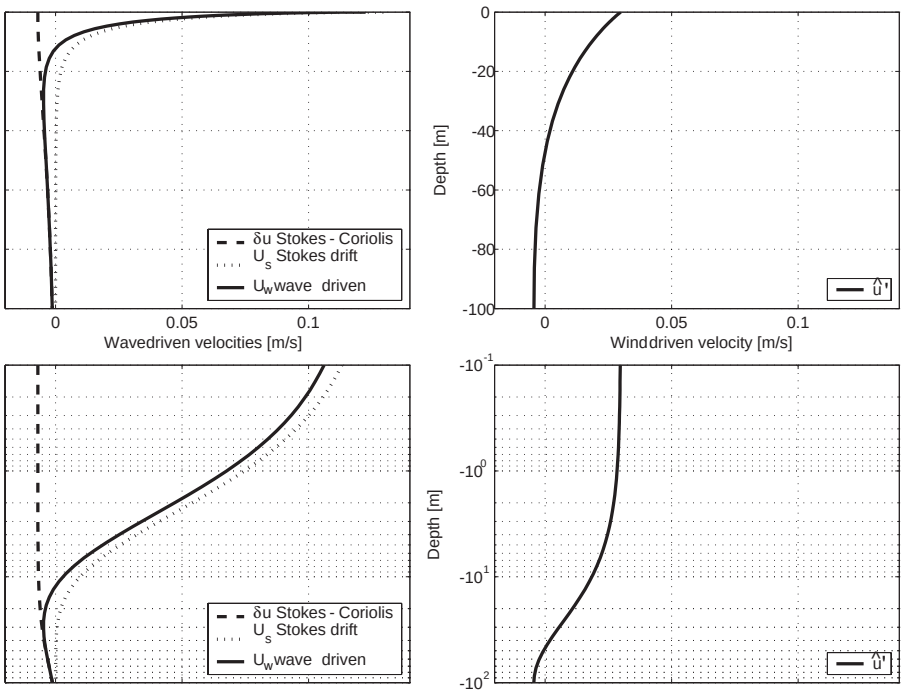

Figure 2.10: Details of the velocity profiles in the downwind direction. Left: Lagrangian drift induced by wave mass transport U_w, equal to Stokes drift U_s plus quasi-Eulerian current driven by the Hasselmann force $\delta\mathrm{u} = \widehat{\mathrm{u}} - \widehat{\mathrm{u}}'$. Right: Wind-driven quasi-Eulerian current (ie the model result without the Stokes-Coriolis term) $\widehat{\mathrm{u}}'$. Left plus right, i.e. $\mathrm{U}_w + \widehat{\mathrm{u}}' = \mathrm{U}_s + \delta\mathrm{u} + \widehat{\mathrm{u}}'$ gives the total Lagrangian velocity U. Curves are for $U_{10} = 10\mathrm{ms}^{-1}$ and fully developed waves (fetch superior to 1000km). Bottom panels are shown on a logarithmic scale.

It can be seen that near the surface the downwind drift in the present model is

essentially due to the Stokes drift (at least 80%), for fully-developed waves. The practical simplification that takes the surface drift to be the sum of the usual Ekman Eulerian current, from an ocean circulation model without the Stokes-Coriolis term, plus the Stokes drift [e.g. *Annika et al.*, 2001], leads to slight over-estimations (less than 5%), for fully-developed waves. For very young waves, the Eulerian current is of same order as the Stokes drift but the Hasselmann force is reduced so that its effect can also be neglected in terms of surface drift.

In the crosswind direction, the wave-induced drift is the quasi-Eulerian current due to the Stokes-Coriolis stress. Although the total transport is zero in this direction, the velocity is not zero at each depth, leading to a small wave-induced drift to the right of the wind near the surface and to the left below (see fig.2.6 and section 2.4.2).

The mean wind-induced drift of a water particle at the surface is not well known. Huang (1979) reviewed field and laboratory experiments about surface drift of water, ice, oil and objects, but laboratory experiments or floating objects observations are not supposed to give the same drift than water particles in presence of developed waves. The different results are scattered roughly around 3% of the wind speed U_{10}. Churchill and Csanady (1983) studied Lagrangian motions of drogues and drifters and found surface drifts between 2 and 2.5% of the wind speed U_{10}. The present model yields smaller velocities, around 1.5%.

This ratio of 1.5% does not vary much with fetch (fig.2.11 and 2.12). For shorter fetches, the Stokes drift is small and the Eulerian velocity is larger, thanks to a small mixing (figure 2.12, dotted lines). Note that we computed the Stokes drift for very short fetches with *Kudryavtsev et al.*'s [1999] spectrum, whereas this spectrum is not expected to behave correctly for such young seas (B. Chapron, personal communication). The effect of the dependence of the atmospheric roughness length with the sea state is also shown : a wind-waves coupling represented by (2.7) is used instead of the Charnock relation (2.6). This coupling leads to an increase of the surface stress for young seas, and thus to a increase of the Eulerian current (dashed-dotted lines). Furthermore, the TKE flux is $\Phi_{oc} = \alpha u_*^3$, where α is also known to depend on the wave age. We use here an analytical fit to the distribution of α as a function of c_p/u_{*a} of fig.8 in Terray et al. (1996). α can be taken around 60 for very young waves (age $Cp/u_{*a} \simeq 5$). It increases to 180 for developing waves ($10 < Cp/u_{*a} < 20$), and then decreases to 80 for fully-developed waves ($Cp/u_{*a} \simeq 30$). As this effect slightly reduces the mixing for very young waves and for fully-developed waves, the quasi-Eulerian current at the surface slightly increases. It is the contrary for developing waves, for which the mixing is slightly enhanced (figure 2.12, solid lines). However,

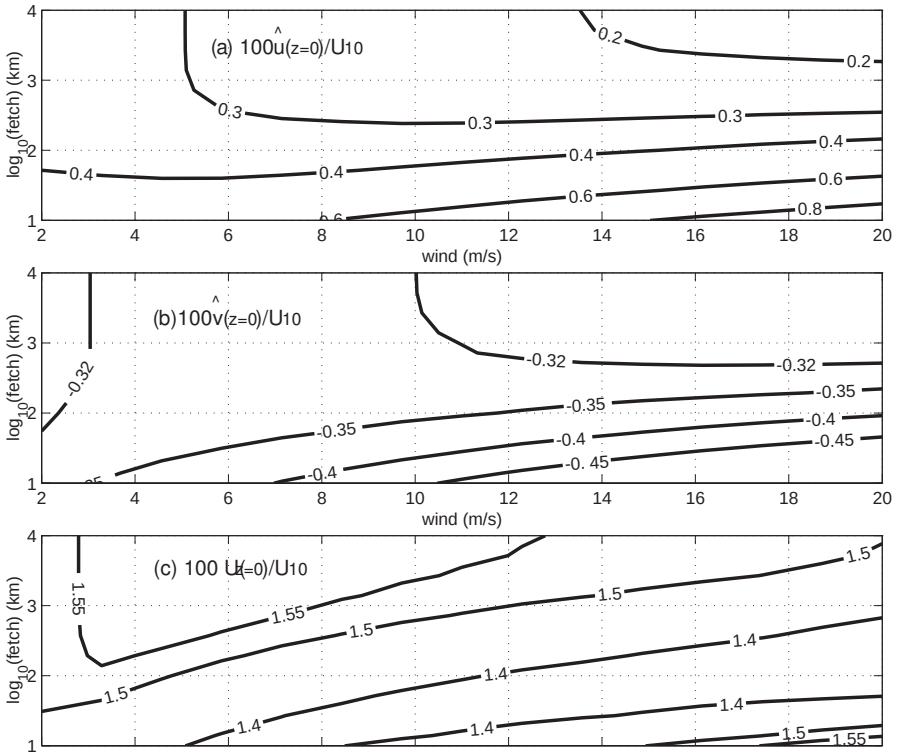

Figure 2.11: (a) quasi-Eulerian current downwind $\hat{u}$, (b) crosswind $\hat{v}$ and (c) total Lagrangian drift $|\hat{\mathbf{u}} + \mathbf{U}_s|$ at the surface, as function of wind speed and fetch. The results are shown as percentages of the wind speed U_{10}. The wind-wave coupling (equ. 2.7) and an estimation of α as a function of the wave age are used.

it is the increase of the roughness length z_0 that dominates the evolution of the near surface mixing with wave development, as expected from Craig and Banner (1994) :

$$K_z \propto u_* \alpha^{1/3} z_0^{0.8} (z_0 - z)^{0.2}. \tag{2.23}$$

The Lagrangian surface drift appears to be almost independent of the fetch (figure 2.11). This drift strongly depends on the depth, due to the vertical shear of the Stokes drift (and also, for short fetches, to the shear of the quasi-Eulerian current).

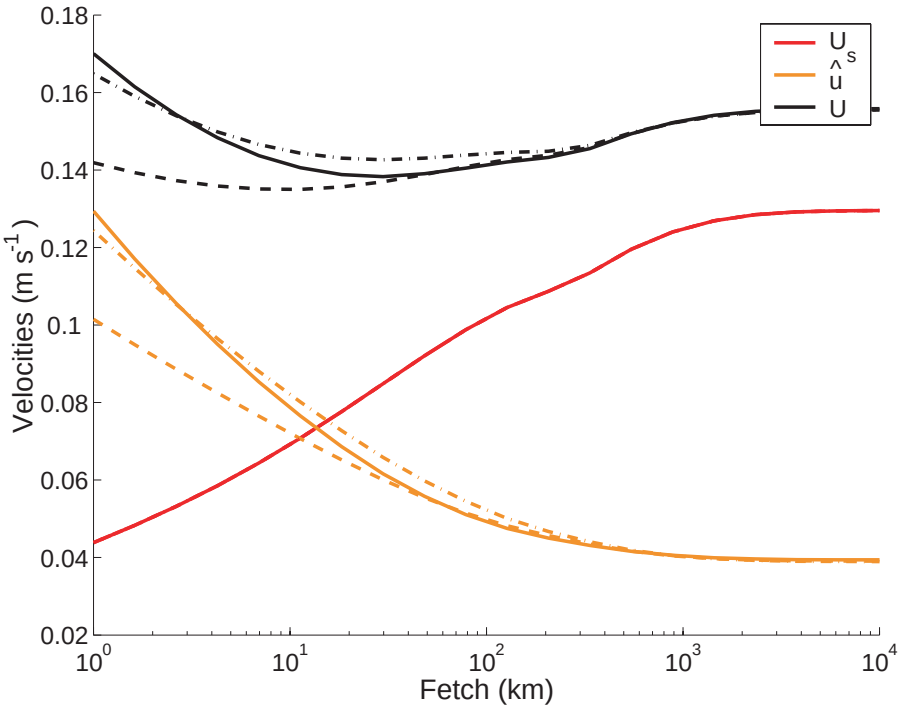

Figure 2.12: Quasi-Eulerian drift $|\widehat{\mathbf{u}}|$, Stokes drift $\mathbf{U}_s$ and total drift $\mathbf{U} = |\widehat{\mathbf{u}} + \mathbf{U}_s|$ at the surface, as function of fetch. Dashed lines : using Charnock's formula and a TKE flux $\Phi_{oc} = \alpha u_*^3$ with $\alpha = 100$. Dashed-dotted lines : using the coupling of Donelan (1998) and $\alpha = 100$. Solid line : using the coupling of Donelan (1998) and a variable α from Terray et al. (1996). The wind is set to $U_{10} = 10\text{ms}^{-1}$.

2.5 General discussion

Clearly, the surface drift is more sensitive to the surface mixing of the model than to the Stokes-Coriolis term. Near surface profiles are, as pointed out by Craig and Banner (1994), strongly dependent on the roughness length. However, if the scaling of Terray et al. (1996) is valid, i.e. z_0 and H_s are of the same order, which is confirmed by observations, then the uncertainty on the quasi-Eulerian velocity is

not that large. A much smaller roughness length like $z_0 = 0.6H_s$, as prescribed by Soloviev and Lukas (2003), leads to Eulerian surface currents 1,5 times larger than with the present value $z_0 = 1.6H_s$. In terms of Lagrangian surface drift, the underestimation would be smaller, from 10% for long fetches to 20% for short fetches. Thus a hopefully more physically sound definition for z_0, such as an average size of breaking waves, is not expected to give significant differences in drift.

Although there is a reasonable agreement between the present model and quasi-Eulerian velocity shears measured by Santala and Terray (1992), there is a large difference between predictions of Lagrangian drift and drifter observations. It is possible that a second order approximation may not be accurate enough for steep waves, and wave-wave interactions (modulations) may enhance the Stokes drift in a random wave field. Melsom and Sæatra (2004) have included fourth-order terms in their estimation of the Stokes drift for monochromatic waves but the effect of these terms is typically less that 10% of the second order terms, even for the steepest waves. It is more likely that turbulent structures associated with breaking fronts may contribute to the drift at the surface, and need to be parameterized.

Breaking wave fronts may cover an area of the order of a few percent of the sea surface. One may use empirically derived distributions $\Lambda(C)dC$ for the length of breaking crest with a phase speed between C and $C + dC$ per unit area [*Melville and Matusov*, 2002], one finds that objects randomly distributed at the surface of the ocean will have an extra drift of

$$\overline{u} = \int LC\Lambda(C)dC, \tag{2.24}$$

with L the displacement at the passage of a breaker. Since breakers propagate at a speed of about 0.8 C and the breaker lifetime is about the wave period $T = 2\pi C/g$, one finds that $\overline{u}$ is of the order of 6×10^{-3} m s^{-1} for $U_{10} = 10$ m s^{-1}, and this velocity increases with the cube of the wind speed. Therefore this effect may become significant for large wind speeds, but it only affects depths down to a small fraction of the wavelength, typically a few percent [*Melville et al.*, 2002]. This calculation only includes transient large-scale breakers. Micro-scale breakers, with a relatively longer lifetime, may yield a larger contribution.

The other turbulent structures that are likely to account for most of the discrepancy between observed drift speeds and the model are the Langmuir circulations. These structures extend down to the base of the mixed layer and have been repeatedly observed as soon as the wave and winds and steady enough that the cells can develop, even in shallow water [e.g. *Marmorino et al.*, 2005]. LCs are characterized by strong variations Δu of the downwind velocity with maxima associated

with convergence zones at the surface. Δu is reported to be of the order of 1–3% of the wind speed by Smith (1998). As a slightly buoyant object would tend to be trapped in the convergence zones, it can easily drift with a mean velocity larger than the actual mean by 1% of the wind speed. This "Langmuir bias" could thus be the principal reason why measured drift velocities are larger than given by the present model, and also larger than the HF-radar measurements by Dobson et al. (1989). Langmuir circulations further raise the issue of the adequacy of the turbulent closure with a $k-l$ model to model mixing due to such organized vortices created by wave-current interactions. Recent studies [e.g. *Noh et al.*, 2004] have investigated Langmuir circulations with Large Eddy Simulations that do not use such a simple closure scheme. However, these studies still need to be validated with field observations such as those of Smith (1999).

Finally, the impact of a density stratification can be included in the present model. A reduced mixed layer depth leads to an increase of the quasi-Eulerian velocity because the Ekman transport is conserved. As shown in fig.2.8, it may increase the quasi-Eulerian velocity by a factor 2 or 3, which would be significant also in terms of Lagrangian surface drift.

2.6 Conclusion

We presented here a model of a uniform and homogeneous ocean driven by wind and associated waves. Distinction is made between wave motion, including the Stokes drift, and a quasi-Eulerian motion, driven by the momentum flux from atmosphere, by the Coriolis force and by the Hasselmann force (also called "Stokes-Coriolis effect"). The waves are supposed to be a linear superposition of monochromatic components which satisfy the usual dispersion relation. The sea state is thus modelled by a directional spectrum of sea surface elevation variance. The Stokes drift and the vertically integrated Stokes transport are respectively the third and first moments of the frequency spectrum, and are therefore sensitive to the high frequency part of the spectrum, i.e. the short waves. Thus a spectrum designed for remote-sensing applications (fitted to reproduce the fourth moment of the spectrum) is supposed to give reasonable results for the Stokes drift calculation. This Stokes drift is found to be around 1.2% of the wind speed U_{10}, and the corresponding Stokes transport around 20 to 30% of the Ekman transport at mid-latitudes, for developed waves. The use of a monochromatic wave cannot represent well the surface drift value, the vertically integrated transport, and the depth involved.

The wave field influences the quasi-Eulerian motion via two different effects : the Stokes drift, in a rotating frame, creates the Hasselmann force which drives an

Eulerian return flow to compensate the Stokes transport. The presence of waves also increases the near surface mixing. A simple turbulent closure scheme gives an eddy viscosity that can be used to represent the latter effect. The roughness length for this closure scheme is evaluated according to observations of TKE dissipation near the surface. The model result is then examined and we can summarize it by comparison to the near surface physics of most ocean circulation models (OCMs), which use small mixing at the surface (represented here by a small roughness length $z_0 < 0.1$m). (i) A surface mixing at least one order of magnitude greater than in current OCMs (and dependant on the sea state) seems realistic. Significant consequences on the sea surface temperature are expected [*Mellor and Blumberg*, 2004]. (ii) As a consequence of this strong mixing, there is a strong reduction of the vertical shear of the quasi-Eulerian velocity near the surface (see fig.2.13). (iii) However, Lagrangian drift velocity is highly sheared due to the shear of the Stokes drift near the surface (see fig.2.13), leading to near surface profiles quite close to those of the Eulerian current in some OCMs. (iv) Although observations of surface drift and comparisons with the wind speed are not very reliable, an important part of the surface drift of objects may be still missing in the present formulation. The "Langmuir bias", which is the correlation of surface convergence and increased velocity, should explain some of this missing drift, as well as the stratification which was not taken into account. (v) The Hasselmann force has a significant impact in terms of vertical profiles of Eulerian velocities (this force leads to current magnitudes of 20 to 30% of the magnitude of currents driven by the wind stress). This impact is relatively small on the surface Lagrangian drift, which could be approximated by the sum of the Stokes drift plus the Eulerian current driven only by the wind stress. (vi) In terms of Lagrangian drift at different depth, stationary waves create a mass transport in the wind-waves direction near the surface, and in the opposite direction below, until a depth of the order of the Ekman depth. If properties are homogeneously distributed in this surface layer then wave transport can be ignored. Otherwise it should be computed. (vii) For really young seas, as it happens in some costal areas or lakes, the near surface dynamics are closer to that described by traditional OCMs, with a small Stokes drift and a relatively weak mixing.

In conclusion, the surface drift and mixing cannot be understood without the waves. However there still are very few datasets that are complete. The reason is that fields experiments on Ekman currents or mixed layers and studies on waves are rarely made simultaneously. Furthermore near surface Lagrangian, Eulerian or quasi-Eulerian averaging are often significantly different but hardly well identified. The present study demonstrates the need for more near surface measurements to gather all this information.

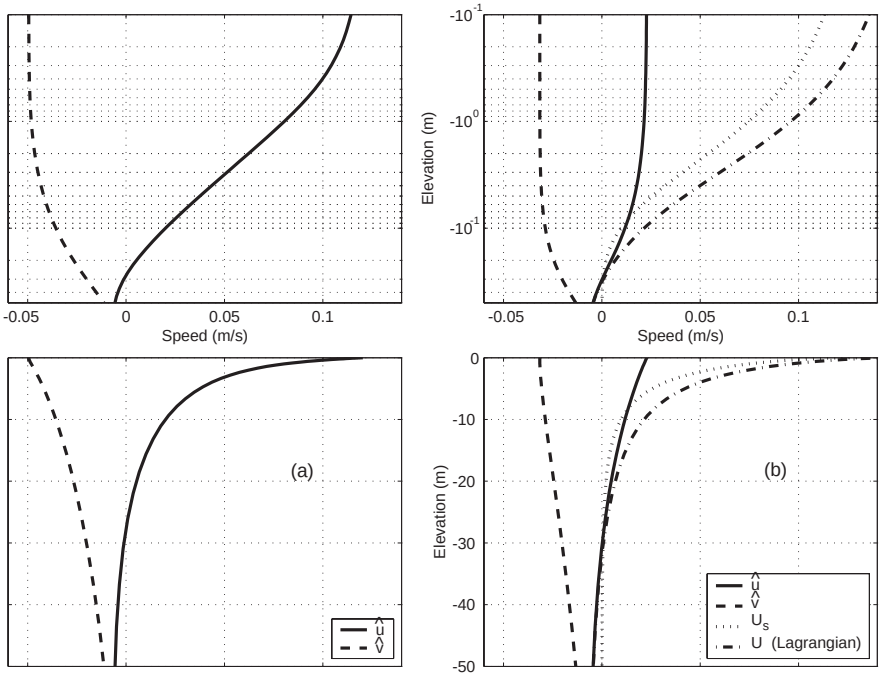

Figure 2.13: Velocity profiles for $U_{10} = 10\text{ms}^{-1}$ and fully developed waves. (a) Quasi-Eulerian velocity from the model without Stokes-Coriolis effect and with $z_0 = 0.1\text{m}$, which represents a small surface mixing in an OCM. (b) Quasi-Eulerian velocity, Stokes drift and Lagrangian velocity from the model with the Stokes-Coriolis effect and $z_0 = 1.6 \times H_s = 4.5\text{m}$. Top panels are shown on a logarithmic scale.

Acknowledgments

The initial version of the computer code for the mixed layer model was kindly provided by P. Craig and M. L. Banner. Many discussions with B. Chapron, N. Reul, V. Kudryavtsev, A.D. Jenkins and P. Daniel were helpful in understand several issues addressed in the paper.

Chapter 3

One-Dimensional description: Part 2: with stratification

This chapter is written as an independent paper :

Drift and mixing under the ocean surface, Part 2: Stratified conditions and model-data comparisons

Nicolas Rascle[(1),(2)], Fabrice Ardhuin[(1)]

Paper submitted to J. Geophys. Res.
27 July 2007

[(1)] *Centre Militaire d'Océanographie, SHOM, BREST, France*
[(2)] *Laboratoire de Physique des Océans, Université de Bretagne Occidentale, Brest, France*

Abstract

A model of the ocean surface currents is presented. It includes the enhanced near-surface mixing due to the waves, the Stokes drift of the waves, the Stokes-Coriolis effect and the stratification. The near-surface current shears from this model are compared with the shears of the quasi-Eulerian currents measured using a wave-following platform during the Shelf Mixed Layer Experiment (SMILE). It is shown that the downwind current shears observed during SMILE are well modelled. However, the observed crosswind shears are in poor agreement with the model. The Stokes-Coriolis (SC) term could qualitatively explain this misfit but it is one order of magnitude too weak. The Ekman-Stokes spiral of the model are compared to the spiral observed during the long time series of measurements Long Term Upper Ocean Study 3 (LOTUS3). The effects of stratification are carefully treated. The mean velocity profiles of the model closely agree with observations. However, we find no evidence of the SC effect on the shape of the observed Ekman spiral. The observed shape is found to be a consequence of the rectification due to the stratification. The SC effect calculated from an accurate numerical wave hindcast is weak, but should have been observed. In fact, it is estimated that the wave-induced bias in the current measurements is larger than the SC effect. Finally, it is shown that the wave age effect on the surface drift, which was found to be small in unstratified conditions, is important in the presence of shallow mixed layers.

3.1 Introduction

Waves are known to dramatically enhance the near-surface mixing. This was inferred from turbulent kinetic energy (TKE) dissipation measurements (Agrawal et al., 1992; Terray et al., 1996), and it was also observed in measurements of downwind current vertical shear very close to the surface during the Shelf Mixed Layer Experiment (SMILE) (Santala, 1991; Terray et al., 2000). Accordingly, the surface mean current is rather weak, around 0.5% of the wind speed at 10 meters U_{10} when the ocean is not stratified and when the waves are developed. This quasi-Eulerian mean current is defined as the Lagrangian drift minus the wave Stokes drift (see for details Jenkins, 1987; Rascle et al., 2006; Ardhuin et al., 2007*b*). This small quasi-Eulerian drift can be overwhelmed by large surface drift due to the wave Stokes drift, which can be as large as 1.2% of U_{10} (Rascle et al., 2006, hereinafter Part 1). However, these processes may not be well represented or, more likely, other processes are important for the drift of surface-trapped buoyant objects to reach surface drifts of the order of 2 or 3% of U_{10} (Huang, 1979). The surface trapping of the Ekman current in the

presence of stratification may be an important factor.

Waves are also associated with a Stokes-Coriolis current (Hasselmann, 1970; Xu and Bowen, 1994; McWilliams and Restrepo, 1999). Namely, in a rotating frame of reference, a wave-induced stress perpendicular to the waves propagation modifies the profile of the Ekman current. In an inviscid ocean, this stress drives a mean current which compensates the Stokes drift of the waves when averaged over the inertial period. However, in the presence of a strong vertical mixing, this return flow is made vertically uniform. Because the Stokes drift of a wind sea is strongly surface trapped, the return flow only compensates the Stokes drift when vertically integrated over depth, and there is a net drift at every depth. This was shown in Part 1 without any stratification, and the question raised is to which extend this remains valid if the Ekman current is also surface trapped, by a shallow mixed layer for instance.

Furthermore, when considering vertically integrated transports, the Stokes-Coriolis effect do compensate the Stokes transport in a steady state. It is also the only mechanism invoked to compensate it. Observations have been made by Smith (2006*a*), in which the modulations of the Stokes drift by the passing wave groups was completely compensated, presumably by the flow associated with long infra-gravity waves. We also note that laboratory measurements fail to reproduce the Stokes drift (Monismith et al., 2007). However, the steady Stokes transport and the Stokes-Coriolis effect on it have never been clearly observed yet. Evidence of this effect has been sought by Lewis and Belcher (2004) and Polton et al. (2005) in the observations of the sub-surface Ekman current during Long Term Upper Ocean Study 3 (LOTUS3) (Price et al., 1987). Unfortunately, neither the wave-enhanced surface mixing nor the quite shallow diurnal mixed layer during LOTUS3 have been taken into account in these previous works, although they can radically change the interpretation of the observed Ekman spiral (Price and Sundermeyer, 1999). Also, evidence of the Stokes-Coriolis forcing have not been sought yet in measurements much closer to the surface, such as those of SMILE.

In this paper the effect of stratification will be added to the model presented in Part 1 in order to make a quantitative comparison with some available observations of near-surface current. More precisely the remaining issues are : How well this model can reproduce the vertical shears observed close to the surface, both in the downwind and the crosswind direction? What is the impact of the Stokes-Coriolis effect on the Eulerian and Lagrangian currents profiles in shallow mixed layers? Is there any observational evidence of this effect? Is the surface drift reaching realistic values in the presence of shallow mixed layers?

The model used for this study is introduced in section 3.2. The near-surface

shears of the quasi-Eulerian currents observed during SMILE are analyzed in section 3.3. The Ekman-Stokes spirals from the LOTUS3 data are analyzed in section 3.4. Finally, the surface drift of the model in the presence of waves and stratification is discussed in section 3.5.

3.2 The model

For the sake of simplicity and because we want to simulate a period of hundreds of days, a simple one dimensional eddy viscosity model with a TKE closure scheme will be used. This model is adapted from Craig and Banner (1994), as discussed in Part 1. It was chosen because it is able to reproduce the wave-enhanced near surface mixing by the addition of a TKE flux at the surface and the specification of a large roughness length z_0. According to Terray et al. (1996), the TKE flux is parameterized as $\Phi_{oc} = \alpha u_*^3$, with $\alpha = 100$ and where u_* is the waterside friction velocity. The roughness length is set to $z_0 = 1.6 H_s$, as in Terray et al. (2000), with H_s the significant wave height of the wind sea, a proxy for the scale of the breaking waves that are responsible for the mixing. The extension to a stratified ocean is taken from Noh (1996). The parameterization of the effects of stratification on the eddy diffusivities is made via a turbulent Richardson number, where the destruction of turbulence by stratification is made regardless of the origin of turbulence, by shear production or by downward diffusion from the wave layer. This model was chosen for its ability to reproduce the diurnal thermocline. Justification for the use of such a simple eddy viscosity model can be found by comparing the velocity profiles of the model to the velocity profiles of more sophisticated models like the large eddy simulations (LES) of McWilliams et al. (1997) or Noh et al. (2004). Such comparisons have shown reasonable agreement (e.g. Kantha and Clayson, 2004).

3.3 Analysis of the near-surface shears - The SMILE data

3.3.1 The experiment

The SMILE data of Santala (1991) are of particular interest because one buoy (the SASS) included measurements of the velocity very close to the surface, at depths smaller than H_s. These unique measurements of the mean current used a surface follower and were corrected for a wave bias due to correlations between the SASS measurements and the waves motion. The most useful measurements occurred on

27 and 28 February 1989. The wind speed was 13.6 m s^{-1} and the wave height was 2.3 m, both approximately aligned and steady. The mixed layer depth was 20 m. More information on this data can be found in Santala (1991) and Terray et al. (2000).

3.3.2 The model

For comparison with these data, the model is run with a steady wind of the observed wind speed. The temperature is initialized to fit the observed profile, with a thermocline around 20 m, and a zero surface heat flux is used in order to reproduce the neutral mixed layer and its slow deepening. To compute the Stokes-Coriolis force, waves are calculated using a JONSWAP spectrum (Hasselmann et al., 1973), assuming a fetch of 100 km, giving the observed significant wave height. The peak period of the waves is slightly underestimated with this method, giving 6.4 s whereas 7.8 s was observed. The Stokes transport of the waves, important to measure the magnitude of the Stokes-Coriolis force, might then be slightly overestimated. The model results, averaged over an inertial period, are plotted on fig. 3.1 (upper panel). For comparison, the model results without stratification are plotted on fig. 3.1 lower panel.

3.3.3 Previous analysis

The measurements have already been analyzed by Santala (1991), and part of its results were used by Terray et al. (2000) and in Part 1. Here we will briefly summarize their analysis and the different technique used in the present analysis.

Four sensors were mounted on the SASS buoy, at depths from 1 to 5m. The vertical shear can be estimated between each pair of adjacent sensors by a finite difference. Santala (1991) scaled the depth with u_*^2/g, which is equivalent to scale with the significant wave height H_s if one supposes a full development and if one omits the swell in H_s. The shear was scaled with u_*/z, the law of the wall scaling. This leads to their figure 7-5, which we reproduce here for the SASS data only (fig. 3.2).

The analysis of this plot, together with deeper measurements from a conventional mooring, leads these authors to infer a description of the downwind shear in a 3 layer structure, namely an upper layer with almost no shear, a lower layer following a log-law and a transition layer in between. However, such a transition is hardly perceptible with only the SASS data, because the lowest shear estimate falls in the transition region (fig. 3.2, upper panel). In the crosswind direction, the shear was found roughly constant with depth. This analysis leads to the figure 7-11 in

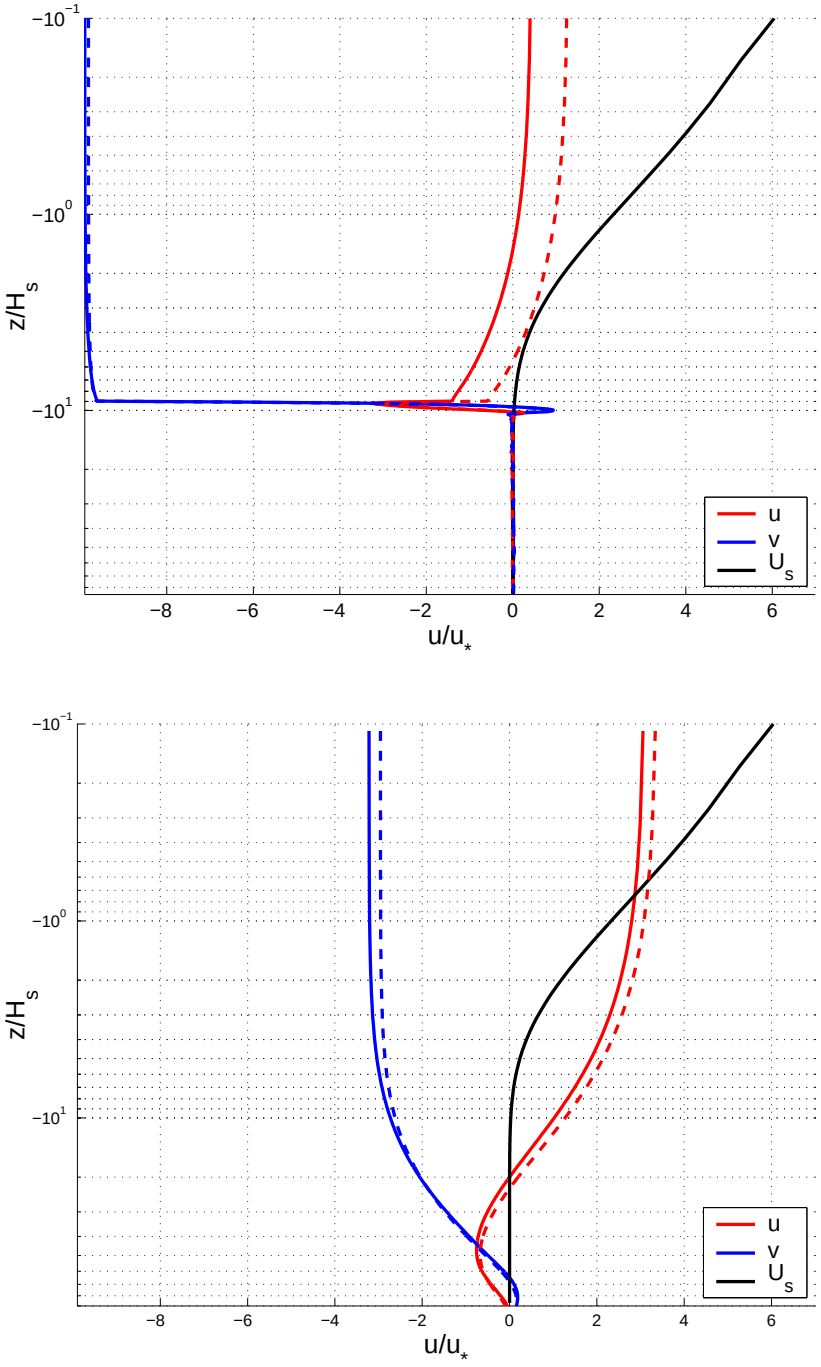

Figure 3.1: Velocity profiles from the model. $\widehat{u}$ is the downwind quasi-Eulerian velocity, $\widehat{v}$ is the crosswind quasi-Eulerian velocity and U_s is the Stokes drift. Velocities and elevation are normalized by the waterside friction velocity u_* and by the significant wave height H_s, respectively. Solid lines and dashed lines are model results with and without the Stokes-Coriolis effect, respectively. Upper panel is with a 20 m deep mixed layer as observed during SMILE and lower panel is without the effect of stratification.

Santala (1991), which was reproduced in Terray et al. (2000) and Part 1, showing the current profiles inferred from this analysis. These profiles were used afterwards

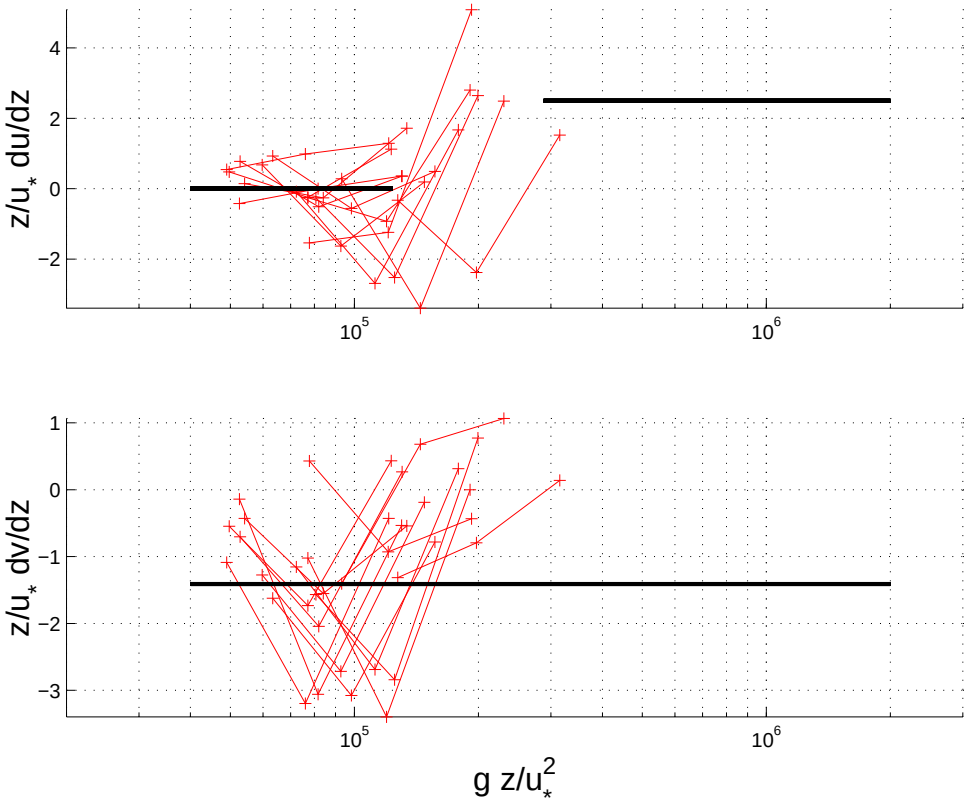

Figure 3.2: Reproduction of the Figure 7-5 of Santala (1991), for the SASS data only. Nondimensional variation of shear with depth for the downwind (upper panel) and for the crosswind (lower panel) directions. The + and thin lines are measurements from the SASS, the thick solid lines are the shears inferred in the original analysis of Santala (1991), with the 3 layers structure in the downwind direction.

in the discussion of Santala (1991).

3.3.4 A less constraining analysis

It is not obvious from fig. 3.2 that the fit to the scatter of finite difference calculated shears should produce a reliable estimation of the mean shear. Given that large scatter, one can wonder if a different analysis of the shears close to the surface cannot lead to a different description of the near surface velocity profiles. For instance, since we are focusing our analysis on the near-surface, where the mixing is enhanced by the waves, the shear should better be scaled with u_*/H_s or g/u_*, according to Craig and Banner (1994)'s eq. 30. But whatever the scaling used for the depth or for the shear, the vertical profiles remain quite noisy (fig. 3.3).

A smoother estimation of the mean vertical shear can be obtained with a linear regression of the current profile over the 4 sensors depths and is shown on fig. 3.4 and fig. 3.5. The observed shear in the downwind direction (fig 3.5, upper panel)

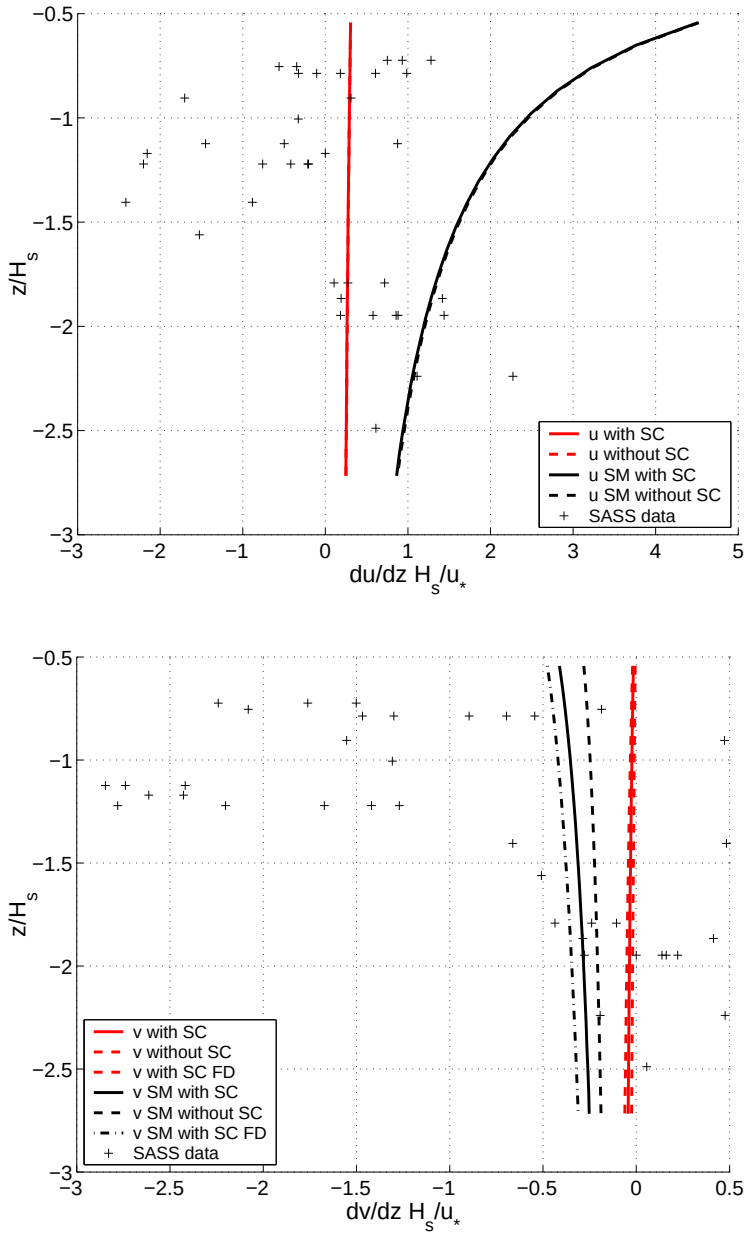

Figure 3.3: (Upper panel) Shear of the downwind component u of the current, normalized with u_*/H_s, plotted as function of the depth normalized with H_s. Shears of the model are calculated by finite difference and shears of the SASS data are calculated by finite difference between each pairs of adjacent sensors. In addition to the default model results, we plotted the results of the model without the Stokes-Coriolis effect (SC) or/and without the wave-induced surface mixing (SM= Small Mixing), obtained with a roughness length of $z_0 = 0.05$ m and no TKE surface flux. (Lower panel) Same as upper panel but for the crosswind component v of the current. As an upper bound of the Stokes-Coriolis effect, the model results when supposing the wave field fully developed (FD) is also shown.

is in relatively good agreement with the shear of the model, this way validating the enhanced near surface mixing as was noted in Terray et al. (2000) and Part 1.

However the observed shear in the crosswind direction (fig. 3.5, lower panel) is one order of magnitude larger than the model prediction.

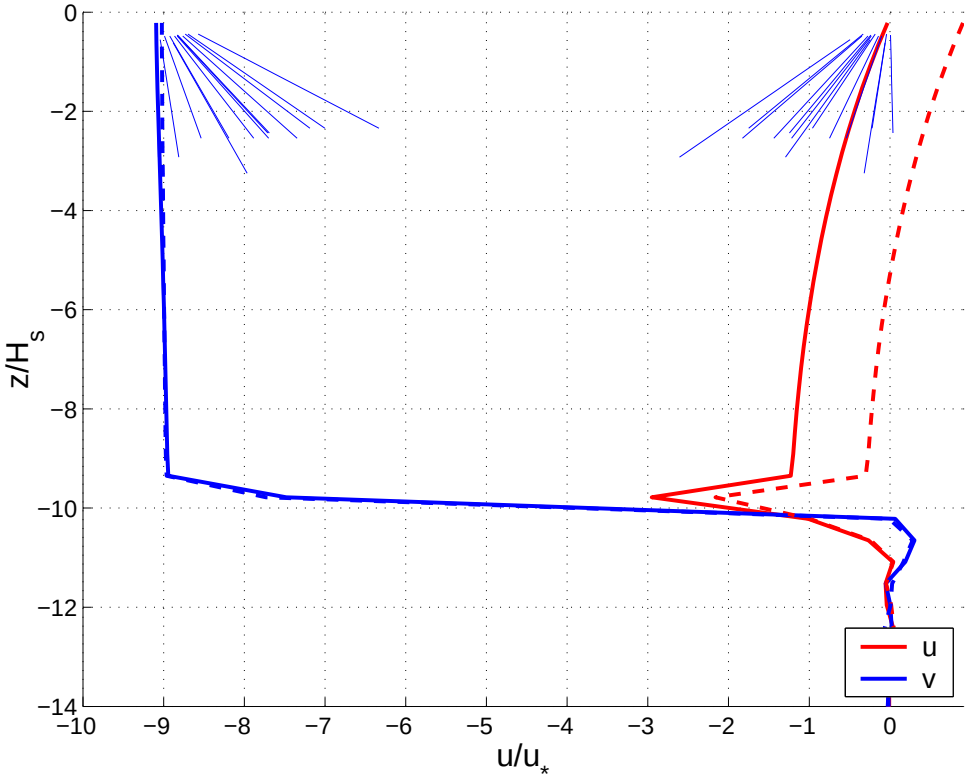

Figure 3.4: Shears observed with the SASS buoy. The shears are calculated with a linear regression over the 4 currents meters and are plotted as thin line segments over the curves of fig. 3.1, upper panel, and with an arbitrary off-set.

The Stokes-Coriolis force, oriented in the crosswind direction, is a possible explanation for that large crosswind shear. Qualitatively, the Stokes-Coriolis force is a good candidate, because it is oriented to the right of the waves propagation, as is the observed bias. Therefore we made a quantitative evaluation of the Stokes-Coriolis impact on the crosswind current. The wave field was not fully developed. The Stokes transport is around 10% of the Ekman transport, which means, according to Polton et al. (2005), that the Stokes-Coriolis effect is equivalent to a surface stress of 10% of the wind stress. The consequent crosswind shear (fig 3.5, lower panel) is quite small, given the strong wave-induced mixing of the model. An upper bound of the Stokes-Coriolis stress can be found by supposing the wave field fully developed. The equivalent stress is then of 35% of the wind stress. But even in this case (fig 3.5, lower panel), the Stokes-Coriolis force is too weak to explain the large crosswind shears observed.

Another possible explanation for those observations is a smaller mixing in the crosswind direction than in the downwind direction. From looking at the vertical

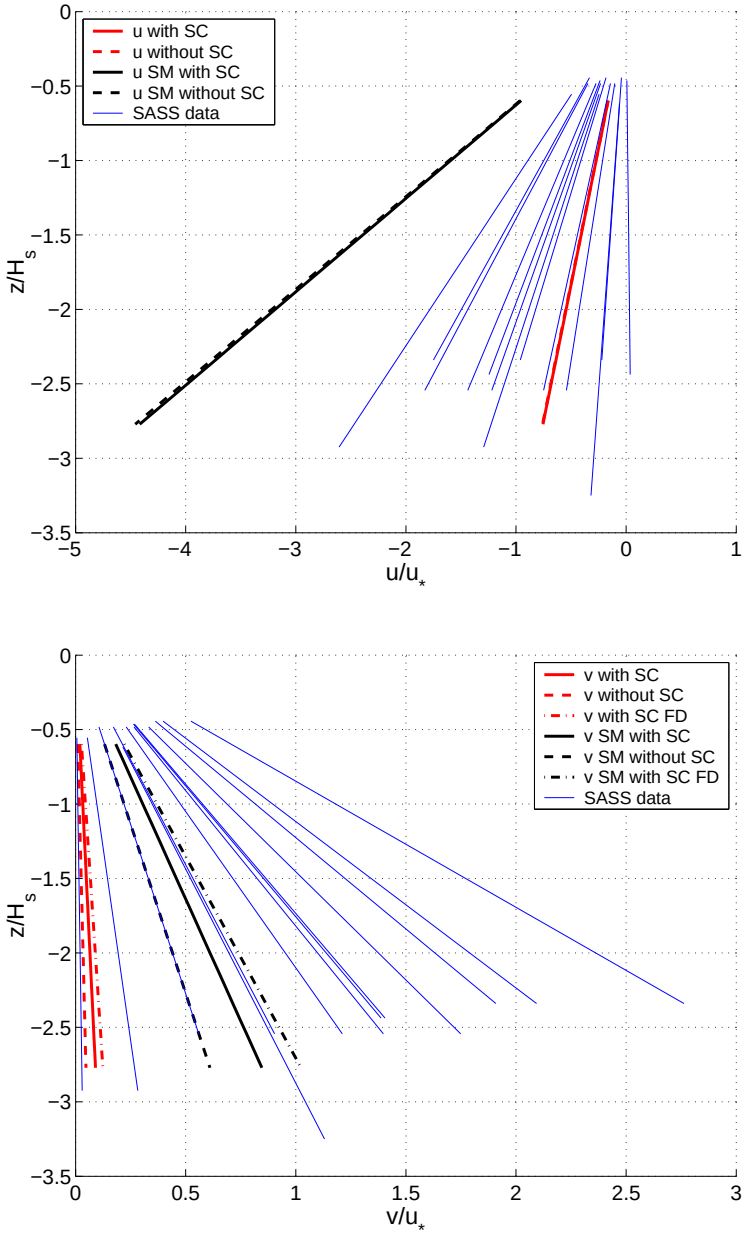

Figure 3.5: (Upper panel) Linear regression of the downwind current u between 1.1 m and 5.8 m deep, the measurement depths of the SASS buoy. The current is normalized with u_* and the depth with H_s. The SASS data are plotted, as well as different model results. In addition to the default model results, we plotted the results of the model without the Stokes-Coriolis effect (SC) or/and without the wave-induced surface mixing (SM= Small Mixing), obtained with a roughness length of $z_0 = 0.05$ m and no TKE surface flux. (Lower panel) Same as upper panel but for the crosswind component v. The SASS data are plotted, as well as different model results. (As in fig 3.3, lower panel, SC is Stokes-Coriolis, SM is Small Mixing and FD is Fully Developed waves.)

profiles of the different LES simulations of the Langmuir turbulence (McWilliams et al. (1997), Noh et al. (2004), ...), it is clear that the mixing due to Langmuir cells

is not isotropic. However none of these simulations are focused enough on the near-surface dynamics to provide any reliable picture of what the mean surface currents and mixing should be.

Also, if Langmuir circulations were present, the SASS buoy could have been trapped into surface convergence zones. Santala (1991) investigated the vertical velocity records and did find a non-zero downward velocity, interpreted as evidence of a non-uniform sampling of the Langmuir cells. The consequent bias of the horizontal velocity measurement cannot be excluded to explain the observed large crosswind shear.

3.4 Analysis of the current magnitude - The LOTUS data

The impact of the Stokes-Coriolis effect and of the stratification is small on the current shear, but is more apparent on the magnitude of the current : the Ekman transport is trapped in the mixed layer, leading to large values of the crosswind current, while the Stokes-Coriolis effect gives small values, if not negative, of the downwind current (see e.g. fig. 3.1, upper panel). Are the observed current in agreement with that expected shape?

Field measurements of the Ekman currents always include a lot of noise, which finds its origins in inertial oscillations and in the diverse transient phenomenons, some of them being surface-trapped. It is thus difficult to separate other processes from the mean wind-driven current. During SMILE (previous section), the currents were averaged over 40 mn. This allows an analysis of the vertical shears but it is insufficient to investigate the magnitude of the current. One solution to get rid of this noise is to average the current over a long time period. This method has been employed by Price et al. (1987) with the LOTUS3 data set. The measurement took place in the summer of 1982, under light to moderate winds and a strong diurnal heating. The current measurement came from a conventional mooring, with the upper measurement at 5 m depth. In the typical light wind encountered, the waves were not really large so that the wave bias, i.e. the correlation between the motion of the mooring and the orbital motion of the waves, was first estimated to be small at the measurement depths using Vector Measuring Current Meters (VMCM) instruments (Schudlich and Price, 1998). We will further discuss this point below. Finally Price et al. (1987) used a coherent averaging method to follow the low frequency changes in wind direction. The resulting current profile can then be quantitatively compared to theoretical models of the Ekman current. These observed current have

the expected profile of an Ekman spiral, with a depth integrated transport in agreement with the Ekman transport. However some features of these currents were unexpected. First, the sub-surface deflection is quite large, around 75° at a depth of 5 m. Second, the decay with depth is stronger than the clockwise rotation (the spiral is 'flat').

To explain this flatness of the spiral, Price and Sundermeyer (1999) invoked the temporal variation of stratification. The mixed layer depth varied typically from 10 m during the day to 25 m at night. The mean current, time-averaged over the diurnal cycle, should then show a different vertical profile than the current inferred from the mean vertical stratification. This difference is a problem of rectification of the Ekman layer (see e.g. McWilliams and Huckle, 2006).

However, Lewis and Belcher (2004) reported potential problems in this interpretation. Mainly, the approach of Price and Sundermeyer (1999) is not able to reconcile the observed large sub-surface deflection of 75° and a small surface deflection of 10 to 45° typically observed (Huang, 1979). Lewis and Belcher (2004), followed by Polton et al. (2005), argued that the Stokes-Coriolis force can explain the large sub-surface deflection, together with a small surface deflection. The agreement between their models and the LOTUS3 observations is then quite good.

Other problems appear in turn in these models. First, the small surface deflections reviewed in Huang (1979) partly comes from observations of Lagrangian surface drift. As noted in Part 1, the Lagrangian surface drift is the sum of the Stokes drift and the quasi-Eulerian current. A large surface deflection of the quasi-Eulerian current is not contrary to a small surface deflection of the Lagrangian drift, because of the Stokes drift. In relation to this, the surface mixing in the models of Lewis and Belcher (2004) and Polton et al. (2005) is likely to be several orders of magnitude too small. But, as noted in Part 1 without stratification, a realistic surface mixing gives a quasi-Eulerian current much more uniform than modelled by the previous authors, ruining the agreement with the data (see Part 1, fig. 7). Stratification is therefore needed to reexamine the LOTUS 3 data. Here we also reexamine whether or not the LOTUS 3 data offer an observational evidence of the Stokes-Coriolis effect on the Ekman current.

3.4.1 A simple model of the diurnal cycle

Following the idealized model of Price and Sundermeyer (1999), the present model is run with the mean wind stress observed during the period, $u_* = 0.0083$ m s^{-1}. The waves are expected to be fully developed with that wind stress, which gives a significant wave height of $H_s = 1.6$ m, based on the JONSWAP spectrum (Hasselmann

et al., 1973).

The temperature is initialized with the temperature observed at the beginning of the field experiment. The surface heat flux is not calculated using a bulk formula because no measurement of the relative humidity was available (see Stramma et al., 1986). Instead, we use an analytical fit of the solar insolation measured during clear sky days and we suppose that a steady heat loss equilibrates the surface heat budget,

$$Q = \max\left(0, 1000\cos\left(\frac{2\pi t}{T_{day}}\right)\right) - \frac{1000}{\pi}, \tag{3.1}$$

where t is the time and T_{day} is a period of one day. With these surface fluxes, the mixed layer depth varies between 8 m and 35 m. Those values agree with the observations of the stratification during LOTUS3. However the vertical profile of the current do not look like the observed current profile. The current of the model is too large and too much homogeneous within the mixed layer (fig. 3.6).

The velocity profile is not well reproduced when we use the observed solar flux but the mean wind stress, and it is not surprising. The rectification over sub-periods with weak wind should not leave a mean velocity profile homogeneous in the upper 8 m. Similarly, if a strong wind event occurred during the period, its effect must be apparent on the mean velocity profile below 30 m deep.

3.4.2 A more elaborate model : constraining the stratification

The previous results are encouraging but the profile of the mean current exhibits a large sensitivity to the mixed layer depth history. The temperature variability is not well reproduced with such a simple model of the diurnal cycle. We will therefore attempt a more realistic simulation of the LOTUS3 data.

Since there is no clear indication of what the damping of the inertial oscillations should be in a one dimensional model (e.g. Mellor, 2001), the wind is supposed to blow in a constant direction, in agrement with the coherent averaging of Price et al. (1987). The bulk formulation of COAMPS (Patrick Marchesiello, personal communication) for the atmospheric boundary layer is used to calculate the wind stress. The relative humidity is set to 75%, as in Stramma et al. (1986). The wind stress is set to the 6 hours low-pass filtered calculated wind stress, updated every 15 mn. Using the averaged wind stress and not the averaged wind speed conserves the stress. This minimizes the rectification errors. Finally, the current of the model, averaged over one hour, is stored and used to calculate the mean over the whole time period (170 days).

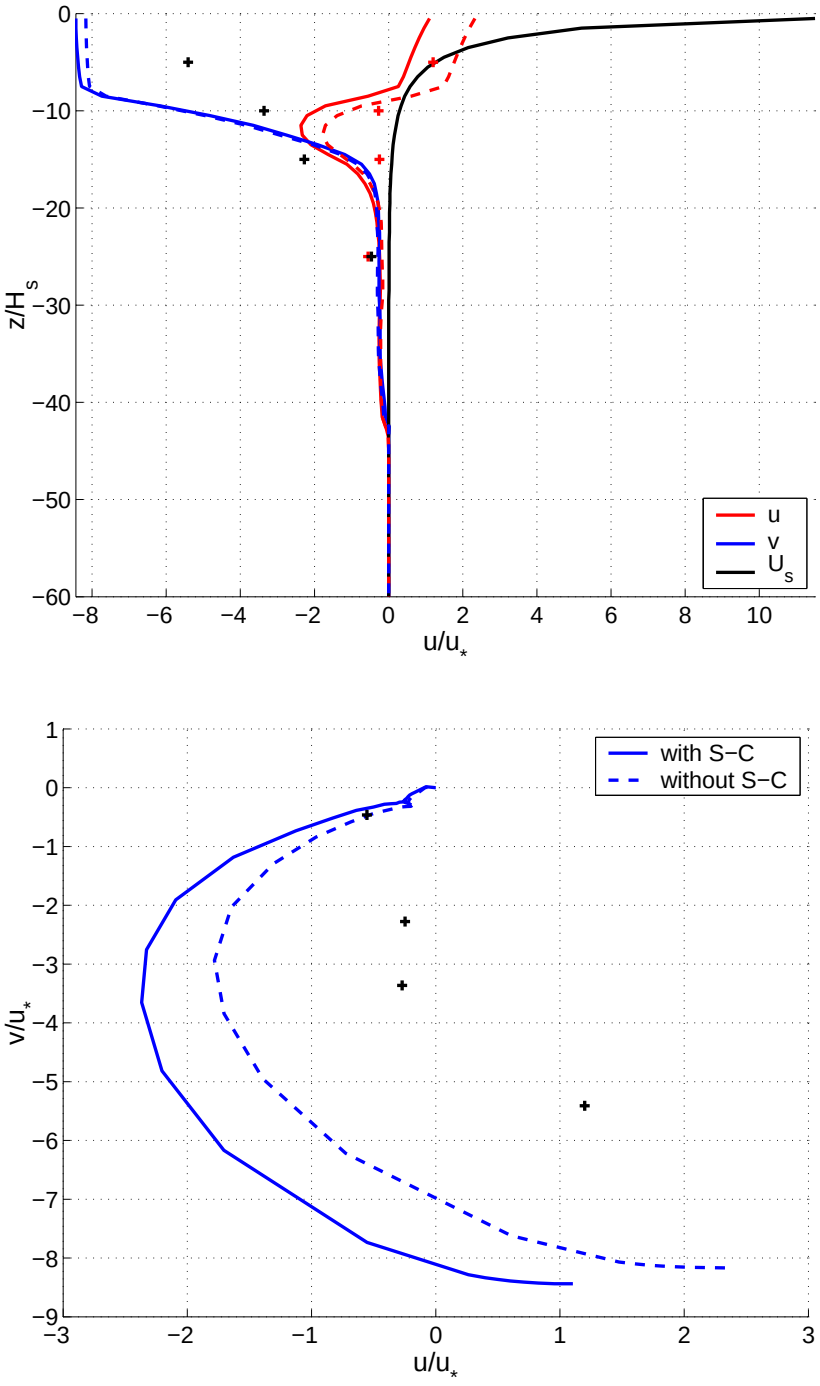

Figure 3.6: Results of an idealized simulation of the diurnal cycle during LOTUS 3: the wind stress is set to the observed mean wind stress over the period and the heat flux is set to a simple diurnal cycle in agrement with the observed solar insolation (equ. 3.1). (Upper panel) Vertical profiles of the mean current $\widehat{u}$, $\widehat{v}$ and of the Stokes drift U_s. (Lower panel) Spirals of the mean current. Velocities are normalized with the waterside friction velocity u_* and depth is normalized with the significant wave height H_s.

When one wants to reproduce the stratification, both the heat budget and the large scale advection of heat come into play (see e.g. Gaspar et al., 1990). We will avoid those problems by constraining the temperature to the observed temperature. A first simulation sets the temperature to the mean observed temperature every 6 hours. The analytical fit (3.1) for the heat flux is still used to reproduce the high-frequency diurnal cycle. The temperature of the simulation is therefore in close agrement with the observed temperature, including the diurnal stratification (shown for a few depths in fig. 3.7), except during a few episodes of exceptionally weak solar insolation. As a consistency check, a second simulation uses a nudging of the temperature to the 6 hours low-pass filtered observed temperature. The time scale of the nudging is 1000 s. The temperature of this second simulation is also in good agreement with the observed temperature, except that the diurnal warming is somewhat weakened by the nudging. The results in terms of mean Ekman current are quite similar between the different methods to reproduce the temperature, validating the reproduction of the impact of the stratification on the current.

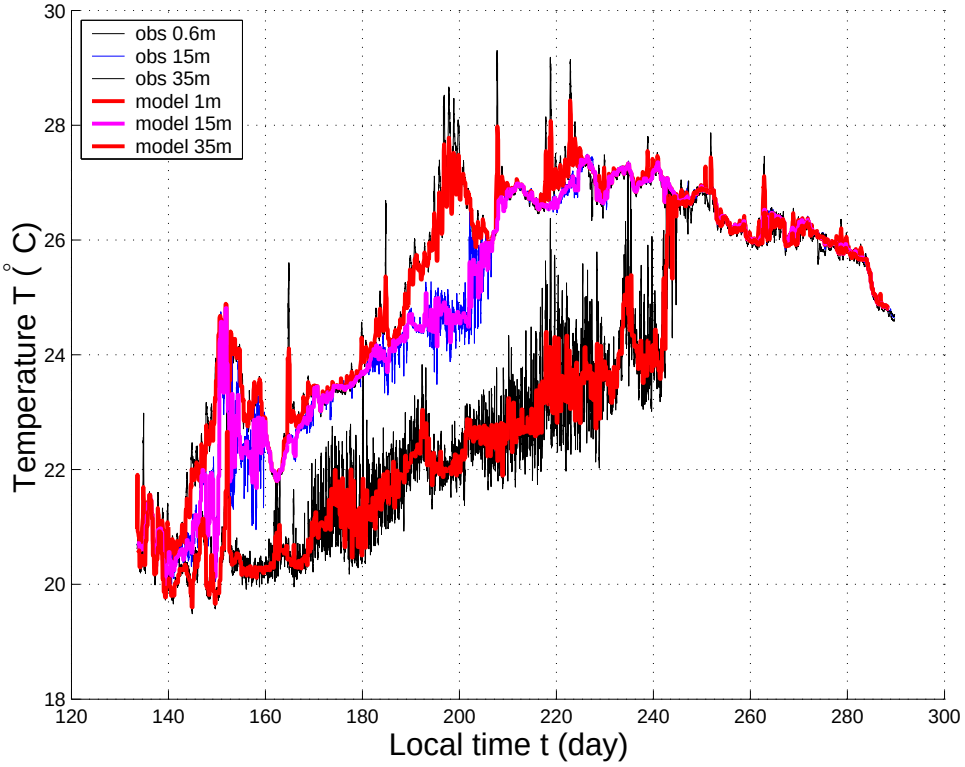

Figure 3.7: Time series of the temperatures observed during LOTUS 3, at depths of 0.6, 15 and 35 m. Also shown is the temperature of the model, constrained to the low-pass filtered observed temperature and with a typical solar insolation. Except during rare events, the temperature is reproduced in a satisfactory manner.

The comparison between the modelled current averaged over the entire period and the coherent averaging of Price and Sundermeyer (1999) is very good (fig. 3.8

and 3.9). The crosswind current agrees very well with the observation. The crosswind transport of the model is equal to the Ekman transport, corresponding to the mean stress, while the crosswind transport calculated with a trapezoidal extension of the data is slightly (8%) inferior (see also Price et al., 1987). The downwind current, if we omit the Stokes-Coriolis effect, is also very close to the observations. Both the downwind transports of the model and of the extrapolation of the data are nil.

3.4.3 Validating the wave-induced mixing parameterization.

Such agreement between the model and the observations is surprising. It provides the opportunity to check the sensitivity to the different parameterizations of the model. In particular, one may wonder if the mean current profiles observed during LOTUS 3 are useful to verify the effects of the wave-induced mixing on the current.

We tested the model sensitivity to the roughness length. As shown in fig. 3.8, the mean velocity profile is mainly determined by the stratification and the consequent rectification effect. The wave-induced mixing is not discernable on velocity measurements below 5 m deep.

3.4.4 The Stokes-Coriolis effect

The Stokes drift has been calculated by supposing the wave field fully developed with the corresponding wind averaged over 6 hours. This gives an upper bound of the Stokes-Coriolis effect.

A more realistic estimation of that effect is also needed. The complete historic of the waves during the period is preferable, because it includes possible correlations between large wave events, strong wind events and particular stratification events like deep mixed layers. Therefore, a global wave model of 1° resolution is used to produce the sea state at the LOTUS3 station (34.0N, 70.0W). The wave model is based on the WAVEWATCH III (WW3) code (Tolman et al., 2002), in which the wind-wave evolution parameterizations have been replaced by those of Bidlot et al. (2005). Although these parameterizations still have some problems in costal and swell-dominated areas (Ardhuin et al., 2007*a*), they provide good results for the mean parameters H_s and T_{m02} when compared to the North Atlantic buoys measurements (Ardhuin and Le Boyer, 2006, Jean Bidlot personal communication). The comparison with the nearby buoy 41001 (34.7N, 72.7W) of the National Data Buoy Center (NDBC) shows an rms error of 0.43 m on H_s (25% of the rms H_s) and of 0.57 s on the mean period T_{m02} (9.8% of the rms T_{m02}), for the period from 14 May to 30 November 1982. Note that no wave data were available at that buoy

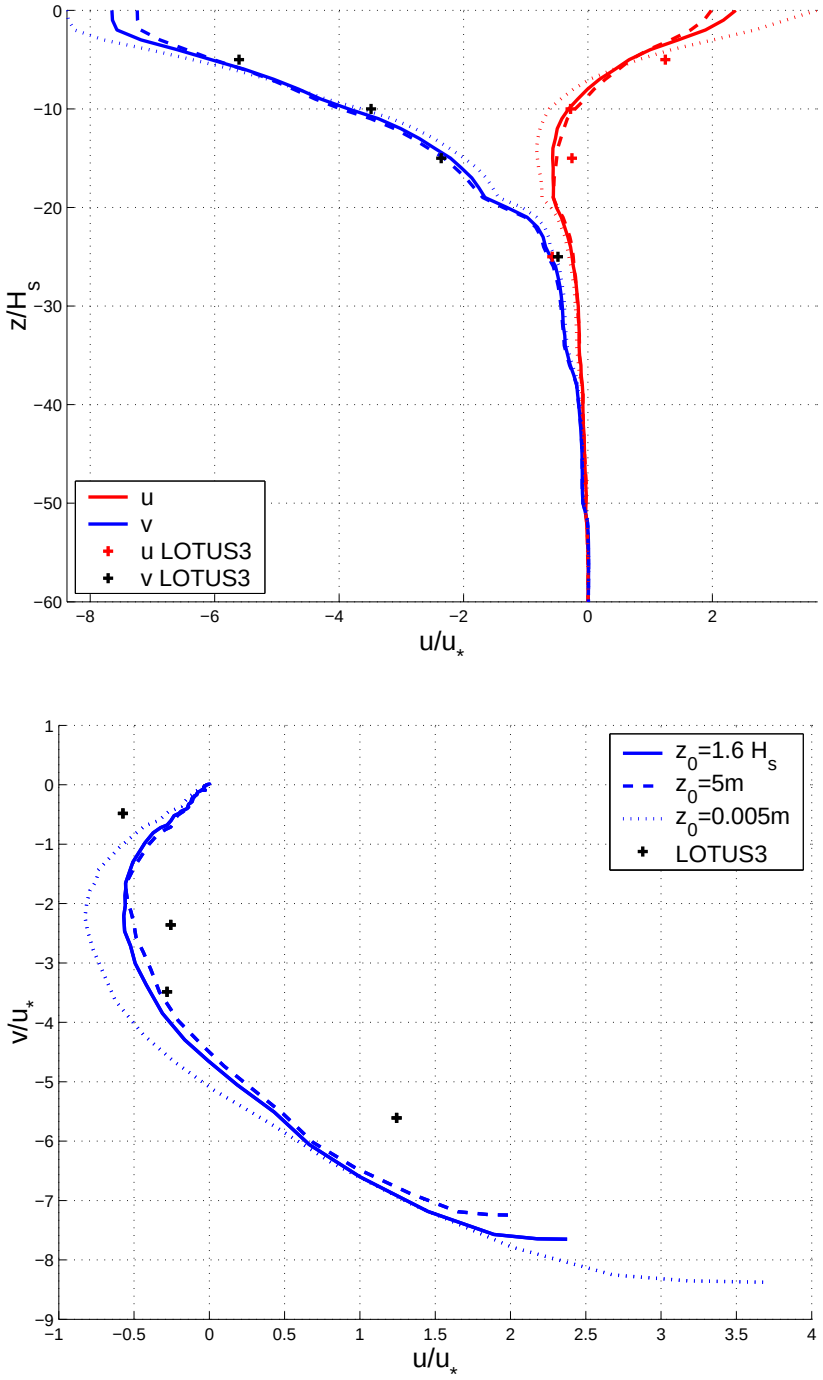

Figure 3.8: Results of the LOTUS 3 simulation, without the Stokes-Coriolis force, with the observed wind stress and with the temperature constrained to the data. (Upper panel) Vertical profiles of the mean current $\widehat{u}$, $\widehat{v}$. (Lower panel) Spirals of the mean current. Solid lines are the default model ($z_0 = 1.6H_s^{FD}$), dashed line are the model with a large surface mixing ($z_0 = 5$ m), and dotted lines, without the wave-induced mixing ($z_0 = 0.005$ m).

from 6 June to 6 August. Our calculation might underestimate the Stokes transport since there is a significant negative bias on the wave height H_s (-0.25 m), and a

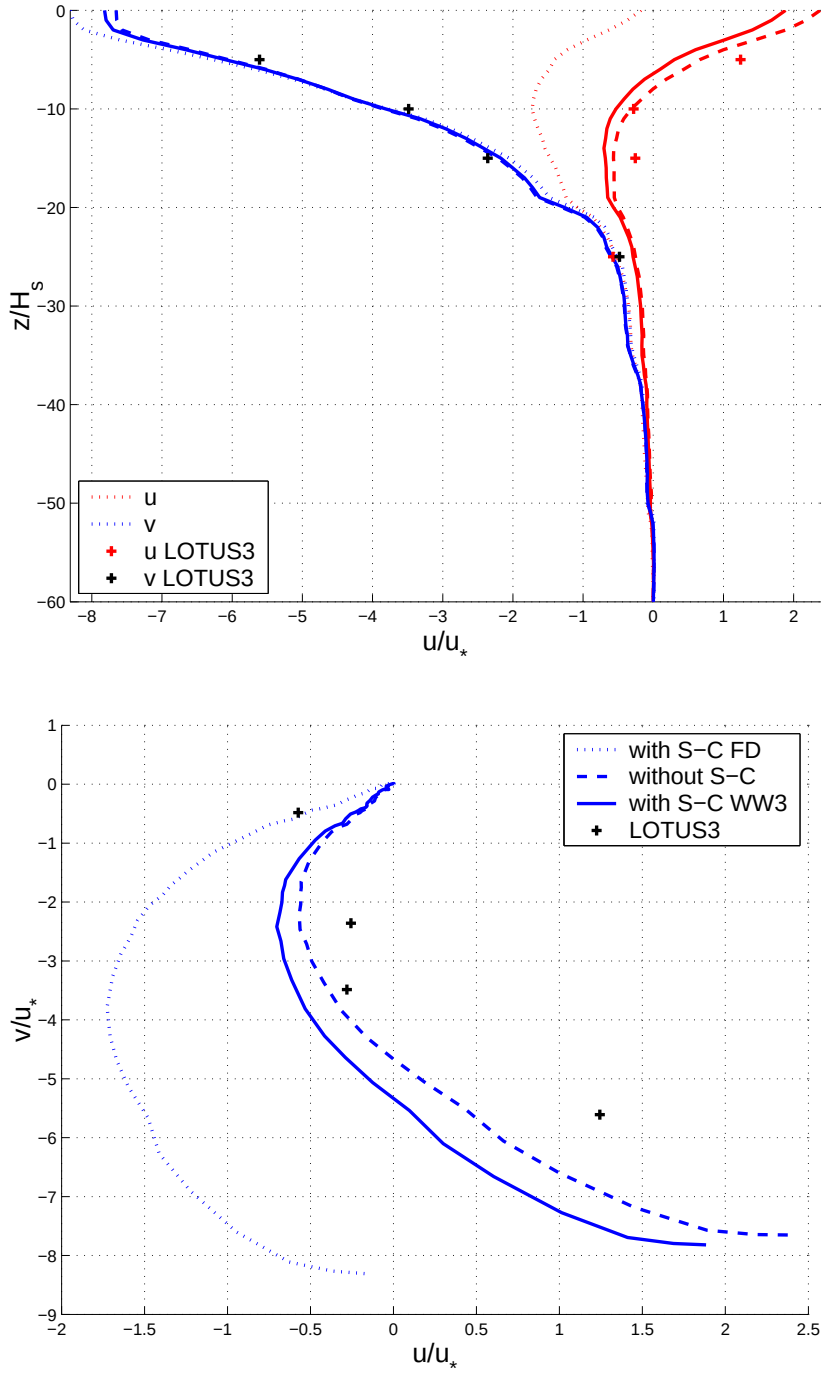

Figure 3.9: Results of the LOTUS 3 simulation, with the observed wind stress and with the temperature constrained to the data. (Upper panel) Vertical profiles of the mean current $\widehat{u}$, $\widehat{v}$. (Lower panel) Spirals of the mean current. Dashed lines are the model results without the Stokes-Coriolis effect. Dotted lines are the model results when supposing the waves fully developed (with the 6 hours low-pass filtered wind), giving an upper bound of the Stokes-Coriolis effect. Solid lines are the models results with the Stokes-Coriolis effect calculated with WW3.

negligible bias on the mean period T_{m02} (-0.07 s).

The wave spectra at the LOTUS3 station were used to compute the Stokes drift. Since the Stokes drift is a high moment of the spectrum, it is often aligned with the wind. Consistently with the average of Price et al. (1987) which follows the wind direction, we used the norm of the Stokes drift and prescribed it aligned with the wind. This avoids any discussions between the observed wind direction and the reanalyzed wind direction.

The numerical results with that lower bound of the Stokes-Coriolis term show that its effect, although small, should be observed from the current measurements. According to the model, the downwind transport should be negative in the observations.

However the observed downwind transport is almost zero. Consistently, the downwind current profile of the model is closer to the data when omitting the Stokes-Coriolis term. In this regard, the present work is consistent with the work of Price and Sundermeyer (1999), showing that the 'flatness' of the spiral results from the stratification, contrary to Polton et al. (2005) which claimed it results from the Stokes-Coriolis effect.

3.4.5 The wave bias

One explanation emerges for that apparent misfit of the model when including the Stokes-Coriolis effect : the nearly zero observed downwind transport was supposed to be Eulerian but could have been contaminated by the wave-induced buoy motion. Schudlich and Price (1998) used the method of Santala (1991) to discuss the wave bias. In particular, one can suppose that the buoy moves vertically with the surface and that the mooring line was taut, a reasonable assumption given the large length of the chain compared to the depths of the current meters considered. Then, for each monochromatic wave train, one gets in addition to the quasi-Eulerian current a bias equal to

$$u_{bias}^{min}(z) = \frac{1}{2}a^2\omega k \exp(-kz), \tag{3.2}$$

where z is the elevation measured downward, a is the wave amplitude, ω is the radian frequency and k the wavenumber. This gives a lower bound of the wave-bias. If one supposes that the buoy moves both vertically and horizontally, then one gets an upper-bound of the wave-bias

$$u_{bias}^{max}(z) = a^2\omega k \exp(-kz). \tag{3.3}$$

For comparison, the Stokes drift of a monochromatic wave is

$$U_s(z) = a^2 \omega k \exp(-2kz). \tag{3.4}$$

As the wave-induced motions of the current meters are larger than the wave-induced motions of the particles, the maximum bias is larger than the Stokes drift (the equality arises at the surface only).

The vertical integral of the bias is bounded by

$$\frac{a^2\omega}{2} \leq \int_{-H}^{0} u_{bias} dz \leq a^2 \omega, \tag{3.5}$$

while the vertically integrated Stokes transport is

$$M^w = \int_{-H}^{0} U_s dz = \frac{a^2\omega}{2}. \tag{3.6}$$

Therefore, if the unbiased theoretical downwind transport is equal to minus the Stokes transport, we then expect to find a biased transport comprised between 0 and $+M^w$. The observed downwind transport in LOTUS 3 is approximately zero. It was interpreted by Price et al. (1987) as an evidence that the Ekman transport is crosswind. Furthermore, in the winter measurements of LOTUS 4, a positive downwind transport was found and was interpreted by Schudlich and Price (1998) as a wave bias, coming from the large winter waves. The present description supports the more nuanced conclusion that both the LOTUS3 and the LOTUS4 measurements are likely biased by the waves in the downwind direction.

3.5 Surface drift

One aim of the present model is a better understanding of the surface Lagrangian drift, for applications to search and rescue, fish larvae recruitment or any other studies following floating materials. The present model, following Garrett (1976) and Jenkins (1989), separates the flow into a wave Stokes drift and an Eulerian current. In particular, the introduction of the wave age should bring new insight in the near-surface dynamics. One remarkable result obtained in Part 1 is that the surface drift is almost independent of the wave age : as the waves gets more mature, the Stokes drift increases. But the mixing is also more efficient and leaves an Ekman current more homogeneous, thus reducing the surface quasi-Eulerian current and compensating the increase of the Stokes drift. This result is recalled in fig. 3.10.

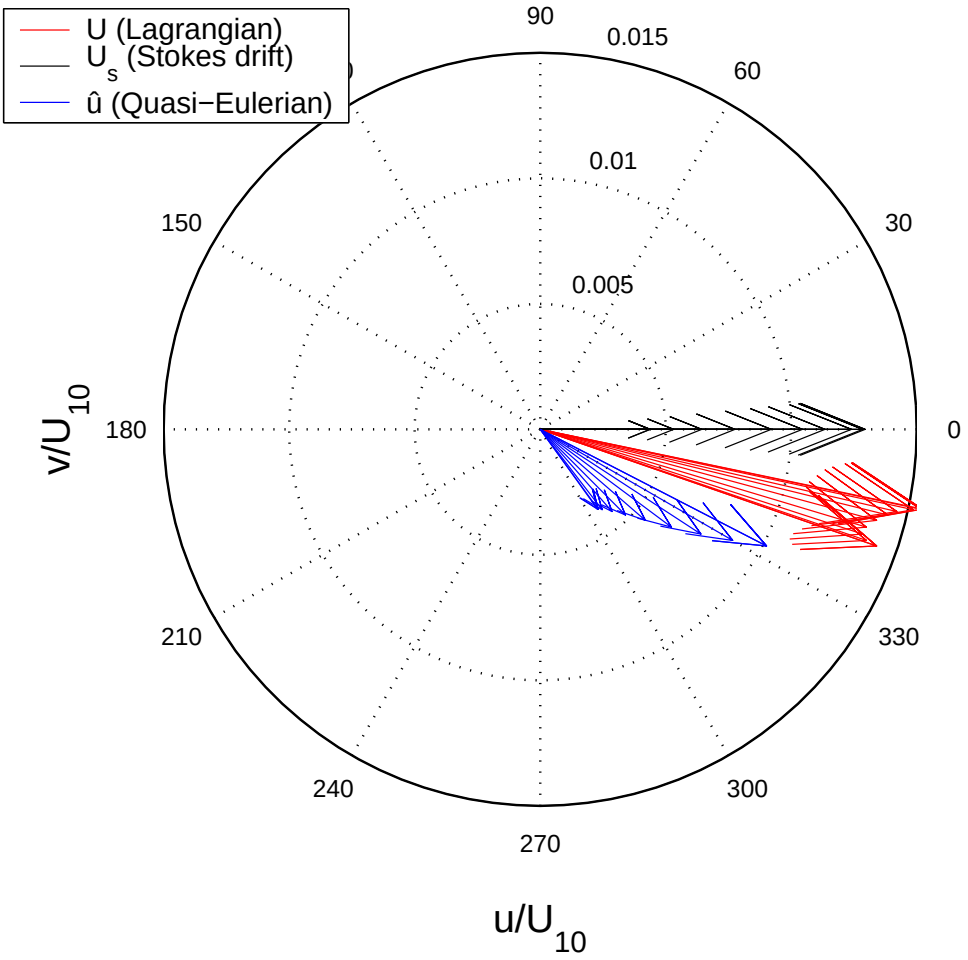

Figure 3.10: Effect of the wave age on the surface values of the Stokes drift, of the quasi-Eulerian current and of the Lagrangian drift, in unstratified conditions. Velocities are expressed as a percentage of the wind speed U_{10}. The density is supposed uniform, as in Part 1. Calculations are made for $U_{10} = 10$ ms^{-1}, and for different stages of wave development (fetches varying from 1 km to 6000 km, corresponding to significant wave height from 0.2 to 2.8 m). As the Stokes drift $\mathbf{U_s}$ increases with more mature waves, the quasi-Eulerian current $\widehat{\mathbf{u}}$ decreases due to the more intense mixing, leading to a Lagrangian surface drift $\mathbf{U} = \mathbf{U_s} + \widehat{\mathbf{u}}$ almost independent of the wave age, both in magnitude and in direction.

Whereas the wave age is a key parameter for the near-surface mixing, it has little influence on the surface drift. A simple parameterization of the surface drift directly from the wind might then be possible. Does this result extends to stratified conditions?

The surface drift depends on the stratification. As the mixed layer gets more shallow, the quasi-Eulerian current increases in magnitude and rotates further from the wind direction. As a consequence, the Lagrangian drift does not vary much in magnitude, but the deviation angle increases (fig. 3.11) with an increasing stabilizing buoyancy flux.

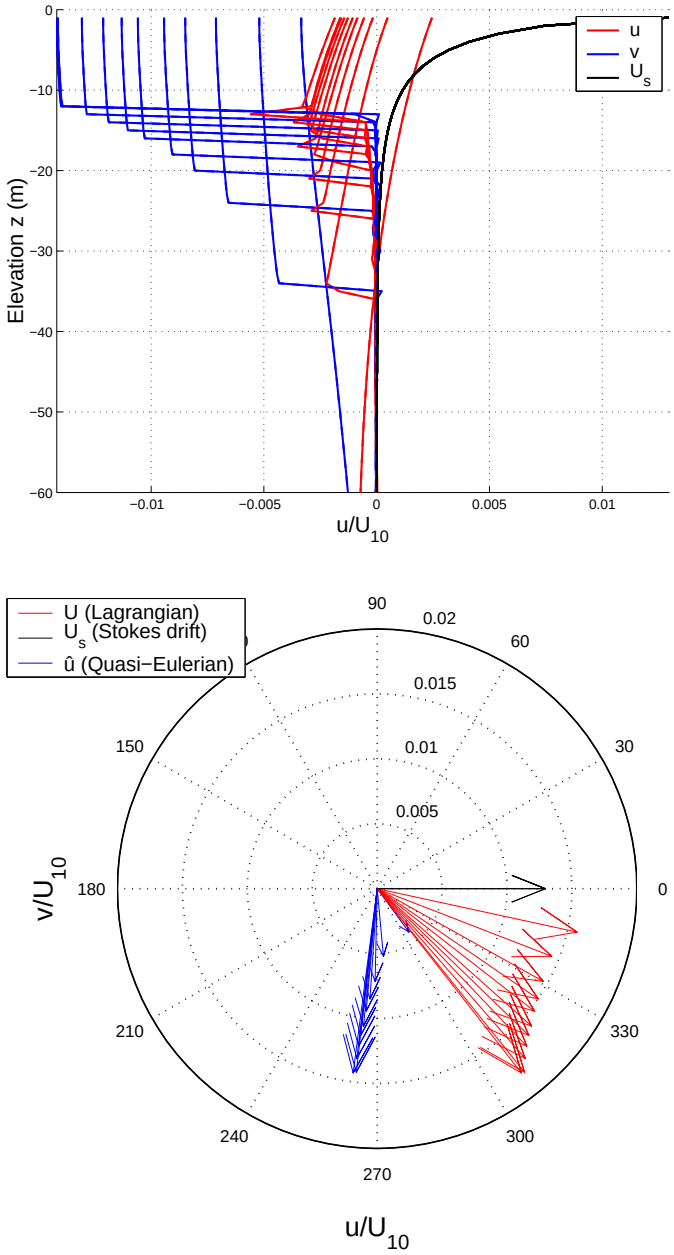

Figure 3.11: Effect of the stratification on the vertical profiles (upper panel) and on the surface values (lower panel) of the Stokes drift, of the quasi-Eulerian current and of the Lagrangian drift, expressed as a percentage of the wind speed U_{10}. Calculations are made for $U_{10} = 10$ ms^{-1}, for fully developed waves ($H_s = 2.80$ m) and for different mixed layer depths obtained with different stabilizing surface heat fluxes (from 0 to 1000 Wm^{-2}). As the mixed layer gets more shallow, the quasi-Eulerian current increases in magnitude and rotates further from the wind direction. As a consequence, the Lagrangian drift does not vary much in magnitude but the deviation angle increases.

The dependance of the surface drift on the wave age in the presence of strong stabilizing buoyancy fluxes is shown in fig. 3.12. For shallow mixed layers, the

quasi-Eulerian current is almost crosswind. Consequently, the reduction of the quasi-Eulerian current, when waves get more developed and mixing more efficient, is not compensated by the increase of the Stokes drift of the waves, contrary to what happens in unstratified conditions. In addition, the mixed layer of the model gets thicker with a larger wave-induced mixing, which increases furthermore the wave age dependance of the surface drift during strong heating events. That latter behavior is physically sound but requires further verifications. This requires a full coupling of the mixed layer with the wave forcing, a task that is beyond the scope of the present study and is left for future work.

3.6 Conclusion

A model of the surface layer of the ocean was presented in Part 1. Essentially, the current was separated into a wave Stokes drift and a quasi-Eulerian current. That physical description leaded to a different analysis of the observations of currents profiles close to the surface, whether the measurements are Eulerian or Lagrangian. That analysis agreed qualitatively with a few available data of Lagrangian drift profiles, of Eulerian velocity profiles and of TKE dissipation rates. Motivated by these results, we added the stratification to the model of Part 1 and tried a more quantitative validation of the current profiles.

We performed a reanalysis of the near-surface quasi-Eulerian velocity measurements during SMILE. The near-surface shears were previously investigated by comparison to shears at greater depths obtained with an additional buoy (Santala, 1991). Here we made no hypothesis on the structure of that shear. The near-surface shears obtained in this more general analysis are found to be in good agreement with the downwind shears expected in the presence of a strong wave-induced mixing. However, crosswind shears found are an order of magnitude larger than expected. The Stokes-Coriolis force (or Hasselmann force) appeared as a good candidate but is too weak in magnitude to produce such shears. Consequently, the physics of the present model is still not sufficient to explain the observed shears. Models and complementary observations of Langmuir cells appear therefore to be necessary for further investigations of these currents measurements.

The long term observations of Ekman spirals during LOTUS 3 provide an opportunity to investigate the Stokes-Coriolis effect. The use of a long time series reduces the noise in the measurement, enabling an analysis of the magnitude of the wind-driven current. However, it introduces rectification effects because of the temporal variations of the wind and of the stratification. The wind variability was taken into account by using the coherent averaging of Price et al. (1987), which follows the

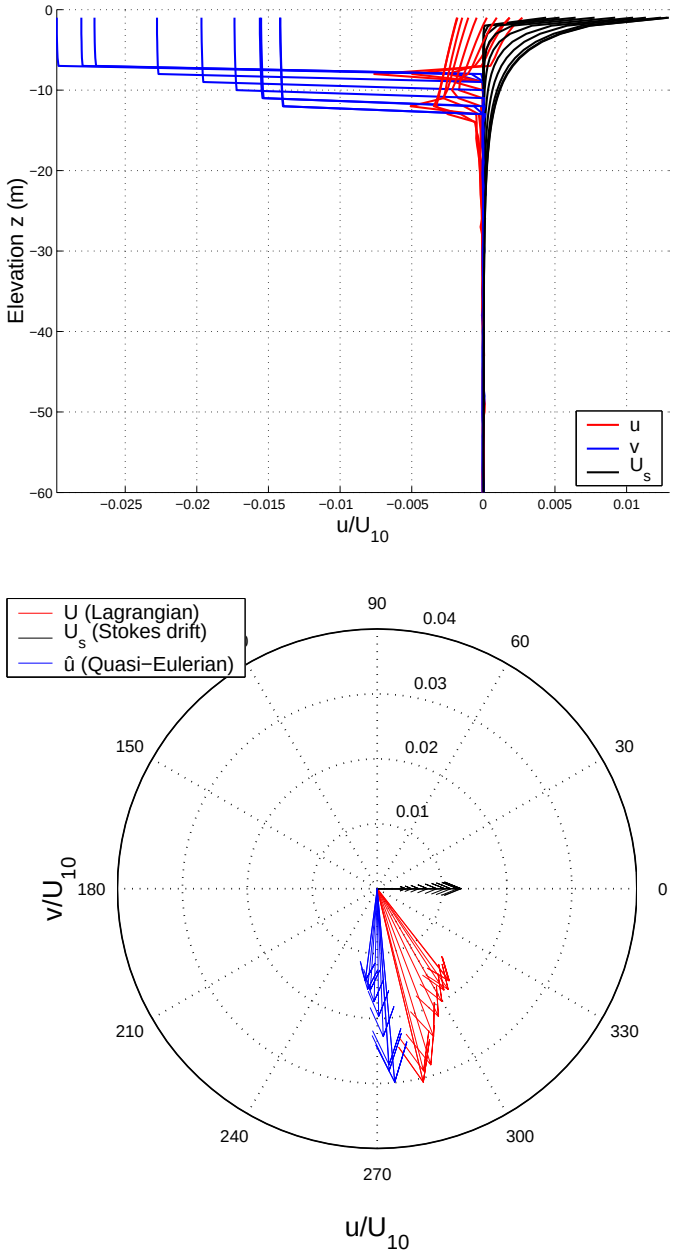

Figure 3.12: Effect of the wave age on the vertical profiles (upper panel) and on the surface values (lower panel) of the Stokes drift, of the quasi-Eulerian current and of the Lagrangian drift. Velocities are expressed as a percentage of the wind speed U_{10}. Here the surface heat flux is set to 1000 Wm^{-2}, leading to very shallow mixed layer, around 8 to 12 m thick, depending on the wave age. Calculations are made for $U_{10} = 10$ ms^{-1}, and for different stages of wave development (fetches varying from 1 km to 6000 km, corresponding to significant wave height from 0.2 to 2.8 m). As the Stokes drift increases with more mature waves, the quasi-Eulerian current decreases due to the more intense mixing. For such shallow mixed layer, the quasi-Eulerian current reduction dominates the increase of the Stokes drift, leading to a Lagrangian surface drift dependent of the wave age, both in magnitude and in direction.

wind direction, and changes in the stratification were represented by constraining the temperature to the observed temperature. The Ekman spiral of the model then showed very good agreement with the observations. However, we did not found any evidence of the Stokes-Coriolis effect, whereas accurate wave hindcasts suggest that it should be significant. The nature of the measurement is then in question, because the bias induced by the waves on near surface measurements from a buoy can be larger than the Stokes transport. Seeking evidence of the Stokes-Coriolis effect such long time averaging, as attempted by Lewis and Belcher (2004) and Polton et al. (2005), still appears to be feasible but preference should be accorded to measurements from fixed towers or bottom mounted Acoustic Doppler Current Profilers (ADCPs) to get rid of that wave bias.

Finally, we investigated the surface drift predictions of the model in the presence of stratification. It is shown that the wave age effect on the surface drift, which was found to be small in unstratified conditions, is important in the presence of shallow diurnal mixed layers. In such case, considering separately the wave field and the mean current should give significant differences on surface drift predictions.

Acknowledgments.

The initial version of the computer code for the mixed layer model was kindly provided by Yign Noh. We acknowledge the National Buoy Data Center (NDBC) and the Upper Ocean Mooring Data Archive of the Woods Hole Oceanographic Institution (WHOI) for their web-available data. N.R. acknowledges the support of a CNRS-DGA doctoral research grant.

Chapter 4

One-Dimensional study: Epilogue and Perspectives

4.1 Is the surface drift due to the wind or due to the waves ?

It was shown in chapter 2 that the surface drift, when the wind-waves are developed, is rather due to the Stokes drift of the waves than to the wind-driven mean current. A fast interpretation could be that the surface drift in the present description is related to the waves and is not related to the local wind anymore. This interpretation must clearly be nuanced.

Firstly, it is true that the Stokes drift not only depends on the wind speed but also depends on the wave age. Developed wind-waves have a larger energy and a larger surface Stokes drift than young wind-waves. But what is the impact of the wave age on the surface drift ? This question has been treated in the previous chapters, showing in particular that, at least in an unstratified ocean, the surface drift is not much modified by the wave development (see fig. 2.12).

Secondly, if the surface drift mainly comes from the waves Stokes drift, is it possible that the swell, i.e. waves not related to the local wind and propagating far from their generation areas, has an important contribution to the surface drift ? We want here to discuss that issue, the impact of the swell on the surface drift.

The contribution of the short waves to the surface Stokes drift is important, because the latter is a third moment of the frequency spectrum (fig. 4.1). Those short waves are less important for the Stokes transport as it is a first moment of the spectrum (fig. 4.1). We note however that the directional spreading of the short waves reduces their contribution to the surface Stokes drift.

Consequently, the Stokes drift of a low frequency swell with a sharp spectral

distribution is much smaller than the Stokes drift of a wind sea of the same energy, especially if the swell period is large. For illustration purpose, we plotted in fig. 4.2 the spectra corresponding to the variance of the surface elevation (the energy, upper panel) and to the surface Stokes drift (lower panel), for young wind-waves, old wind-waves, long period and small period swells. The swell were supposed to be narrow-banded, with a Gaussian distribution of the energy around the peak frequency, with a spreading of 0.02 Hz. The surface Stokes drift of the young wind-waves (fetch of 100 km, $H_s = 1.6$ m, $T_p = 5.5$ s) is 10.2 cm s^{-1}, that of the developed wind-waves (fetch larger than 1000 km, $H_s = 2.8$ m, $Tp = 8$ s) is 12.9 cm s^{-1}, that of the short period swell ($H_s = 2.8$ m, $T_p = 8$ s) is 5.2 cm s^{-1} and that of the long period swell ($H_s = 2.8$ m, $T_p = 12$ s) is 1.6 cm s^{-1}.

The surface drift, even if it was found mainly due to the Stokes drift of the waves, remains then correlated to the local wind, with only a small contribution of the swell, typically of the order of a few centimeters per second in deep water.

4.2 Further verifications of the present description

4.2.1 The drifters observations and the model of Kudryavtsev et al. (2007)

The major weakness of the model presented in this part is its high dependency on the roughness length, whereas that latter is poorly physically defined. Such additional tuning parameters might denote that the physics of the model fails to described the near-surface zone. One of the interpretation of this roughness length is that it is a substitute for the depth injection of TKE and momentum due to wave breaking. In chapter 2, we used the model of Sullivan et al. (2004) and the observations of Melville et al. (2002) to inject the momentum and the TKE over a certain depth. Our conclusion was that this cannot substitute to the use of a large roughness length, of the order of H_s. Kudryavtsev et al. (2007) injected the TKE and the momentum to a depth proportional to the wavenumber of the wave that dissipates and they found that their model is consistent with previous observations of TKE dissipation rates close to the surface, and also with new observations of near-surface drifters. Interestingly, they do not need a large roughness length to obtain this agreement (they set z_0 to a few centimeters). The differences with our similar experiment made in chapter 2 are not clear. The depth injection of TKE and momentum is around $\lambda/5$ in our work and is around $1/k = \lambda/2\pi$ in their model.

More interestingly, Kudryavtsev et al. (2007) argued that the quasi-Lagrangian motion expected for a drogue in the presence of waves, almost similar to the Stokes

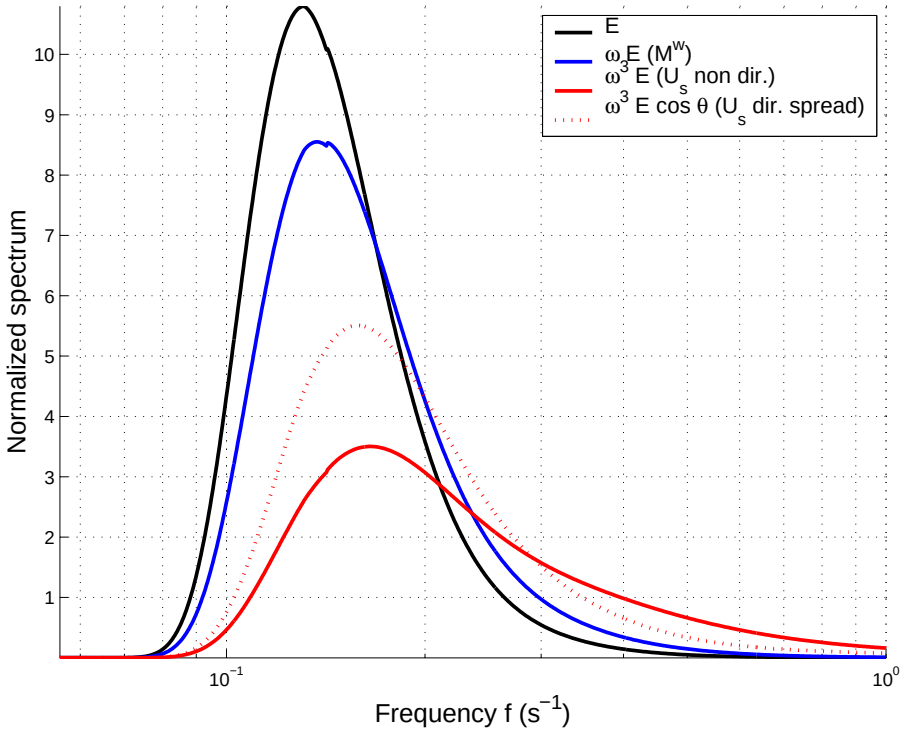

Figure 4.1: Frequency spectrum integrated over the direction $\int E(f,\theta)d\theta$, for a wind sea with a wind speed of $U_{10} = 10$ m s^{-1} and a fetch larger than 1000 km (fully developed sea, period $Tp = 8$s, significant wave height $H_s = 2.8$m), based on the KMC spectrum [Kudryavtsev et al. (1999)]. Also shown is the first moment of the spectrum $f \int E(f,\theta)d\theta$ (corresponding to the the Stokes transport), the third moment $f^3 \int E(f,\theta)d\theta$ and the effect of the directional spreading on the third moment $f^3 \int E(f,\theta)cos(\theta)d\theta$ (corresponding to the Stokes drift). Each spectrum is normalized with its integral over frequency. One can see that the Stokes drift depends on the most energetic waves near the spectral peak but with non negligible importance of the small waves, although the directional spreading of the small waves reduces this importance.

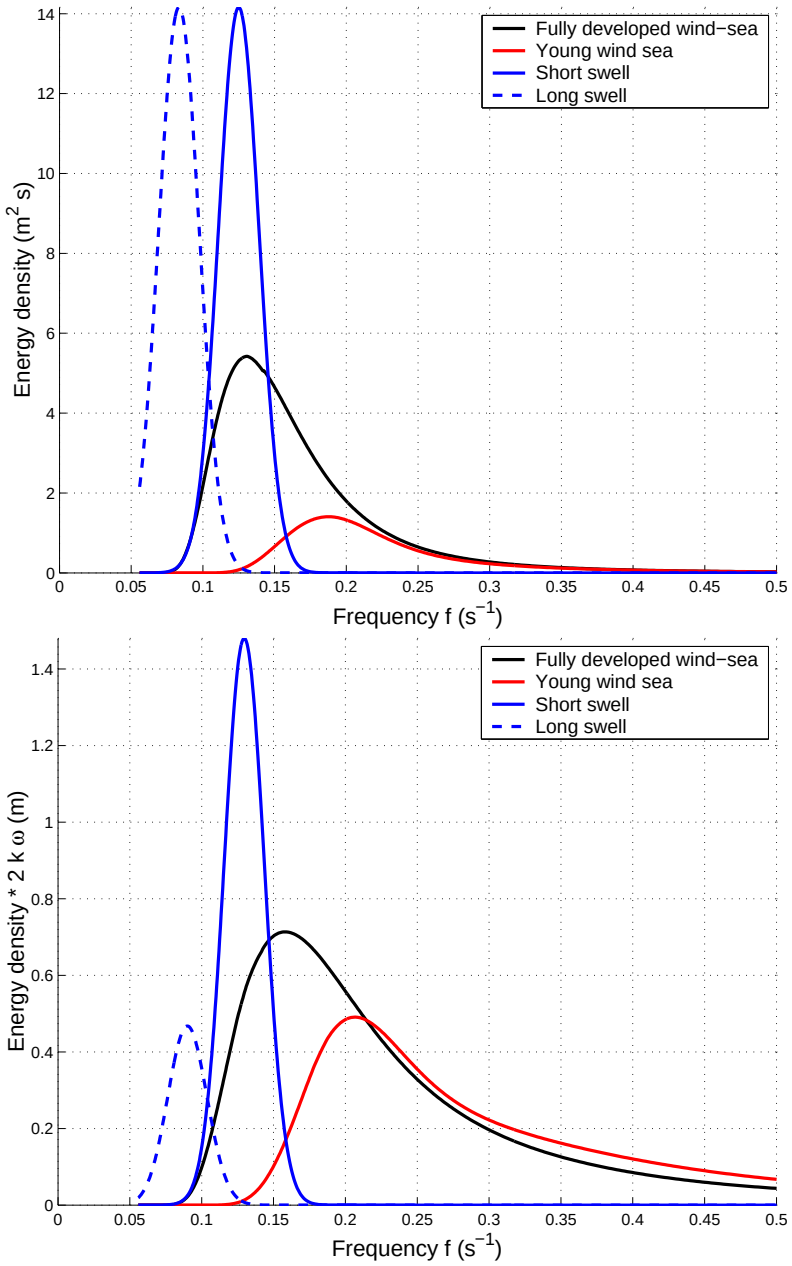

Figure 4.2: (Upper panel) Frequency spectrum integrated over the direction $\int E(f,\theta)d\theta$. The integrals over frequency gives the "energy" E, i.e. the variance of the surface elevation, related to H_s by $H_s = 4 * \sqrt{E}$.(Lower panel) $\int E(f,\theta)2k\omega d\theta$, which integrates over frequency to give the surface Stokes drift U_s. The wind speed is set to $U_{10} = 10$ m s^{-1}. Four different spectra are shown: in red, the waves are young (fetch of 100 km, $H_s = 1.6$ m, $T_p = 5.5s$), in black the waves are fully-developed (fetch larger than 1000 km, $H_s = 2.8$ m, $Tp = 8$ s), based on the KMC spectrum (Kudryavtsev et al., 1999). In blue, we show the case of swells with a gaussian spectral distribution with the same energy than developed waves ($H_s = 2.8$ m) and for two different peak periods, $T_p = 8$ s in solid line and $T_p = 12$ s in dashed line. By comparing the areas below each curves, one can see the increase of both the wave height and the surface Stokes drift as the wind sea gets more developed. One can also see that a narrow-banded swell, although of same energy than developed wind-waves, creates a small surface Stokes drift, and even smaller as the swell period gets larger.

drift that would experience a perfect Lagrangian drifter, is much smaller than the observed displacements. Consequently, they analyzed the drifters motions in terms of mean current only, without any considerations of the Stokes drift of the waves. This approach would appear to completely contradict the results obtained in chapter 2 for fully developed waves. However, the quite small waves encountered during their field measurement ($H_s \leq 0.5$ m) suggest that either the wind was quite low or the fetch quite short. As noted in chapter 2, for short fetches, the Stokes drift is small and the Eulerian current may dominate the surface drift. Further work is clearly needed to reconcile the two models.

4.2.2 Other determinations of the roughness length

We essentially used the works of Terray et al. (1996, 2000) which relates the roughness length to the significant wave height : $z_0 = 1.6H_s$. These results were inferred from observations of TKE dissipation close to the surface.

The same kind of calculation was conducted by Soloviev and Lukas (2003) and they found smaller value of the proportionality constant $z_0 = 0.6H_s$. However, if a swell was present in this Central Pacific experiment, this constant might be slightly underestimated.

Also, Gemmrich and Farmer (1999) used measurements of temperature gradients close to the surface and found smaller values of the roughness length, $z_0 \simeq 0.2$m. Although this different measurement technique could be argued to produce naturally different results, Gemmrich and Farmer (2004) also estimated dissipation rates from near-surface wavenumber spectra of velocity. These latter measurements are found to be generally consistent with smaller z_0 values than expected from Terray et al. (1996). In this case, their measurement device was following the up and down motion of the waves, and would thus be a more adequate measurement than those made at fixed depth by Terray et al. (1996). We may only conclude that measurements of turbulence in the upper ocean are clearly consistent with values of z_0 that are a significant fraction of a meter, but with an elusive scaling, logically related to the height of breaking waves, but only tentatively related to the wind sea wave height.

Part II

Impact of waves on the ocean mixed layer

Chapter 5

Impact of waves on the ocean mixed layer

Part I of the present thesis analyzed the velocity profiles in the surface layer. It was made clear that the vertical shear of the velocity close to the surface is mainly due to the Stokes drift of the waves, rather than due to a sheared surface current. This is a consequence of the observed strong near-surface mixing, likely due to wave breaking, at moderate and high wind speeds.

In parallel, since this expected strong wave-induced surface mixing has been actually measured, several authors have discussed its influence on the temperature of the surface layers of the oceans. Namely, the whole description of the turbulence in the near-surface layer was modified. The classical view on the ocean mixed layer is a transposition of the atmospheric boundary layer over land, which is well described by Monin-Obukhov theory, as verified in the Kansas experiments. Turbulent kinetic energy (TKE) is produced by velocity shears and unstable stratification, and may be destroyed by stable stratification. In stably stratified cases, this leads to a description of the mixed layer depth through a competition between the shear production by the mean current and the buoyancy damping, leading to definitions of Richardson numbers based on their ratio.

A significant difference in the ocean mixed layer is given by the surface flux of TKE, associated with wave breaking, which dominates by far the production by the mean shear (e.g. Terray et al., 1996). Noh (1996) showed that this surface flux of turbulence is a necessary ingredient to obtain a thermocline in the presence of both wind and stabilizing buoyancy flux. This explain why the diurnal ocean surface layer exhibits a thermocline while the nocturnal atmospheric bottom boundary layer does not.

Li et al. (1995) studied the impact of Langmuir cells on the mixed layer depth.

This impact was inferred from an investigation of the downward velocity due to Langmuir cells at the base of the mixed layer. This cause of thermocline erosion was then compared to erosion due to the shear current of inertial oscillations. However, the shear of the mean flow was considered as the dominant source of turbulence, whereas for shallow mixed layers, the downward diffusion from the surface might certainly dominate.

5.1 A methodology to study the impact of waves on the mixed layer depth

Large Eddy Simulations (LES) are the most realistic models of the mixed layer. They are able to resolve the full 3D turbulence, including wave-induced turbulence, with a resolution of about 1 m. They are used to understand special aspects of the near-surface dynamics, to interpret small scales observations, and even to substitute to missing (because difficult to achieve) measurements. But due to their high computational costs, they are not suited for seasonal or annual simulations of mixed layers, and they also cannot be implemented in a Ocean General Circulation Model (OGCM) to produce simulations and analysis of mixed layers where horizontal advection is important.

Therefore the traditional approach of mixed layers studies uses LES, in idealized situations, to analyze the impact of the different important physical processes : Langmuir circulations (McWilliams et al., 1997), horizontal Coriolis force, wave breaking (Noh et al., 2004), surface heating (Min and Noh, 2004),...

Results of these LES studies are used to construct simpler and computationally less expensive parameterizations (e.g. Kantha and Clayson, 2004; McWilliams and Sullivan, 2001; Smyth et al., 2002), and to implement them either in 1D vertical models or in full 3D OGCM to include horizontal advection. Long term, seasonal or annual, mixed layers predictions of such models are then considered as indirect checks of the role of the different physical processes included (Gaspar et al., 1990; Large et al., 1994; Noh et al., 2005; Mellor and Blumberg, 2004).

We note, however, that LES models of the ocean mixed layer have failed so far to actually include wave motions, and only phase-averaged parameterizations have been used with, in some cases, the addition of momentum and TKE pulses meant to represent breaking waves. Recent model results on breaking waves (Lubin et al.2006) could likely be applied to this problem.

Here we will not attempt another LES simulation to evaluate the impact of waves on the mixed layer depth. Instead, we will focus on the following step of the

approach described above : we will use previous theoretical works to identify which parameters are useful to represent the wave-induced mixing. Then we will turn our interest on an estimation of these parameters, using a global wave model. We finally will evaluate the impact of such parameters on mixed layer depths calculated with an OGCM. In particular, we want to examine whether waves are a plausible candidate to explain mixed layer depths misfits of OGCMs compared to unresolved inertial oscillations, uncertainty on the surface fluxes, unresolved internal waves or others.

5.2 Which parameters for wave-induced mixing ?

5.2.1 Wave-induced mixing in the near-surface zone

Whitecaps of surface waves provide an intense source of TKE compared to the shear of the mean current. Also, waves are believed to be at the origin of the Langmuir cells (Langmuir, 1938), which generally dominate the vertical mixing produced by the breaking waves (Noh et al., 2004), except probably in the near-surface zone.

Regardless of it physical origin, that near-surface mixing, enhanced in the presence of waves compared to the mixing close to a rigid wall, has been successfully modeled with simple Mellor-Yamada type TKE models, by adding a TKE surface flux Φ_{oc} and by setting the mixing length at the surface z_0 proportional to the wave height (see Part I). The surface flux of TKE comes from the dissipation of waves.

5.2.2 Wave-induced mixing through the whole mixed layer

Observations of Langmuir turbulence have revealed that the turbulent velocity w_{rms} associated with the Langmuir cells scales with the surface Stokes drift (Smith, 1998). Also, Langmuir turbulence is supposed to occur for small values of the Langmuir parameter $La = \sqrt{u^*/U_s(z=0)}$. Nevertheless, we note that the vertical shear of the Stokes drift is absent from these dimensional analysis, whereas the tilting of the vorticity of the mean flow by the Stokes drift shear is a dominant mechanism for the generation of Langmuir cells. Recently, Harcourt and D'Asaro (2006) proposed a revised Langmuir parameter La_{St}, in which the mean Stokes drift between the surface and one fifth of the mixed layer depth is used instead of its surface value. That number was chosen to include in the dimensional analysis the ratio of the mixed layer depth to the Stokes depth, which characterizes the vertical shear of the Stokes drift through the mixed layer. Based on LES simulations, the turbulent velocity of the Langmuir cells was found to depend on that modified Langmuir number by

the formula $w_{rms} = u^* La_{St}^{-2/3}$. These authors further argued that the observations hardly exhibit such trend because of inverse correlations between winds speeds and wave ages in the field measurements.

5.3 Estimations of the wave-related parameters

Wave-related parameters may be obtained from numerical models. One should be carelful that such models are mostly verified in terms of significant wave height and peak or mean period only, so that other parameters, in particular those related to the high-frequency end of the spectrum may not be well estimated. Here we have chosen to use the spectral phase-averaged model WAVEWATCH III (Tolman, 2002), as modified by Ardhuin et al. (2007*a*) to include the generation and dissipation parameterizations of Bidlot et al. (2005). Although these parameterizations still result in large biases (about 30%) in the swell-dominated Eastern tropical Pacific, due to a lack of swell attenuation by the wind, they also provided the smallest random errors of all other parameterizations in use in operational wave models for mid and high latitudes (Jean Bidlot, personnal communication). Our model configuration is global (80°S to 80°N) with 1° resolution, and has been extensively validated against all in situ buoys reporting to the WMO Global Transmission System and all satellite altimeters (Fabrice Ardhuin and Pierre Queffeulou, personnal communication). This model is forced here with 10-m winds and sea ice concentrations from the European Center for Medium-Range Forecasts (ECMWF) 40-year reanalysis (ERA40).

5.3.1 The Stokes drift U_s

The Stokes drift at the surface was estimated by Kenyon (1969). He supposed that the waves are fully-developed and computed the Stokes drift with the spectrum of Pierson and Moskowitz (1964). He obtained values around 3% of the wind speed at 10 m. These results were reevaluated in Part I, using the more realistic spectrum of Kudryavtsev et al. (1999), and we obtained that the Stokes drift can reach a maximum value of 1.2% of the wind speed. This ratio was found to be maximum for high wind speeds. However, for strong winds, the waves are seldom fully developed. Therefore we estimated the Stokes drift using the waves hindcasts. Here the Stokes drift is only computed over the frequency range of the spectrum, i.e. with a maximum frequency of 0.4 Hz. The mean ratio over January 2004 is shown in fig. 5.2. This ratio is around 0.3% at low latitudes and about 0.6% at mid-latitude. Maximum values are only around 1.0%, in areas of large wind speeds.

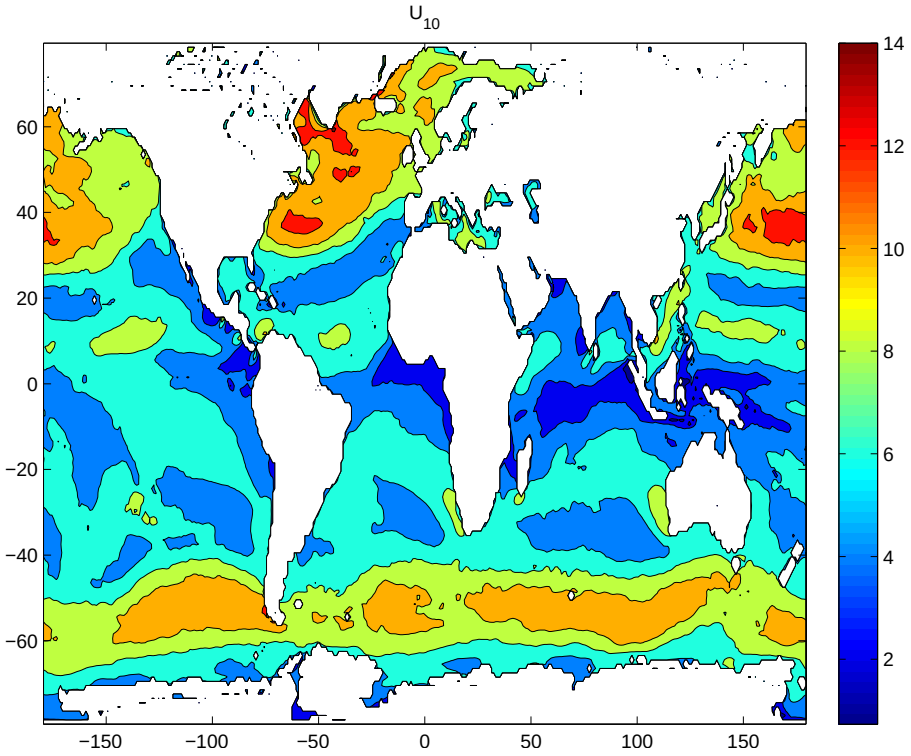

Figure 5.1: Wind speed U_{10} (m s^{-1}) at 10m. Values shown are mean values over January 2004.

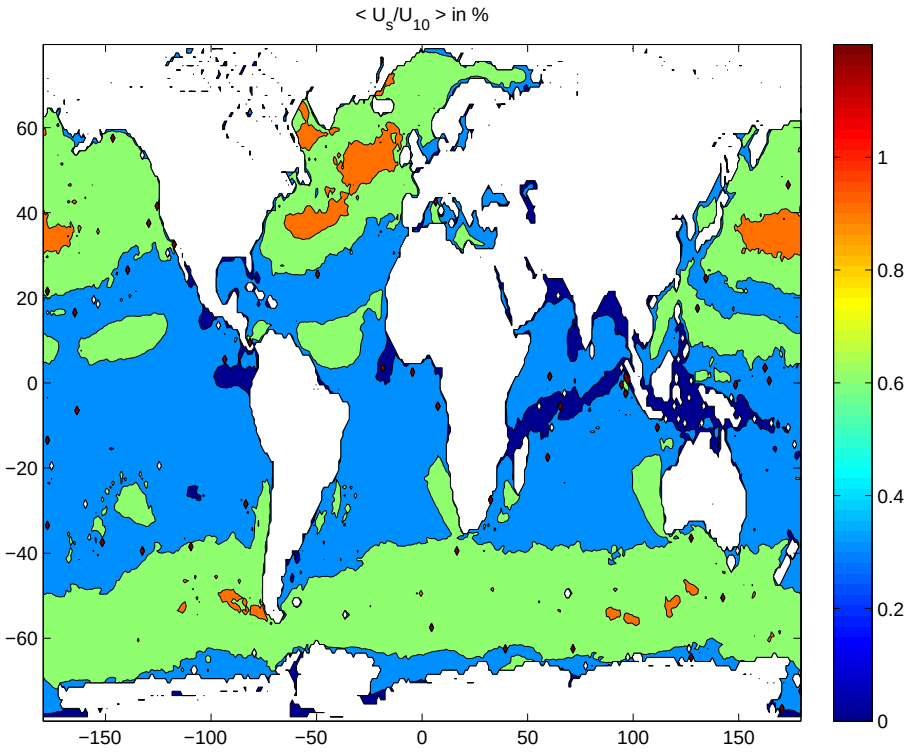

Figure 5.2: Ratio of the surface Stokes drift $U_s(z=0)$ to the wind speed U_{10} at 10 m, in percentage. Values shown are mean values of the ratio, $< U_s(z=0)/U_{10} >$, over January 2004.

5.3.2 The Stokes transport T_s

The Stokes transport (i.e. the vertically integrated Stokes drift) of a wind sea was estimated by McWilliams and Restrepo (1999) and Polton et al. (2005), using the spectrum of Pierson and Moskowitz (1964). It was shown to reach maximum values around 40% of the corresponding Ekman transport, depending on the latitude. In part I, we reevaluated this ratio using the spectrum of (Kudryavtsev et al., 1999) and found smaller values, around 30% at best at 45° of latitude. The ratio was shown to reach maximum values for high wind speeds. However, once again, waves are seldom fully developed for large wind speeds. Indeed, Pierson and Moskowitz only found about 20 cases of fully developed waves in several years of data (see also Alves et al. 2003). Therefore we reevaluated this ratio using a wave hindcasts. The atmospheric boundary layer of the wave model is used to calculate the surface stress. The fig. 5.3 shows that monthly mean values of the ratio are around 5%. Maximum values only reach 10%, and are found in the vicinity of areas with large wind speeds.

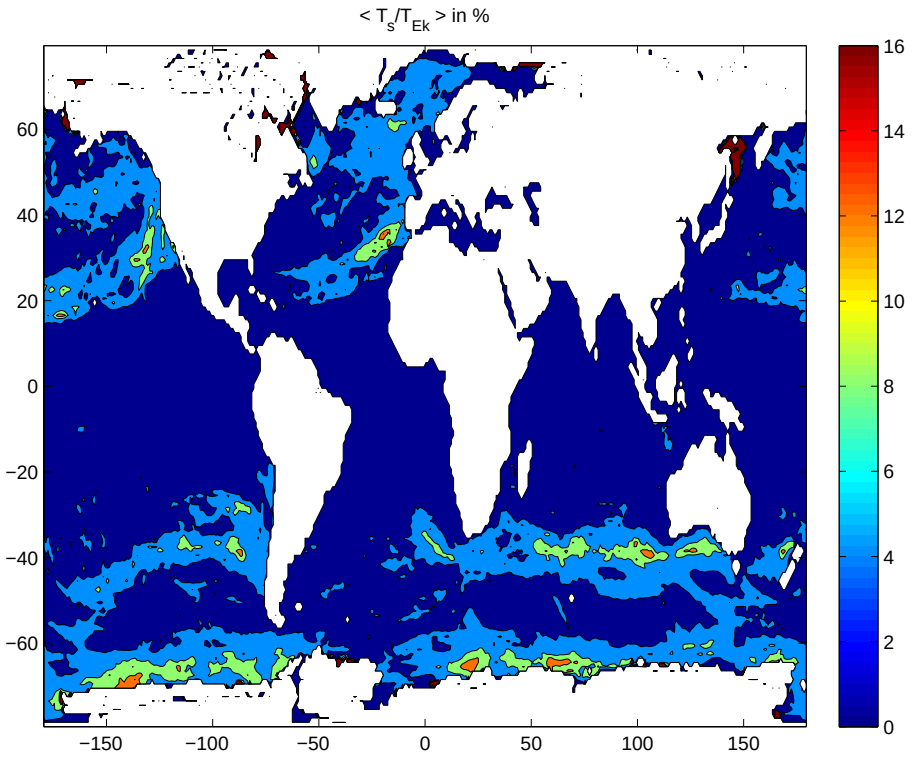

Figure 5.3: Ratio of the Stokes transport T_s to the Ekman transport $T_{Ek} = u^{*2}/f$, in percentage. Values shown are mean values of the ratio, $< T_s/T_{Ek} >$, over January 2004. Values of the ratio as much as 200 are obtained during particular events of very light wind and presence of swell. Such events introduce highly localized bias in the monthly mean and were avoided by averaging only over the events with $T_s/T_{Ek} < 1$.

5.3.3 The roughness length z_0

The roughness length z_0 is physically understood as the scale of the breaking waves responsible for the high mixing levels close to the surface. It has been shown by Craig and Banner (1994) and by Mellor and Blumberg (2004) that this length scale is even more important in terms of mixing than the amount of TKE injected. This means that the actual size of the mixing pattern is important, even more than the energy of this mixing. That length scale has been related to the significant wave height H_s of the waves (Terray et al., 1996, 2000) with

$$z_0 = 1.6 H_s. \tag{5.1}$$

Given that the swells (waves not related to the local wind) have a small surface slope and generally do not break, the wave height of the wind sea only (H_{sws}) is probably the appropriate parameter in 5.1. We performed the separation between swell and wind-waves by imposing that wind-waves must experience a positive forcing from the wind, namely

$$H_{sws} = 4\sqrt{\int_{S_{in}(k)>0} E(k)dk}, \tag{5.2}$$

where $E(k)$ is the variance of the surface elevation for a given wavenumber k and S_{in} is the energy input term in the wave energy equation. For developped waves a large fraction of the energy corresponds to waves propagating slightly faster than the wind and for which $S_{in} < 0$. Our definition (5.2) thus yields a smaller height than the usual swell-sea partition based on the analysis of local minima in the spectrum. As a consequence, for a young wind-sea without swell, $H_{sws} = H_s$, whereas for a fully-developed wind sea, $H_{sws} < H_s$. This is consistent with the Fig. 9 of Banner et al. (2000) which showed observations that waves around the spectral peak do not break when the waves are fully-developed. It might also be consistent with a smaller value of z_0/H_s found by Soloviev and Lukas (2003) for developed waves. The fig. 5.4 shows the mean values of H_{sws} over January 2004.

Mellor and Blumberg (2004) have related the roughness length z_0 to the wind stress u^*, using an approximate equation for the height of the waves as a function of the wind stress,

$$\left\{ \begin{array}{rcl} H_s & = & \frac{\beta}{0.85}\frac{u^{*2}}{g}, \\ \beta & = & 665\left(\frac{C_p}{u_a^*}\right)^{1.5}, \end{array} \right. \tag{5.3}$$

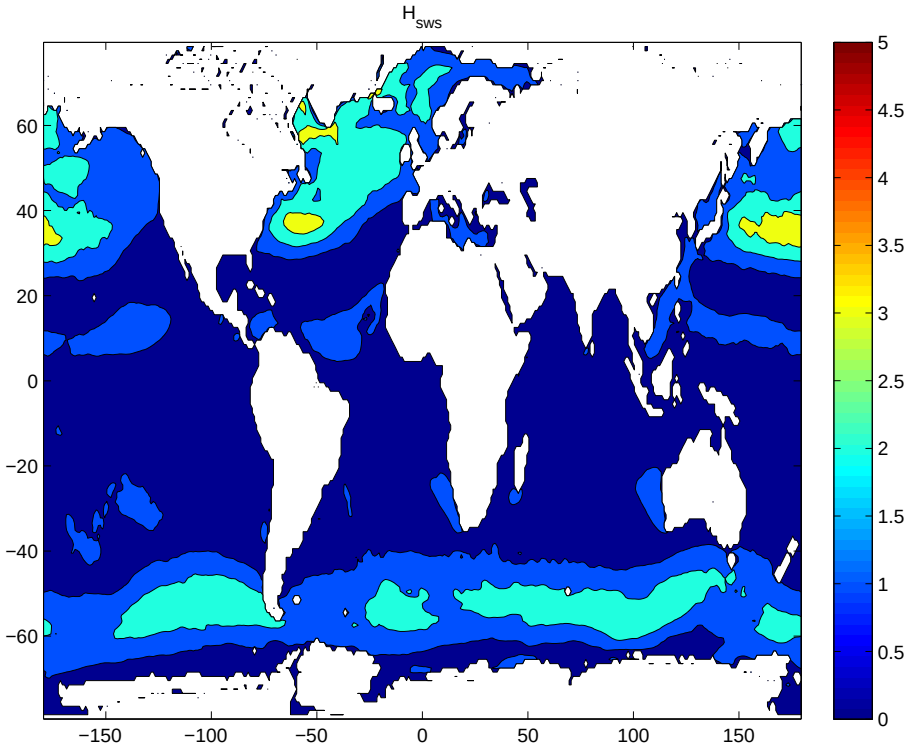

Figure 5.4: Significant wave height of the wind sea, H_{sws} (m), as estimated from the wave model with 5.2. Values shown are mean values $< H_{sws} >$ over January 2004.

where C_p/u_a^* is the wave age, i.e. the ratio of the phase speed of the dominant waves to the atmospheric friction velocity.

Note that Mellor and Blumberg (2004) did use the definition of the mixing length $l = \kappa \max(z_0', |z|)$, with the corresponding roughness length $z_0' \simeq 0.85 H_s$ (Terray et al., 2000), whereas, as already discussed in Part I, we stayed with $l = \kappa(z_0 + |z|)$ and $z_0 \simeq 1.6 H_s$. Because of these different definitions of the roughness length, we will rather discuss here the values of the wave height.

For a wave age of $C_p/u_a* = 30$, i.e. fully developed waves, formula 5.3 gives

$$\left\{ \begin{array}{rcl} H_s & = & \frac{\beta}{0.85}\frac{u^{*2}}{g}, \\ \beta & = & 1.E5. \end{array} \right. \tag{5.4}$$

Estimations of z_0 by Stacey (1999), from velocity profiles observations, gave value of β even larger, $\beta = 2.E5$, although the waves were quite young during their Canadian fjord measurements. Therefore Mellor and Blumberg (2004) investigated values of β between $1.E5$ and $2.E5$.

Indeed, waves are not always fully-developed, and the comparison between the parameterization 5.4 of the wave height and the calculation from the wave model, using 5.2, shows a large discrepancy at mid-latitude (fig. 5.5). Note however that

the agreement is acceptable at low latitude.

The wave age C_p/u_a^* is obviously missing in a direct parameterization of the wind-wave height from the wind. However, seeking for such a simple parameterization, why do the authors suppose fully developed waves ? Waves are always fully-developed under weak winds and are often quite young under strong winds (fig. 5.6). Although we warmly recommend using wave parameters from a wave model, we nevertheless propose here a better approximation of the wind-wave height, for those who do not want to use a wave model. This approximation supposes that the wave age is a function of the wind speed,

$$\frac{C_p}{u_a^*} = 30 \tanh \frac{u_{ref}^*}{u^*}, \tag{5.5}$$

where u_{ref}^* is a typical friction velocity above which the wave growth is duration limited (see fig. 5.8, left panel). Here we set $u_{ref}^* = 0.020$. The wave height is then

$$\left\{ \begin{array}{rcl} H_s & = & \frac{\beta}{0.85} \frac{u^{*2}}{g}, \\ \beta & = & 665 \left(30 \tanh \frac{u_{ref}^*}{u^*} \right)^{1.5}. \end{array} \right. \tag{5.6}$$

It is shown in fig. 5.7 that this parameterization 5.6 corrects the overestimation of the wave height at mid-latitude.

We modestly propose the use of the formula 5.6 instead of 5.4 to roughly parameterize the wave-breaking effect on the mixing, for instance for application to an OGCM.

The next step to built a more accurate simple formula could be to suppose that the wave age is a function of both the wind speed and the space, $C_p/U_{10} = f(U_{10}, x, y)$. This would lead us to built a climatology of wave ages, and could roughly represent the young sea states in the west parts of the oceans, due to the fetch limited growths of the waves.

However, as is emphasized in section 5.4, the use of a wave model in addition to the ocean circulation model is by far preferable to such simple climatological parameters.

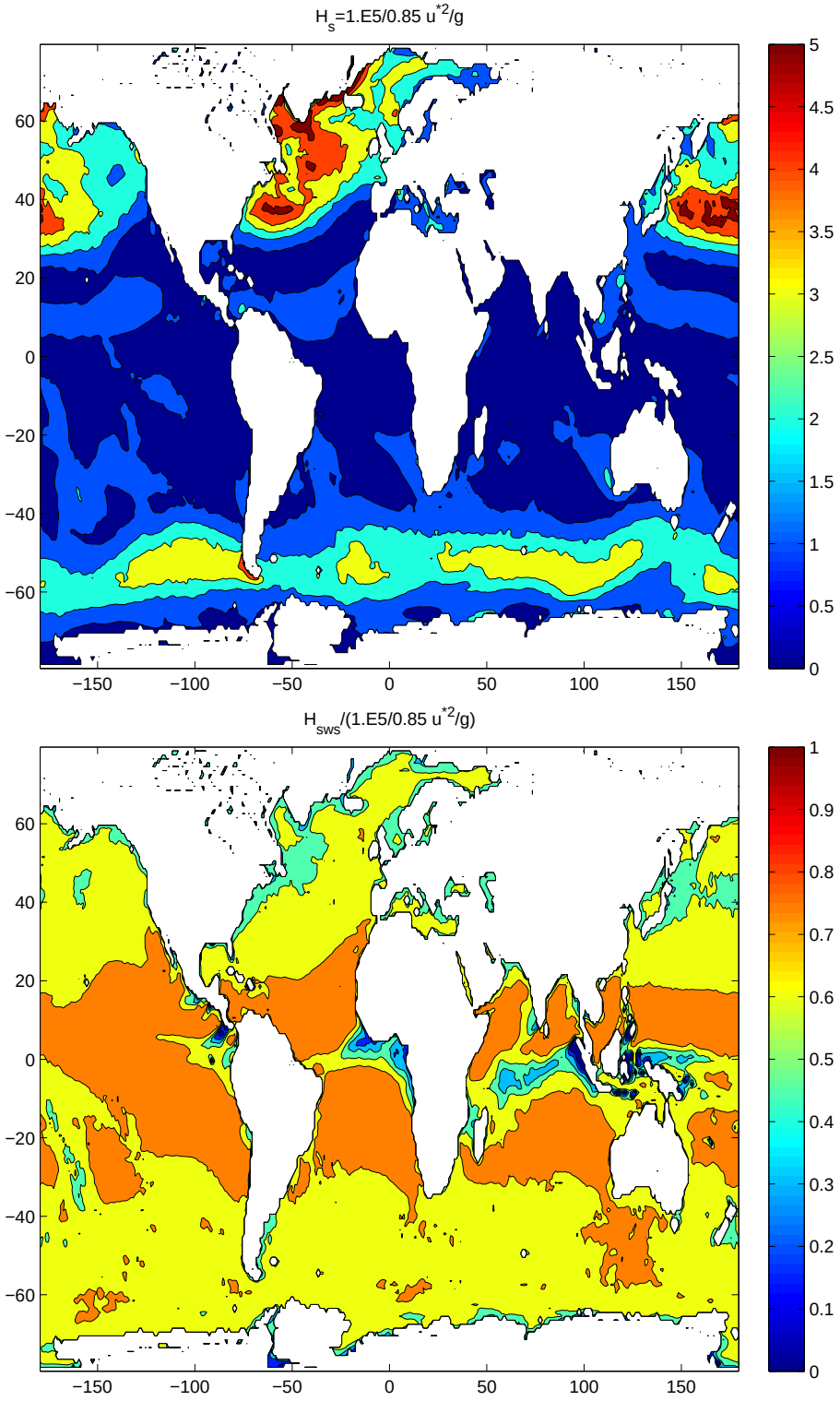

Figure 5.5: (Upper panel) Significant wave height (m), calculated from the wind stress with 5.4. Values shown are mean values $< \beta u^{*2}/(0.85g) >$, with $\beta = 1.E5$, over January 2004. Color scale stops at 5m although values up to 10m are found at mid-latitude. (Lower panel) Ratio of the significant wave height of the wind sea as inferred from 5.2 to the estimation with 5.4. Values shown are ratio of the mean values, $< H_{sws} > / < \beta u^{*2}/(0.85g) >$, over January 2004. The estimation supposing fully-developed waves is not bad at low latitudes but largely overestimates the wave height at mid-latitudes.

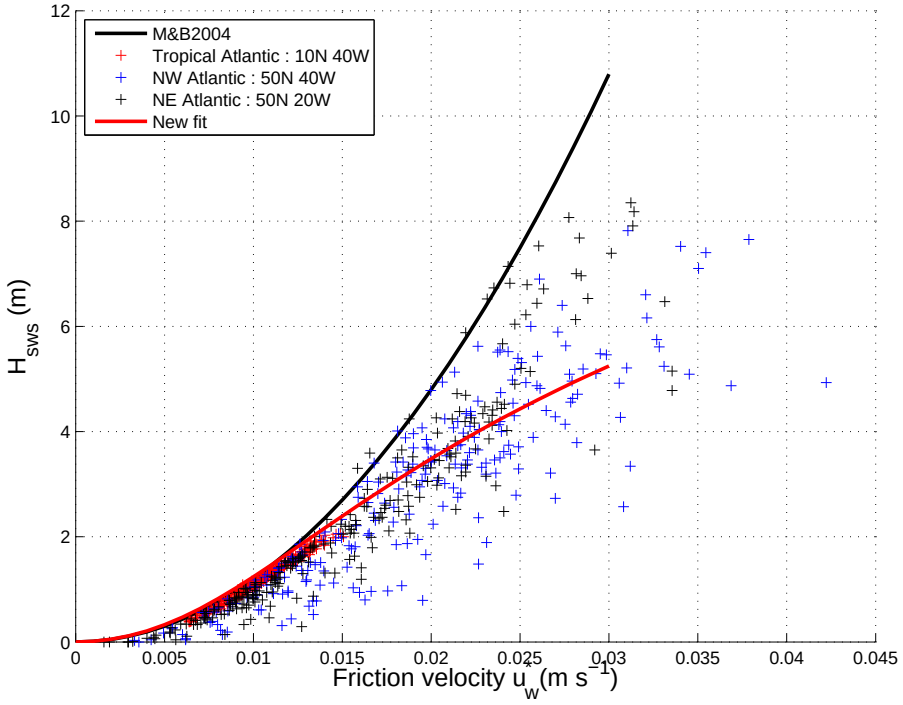

Figure 5.6: Significant wave height of the wind sea H_{sws} as a function of the waterside friction velocity u^*. One value corresponds to one wave model output, every 3 hours, for January 2004. Three locations of the North Atlantic are shown, one from the Tropical Atlantic, one from the North-East Atlantic and one from the North-West Atlantic. Also shown is the significant wave height of the wind sea as inferred from 5.4, which supposes full development. At low wind speed, the waves are often close to full development. However, for large wind speeds at mid-latitudes, waves are less developed, especially in the west part of the ocean. Therefore, we also show the significant wave height obtained by supposing that the wave age is a function of the wind speed (equ. 5.5 and 5.6).

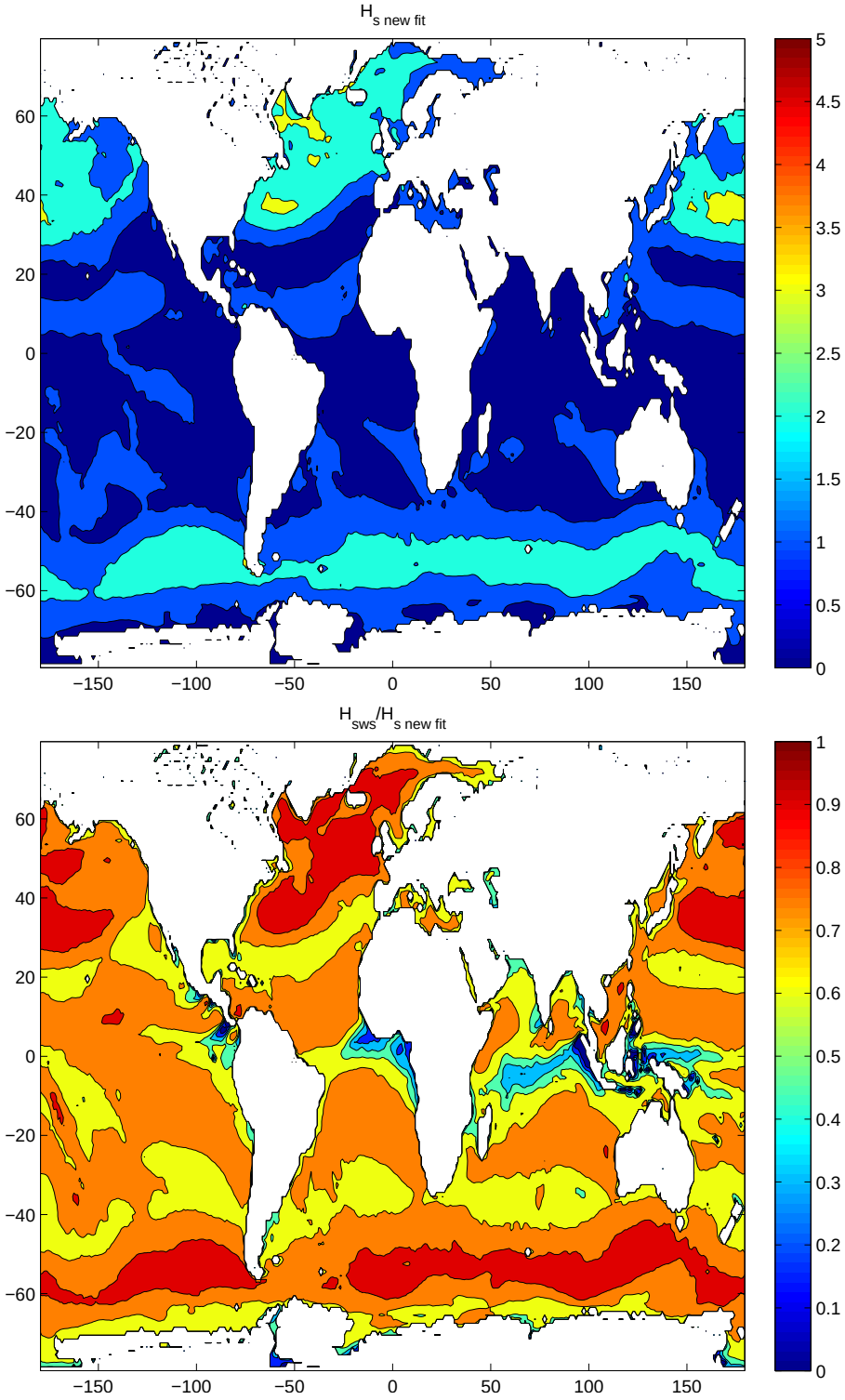

Figure 5.7: (Upper panel) Significant wave height $H_{snewfit}$ (m) calculated from the wind stress with 5.6. Values shown are mean values $< H_{snewfit} >$ over January 2004. (Lower panel) Ratio of the significant wave height of the wind sea as inferred from 5.2 to the estimation $H_{snewfit}$ with 5.6. Values shown are ratio of the mean values, $< H_{sws} > / < H_{snewfit} >$, over January 2004. The estimation supposing fully-developed waves is still good at low latitudes but the large overestimation of the wave heights at mid-latitudes, due to duration limited growths, has been corrected.

5.3.4 The TKE flux αu^{*3}

The TKE flux Φ_{oc} to the ocean comes from the dissipation of the waves. It has been modelled during the past as $\Phi_{oc} = \alpha u^{*3}$. Terray et al. (1996) calculated the dissipation of the waves using the energy input from the wind, S_{in}, from Donelan and Pierson (1987), integrated over a large variety of observed wave energy spectrum. They obtained values of α between 50 and 150, depending on the wave age (see the fig. 8 of Terray et al. (1996)). Nevertheless, it should be noted that the wind-wave growth term of Donelan and Pierson (1987) was later revised by Donelan (1990), with the dimensionless growth constant increased from 0.19 to 0.28. We thus expect such a proportional increase to apply to Φ_{oc}. Mellor and Blumberg (2004) fitted the (underestimated) flux data shown in Terray et al.'s figure 8 (see fig. 5.8, right panel), with the expression

$$\alpha = 15\frac{C_p}{u_a^*}\exp\left[-\left(0.04\frac{C_p}{u_a^*}\right)^4\right]. \tag{5.7}$$

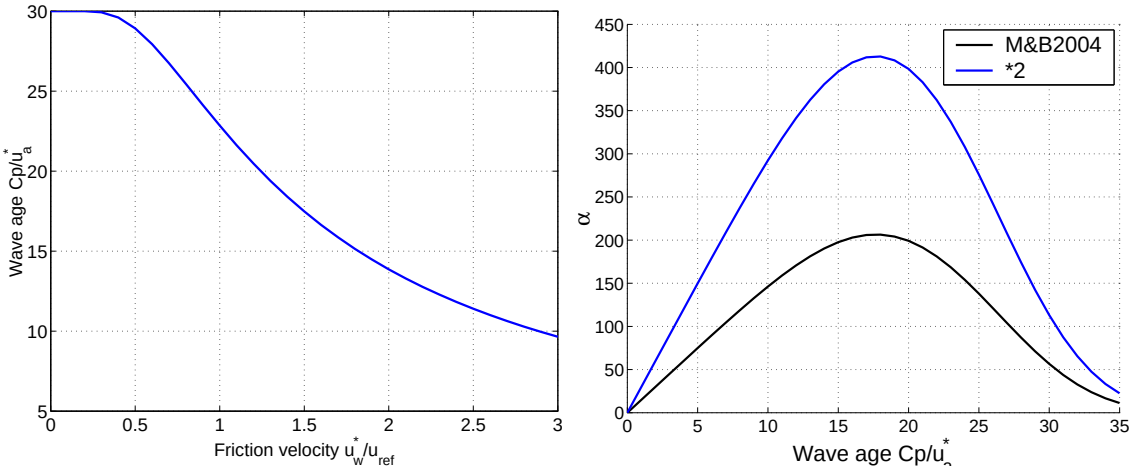

Figure 5.8: (Left panel) Wave age C_p/u_a^* as function of the friction velocity u^*/u_{ref}^*, from our estimation 5.5. (Right panel) Fit of the parameter $\alpha = \Phi_{oc}/u^{*3}$ of the TKE flux from the waves to the ocean, as a function of the wave age C_p/u_a^*. Black line is the fit made by Mellor and Blumberg (2004) over the fig. 8 of Terray et al. (1996), which used the wind-wave growth term of Donelan and Pierson (1987). Blue line is twice the black line, as the present wave model uses a larger growth term.

Janssen et al. (2004) evaluated with the 2003 version of the ECMWF wave model (ECWAM) the monthly mean values of α. As shown by this author, the monthly mean value of this parameter, namely $< \alpha >=< \Phi_{oc}/u^{*3} >$, was of the order of the estimations of Terray et al. (1996), i.e. around $50 - 150$ (Janssen et al., 2004, fig. 14). Our estimations of the monthly mean values of α is of the same order

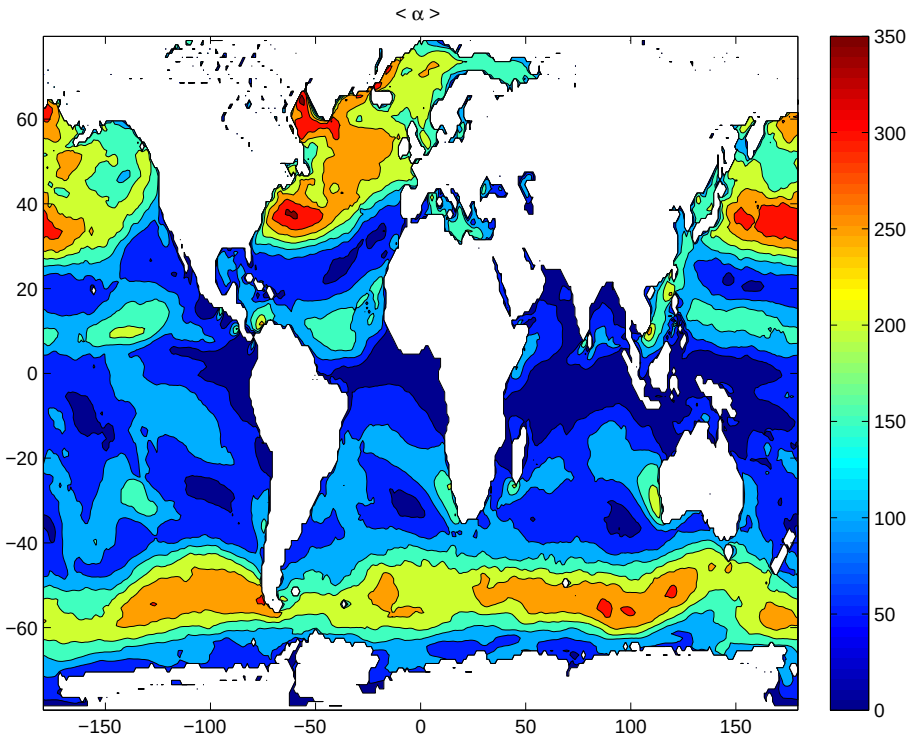

Figure 5.9: Monthly mean parameter $\alpha = \Phi_{oc}/u^{*3}$ of the TKE flux from the waves to the ocean. Values shown are mean values of α, calculated as $< \Phi_{oc}/u^{*3} >$, over January 2004.

than the one of Janssen et al. (2004), also slightly larger, by a factor of roughly 1.5. This might come from a different parameterization of the dissipation in the wave model, since it was later changed by Bidlot et al. (2005). But more importantly, the monthly mean largely hides the variability of the parameter α. Under strong winds, α can reach values as large as 600 (fig. 5.10).

Janssen et al. (2004) further highlighted the spatial distribution of the parameter α, which exhibits a strong latitude dependency, because the wave field is often less developed at mid-latitudes (see their fig. 14). Once again, the wave age is often correlated with the wind stress, leading to a correlation between the parameter α and the wind stress (fig.5.10). Rather than supposing the parameter α constant, a simple parameterization of α as a function of the wind stress would be more accurate. Of course, we again insist that using a wave model to derive these parameters would be better, since such an empirical fit cannot reproduce the full variability due to the wave field. If, as in the previous section, one supposes that the wave-age depends on the wind stress via 5.5, then one could use the formula 5.7 to estimate α directly from the wind stress. It is shown in fig. 5.10 that such estimation of α exhibits the good trend, and we propose its use in an OGCM instead of a fixed value of α. However, as already noted, the formula 5.7 seems to underestimate the wind input

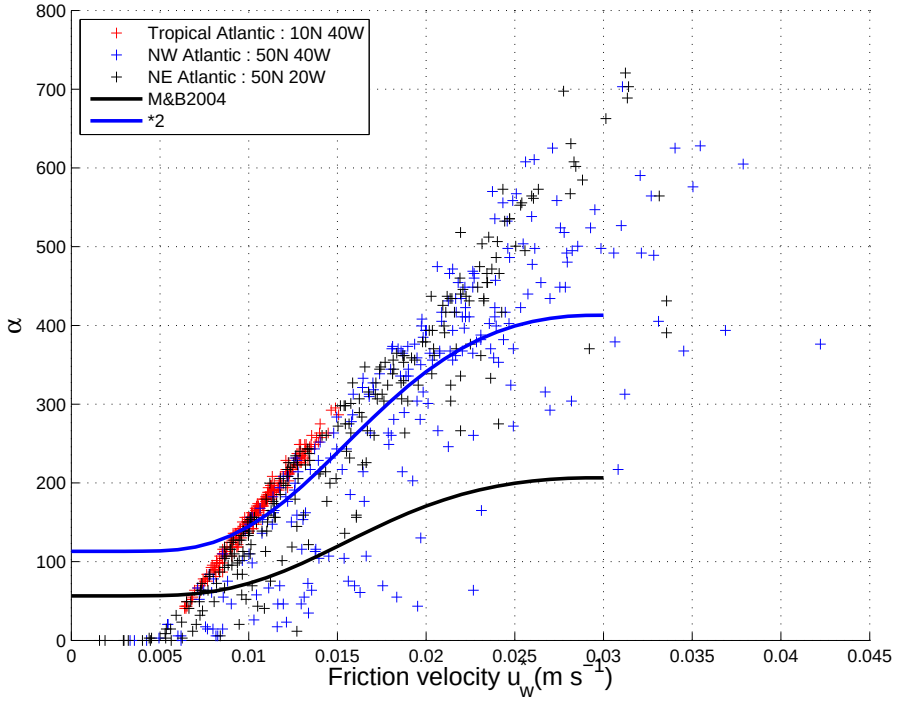

Figure 5.10: Parameter $\alpha = \Phi_{oc}/u^{*3}$ of the TKE flux from waves to the ocean, as a function of the waterside friction velocity u^*. One value corresponds to one wave model output, every 3 hours, for January 2004. Three locations of the North Atlantic are shown, one from the Tropical Atlantic, one from the North-East Atlantic and one from the North-West Atlantic. The parameter α, over 3 hours, largely overtakes the usual values of $50-150$, and so does the daily mean (not shown). Also shown in black solid line is the parameter α by supposing that the wave age is a function of the wind speed (equ. 5.5), and with formula 5.7. As the latter formula appears to underestimate the wind input of our wave model, we have also plotted a blue solid line equal to twice the black line.

of our wave model, by a factor 2 (fig. 5.10).

5.4 The spatial and temporal distribution of mixing events. A direct parameterization from the wind ?

In the previous section, we have evaluated the wave-induced mixing parameters. It was highlighted that most of them are strongly correlated to the wind speed, for instance, the roughness length proportional to the height of the breaking waves, the TKE surface flux, the Stokes drift at the surface. A rough approximation of the wave age as a decreasing function of the wind speed was found to roughly represent the smallest wave development at mid-latitude, due to the short durations of the storms. The main features of the wave field at a global scale were obtained, except the short fetches effects in the west part of the oceans in the westerlies regimes.

However, for costal studies or when details matter, a direct representation of the mixing with the wind is clearly not precise enough. In this section, we wish to insist on the different features of the wave-related mixing compared to a wind-related mixing.

At a global scale, as already mentioned, the highest waves areas are shifted to the west compared to the highest wind speeds areas (fig. 5.6) at mid-latitudes. But such differences also occur at smaller scales. It is obvious, when considering the wave height, that the wave field exhibits less spatial variability than the wind field. Waves act like a spatial filter, damping the high wavenumber components of the wind stress. For instance, the spatial extension of a storm is largely thinner if one considers the track of the high winds areas than the track of the large waves areas (fig. 5.11). Note however that our strict definition of the wind-waves, as waves experiencing a positive forcing from the wind, which might be suited for the breaking-waves, reduces the spreading of the wave-induced mixing compared to the wind-induced mixing.

We also note finally that the waves, in addition to the spatial filtering, constitute a temporal integrator of the wind. This has already been discussed by Janssen et al. (2004), with the analysis of the case of a passing front. Both the momentum and the TKE fluxes to the ocean were shown to slowly relax after the sudden wind change.

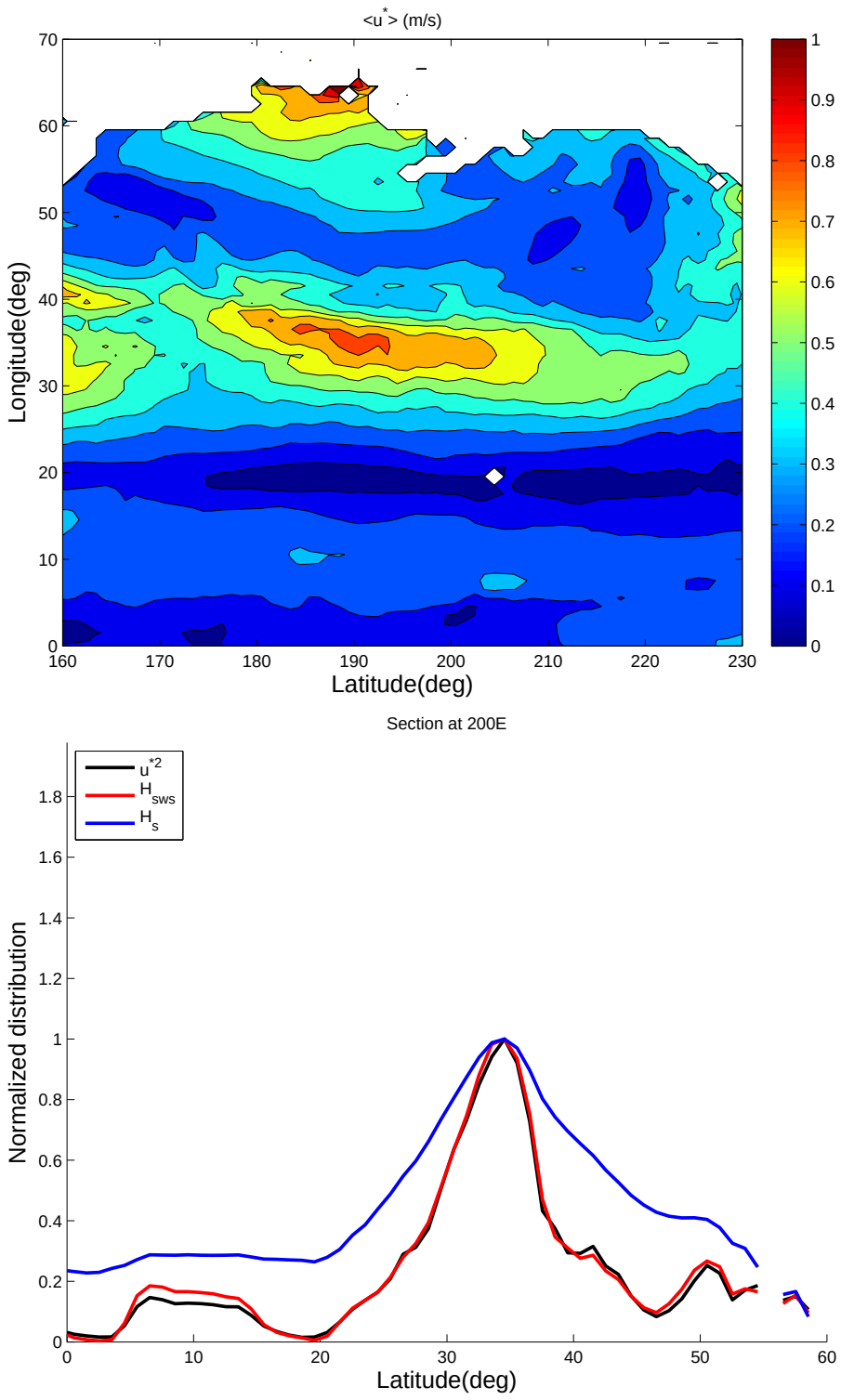

Figure 5.11: (Upper panel) Mean friction velocity $< u^* >$, averaged over the period 8th-10th January 2004. The track of a west propagation storm in the North Pacific is apparent. (Lower panel) Section along the longitude 200E, showing the mean wind stress $< u^{*2} >$, significant wave height of the wind sea $< H_{sws} >$, and the total significant wave height H_s, averaged over the period 8th-10th January 2004. A similar storm in the early spring might constitute an important mixing event and thus largely impact on the mixed layer depth.

5.5 The different kinds of vertical mixing models for applications in OGCMs

There are different kinds of vertical mixing models for the mixed layer of the ocean.

The bulk models consider that the mixed layer is approximately uniform in terms of temperature and velocity. The mixed layer depth evolves then using considerations on buoyancy content, depending on the surface fluxes and the buoyancy just below the mixed layer, and considerations on the TKE, with strong importance of the TKE at the base of the mixed layer to deepen the mixed layer.

On the other hand, there are models which solve a full vertical distribution of the mixed layer. These models generally parameterize the vertical turbulent transports with eddy diffusivities. These diffusivities are determined using the TKE and an additional parameter, such as a mixing length or a dissipation rate.

One of the major drawbacks of these models is their use of eddy viscosity. The turbulent transport is then locally parameterized as a down-gradient flux. This remains true as long as the typical length scale of the important eddies is less than the vertical discretisation of the model. Otherwise, larger but unresolved eddies (because of hydrostatic assumption for example) can carry fluxes which are not necessary down-gradient. For that reason, models have appear which use bulk parameters of the mixed layer in addition to local parametrization. The most widely used model in that class is the K-profile parameterization (KPP) of Large et al. (1994).

5.6 A model to estimate the impact of waves on the mixed layer depth

If, for any physical reason, waves are important in terms of the mixed layer depth, then all the different models presented above might already include, to some extend, an implicit parameterization of the effect of waves on the mixing, because these models are calibrated to give realistic values of the mixed layer depths compared to the observations.

However, we wish here to isolate the wave effects on these models, in order to investigate the mixed layer structure under different wave conditions. We leave aside the bulk models (e.g. Li et al., 1995), because vertical profiles are her under interest, but we also leave aside the KPP model, because the mixed layer depth of the model is calculated using a bulk formulation with the near-surface velocity and density. For instance, any modification of the diffusivity profile close to the surface to better parameterize the wave-breaking, such as the one proposed by McWilliams and

Huckle (2006), modifies the surface velocity and consequently the bulk Richardson number used to calculate the depth of the mixed layer. This modification is not physically sounded, because in this case the TKE flux from the surface dominates the TKE production by the shear of the current.

In contrast, the models with a TKE calculation, including TKE diffusion, appear particularly well designed for our purpose. Also, the wave breaking effects have already been added to such models, with a surface flux of TKE and with a surface roughness length (see part I).

5.7 Preliminary results on the impact of waves on the mixed layer depth

The model used in this section is the model of Noh (1996). This model is quite similar to the model of Gaspar et al. (1990). The main common feature is that the roughness length is equal to the buoyant length scale when the stratification is strong.

However, strange features of the model of Gaspar et al. (1990) were observed. The model was used with a vertical grid of 1 m. Depending on the time step dt, the mixed layer depth obtained under wind mixing ($u^* = 0.001$ m s^{-1}) and stabilizing buoyancy flux (500 W m^{-2}) was either proportional to the Ekman depth (for $dt \simeq 300$ s) or proportional to the Monin-Obukov length (for $dt \simeq 10$ s), this time without any dependency on the Coriolis parameter f. With the low temporal resolution, the thermocline appears only after 1 day, whereas it appears immediately with the high temporal resolution. The reason for this is unclear, but clarification of this might be of importance for a high temporal resolution aiming to include the diurnal cycle with this kind of model.

The model of Noh (1996) was run, as in part I, with a time step $dt = 10$ s. It is shown in fig. 5.12 that the mixed layer depth obtained with this model in the presence of both wind- and wave-induced mixing and a stabilizing buoyancy flux strongly depends on the sea state. Also, in a case without buoyancy flux, the rate of thermocline erosion by the wind- and wave-induced mixing depends on the sea state.

This sensitivity study confirms that, as the near surface mixing depends on the sea state, the mixed layer depth also depends on the wave age. This result is relevant for shallow mixed layers. An estimation of the depths reached by the downward flux of the TKE is around a few times z_0 (see Craig and Banner, 1994, their equ. 27). That downward flux of TKE due to surface waves might then be important for

depths of the order of a few tens of meters.

However at greater depths, other processes might dominate the mixing. Among them one can cite the Langmuir circulations and the current shear due to inertial oscillations (Li et al., 1995). Clearly, more sophisticated models are needed to compare the intensity and the depths those different sources of mixing can reach.

Similarly, the TKE dissipation measurements used to build simple TKE models of the near-surface wave-induced mixing where made at quite shallow depths (e.g. Terray et al., 2000). Extension of these results to greater depths must be checked with other measurements.

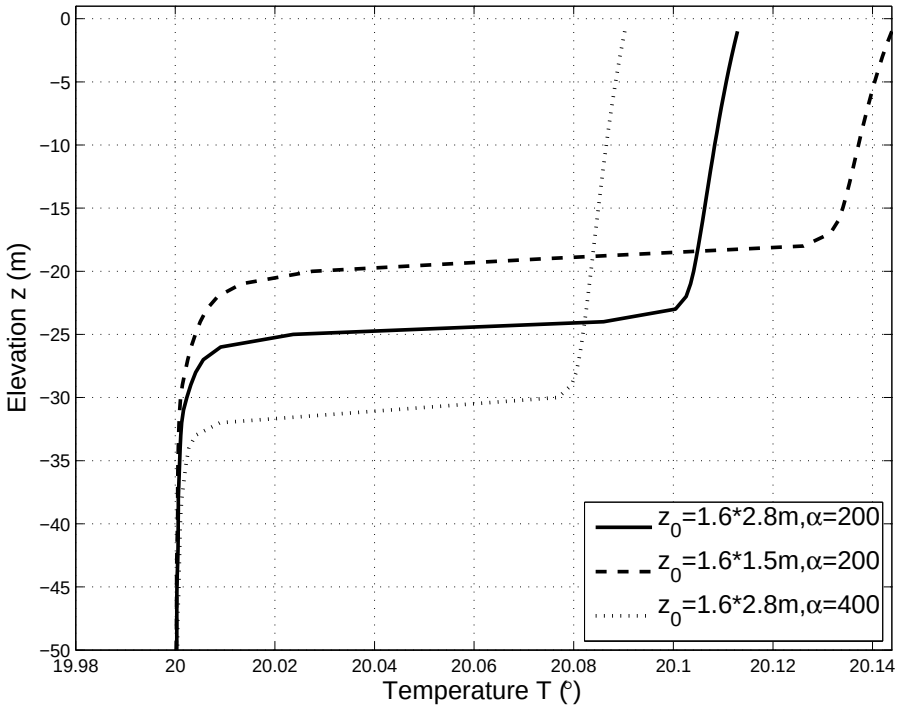

Figure 5.12: Impact of the wave development on the diurnal mixed layer depth, as inferred from a simple TKE model (Noh, 1996; Noh and Kim, 1999). The temperature profile is calculated from an initially uniform temperature of $T = 20°\mathrm{C}$, after 6 hours of stabilizing buoyancy flux of $500\mathrm{Wm}^{-2}$ and of mixing due to a wind of $10\mathrm{ms}^{-1}$ and its associated wind sea. Solid line is for fully developed waves ($H_s = 2.8$ m) while dashed line is for a limiting fetch of 100km ($H_s = 1.5$ m). Those are typical on a continental shelf during onshore and offshore wind events. More developed waves provide more intense near-surface mixing, which creates a deeper diurnal mixed layer. Also shown is the impact of variations of the TKE flux : dotted line is with a parameter α twice as large.

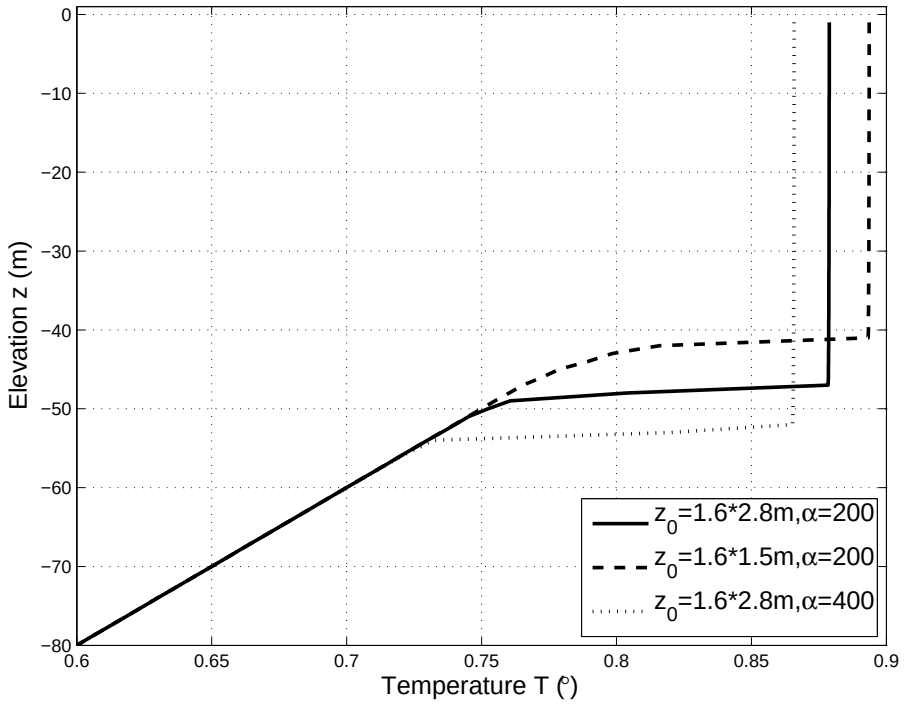

Figure 5.13: Impact of the wave development on the deepening of the mixed layer. The initial temperature is calculated from an initial profile $T = 1 + 0.005z$, where $z \leq 0$, after 120 hours of erosion of the stratification without any buoyancy flux but of with mixing due to a wind of 10ms^{-1} and its associated wind sea. Solid line is for fully developed waves ($H_s = 2.8$ m) while dashed line is for a limiting fetch of 100km ($H_s = 1.5$ m). Also shown is the impact of variations of the TKE flux : dotted line is with a parameter α twice as large. It is shown that the different stages of wave development may have an impact on the thermocline erosion : more intense mixing provides faster erosion.

Part III

Impact of waves on the nearshore and shelf circulation

Chapter 6

Nearshore and Shelf circulation : Introduction

6.1 Introduction

In the previous parts of this thesis, the wave field was supposed horizontally homogeneous. More precisely the gradients of the radiation stresses due to inhomogeneous wave field were supposed much smaller than the leading terms in the steady offshore momentum balance that are the Coriolis force, the Stokes-Coriolis force and the vertical mixing. However, close to the shore, variations of the wave field are much more important, mainly because of shoaling, refraction and intense breaking in the surf zone. Waves are then a dominant forcing of the circulation.

I will attempt here a short review of the theories of wave-forced currents. I will not focus on the feedback of currents on waves, although it is to some extend included in the wave momentum equation (see section 6.4), which is a necessary step to proceed to the analysis of the mean flow.

To fix the ideas, I will take the following example : we suppose that the flow is uniform in the y direction along shore, and we can consider a swell normally incident in the x direction, supposing that a steady state is reached. I will shortly discuss the vertically integrated equations, following Smith (2006*b*). Here I will only show a sketch of the wave-driven momentum equations, with emphasis on the origin of the important terms. The complete GLM equations can be found in chapter 7.

6.2 Total flow equations

The radiation stress tensor is similar to the Reynolds tensor for the turbulent motion : the wave fluctuations induce a flux of momentum. Gradients in the wave field leads

to gradients in that momentum flux, which is equivalent to a force. That force acts on the total momentum $M = \int_{-h}^{\overline{\eta}} \overline{u}^L dz$, which is the sum of the wave Pseudo-momentum $M^w = \int_{-h}^{\overline{\eta}} P dz$ and the mean current momentum $M^m = \int_{-h}^{\overline{\eta}} \widehat{u} dz$.

For our example, the total momentum balance is (e.g Smith, 2006*b*; Ardhuin, 2005)

$$\left\{ \begin{array}{lcll} \frac{\partial M_x}{\partial t} + \frac{\partial UM_x}{\partial x} - fM_y & = & -\left(gD + \frac{p^w}{\rho}\right)\frac{\partial \overline{\eta}}{\partial x} & -\frac{\partial}{\partial x} S_{xx}^{rad} \\ \frac{\partial M_y}{\partial t} + \frac{\partial UM_y}{\partial x} + fM_x & = & & -\frac{\partial}{\partial x} S_{xy}^{rad}, \end{array} \right. \tag{6.1}$$

where p^w is the mean Eulerian pressure, $D = h + \overline{\eta}$ is the water depth and $U = M_x/D$ is the barotropic cross-shore velocity associated with the mass transport. As the waves are normally incident, the 2D form of the radiation stress is

$$S^{rad} = \begin{pmatrix} S^j + C_g M_x^w & 0 \\ 0 & S^j \end{pmatrix}. \tag{6.2}$$

The isotropic part of the radiation stress is called S^j,

$$S^j = gD \frac{kE}{\sinh(2kD)}. \tag{6.3}$$

.

When the waves shoal on the inner-shelf and break in the surf zone, a supplementary forcing arises from the divergence of the radiation stress S^{rad}.

Longuet-Higgins and Stewart (1962) first introduced the concept of the radiation stress, for the vertically integrated equations. This 2D radiation stress concept has been widely used in nearshore modelling (see Battjes (1988) for a review). In these descriptions, the total momentum is obtained, including the wave Pseudo-momentum. The latter is then either ignored or subtracted from a separate computation. Several studies have used vertical extensions of this theory (e.g. Stive and Wind, 1986) or discussed it (Rivero and Arcilla, 1995), most of them in an Eulerian frame. Recently, Mellor (2003) used a vertical coordinate transformation to derive a more rigorous vertical extension of the equations and found supplementary terms for the 3D radiation stress, compared to the previous extensions. Also, the GLM of Andrews and McIntyre (1978*a*) was used by Groeneweg (1999) to obtain 3D equations for the total momentum.

6.3 Mean flow equations

The radiation stress determines the evolution of the total momentum. But part of the radiation stress divergence is in fact a divergence of the wave momentum flux. For various reasons (see section 1.3), it is be advantageous to consider the evolution of the mean flow only, and to parameterize the evolution of the wave pseudo-momentum separately.

The wave momentum equation is

$$\frac{\partial M_x^w}{\partial t} + \frac{\partial}{\partial x}\left(\overline{u} + C_g\right) M_x^w = \frac{1}{\rho}\tau_x^{ds} - \frac{S^j}{D}\frac{\partial D}{\partial x} - M_x^w \frac{\partial \overline{u}}{\partial x}, \tag{6.4}$$

where $-\tau_x^{ds}$ is the momentum released by the waves to the current when they dissipate, and $\overline{u}$ is the advection velocity of waves by the mean flow, equal here to the barotropic velocity $\overline{u} = M_x^m/D$.

The divergence of the radiation stress can then be written as a gradient of a Bernoulli head plus the wave dissipation,

$$\begin{aligned}
\frac{\partial}{\partial x} S_{xx}^{rad} &= \frac{\partial}{\partial x} S^j + \frac{\partial}{\partial x} C_g M_x^w - \frac{\partial M_x^w}{\partial t} \\
&= \frac{\partial}{\partial x} S^j - \frac{S^j}{D}\frac{\partial D}{\partial x} + \frac{1}{\rho}\tau_x^{ds} - M_x^w \frac{\partial U}{\partial x} - \frac{\partial M_x^w}{\partial t} \\
&= D\frac{\partial}{\partial x}\frac{S^j}{D} + \frac{1}{\rho}\tau_x^{ds} - M_x^w \frac{\partial U}{\partial x} - \frac{\partial M_x^w}{\partial t}.
\end{aligned} \tag{6.5}$$

The two remaining terms on the right in 6.5 are an advective term, which combines with the total momentum advection to give a vortex force, and the time variation of the wave field, contained in the time variation of total momentum. One thus obtain from 6.1 and 6.4 an equation for the cross-shore mean flow

$$\left\{\begin{array}{llll}
\frac{\partial M_x^m}{\partial t} & + \frac{\partial}{\partial x}\left(\int_{-h}^{\overline{\eta}} \overline{uu} dz\right) & - f M_y^m = & - \left(gD + \frac{p^w}{\rho}\right)\frac{\partial \overline{\eta}}{\partial x} \qquad + D\frac{\partial}{\partial x}\frac{S^j}{D} \quad + \frac{1}{\rho}\tau_x^{ds} \\
\frac{\partial M_y^m}{\partial t} & + \frac{\partial}{\partial x}\left(\int_{-h}^{\overline{\eta}} \overline{uv} dz\right) & + f M_x^m = & - \left(f + \Omega\right) M_x^w
\end{array}\right. \tag{6.6}$$

This kind of equations for the mean flow have been discussed after the introduction of the radiation stress. Hasselmann (1971) introduced the concept of the interaction stress to denote the part of the radiation stress that acts on the mean flow. Also, the impact of waves on the mean flow, written with a vortex force formulation, have been used for a long time to explain the Langmuir circulation (Craik and Leibovich, 1976; Garrett, 1976). Smith (2006*b*) extended the initial 2D equations of Garrett (1976) to deep water. A 3D extension was made by McWilliams et al. (2004), with a rigorous asymptotic expansion assuming small parameters (essentially

wave slope and current-waves ratio) and using an Eulerian frame (see also Newberger and Allen, 2007*b*). Recently, Ardhuin (2005) tried to derive similar equations for the mean flow while avoiding the ambiguous Eulerian averaging close to the surface. The vertical coordinate change of Mellor (2003) was investigated but left aside for practical reasons (Ardhuin et al., 2007*c*), as well as the GLM equations for the total flow (Ardhuin, 2005). Finally the GLM equations for the mean flow were chosen (Ardhuin et al., 2007*b*), leading to equations similar to those of McWilliams et al. (2004). This similarity between the two different sets of equations can be considered as a verification of the different derivations from the Navier-Stokes equations. It also provides a physical interpretation to the not-quite-Eulerian average of McWilliams et al. (2004).

6.4 On the coupling of waves and current

It must be noted that the equations for the mean flow involve a vortex force and a Bernoulli head. These equations are obtained in the different theory by using the wave momentum equation. In particular, the vortex force comes from the advection of current by the waves. In other words, the equations for the mean flow have included a coupling between the waves and the current. Even if the waves are prescribed as a forcing without any coupling with the current, this coupling is to some extend included via the use of the equations for the mean momentum (see also the discussion in McWilliams et al. (2004) section 14). Lane et al. (2007) showed that the use of the decomposition into a Bernoulli head and a vortex force, although equivalent with the interaction stress representation, incorporates more information on the wave-current coupling, and therefore leads to approximations more consistent than the interaction stress formulations.

6.5 Models and observations

For historical reasons, there has been a gap between the large scale ocean circulation research community and the nearshore community. This gap applies both to the model and to the observations : large scale models usually end at the offshore boundary of the surf zone, where begin the nearshore models. Recently, with the apparition of 3D primitive equations for the wave-driven currents, models have appeared which begin to fill this gap : Delft 3D (Walstra et al., 2001), POM (Newberger and Allen, 2007*a*), Symphonie (Denamiel, 2006), ROMS (Warner et al., 2006, and the present thesis). Also in the field measurements, very few studies have focused on the inner-shelf zone (i.e. between the surf zone, around 10 or 15m deep,

and the mid-shelf, around 50 to 100m). Among them, one can cite the work of Lentz et al. (1999), which showed that the radiation stress is important for the momentum balance even outside the surf zone. However a clear separation of the wave momentum and of the mean momentum is still missing in their discussion, especially when they examine current measurements from fixed towers and interpret them as total flows, whereas the wave part is obviously absent from the measurement. For instance, Lentz et al. (1999) discussed the uncorrelation between the alongshore Coriolis force fu and the forcings, fu being identified to $f(\widehat{u}+P)$. If only the mean flow was measured at the 4m and 8m depth locations, then analysis in term of mean flow momentum balance includes different terms, such as the Stokes-Coriolis term fP which is, as noted by Xu and Bowen (1994), of the order of the measured $f\widehat{u}$ and might partly cancel it. The figure 6.1 illustrates this inconsistency. In passing, the figure 6.2 shows the importance of the Stokes-Coriolis force on the wave-driven velocity profiles.

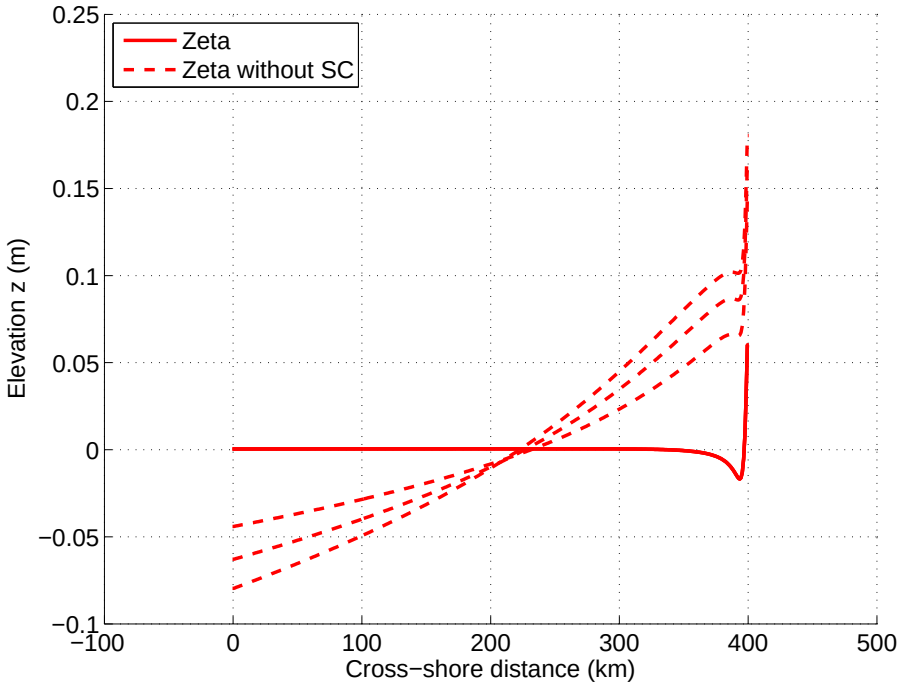

Figure 6.1: Results from a numerical simulation of the alongshore-uniform circulation induced by a normally incident swell (narrow-banded, with an off-shore significant wave height $H_s = 3$m and a period of $T = 12$s) over a narrow shelf (linear beach profile, with a slope of 0.1%). The reader is referred to the next chapter for more details, with a similar simulation but with a different bottom slope, with obliquely incident swell and more focused on the nearshore zone. Here we show the sea surface elevation. The set-down and set-up in the surf zone are visible on the right. Solid line is the surface elevation if the Coriolis and Stokes-Coriolis term are included, dashed line is the one if the Stokes-Coriolis term is omitted but the Coriolis term included. The mean flow is seaward, as it compensates the shoreward mass transport of the waves. If the Stokes-Coriolis term is omitted, as in Lentz et al. (1999), the Coriolis force acts on the mean flow to create an alongshore jet, which increases in time. This jet is in geostrophic equilibrium with a surface elevation. This surface elevation do not appear if the Stokes-Coriolis force is included.

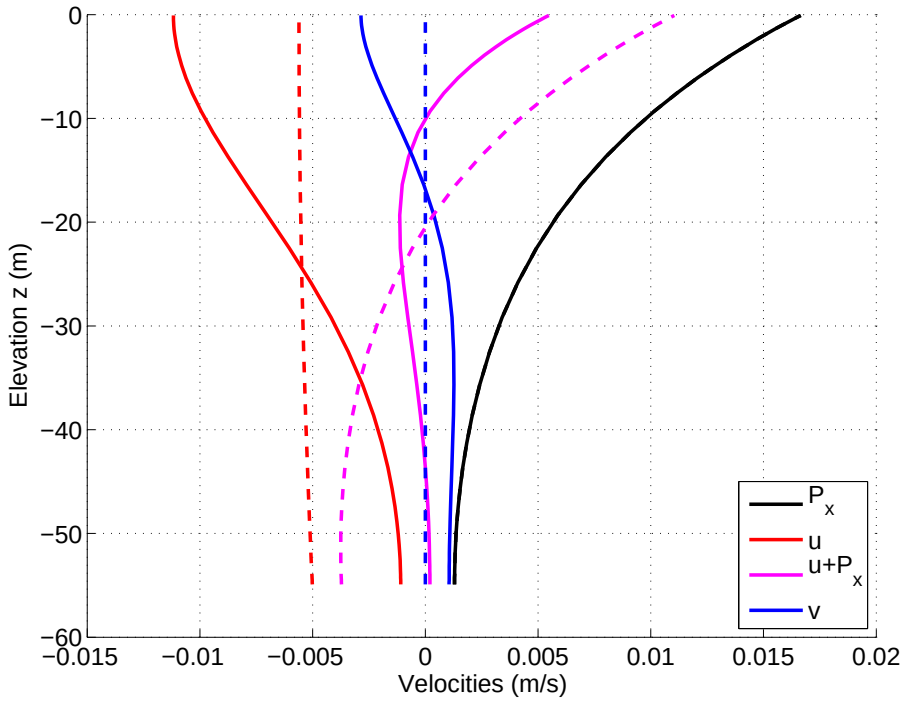

Figure 6.2: Results from the same numerical simulation as described in fig. 6.1. Here we show the vertical profiles of the mean current $(\widehat{u}, \widehat{v})$, of the wave pseudo-momentum P_x and of the Lagrangian drift $\widehat{u} + P_x$. In solid lines, the Coriolis and the Stokes-Coriolis terms are included. In dashed lines, both are omitted. It is shown that the vertically integrated wave mass transport is compensated by the seaward mean flow, but if the two rotation terms are included, the mean flow tends to compensate the wave pseudo-momentum at each depth and not only in terms of vertically integrated transport. This shows the transition between the nearshore dynamics and the off-shore dynamics, as studied in part I.

Chapter 7

Nearshore and Shelf circulation: A two dimensional study

This chapter is written as an independent paper :

Wave-forced shelf circulation using approximate GLM equations

Nicolas Rascle[(1),(2)], Fabrice Ardhuin[(1)]

Paper in preparation
July 2007

[(1)] *Centre Militaire d'Océanographie, SHOM, BREST, France*
[(2)] *Laboratoire de Physique des Océans, Université de Bretagne Occidentale, Brest, France*

Abstract

An approximate Generalized Lagrangian Mean (GLM) is used to modify a primitive equation model, taking into account the effects of surface gravity waves. The model is run here in a simple two-dimensional test case. To the representation of wave effects by a vortex force and a Bernoulli head, the GLM theory adds the effect of the current shear on the Bernoulli head. That latter effect both modifies the wave set-up and the strength of the nearshore circulation. Also, the depth-distributed wave pseudo-momentum modifies the momentum exchange between the waves and the mean flow compared to a surface wave pseudo-momentum often used. Finally, the effect of the current shear on the wave pseudo-momentum is discussed, as well as a finite amplitude effect. The latter give rise to a large shoreward drift under incipient breaking waves, even outside the surf zone.

7.1 Introduction

Recently, three-dimensional primitive equation models have been modified to reproduce the wave-averaged nearshore currents (Walstra et al., 2001; Newberger and Allen, 2007*a*; Denamiel, 2006; Warner et al., 2006). Advantageously such models could be used from the surf zone to the shelf, including the important but still poorly understood inner-shelf zone (Lentz et al., 1999). These models include the effects of wind, waves, Earth rotation and tides, thus filling the gap existing between models of the nearshore circulation, mainly wave-driven, and of the shelf circulation, where waves are often ignored. These models might therefore bring a new framework for applications to sediment transport, pollutants dispersion or larval migrations. They could also be embedded into larger scale costal models, for instance for application to biochemistry of costal waters. Furthermore, by properly representing the wave-current interactions, these models might bring better parameterizations in existing nearshore models (e.g. Apotsos et al., 2007), and should also be relevant for the analysis of rip currents and surf-zone macro-vortices (Büler, 2000; Brocchini et al., 2004).

To achieve such modelling, a number of theoretical developments have been made to derive practical equations for the wave-induced forcing on the wave-averaged mean flow. Among the latest developments are the equations for the Lagrangian flow of Mellor (2003), with a proper averaging of the moving surface, the equations for the mean flow of Newberger and Allen (2007*b*) and the adiabatic equations for the mean flow of McWilliams et al. (2004), with an asymptotical derivation from an Eulerian averaging. However, Ardhuin et al. (2007*c*) reported problems in the derivation of

the equations of Mellor (2003). In order to overcome these limitations, Ardhuin et al. (2007*b*) approximated the Generalized Lagrangian Mean (GLM) equations of Andrews and McIntyre (1978*a*) to derive equations for the mean flow, called GLM2z. The latter equations are generally consistent with the equations of McWilliams et al. (2004), derived for adiabatic small amplitude waves. Both the equations of Ardhuin et al. (2007*b*) and of McWilliams et al. (2004) can be considered as extensions of the work of Newberger and Allen (2007*b*), with some relaxations of hypotheses. Namely, Newberger and Allen (2007*b*) represented the wave mass transport as a surface mass flux. They further assumed that the adiabatic part of the wave forcing was depth-uniform and also neglected effects of the vertical shear of the mean current. Yet no attempt was made to implement the GLM2z equations for the mean flow in a 3D primitive equations model and to describe the physics of the different terms. It is the goal of this paper.

Neither the equations of McWilliams et al. (2004), with an addition of the diabatic processes, nor those of Ardhuin et al. (2007*b*) or those of Newberger and Allen (2007*b*), apply properly in the surf zone, mainly because they all are derived assuming small wave slope. But it is common practice to assume that the physics derived theoretically under simplifications (linear wave theory for instance) is robust to a relaxation of the hypothesis, in spite of known large bias (e.g. Cokelet, 1977). However, because the original GLM equations are exact, the GLM2z equations can be corrected for errors made in the approximations.

Newberger and Allen (2007*a*) have implemented in a 3D primitive equations model the equations of Newberger and Allen (2007*b*) for the wave-forced mean flow. They compared its results to the field measurement obtained during DUCK94. The results in terms of undertow profile and alongshore jet were especially evaluated and a sensitivity study to various parameterizations, such as the bottom boundary layer, the surface layer, the inclusion of a roller model and even the uncertainty on the wave incidence angle, was conducted. Such a sensitivity study will not be repeated here. Instead, and because the GLM2z equations are to some extend similar to those of Newberger and Allen (2007*b*), we shall focus on the physics added by the GLM2z equations. In addition to the results in terms of cross-shore mean undertow and alongshore jet, the results in terms of Lagrangian motion, essential for the practical applications of such nearshore models, will be discussed.

The GLM2z equations are recalled in section 7.2. The simple steady test case for our numerical experiment is described in section 7.3, as well as the wave model and the circulation model. The basic features of the solution, namely the alongshore jet, the set-up of the sea level, the undertow, and the associated momentum and mass equilibrium, are described in section 7.4. The model is compared to the one

of Newberger and Allen (2007*a*) in section 7.5. The effect of the current shear on the Bernoulli head and on the wave pseudo-momentum is discussed in section 7.6. Finally, the non-linear effect on the pseudo-momentum of nearly breaking waves is discussed in section 7.7.

7.2 GLM description of the flow

In this section, the essential features of the work of Ardhuin et al. (2007*b*) are recalled.

7.2.1 Wave / mean flow separation

The flow is averaged using the GLM theory which provides a clean averaging close to the surface and also separates the Lagrangian velocity $\overline{\mathbf{u}}^L$ into a wave pseudo-momentum $\mathbf{P}$ and a quasi-Eulerian mean momentum $\widehat{\mathbf{u}} = \overline{\mathbf{u}}^L - \mathbf{P}$. Below the wave troughs, that separation of $\overline{\mathbf{u}}^L$ into $\widehat{\mathbf{u}} + \mathbf{P}$ is not very different from the separation into Eulerian mean flow $\overline{\mathbf{u}}$ plus Stokes drift $\overline{\mathbf{u}}^S$.

$\mathbf{P}$ can be approximated using linear wave theory for weak current curvature,

$$P_\alpha \simeq \frac{mE}{\sinh^2(kD)} \left[\sigma k_\alpha \cosh(2kz+2kh) + mk_\alpha \sinh(2kz+2kh) \mathbf{u}_\theta \cdot \frac{\partial \overline{\mathbf{u}}}{\partial z} + m^2 \frac{k_\alpha}{\sigma} \sinh^2(kz+kh) \left| \frac{\partial \overline{\mathbf{u}}}{\partial z} \right|^2 \right], \qquad (7.1)$$

where $\mathbf{k}$ is the wavenumber of the wave, σ the intrinsic radian frequency, a the wave amplitude, D the water depth, h the bottom elevation and m a shear correction parameter here set to unity for the sake of simplicity. z is the vertical coordinate oriented upward, $\mathbf{u}_\theta$ is a unit vector in the direction of wave propagation, $\alpha = 1, 2$ is the index for the horizontal components. The last two terms in 7.1 are corrections coming from the vertical shear of the mean flow and are further discussed in section 7.6.1.

The vertical component of the pseudo-momentum is

$$P_3 \simeq -P_\alpha(-h) \frac{\partial h}{\partial x_\alpha} - \int_{-h}^{z} \frac{\partial P_\alpha(z')}{\partial x_\alpha} dz', \qquad (7.2)$$

where the summation is implicit over repeated indices.

7.2.2 Equations of motion

The equations of motion are the following :

1. The mass conservation is

$$\frac{\partial \widehat{u}_\alpha}{\partial x_\alpha} + \frac{\partial \widehat{w}}{\partial z} = 0. \tag{7.3}$$

2. The horizontal momentum equation is

$$\begin{aligned} &\frac{\partial \widehat{u}_\alpha}{\partial t} + \widehat{u}_\beta \frac{\partial \widehat{u}_\alpha}{\partial x_\beta} + \widehat{w}\frac{\partial \widehat{u}_\alpha}{\partial z} + \underbrace{P_3 \frac{\partial \widehat{u}_\alpha}{\partial z}} + \epsilon_{\alpha 3\beta} f \widehat{u}_\beta + \underbrace{\epsilon_{\alpha 3\beta}\left(f+\omega_3\right) P_\beta} \\ = \; & -\frac{1}{\rho}\frac{\partial p^H}{\partial x_\alpha} + D_h + D_v - \underbrace{\frac{\partial}{\partial x_\alpha}\left(S^{\mathrm{J}} + S^{\mathrm{shear}}\right)} - \underbrace{T_\alpha^{\mathrm{wc}} - T_\alpha^{\mathrm{turb}} - T_\alpha^{\mathrm{bfric}}}, \end{aligned} \tag{7.4}$$

where the underbrace highlights the wave forcing terms and where f is the vertical Coriolis parameter, ω_3 is the vertical component of the vorticity,

$$\omega_3 = \frac{\partial \widehat{u}_2}{\partial x_1} - \frac{\partial \widehat{u}_1}{\partial x_2}, \tag{7.5}$$

ρ is the water density, p^H is the hydrostatic pressure, D_h and D_v represent horizontal and vertical diffusions of momentum, respectively. S^J and S^{shear} make up the isotropic Bernoulli's head,

$$S^J = \frac{gkE}{\sinh 2kD}, \tag{7.6}$$

$$\begin{aligned} S^{\mathrm{shear}} = \; & - \; E\left[m\sigma \mathbf{u}_\theta \cdot \frac{\partial \mathbf{u}}{\partial z}(\overline{\zeta})\tanh(kD) + \frac{m^2}{2}\left|\frac{\partial \mathbf{u}}{\partial z}(\overline{\zeta})\right|^2\right] \\ & - \; \int_{-h}^{\overline{\zeta}} \widehat{u}_\alpha \frac{\partial P_\beta}{\partial x_\beta} dz, \end{aligned} \tag{7.7}$$

where g is the gravity and $\overline{\zeta}$ is the mean surface elevation.

3. The vertical momentum equation is reduced to the hydrostatic equilibrium

$$\frac{\partial p^H}{\partial z} = -\rho g, \tag{7.8}$$

because the mean flow is assumed hydrostatic and the wave-modified pressure terms are integrated to provide the terms S^J and S^{shear}.

4. The tracer equation, written here for the temperature T, is

$$\frac{\partial T}{\partial t} + \widehat{u}_\beta \frac{\partial T}{\partial x_\beta} + \underbrace{P_\beta \frac{\partial T}{\partial x_\beta}} + \widehat{w}\frac{\partial T}{\partial z} + \underbrace{P_3 \frac{\partial T}{\partial z}} = F_T + D_T, \tag{7.9}$$

where F_T and D_T are forcing and diffusive terms for the temperature, respectively.

7.2.3 Vertical boundary conditions

The vertical boundary conditions can be prescribed as follows :

1. The surface kinematic condition is

$$\frac{\partial \overline{\zeta}}{\partial t} + \widehat{u}_\alpha \frac{\partial \overline{\zeta}}{\partial x_\alpha} + \underbrace{P_\alpha \frac{\partial \overline{\zeta}}{\partial x_\alpha}} = \widehat{w} + \underbrace{P_3} \quad \text{at} \quad z = \overline{\zeta}. \tag{7.10}$$

2. The surface flux of momentum is

$$\rho_w K_z \frac{\partial \widehat{u}_\alpha}{\partial z} = \tau_\alpha^a - \underbrace{\tau_\alpha^w} - \underbrace{\tau_\alpha^{ds}} \quad \text{at} \quad z = \overline{\zeta}, \tag{7.11}$$

where τ_α^w is the flux of momentum from atmosphere to waves (the form drag), and τ_α^{ds} is the release of wave momentum to the ocean due to breaking, interactions with turbulence or viscous effects. It must be noted that we made no separation between the dissipation occurring at the surface, like the viscous virtual wave stress, and the other processes occurring through the water column. Here, for simplicity, all the momentum coming from the wave field, mainly because of breaking, is injected at the surface of the ocean, although a depth-distributed mean force or depth-distributed intermittent breakers may be more appropriate. However, the dissipation of waves due to bottom friction is omitted in the term τ^{ds} as, if the bottom wave boundary layer (where the streaming occurs) is not resolved, the flux of momentum from the waves ends up directly in the bottom (see Ardhuin, 2006, and Ardhuin et al., 2007*b*, for details).

3. The surface flux of tracer is

$$K_T \frac{\partial T}{\partial z} = Q \quad \text{at} \quad z = \overline{\zeta}, \tag{7.12}$$

where Q is the heat flux at the surface.

4. The bottom kinematic condition is

$$\overline{u}_\alpha^L \frac{\partial(-h)}{\partial x_\alpha} = \widehat{w} + \underbrace{P_3} \quad \text{at} \quad z = -h. \tag{7.13}$$

5. The bottom flux of momentum is

$$\rho_w K_z \frac{\partial \widehat{u}_\alpha}{\partial z} = \tau_\alpha^b \quad \text{at} \quad z = -h, \tag{7.14}$$

where the bottom stress τ_α^b is calculated using a quadratic drag law. The bottom flux of momentum could be modified to include the streaming, without resolving the wave bottom boundary layer, by specifying a non-zero velocity at the bottom of the lowest grid box. However, we have neglected this effect for simplicity and let the latter velocity to zero.

6. The bottom flux of tracer is zero,

$$K_T \frac{\partial T}{\partial z} = 0 \quad \text{at} \quad z = -h. \tag{7.15}$$

7.3 Description of the numerical experiment

We want to estimate the different terms of the GLM2z description, in a simple but realistic case. We consider a west coast, with the x axis to the east and y to the north. The bathymetry is uniform in the alongshore direction. The swell is narrow-banded, with an off-shore significant wave height $H_s = 3$m and a period of $T = 12$s. This swell is obliquely incident from the North-West, with an off-shore angle of 20° relative to the beach normal. The beach profile is linear, with a slope of 1%.

7.3.1 The wave model

The evolution of the wave energy and derived parameters is based on the model of Thornton and Guza (1983), using a coefficient $B = 1$ (i.e. the dissipation in a breaking wave is given by the dissipation in a hydraulic jump of the same height), and a breaking to depth ratio γ given by Battjes and Stive (1985). Recent works suggest that this latter expression is not optimal (Ruessink et al., 2003). However, the main source of error in such a model is probably the underlying assumption of linear wave theory that is used to estimate the energy flux and the momentum flux. We note in particular that in recent investigations with such a model, the set-up is typically underestimated by about 30% at the beach face (Apotsos et al., 2007),

which is of the order of the expected bias on the momentum flux (Cokelet, 1977, figure 18).

7.3.2 The ocean model

The Regional Ocean Modelling System (ROMS) has been modified to resolve the GLM2z equations. More details are given in Appendix A. The temperature and salinity are supposed homogeneous. For the sake of simplicity, the turbulence closure scheme is discarded and the vertical viscosity and diffusivity are set to $K_z = 0.03\text{m}^2\text{s}^{-1}$. The bottom stress is quadratic, with a roughness length of 10^{-3}m. No wave-current interactions were used in the bottom boundary layer. The Coriolis parameter is set to $f = 10^{-4}$. The horizontal resolution of the model is 10m, extending to 4km off shore, and the model has 40 vertical σ-levels. The baroclinic time step is dt= 3s, and there are 50 barotropic time steps of the 2D submodel within one baroclinic step. The ocean is initially at rest and the swell is added until a steady state is reached. Close to the shore, the steady state is reached after a few hours, whereas off-shore the Coriolis force gives a longer spin-up time.

7.4 Analysis of the solution

7.4.1 Description of the different terms of the equations

The wave forcing acts on the mean flow in different ways. As the wave pseudo-momentum is shoreward outside the surf zone and zero at the coast, the wave mass transport is convergent in the surf zone. As a consequence the mass conservation drives a vertically averaged mean flow seaward.

The radiation stress adds on this effect and is composed of two parts : a Bernoulli's head $-\nabla(S^J + S^{\text{shear}})$ and the diabatic part τ^{ds}. The latter comes from the release of momentum by the waves as they break, modelled here for simplicity as a surface stress. The cross-shore component of this stress is responsible for the set-up of the sea level in the surf zone (fig. 7.1), and it also drives a vertical recirculation of the mean flow, shoreward close to the surface and seaward close to the bottom, the undertow (fig. 7.2). The alongshore component of this stress drives an alongshore jet southward.

The term $-\nabla S^J$ is depth-uniform and corresponds to the modification of the pressure by the waves. It only modifies the sea level. As the wave shoal outside the surf zone, this term is negative (fig. 7.3) and therefore yields a set-down (fig. 7.1). In the surf zone, this term becomes positive and gives a slight set-up.

The term $-\nabla S^{\text{shear}}$ will be described in the section 7.6.2.

The vortex force $-\epsilon_{\alpha 3\beta}\omega_3 P_\beta$ has a component in the cross-shore direction, $\omega_3 P_y$, which tends to concentrate the jet. But this component is very small and negligible compared to the others cross-shore forcings (fig. 7.3). On the contrary the alongshore component $-\omega_3 P_x$ is a dominant alongshore forcing (fig. 7.6, upper panel). It drives the jet closer to the shore and in its absence the jet tends to widen (fig. 7.5).

The Stokes-Coriolis term $-\epsilon_{\alpha 3\beta} f P_\beta$ is the only term subsisting off-shore, where the horizontal gradients are small (Hasselmann, 1970). The momentum balance then writes

$$\epsilon_{\alpha 3\beta} f \widehat{u}_\beta + \epsilon_{\alpha 3\beta} f P_\beta = \frac{\partial}{\partial z} K_z \frac{\partial \widehat{u}_\alpha}{\partial z}. \tag{7.16}$$

This Stokes-Coriolis force is oriented to the right of the wave propagation and drives a vertically-integrated mass transport which cancels the vertically integrated waves mass transport. In the limit of a Stokes length scale $\delta_s = 1/2k$ much larger than the Ekman scale $\delta_e = \sqrt{2K_z/f}$, this cancellation is perfect at each depth, $\widehat{\mathbf{u}} = -\mathbf{P}$ (see for example Polton et al., 2005, their equ. 13). For the swell considered here, $\delta_s = 18$m and $\delta_s = 24$m, so that this trend is hardly perceptible in a water depth of 40m, our off-shore maximum depth.

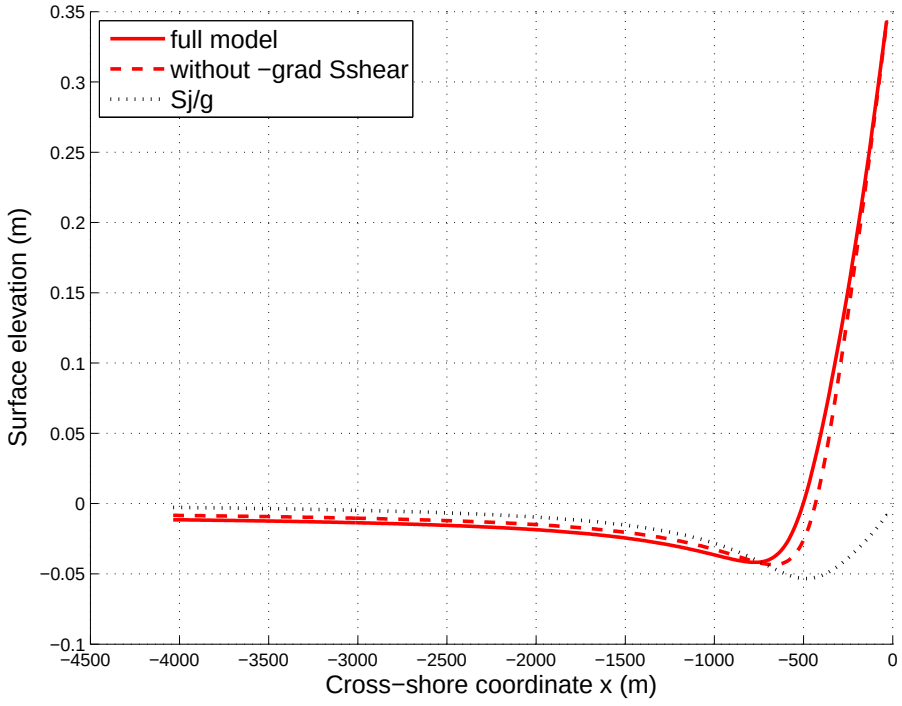

Figure 7.1: Sea surface elevation with and without the term $-\nabla S^{\text{shear}}$. The dotted line is the surface set-down from an adiabatic equilibrium between the pressure gradient and the wave-induced pressure gradient $-\partial S^J/\partial x$.

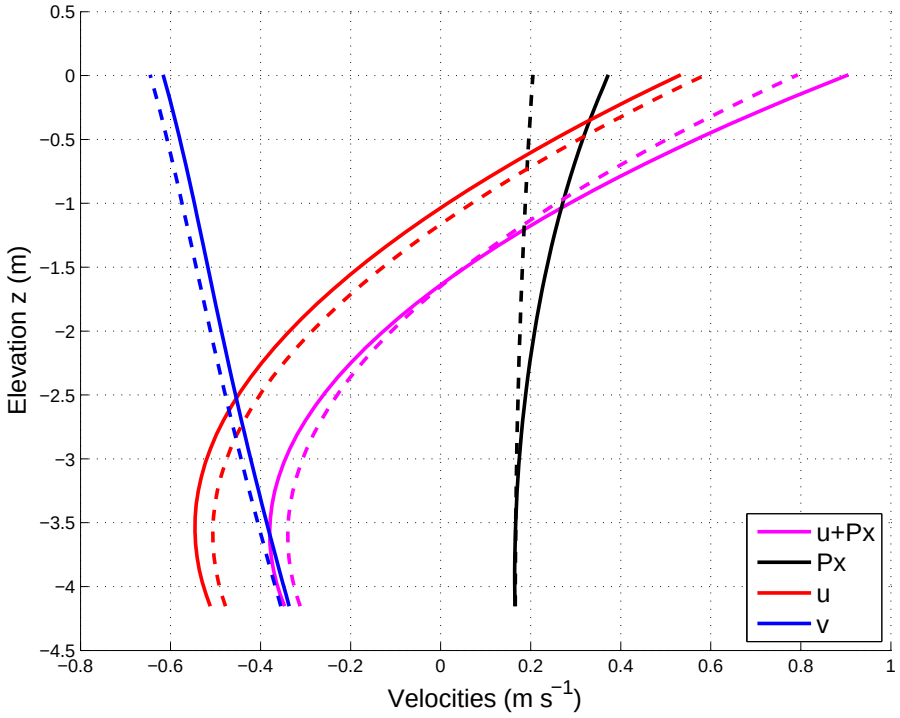

Figure 7.2: Vertical profile of the velocities at 400m off-shore (in the surf zone). Solid lines are the full model whereas dashed lines are the model without the effect of the current shear on the wave pseudo-momentum $\mathbf{P}$.

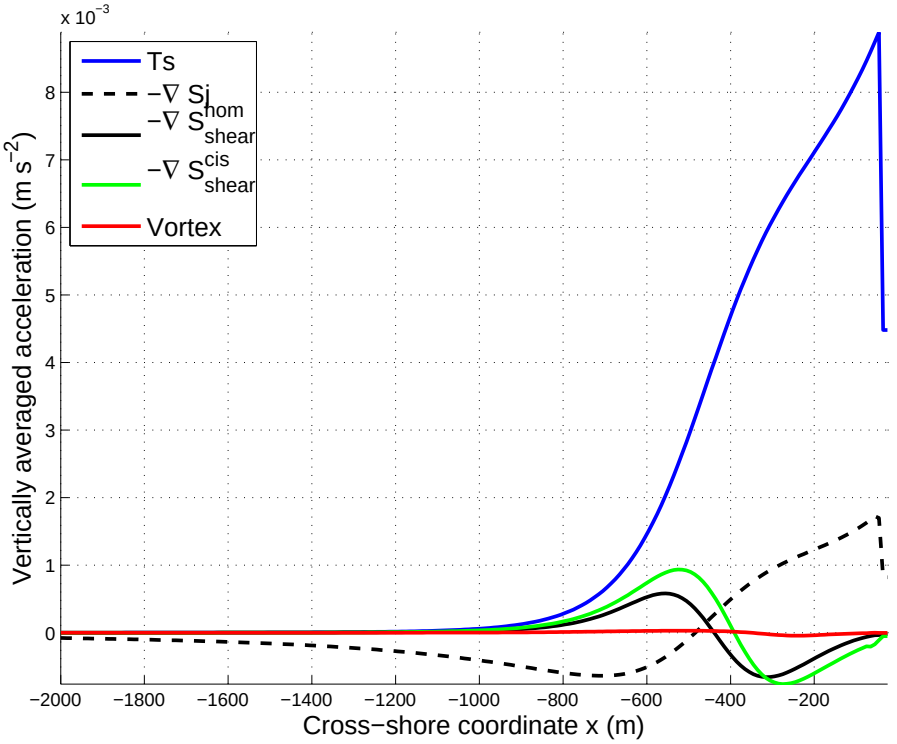

Figure 7.3: Depth-averaged values of the different cross-shore wave-induced forcing terms of the mean flow, the surface momentum flux T_x^{ds}, the 3 terms of the Bernoulli's head $-\partial/\partial x S^J$, $-\partial/\partial x S^{\text{shear}}_{hom}$ and $-\partial/\partial x S^{\text{shear}}_{cis}$, and the vortex force.

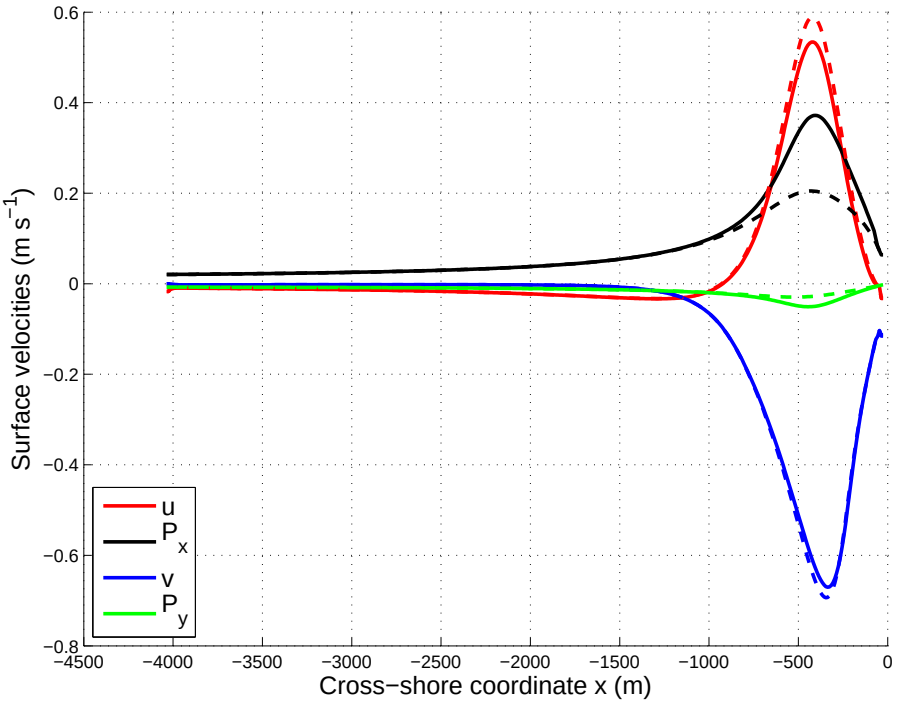

Figure 7.4: Surface velocities. Solid lines are the full model whereas dashed lines are the model without the effect of the current shear on the wave pseudo-momentum $\mathbf{P}$.

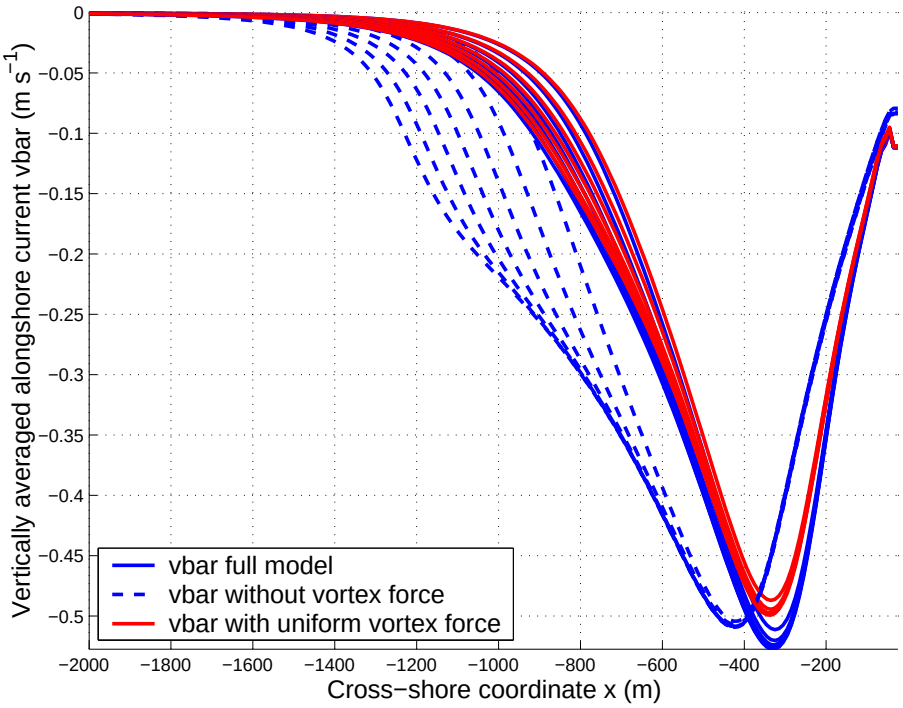

Figure 7.5: Vertically averaged alongshore velocity ($\overline{\widehat{v}}$). Solid blue line is for the full model, dashed blue line is without the vortex force and red with an uniform vortex force as in NA07. Without the vortex force, the alongshore jet is further off-shore and wider. The time scale for the establishment of the jet is about 3-4 hours without the vortex force, with a slow widening of the jet.

7.4.2 Description of the alongshore and cross-shore momentum balance

The alongshore momentum balance is detailed in fig. 7.6, upper panel. The main equilibrium is between the southward surface stress, which drives the southward alongshore jet, and the northward bottom stress. But that main equilibrium is modified by the vortex force, which shifts the jet towards the shore, and the advection.

The cross-shore momentum balance is detailed in fig. 7.6, lower panel. The cross-shore momentum balance is between the shoreward surface stress and the pressure gradient. This creates the set-up of the sea level, which is slightly enhanced by the shoreward bottom stress. The advection also slightly modifies this equilibrium.

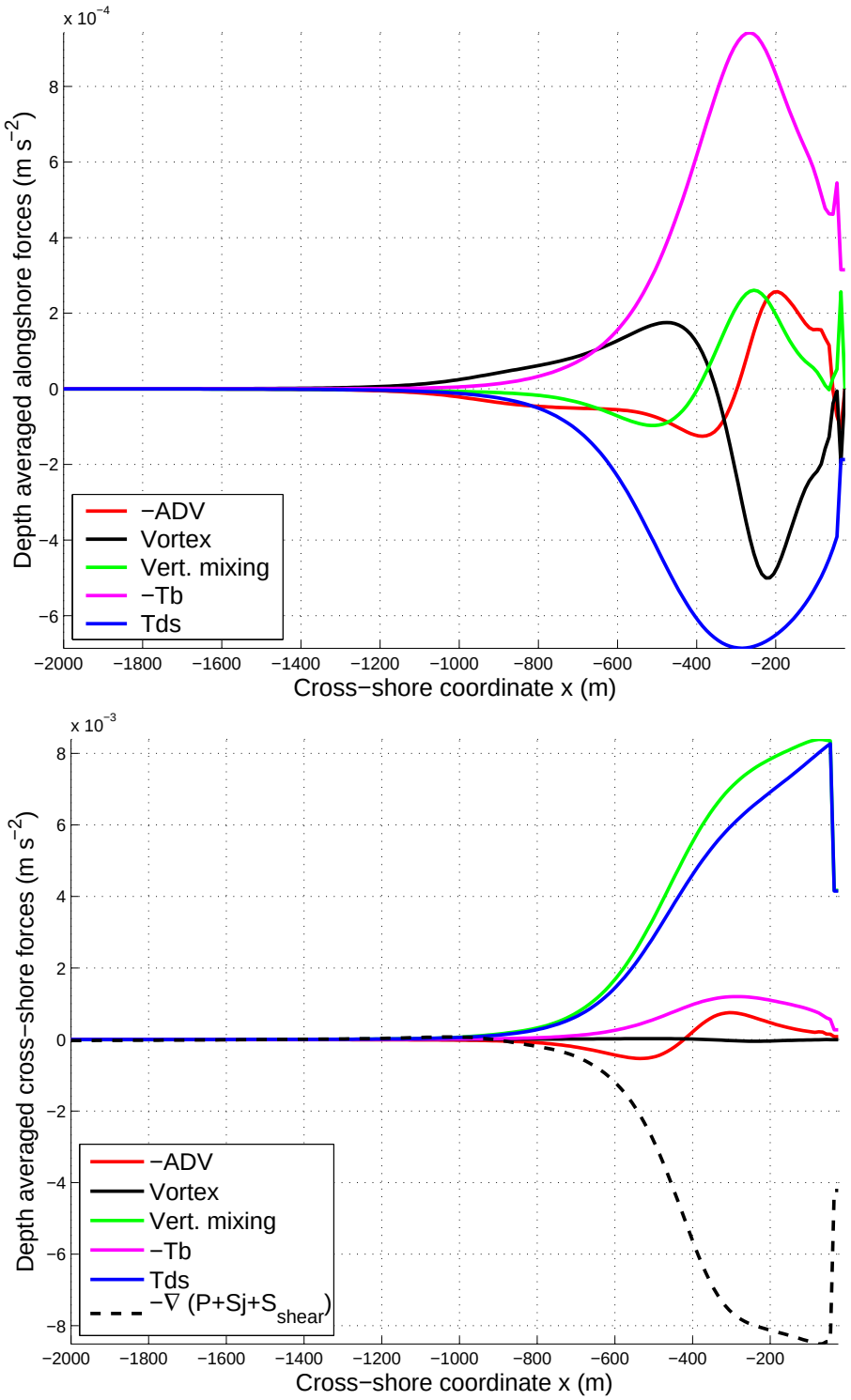

Figure 7.6: (Upper panel) Depth-averaged values of the terms in the alongshore momentum balance, the advection, the vortex force and the vertical mixing. The latter is split into the surface stress T_y^{ds} plus the bottom stress $-T_y^b$. (Lower panel) Depth-averaged values of the terms in the cross-shore momentum balance, the advection, the vortex force,the vertical mixing, split into surface stress T_x^{ds} and bottom stress $-T_x^b$, and the pressure plus Bernoulli's head gradient $-\partial/\partial x\left(p^H/\rho + S^J + S_{hom}^{\text{shear}} + S_{cis}^{\text{shear}}\right)$.

7.5 Comparison with the model of Newberger and Allen (2007*a*)

If we omit the effects of the vertical shear of the mean flow on the wave pseudo-momentum (see section 7.6 and if we omit S^{shear}, the GLM2z equations are then very close to the equations of NA07. The Earth rotation is omitted in NA07. Its effect has been discussed above. The only other differences remain in the description of the Lagrangian mass flux and in the vertical distribution of the vortex force.

7.5.1 Lagrangian mass flux in NA07

Consistently with the Eulerian description of Hasselmann (1971), all the Stokes transport occurs at the surface in the work of NA07. This leads to the following equations,

$$\frac{\partial \widehat{u}_\alpha}{\partial x_\alpha} + \frac{\partial \widehat{w}}{\partial z} = 0, \tag{7.17}$$

with

$$\widehat{w} = \frac{\partial \overline{\zeta}}{\partial t} + \widehat{u}_\alpha \frac{\partial \overline{\zeta}}{\partial x_\alpha} + w_0 \quad \text{at} \quad z = \overline{\zeta}, \tag{7.18}$$

where

$$w_0 = \frac{\partial}{\partial x_\alpha} \int_{-h}^{\overline{\zeta}} P_\alpha dz. \tag{7.19}$$

These equations are consistent with the GLM2z equations, but the advections are different.

In NA07, the momentum and tracer advections are

$$\frac{\partial \widehat{u}_\alpha}{\partial t} + \widehat{u}_\beta \frac{\partial \widehat{u}_\alpha}{\partial x_\beta} + \widehat{w} \frac{\partial \widehat{u}_\alpha}{\partial z}, \tag{7.20}$$

$$\frac{\partial T}{\partial t} + \widehat{u}_\beta \frac{\partial T}{\partial x_\beta} + \widehat{w} \frac{\partial T}{\partial z}, \tag{7.21}$$

respectively, while the corresponding GLM2z advections are

$$\frac{\partial \widehat{u}_\alpha}{\partial t} + \widehat{u}_\beta \frac{\partial \widehat{u}_\alpha}{\partial x_\beta} + \widehat{w} \frac{\partial \widehat{u}_\alpha}{\partial z} + P_3 \frac{\partial \widehat{u}_\alpha}{\partial z}, \tag{7.22}$$

$$\frac{\partial T}{\partial t} + \widehat{u}_\beta \frac{\partial T}{\partial x_\beta} + \widehat{w} \frac{\partial T}{\partial z} + P_\beta \frac{\partial T}{\partial x_\beta} + P_3 \frac{\partial T}{\partial z}. \tag{7.23}$$

Clearly, the last term in 7.22 and the last two terms in 7.23 are omitted in NA07.

The implementation of the NA07 equations in a 3D primitive ocean model is much more simple than the GLM2z equations because, in the interior, the wave pseudo-momentum is zero and there is only the mean flow.

On the contrary, in the GLM equations, the difference between the quasi-Eulerian momentum advection and the Lagrangian tracer advection complicates the implementation in a model with a mode baroclinic / barotropic mode splitting. In fact, the time-stepping of such model is designed to conserve both the integral and the constancy of the tracer. For that, one needs to compute a mass conservation and an advection in perfect agreement. This would be simple for the barotropic variables, but as the tracer is advected once a baroclinic step, one needs it for the baroclinic variables and this leads to a fairly complicated time-stepping (Shchepetkin and McWilliams, 2003). The addition of different advections for the momentum and for the tracer further complicates the time-stepping.

Instead, complications like those do not arise with a wave pseudo-momentum at the surface, as in NA07. It is then of practical importance to clarify whether or not the physical simplification of the NA07 description leads to strong differences compared to the GLM formulation.

The tracer horizontal advection by the waves is obviously missing in NA07 (the last but one term in 7.23). Therefore we will not discuss further the tracer but we will focus on the quasi-Eulerian current.

In the momentum equation 7.20 of NA07, one vertical advection term is missing compared to 7.22. This term modifies the momentum exchange between the waves and the mean flow. That momentum exchange, corresponding to the mass exchange between the waves and the mean flow, can be seen when vertically integrating the equation for the momentum advection,

$$\frac{\partial \widehat{u}_\alpha}{\partial t} + \widehat{u}_\beta \frac{\partial \widehat{u}_\alpha}{\partial x_\beta} + \widehat{w} \frac{\partial \widehat{u}_\alpha}{\partial z} \tag{7.24}$$

transforms, using the mass conservation, to the flux form

$$\frac{\partial \widehat{u}_\alpha}{\partial t} + \frac{\partial \widehat{u}_\beta \widehat{u}_\alpha}{\partial x_\beta} + \frac{\partial \widehat{w} \widehat{u}_\alpha}{\partial z}, \tag{7.25}$$

which in turns integrates to

$$\frac{\partial}{\partial t} \int_{-h}^{\overline{\zeta}} \widehat{u}_\alpha dz + \frac{\partial}{\partial x_\beta} \int_{-h}^{\overline{\zeta}} \widehat{u}_\beta \widehat{u}_\alpha dz + w_0 \widehat{u}_\alpha(\overline{\zeta}). \tag{7.26}$$

The last term represents the exchange of momentum due to the exchange of mass. The velocity of the water mass exchanged between the wave part and the mean flow is the velocity of the surface current.

On the contrary, the mass flux is distributed through the whole water column in the GLM2z equations, leading to the corresponding exchange of momentum

$$\begin{aligned} & \frac{\partial \widehat{u}_\alpha}{\partial t} + \widehat{u}_\beta \frac{\partial \widehat{u}_\alpha}{\partial x_\beta} + \widehat{w} \frac{\partial \widehat{u}_\alpha}{\partial z} + P_3 \frac{\partial \widehat{u}_\alpha}{\partial z} \\ = & \frac{\partial \widehat{u}_\alpha}{\partial t} + \frac{\partial \widehat{u}_\beta \widehat{u}_\alpha}{\partial x_\beta} + \frac{\partial \widehat{w} \widehat{u}_\alpha}{\partial z} + \frac{\partial P_3 \widehat{u}_\alpha}{\partial z} + \widehat{u}_\alpha \frac{\partial P_\beta}{\partial x_\beta}, \end{aligned} \tag{7.27}$$

where we have used the mass conservation (7.3). The velocity of the water mass exchanged between the wave part and the mean flow at the depth z is in the GLM description the velocity of the current at the depth z. Equ. 7.27 integrates to

$$\begin{aligned} & \frac{\partial}{\partial t} \int_{-h}^{\overline{\zeta}} \widehat{u}_\alpha dz + \frac{\partial}{\partial x_\beta} \int_{-h}^{\overline{\zeta}} \widehat{u}_\beta \widehat{u}_\alpha dz \\ + & \frac{\partial \overline{\zeta}}{\partial x_\beta} \widehat{u}_\alpha(\overline{\zeta}) P_\beta(\overline{\zeta}) - \frac{\partial(-h)}{\partial x_\beta} \widehat{u}_\alpha(-h) P_\beta(-h) + \int_{-h}^{\overline{\zeta}} \widehat{u}_\alpha \frac{\partial P_\beta}{\partial x_\beta} dz. \end{aligned} \tag{7.28}$$

The last three terms can be rewritten as

$$\begin{aligned} & \frac{\partial \overline{\zeta}}{\partial x_\beta} \widehat{u}_\alpha(\overline{\zeta}) P_\beta(\overline{\zeta}) - \frac{\partial(-h)}{\partial x_\beta} \widehat{u}_\alpha(-h) P_\beta(-h) + \int_{-h}^{\overline{\zeta}} \widehat{u}_\alpha \frac{\partial P_\beta}{\partial x_\beta} dz \\ = & \frac{\partial}{\partial x_\beta} \int_{-h}^{\overline{\zeta}} \widehat{u}_\alpha P_\beta dz - \int_{-h}^{\overline{\zeta}} \frac{\partial \widehat{u}_\alpha}{\partial x_\beta} P_\beta dz \\ = & u_{A\alpha} \frac{\partial}{\partial x_\beta} \int_{-h}^{\overline{\zeta}} P_\beta dz + \frac{\partial u_{A\alpha}}{\partial x_\beta} \int_{-h}^{\overline{\zeta}} P_\beta dz - \int_{-h}^{\overline{\zeta}} \frac{\partial \widehat{u}_\alpha}{\partial x_\beta} P_\beta dz \end{aligned} \tag{7.29}$$

where we have defined the advection velocity

$$u_{A\alpha} \int_{-h}^{\overline{\zeta}} P_\beta dz = \int_{-h}^{\overline{\zeta}} \widehat{u}_\alpha P_\beta dz. \tag{7.30}$$

Supposing that the last two terms in equ. 7.29 approximately cancel, equ. 7.28 becomes

$$\frac{\partial}{\partial t} \int_{-h}^{\overline{\zeta}} \widehat{u}_\alpha dz + \frac{\partial}{\partial x_\beta} \int_{-h}^{\overline{\zeta}} \widehat{u}_\beta \widehat{u}_\alpha dz + u_{A\alpha} \frac{\partial}{\partial x_\beta} \int_{-h}^{\overline{\zeta}} P_\beta dz, \tag{7.31}$$

which we can compare to equ. 7.26. Clearly, when the current is vertically uniform, the momentum exchange between the wave part and the mean flow is similar between the GLM and NA07. This is not true in the case of a vertically sheared mean current, because of the different locations of the mass exchange.

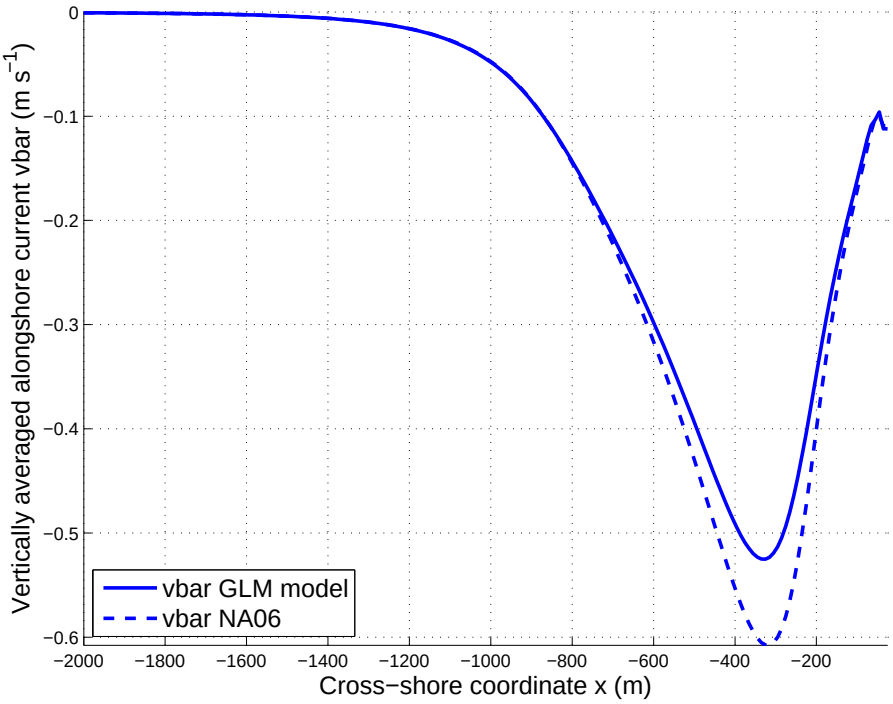

Figure 7.7: Vertically averaged cross-shore velocity ($\overline{\widehat{v}}$). Solid blue line is for the full GLM model, dashed blue line is with the source of mass at the surface as in NA07. Without the surface source of mass, the alongshore jet is stronger.

As an illustration of this, the cross-shore vertically integrated source of momentum has a different sign if the mass exchange is at the surface, where the mean current is shoreward, compared to that if the mass exchange is distributed through the water column, where the current is essentially seaward (fig. 7.8, middle panel). However this term is of little impact on the cross-shore velocities because the advection is not a dominant term in the cross-shore momentum balance (fig. 7.6, lower panel). On the contrary, the alongshore vertically integrated source of momentum is stronger with a surface wave mass flux than with a depth-distributed one, because the alongshore jet is stronger at the surface (fig. 7.9, middle panel). As the advection is important in the alongshore momentum balance (see fig. 7.6, upper panel), the resulting alongshore jet is stronger with the NA07 description of the source of mass than with the GLM description, as shown in fig. 7.7.

In short, the numerical results do not show many differences in the cross-shore circulation between the wave mass flux as in NA07 and as in GLM2z. However in the alongshore direction, the jet is stronger with a surface mass flux. This difference is due to the different momentum exchange between the waves and the mean flow in the two descriptions. That momentum exchange is important compared to the

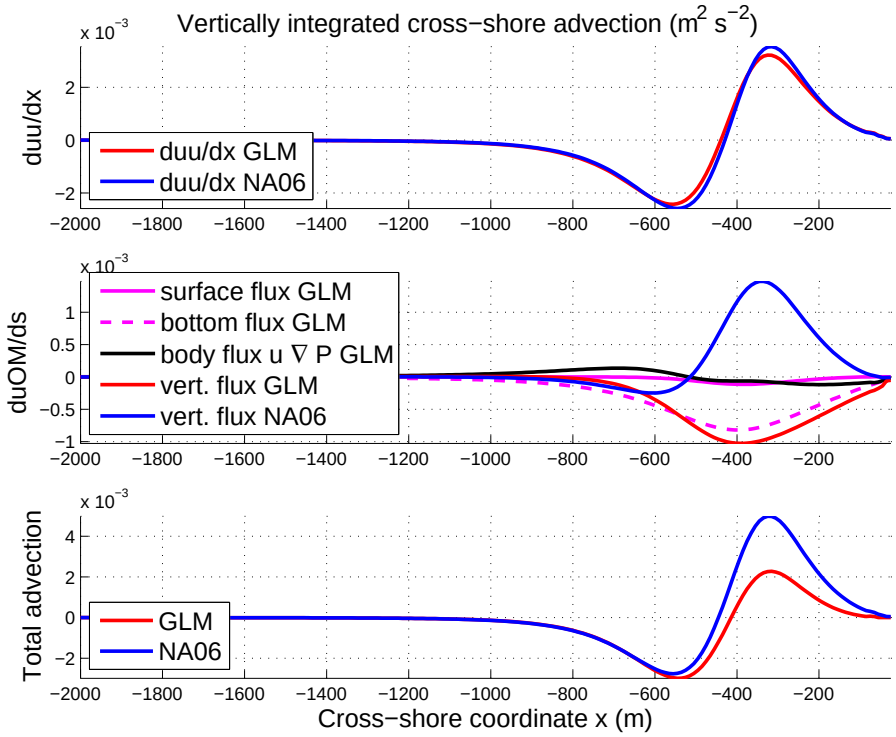

Figure 7.8: Vertically integrated cross-shore advection as in equ. 7.26 and 7.28. Upper panel is the horizontal advection ($-\frac{\partial}{\partial x}\int \widehat{u}\widehat{u}dz$), middle panel is the vertically integrated source of momentum ($-w_0\widehat{u}(\overline{\zeta})$ for NA07, $-\frac{\partial\overline{\zeta}}{\partial x_\beta}\widehat{u}(\overline{\zeta})P_\beta(\overline{\zeta}) + \frac{\partial(-h)}{\partial x_\beta}\widehat{u}(-h)P_\beta(-h) - \int_{-h}^{\overline{\zeta}}\widehat{u}\frac{\partial P_\beta}{\partial x_\beta}dz$ for the GLM). Lower panel is the total advection. The cross-shore advection is modified by the different locations of the source of mass and by the associated different momentum exchanges.

horizontal advection. But the advection is negligible in the cross-shore momentum balance, whereas it is not in the alongshore balance, which explains why the alongshore velocities are modified between the two descriptions, whereas the cross-shore velocities are not.

7.5.2 Vortex force in NA07

Another difference is that the vortex force is vertically uniform in the work of NA07 ($\epsilon_{\alpha 3\beta}\overline{P_\beta}\partial\overline{\widehat{v}}/\partial x$, where the overline denotes a depth averaging), whereas it is depth distributed according to the Stokes drift profile and to the vertical vorticity profile in the GLM equations ($\epsilon_{\alpha 3\beta}P_\beta\partial\widehat{v}/\partial x$). The figure 7.5 shows the alongshore jet change in strength and position with a depth-uniform vortex force. As the vertical vorticity and the pseudo-momentum are both maximum at the surface, ignoring their depth distributions results in a slight underestimation of the depth-averaged vortex force and neglects the torque of the vortex force. However, for the averaged circulation

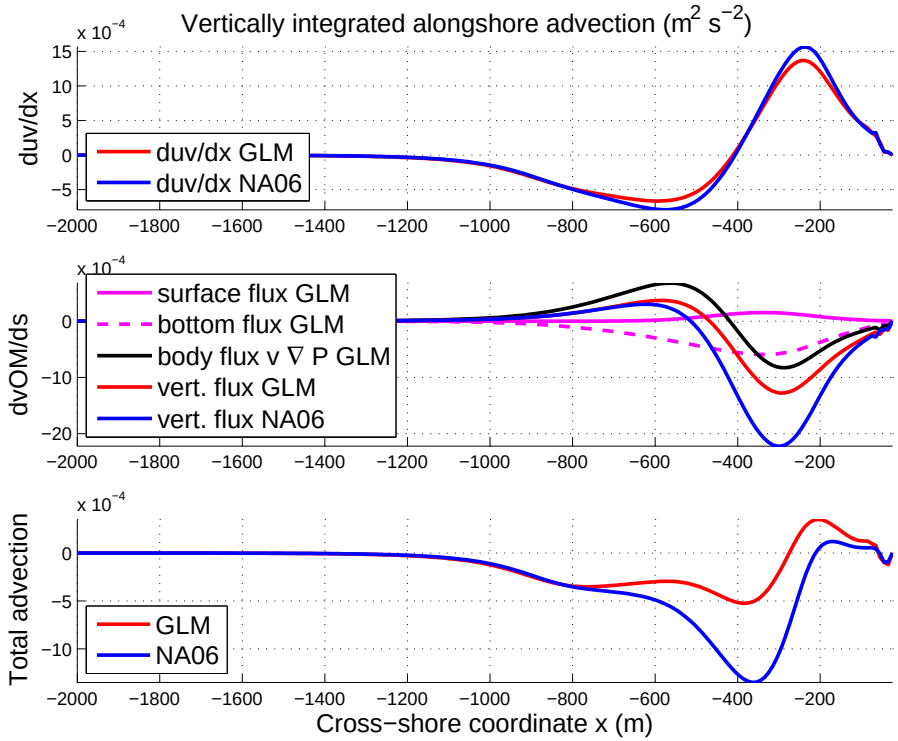

Figure 7.9: Same as fig. 7.8 but for the alongshore advection. The alongshore advection is modified by the different locations of the source of mass and by the associated different momentum exchanges.

studied here, these changes are quite modest.

7.6 Effect of the current shear

7.6.1 Effect of the current shear on the Stokes drift

Without mean current, the orbits of the particles during a wave period are not exactly closed. The corresponding mean drift in the wave propagation direction is the wave pseudo-momentum $\mathbf{P}$. In the presence of a mean current shear, the orbits are further modified, and so is the wave pseudo-momentum $\mathbf{P}$. This results in the last two terms in 7.1.

The wave pseudo-momentum is modified by the current shear with terms of the order of $1/\sigma \partial u/\partial z$. These terms become important when approaching the surf zone, where $\partial u/\partial z$ is of the order of σ (fig. 7.4). The wave pseudo-momentum without current shear effect is almost depth-uniform for linear waves in shallow water. On the contrary the wave pseudo-momentum is largely enhanced with the current shear effect and exhibits a strong surface shear, related to the shear of the cross-shore current in the surf zone (fig. 7.2). As a consequence of the enhanced

shoreward wave mass transport, the undertow and all the vertical recirculation are also enhanced.

7.6.2 Effect of the current shear on the radiation stress

When taking into account the current shear effect, 2 supplementary terms $-\nabla S_{hom}^{\text{shear}}$ and $-\nabla S_{cis}^{\text{shear}}$ add to the Bernoulli's head $-\nabla S^J$ of the radiation stress.

The first term, $-\nabla S_{hom}^{\text{shear}}$ where

$$S_{hom}^{\text{shear}} = -E\left[\sigma \mathbf{u}_\theta \cdot \frac{\tau^{ds}}{\rho K_z} tanh(kD) + \frac{1}{2}\left|\frac{\tau^{ds}}{\rho K_z}\right|^2\right], \tag{7.32}$$

is vertically uniform and thus only modifies the set-up equilibrium. This term is negative close to the shore as both the wave amplitude and the surface stress due to the wave dissipation are decreasing toward the shore (fig. 7.3). However in the off-shore part of the surf zone, the surface stress is increasing toward the shore so that $-\nabla S_{hom}^{\text{shear}} > 0$. As a consequence of this term, the transition from set-down to set-up is displaced further off-shore and the slope of the surface is reduced (fig. 7.1).

The second term, $-\nabla S_{cis}^{\text{shear}}$ where

$$S_{cis}^{\text{shear}} = -\int_{-h}^{\overline{\zeta}} \widehat{u}_\alpha \frac{\partial P_\beta}{\partial x_\beta} dz, \tag{7.33}$$

is vertically non uniform and so drives both a barotropic response and a vertical recirculation. At any depth z, $S_{cis}^{\text{shear}}(z)$ increases from the offshore value, reaches a maximum inside the surf zone and then decreases approaching the beach. The effect of the depth integral of $-\nabla S_{cis}^{\text{shear}}$ on the set-up is then similar to the effect of $-\nabla S_{hom}^{\text{shear}}$, i.e. an off-shore displacement of the transition from set-down to set-up and a reduction of the slope of the set-up. Also, $-\nabla S_{cis}^{\text{shear}} = 0$ at the surface and its absolute value increases with depth. The resulting torque amplifies the undertow recirculation close to the beach whereas it is opposed to this recirculation in the offshore part of the surf zone.

7.7 Effect of the wave non-linearity

The linear wave theory have been used for simplicity in many nearshore circulation models. This is justified because the wave energy, the wave phase speed or the group speed are roughly well predicted with linear theory. The vertically integrated wave pseudo-momentum is also well approximated (Rascle and Ardhuin, manuscript in preparation). Without the current shear effects, the linear theory predicts a wave pseudo-momentum almost depth-uniform in shallow water $kD \ll 1$. On the contrary, the pseudo-momentum of a steep wave, with non-linear effects, exhibits significant deviations from the linear theory, becoming strongly sheared close to the surface. In this section, we will evaluate the impact of such phenomenon on our steady test case.

In Rascle and Ardhuin (manuscript in preparation), it is proposed a correction of the linear wave pseudo-momentum $\mathbf{P}$, based on a numerical fully non-linear solution of the potential flow over a flat bottom. This formula is valid for nearly breaking wave. In order to obtain a first upper-bound of this effect, we will thus suppose that all the waves reach this limiting steepness.

First, for comparison with the linear theory used above, the wave energies, amplitudes and wavenumbers are not corrected from the linear values. The vertically integrated mass transport of the waves is then similar between the linear and the non-linear calculations, only the vertical profile of $\mathbf{P}$ has been changed. It is shown in fig. 7.10 that the strongly sheared pseudo-momentum does not modify the quasi-Eulerian current, as long the vertically integrated transport is not modified. If, as inferred from the non-linear analysis, the transport is enhanced by 10 or 20%, the undertow is enhanced proportionally, but the other features of the circulation, such a the strength of the jet and the set-up level, remain unmodified (not shown).

The main modification from the wave non-linearity is on the shoreward Lagrangian drift close to the surface. This drift is largely enhanced, by a factor 2 (fig. 7.10). This is especially important immediately seaward of the surf zone (around 1000 m offshore, fig. 7.10), were the shoreward mean current is small.

Probably even more important is the significant larger momentum flux associated with finite amplitude waves. Cokelet (1977) reported potential errors up to 40% in the radiation stress component S^{xx}. Such errors may be even larger in the presence of a vertical current shear. That effect may be computed with the original GLM equations and parameterized with a bias in the surface stress τ_{ds} and in the Bernoulli head S^J. It may then account for most of the errors in set-up predictions (Apotsos et al., 2007).

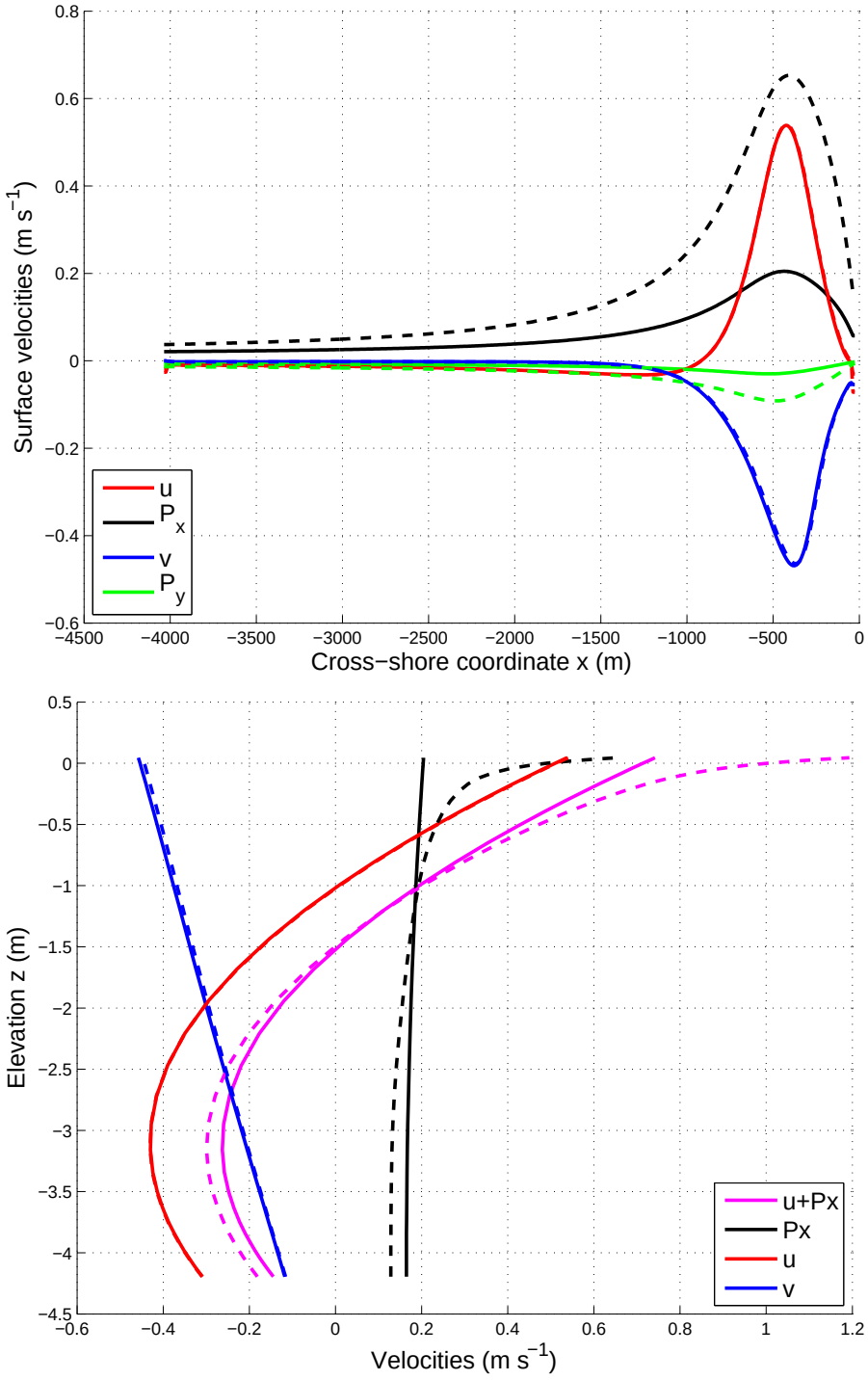

Figure 7.10: (Upper panel) Surface velocities. (Lower panel) Vertical profile of the velocities at 400m off-shore (in the surf zone).. Solid lines are the full model without the current shear effect on the wave pseudo-momentum $\mathbf{P}$, i.e. with the Stokes drift from the linear wave theory, whereas dashed lines are the model with the non-linear effect on the wave pseudo-momentum $\mathbf{P}$.

7.8 Conclusion

In this paper, the recently derived GLM2z equations for the wave-forced mean flow (Ardhuin et al., 2007*b*) have been used in a simple two-dimensional steady simulation of the shelf circulation, including the surf-zone . These approximate GLM equations represent the adiabatic wave-forcing with a vortex force and a Bernoulli head. Such representation has already been studied and compared to measurements in Newberger and Allen (2007*a*). But the GLM2z formulation further brings new physics compared to this previous description :

Firstly, in the GLM description, the wave pseudo-momentum is distributed along the vertical. Consequently, a diverging horizontal wave pseudo-momentum within the water column modifies the momentum exchange between the wave part and the mean flow, compared to a diverging surface wave pseudo-momentum as in Newberger and Allen (2007*a*). This effect is equal to the addition of the vortex force due to the vertical wave pseudo-momentum P_3, as derived in McWilliams et al. (2004).

Secondly, the GLM description includes current shear effects. The current shear modifies the Bernoulli head via two terms. The first one is depth-uniform while the second one creates a small torque, enhancing the vertical recirculation of the surf zone onshore of the jet and reducing it offshore. Both terms shift the transition from set-down to set-up slightly seaward. The current shear also enhances the wave pseudo-momentum, and thus the undertow strength.

Thirdly, the GLM formalism, by separating the mean flow and the wave pseudo-momentum, enables an analysis of the Lagrangian drift within and outside of the surf-zone. In this regard, the effect of the wave non-linearity in increasing the vertical shear of the wave pseudo-momentum, is discussed. This effect strongly alters the description of the near-surface drift, giving rise to surface shoreward velocities as large as $0.5\mathrm{m\,s^{-1}}$. This is believed to be especially important in the proximity of the surf-zone, because steep waves might then be able to drive buoyant objects towards the surf zone.

The present work only gave a simple illustration of the wave-forced circulation on the shelf inferred from the GLM2z equations. However, it is believed that this equations might give more spectacular results in modelling more complex wave-current interactions phenomena, such as the rip currents or the macro-vortices.

7.9 Appendix A : modification of ROMS to solve the GLM equations

7.9.1 Equations in σ-coordinates

Equations solved in ROMS are equations for the "semi-Lagrangian" flow $(\widehat{u}_\alpha, \overline{w}^L)$, i.e. for the quasi-Eulerian flow $(\widehat{u}_\alpha, \widehat{w})$ plus the vertical pseudo-momentum $(0, P_3)$. They are transformed into σ-coordinates using $H_z \equiv \frac{\partial z}{\partial s}$.

The mass conservation writes

$$\frac{\partial H_z}{\partial t} + \frac{\partial H_z \widehat{u}_\alpha}{\partial x_\alpha} + \frac{\partial H_z \overline{\Omega}^L}{\partial s} + \underbrace{\frac{\partial H_z P_\alpha}{\partial x_\alpha}} = 0, \tag{7.34}$$

where we have defined the Lagrangian sigma-vertical velocity

$$\overline{\Omega}^L = \frac{1}{H_z}\left(\widehat{w} - \frac{\partial z}{\partial t} - \widehat{u}_\alpha \frac{\partial z}{\partial x_\alpha} - P_\alpha \frac{\partial z}{\partial x_\alpha}\right). \tag{7.35}$$

The time derivative and advective terms in momentum equation transform to the stretched coordinates to

$$\frac{1}{H_z}\left[\frac{\partial H_z \widehat{u}_\alpha}{\partial t} + \frac{\partial H_z \widehat{u}_\alpha \widehat{u}_\beta}{\partial x_\beta} + \frac{\partial H_z \widehat{u}_\alpha \widehat{\Omega}}{\partial s} + \widehat{u}_\alpha\left(H_z \frac{\partial P_\alpha}{\partial x_\alpha} - \frac{\partial z}{\partial x_\alpha}\frac{\partial P_\alpha}{\partial s}\right)\right], \tag{7.36}$$

which writes alternatively

$$\frac{1}{H_z}\left[\frac{\partial H_z \widehat{u}_\alpha}{\partial t} + \frac{\partial H_z \widehat{u}_\alpha \widehat{u}_\beta}{\partial x_\beta} + \frac{\partial H_z \widehat{u}_\alpha \widehat{\Omega}}{\partial s} + \widehat{u}_\alpha\left(\frac{\partial H_z P_\alpha}{\partial x_\alpha} + \frac{\partial H_z\left(\overline{\Omega}^L - \widehat{\Omega}\right)}{\partial s}\right)\right], \tag{7.37}$$

where we have defined

$$\widehat{\Omega} = \frac{1}{H_z}\left(\widehat{w} - \frac{\partial z}{\partial t} - \widehat{u}_\alpha \frac{\partial z}{\partial x_\alpha}\right), \tag{7.38}$$

the "semi-Lagrangian" sigma-vertical velocity. Note that a correction arise from the advective form to the flux form of the equations due to the diverging "semi-Lagrangian" velocity field. This correction does not appear in the time derivative and advection of the tracer because it is advected by the Lagrangian velocity which is a non-divergent field :

$$\frac{1}{H_z}\left[\frac{\partial H_z T}{\partial t} + \frac{\partial H_z \widehat{u}_\beta T}{\partial x_\beta} + \underbrace{\frac{\partial H_z P_\beta T}{\partial x_\beta}} + \frac{\partial H_z \overline{\Omega}^L T}{\partial s}\right]. \tag{7.39}$$

The boundary conditions are simplified :

$$\overline{\Omega}^L = 0 \quad \text{at} \quad s = 0 \quad \text{and} \quad s = -1, \tag{7.40}$$

7.9.2 Depth-integrated equations

The depth average of a quantity A is given by

$$\overline{A} = \frac{1}{D}\int_{-1}^{0} H_z A ds, \tag{7.41}$$

where $D = \eta(t,x,y) + h(x,y)$ is the total depth of the water column.

The depth average of the mass conservation (equ. 7.34) is

$$\frac{\partial \eta}{\partial t} + \frac{\partial D\overline{\widehat{u}_\alpha}}{\partial x_\alpha} + \underbrace{\frac{\partial D\overline{P_\alpha}}{\partial x_\alpha}} = 0, \tag{7.42}$$

where we have used

$$\frac{\partial H_z}{\partial t} = \frac{\partial \eta}{\partial t} \tag{7.43}$$

and the boundary conditions 7.10 and 7.13.

The fast evolving part of the 2D equation must be separated from another part that will remain constant during the barotropic steps. The depth average of the momentum advection (equ. 7.37) is

$$\begin{aligned}\frac{\partial D\overline{\widehat{u}_\alpha}}{\partial t} + \frac{\partial D\overline{\widehat{u}_\alpha \widehat{u}_\beta}}{\partial x_\beta} + \widehat{u}_\alpha(0)P_\beta(0)\frac{\partial z}{\partial x_\beta} - \widehat{u}_\alpha(-1)P_\beta(-1)\frac{\partial z}{\partial x_\beta} \\ + \int_{-1}^{0} \widehat{u}_\alpha \left(\frac{\partial H_z P_\alpha}{\partial x_\alpha} + \frac{\partial H_z \left(\overline{\Omega}^L - \widehat{\Omega}\right)}{\partial s} \right) ds,\end{aligned} \tag{7.44}$$

where we have used

$$\widehat{\Omega} = \overline{\Omega}^L + \frac{1}{H_z}\left(P_\alpha \frac{\partial z}{\partial x_\alpha}\right). \tag{7.45}$$

No simple expression of the 2D momentum advection in terms of the fast evolving 2D velocities $\overline{\widehat{u}_\alpha}$ was found. Therefore the fast part was left as in the original ROMS formulation,

$$\frac{\partial D\overline{\widehat{u}_\alpha}}{\partial t} + \frac{\partial D\overline{\widehat{u}_\alpha}\,\overline{\widehat{u}_\beta}}{\partial x_\beta} + \epsilon_{\alpha 3\beta} f D\overline{\widehat{u}_\beta} = -\left(\frac{D}{\rho_w}\frac{\partial \overline{p}^H}{\partial x_\alpha}\right)_{fast} + D_{\overline{u}} - \tau_b + R_{slow}, \tag{7.46}$$

with R_{slow} containing the baroclinic to barotropic contribution, i.e. the remaining part of the 2D equations (terms like $\overline{\widehat{u}_\alpha \widehat{u}_\beta} - \overline{\widehat{u}_\alpha}\ \overline{\widehat{u}_\beta}$) left constant during the fast barotropic time step.

The modifications in the 2D sub-model are then restricted to the 2D free surface evolution. All the terms added by the wave forcing are kept constant during a baroclinic time step.

7.10 Complements : Numerical implementation of the GLM equations in ROMS

7.10.1 Modification of the time stepping to include the diverging mean flow

Hereinafter, we do not make any distinction between Stokes drift, noted *ust*, and the horizontal wave pseudo-momentum **P**. The main routines of a time step, old ones and new ones, are described below, following their order of appearance during the baroclinic step (in **step**).

- **ana_stokes** At the beginning of each baroclinic time step, the Stokes drift *ust* at t_n is calculated.

- **set_HUVstokes** The lateral mass flux of the grid box due to the Stokes drift $Huson = \frac{Hz\,ust}{n}$ is calculated correspondingly to $Huon = \frac{Hz\,u}{n}$ as calculated in **set_HUV**

- **omega** $W = \frac{Hz\overline{\Omega}^L}{mn} = -div\,Huon - div\,Huson$ is the σ-vertical velocity of the Lagrangian flow. Additional vertical velocity $W_{stqe} = \frac{Hz\widehat{\Omega}}{mn}$ for the mean flow advection is calculated using $W_{stqe} = W + \frac{ust}{n}\frac{\partial z}{\partial \xi}$.

- **prsgrd** not modified

- **rhs3d** W_{stqe} is used for the vertical advection, as well as terms for the correction to the flux form (last term in equ. 7.37)

- **pre_step3d** In the preliminary step, the pseud-compressible algorithm for the calculation of Hz_{half} uses the divergence of $W + Huon + Huson$ consistently with the modified mass conservation. The tracer is calculated at time $n + \frac{1}{2}$ (predictor) including the horizontal advection by the Stokes drift. The advance of the velocity u has not been changed. In particular, the barotropic mass flux of the velocity u at time $t_{n+\frac{1}{2}}$, unknown at this moment, is set as in the original version as an interpolation of the velocity at time t_n and time t_{n-1}.

- **u3dmix** not modified

- **step2D** The barotropic submodel is modified using *ustbar* the vertical average of the Stokes drift. The free surface evolves using the divergence of the lateral mass flux of the Stokes drift $Duston = \frac{Dustbar}{n}$ in addition to the mass flux of the Eulerian velocity $Duston = \frac{Dubar}{n}$.

ustbar, as *ust*, is kept constant during the barotropic time steps, but as the free surface evolves, *Duston* also evolves. Consequently, *Duston* is averaged in time as *Duon* for the purpose of coupling with the 3D equation, leading to $DUST\_avg1$ and $DUST\_avg2$ to correct the Stokes velocity at time step t_{n+1} and $t_{n+\frac{1}{2}}$, respectively.

- **set_HUV2** As well as for the velocity, the Stokes drift *ust* is corrected using the result $DUST\_avg2$ from the 2D submodel and the flux *Huson* at time $t_{n+\frac{1}{2}}$ is computed.

- **omega** treated above

- **prsgrd** not modified

- **rhs3d** treated above

- **step3d_uv1** not modified

- **step3d_uv2** *ust* at time t_n is corrected using $DUST\_avg1$ from the 2D submodel. Then *ust* is interpolated back to time $t_{n+\frac{1}{2}}$ using the values of t_n, t_{n+1} and the result $DUST\_avg2$ from the 2D submodel. Finally *Huson* at time $t_{n+\frac{1}{2}}$ is recomputed.

- **omega** treated above

- **step3d_t** Finalize the advance of the tracer with *div Huson* added to *div Huon*+ *div W*. All values at time $t_{n+\frac{1}{2}}$ were then corrected to give a tracer time step both conservative and constancy preserving, as in the original ROMS code.

7.10.2 Discussion

The development of ROMS to solve the GLM equations is much complicated due to the body source of mass when one solves only the "semi-Lagrangian" velocities $(\widehat{u}, \widehat{w} + P_3) = (\widehat{u}, \overline{w}^L)$. The flow is then divergent, as well as the horizontal wave part P_x, and the tracer is not advected in a similar way. A sketch of the "semi-Lagrangian" equations is

$$\left\{\begin{array}{rrll} & \frac{\partial \widehat{u}}{\partial x} + \frac{\partial \overline{w}^L}{\partial z} & + \frac{\partial P_x}{\partial x} & = 0, \\ \frac{\partial \widehat{u}}{\partial t} + & \widehat{u}\frac{\partial \widehat{u}}{\partial x} & + \overline{w}^L \frac{\partial \widehat{u}}{\partial z} & = F_u, \\ \frac{\partial T}{\partial t} + & (\widehat{u} + P_x)\frac{\partial T}{\partial x} & + \overline{w}^L \frac{\partial T}{\partial z} & = F_T, \\ & \frac{\partial \overline{\zeta}}{\partial x} + \widehat{u}\frac{\partial \overline{\zeta}}{\partial z} & + P_x \frac{\partial \overline{\zeta}}{\partial x} & = \overline{w}^L \quad \text{at} \quad z = \overline{\zeta}. \end{array}\right. \tag{7.47}$$

This approach was chosen because we originally omitted the vertical component of the wave pseudo-momentum P_3. On the contrary, the introduction of the vertical wave pseudo-momentum P_3, consistently with the Stokes pseudo-vertical velocity of McWilliams et al. (2004), separates the mean flow and the wave part such that both are non-divergent. Does this lead to much simpler equations to implement ? The equations of motion become :

$$\left\{\begin{array}{rcl} \frac{\partial \widehat{u}}{\partial x}+\frac{\partial \widehat{w}}{\partial z} & = & 0, \\ \frac{\partial \widehat{u}}{\partial t}+\widehat{u}\frac{\partial \widehat{u}}{\partial x}+\widehat{w}\frac{\partial \widehat{u}}{\partial z} & = & F_u - P_3\frac{\partial \widehat{u}}{\partial z}, \\ \frac{\partial T}{\partial t}+\widehat{u}\frac{\partial T}{\partial x}+\widehat{w}\frac{\partial T}{\partial z} & = & F_T - P_x\frac{\partial T}{\partial x} - P_3\frac{\partial T}{\partial z}, \\ \frac{\partial \overline{\zeta}}{\partial x}+\widehat{u}\frac{\partial \overline{\zeta}}{\partial z}+P_x\frac{\partial \overline{\zeta}}{\partial x} & = & \widehat{w}+P_3 \quad \text{at} \quad z=\overline{\zeta}. \end{array}\right. \tag{7.48}$$

These equations can now be solved in terms of $(\widehat{u},\widehat{w})$, which is a non divergent field. The vertical advection by P_3 appears now on the right hand side of the momentum equation and can be considered as the missing component of the full 3D vortex force. Also, the boundary condition for $\overline{w}^L$ are changed to boundary condition for $\widehat{w}$ (see also McWilliams et al., 2004, equ. 9.12). However it seems that the difficulties to obtain a time step both integral and constancy preserving are not much reduced using this form of the equations, because the advective terms for the tracer equation are still different than those for the momentum, involving the horizontal advection by the wave pseudo-momentum.

Another option to simplify the numerical implementation is to suppose that the wave mass transport occurs at the surface, as in Newberger and Allen (2007*a*). Then, we only need to add a surface vertical velocity and the only routines to be modified are **omega** and 2D submodel **step2D**. However, the simplification is only valid if the tracer advection is not considered, as the advection by the horizontal wave pseudo-momentum P_x is important compared to the advection by the mean flow.

7.10.3 Momentum forcing terms

The additional momentum source terms due to the waves are added through different ways.

The dissipation of the waves is put as a surface stress.

Gradients of the Bernoulli's head are added to the pressure gradient (routine **prsgrd**). Some terms are vertically uniform (S_J, S_{sh}^{hom}) and are simply added to the surface pressure, while the term S_{sh}^{cis} is added separately.

Wave forcing terms like the vortex force and the Stokes-Coriolis force are added to the right hand side of the momentum equation ru in the routine **rhs3d**.

There is no need to add those forces in the 2D submodel if they are supposed to remain constant during the barotropic steps.

7.10.4 Volume conservation and boundary conditions

The overall volume is conserved if the mass which enters with the wave field is compensated by an outgoing mass of the mean flow. Namely

$$\int\int (\hat{\mathbf{u}} + \mathbf{U_s}) \cdot \mathbf{n} = 0, \tag{7.49}$$

where the integral is over the boundary of the domain and $\mathbf{n}$ is the normal to the surface. At a global scale, the wave field is nil at the boundary so that the volume is conserved. However at the regional scale, we need to add additional boundary condition to ensure that conservation. We used $\hat{\mathbf{u}} = -\mathbf{U_s}$ at the off-shore boundary, whereas $\overline{\hat{\mathbf{u}}} = -\overline{\mathbf{U_s}}$ would be sufficient and less imposing. However, imposing the profile of the outgoing mass does not seem to impact strongly on the interior circulation, except in the vicinity of the boundary.

General conclusion

In this PhD thesis, we studied the impact of waves on the near-surface and on the nearshore ocean circulations. This study was made with a separation of the wave part and of the mean flow using the Generalized Lagrangian Mean (GLM) formalism of Andrews and McIntyre (1978*a*). The mean flow is described in a quasi-Eulerian average, which is close to an Eulerian average below the troughs but is also well defined, although difficult to measure, from the trough to the mean sea surface. In addition, a Lagrangian Stokes drift, or wave pseudo-momentum, is associated with the waves.

The Stokes drift of wind-sea waves has been calculated with an appropriate spectrum, and was shown to reach a significant fraction of the wind speed U_{10}, around 1.2% when the waves are developed. That Stokes drift depends on the wave development, but also depends on the wind : for a narrow-banded swell, this drift is quite small, of the order a few centimeters per second.

Waves also induce a strong near-surface mixing. This mixing can be well represented with a Mellor-Yamada type model, by specifying a surface mixing length of the order of the wave height and by including an additional Turbulent Kinetic Energy (TKE) source coming from the energy dissipation of the waves.

There is also, in addition to the momentum flux from the wind to the mean flow, a Stokes-Coriolis force associated with the waves. This force can be understood as the action of the Coriolis force on the wave pseudo momentum, this momentum flux being in turn released to the mean flow through the Stokes-Coriolis force.

In part one, all these ingredients were gathered to study the impact of waves on the open ocean near-surface dynamics. Offshore, where the horizontal gradients of the wave field and the associated forces can be neglected, the mean flow momentum balance reduces to an Ekman-Stokes equilibrium, i.e. an equilibrium between the Coriolis force and the diffusion of momentum from both the wind and the Stokes-Coriolis stress. There are two important features of this equilibrium : Firstly, due to the strong wave-induced mixing, the mean flow is rather uniform close to the surface, reaching only to small surface values, around 0.5% of the wind speed. Secondly,

the Stokes-Coriolis force, which drives a vertically integrated mean flow transport opposed to the Stokes transport, does not drive a surface mean flow which cancels the surface Stokes drift, because of the strong mixing.

As a consequence of those features, it was made clear that the surface Lagrangian drift due to the wind is dominated by the Stokes drift when the waves are developed. Thus, if the surface drift can be well represented in ocean circulation models ignoring waves, this will be to the detriment of the near-surface mixing. On the contrary, waves and the associate Stokes drift can reconcile a large surface mixing and a realistic surface drift.

This first result has been confronted to observations. The mixing is comparable to the observations of TKE dissipation rates close to the surface, as the mixing model was designed for that purpose. The comparison with current measurements is likely to be of the good magnitude order, but a precise validation is difficult to achieve. In fact, useful data sets should include wave measurements, it must be determined whether the current is Eulerian, quasi-Eulerian of Lagrangian, and the wind- and wave-induced components must be separated from the other processes. We attempted a reanalysis of the SMILE and LOTUS3 data-sets, since they have already been used for this kind of studies during the past (Santala, 1991; Terray et al., 2000; Polton et al., 2005) and they appeared to be suited for that purpose. However, it did not lead to clear conclusions, contrary to what has been claimed in the past.

A second part aimed to evaluate the impact of the wave mixing on the mixed layer depth. The role of the Langmuir cells has not been investigated, as it needs specific numerical simulations, based on LES for instance. However, it is likely that the wave-breaking is an important source of mixing close to the surface. Related parameters such as the surface value of the mixing length z_0 and the surface flux of TKE Φ_{oc} ($= \alpha u^{*3}$) have been calculated from a wave model and analyzed in terms of global distributions. Compared to previous estimations of these parameters, it has been shown that the wave height is largely overestimated when supposing full development at high latitude, and more importantly, it has been shown that the parameter α was strongly underestimated by the previous analysis of Terray et al. (1996) or by the monthly mean analysis of Janssen et al. (2004).

The importance of these two parameters z_0 and α has been highlighted with mixed layer numerical simulations, using a simple TKE mixing model. It was shown that the diurnal mixed layer is much thinner when the waves are young than when the waves are developed. It was also shown that the erosion of a thermocline is more efficient when the waves get more developed.

We note that many uncertainties remain : The dissipation term of the wave model is still more poorly constrained than the wave energy. Also, a precise estimation of the roughness length is still to be sought, and we believe that a comparison with the breaking wave height, like calculated here, might be helpful.

Finally, practical parameterizations directly from the wind speed have been proposed, but it is argued that the wave parameters should better be calculated with a wave model, instead of adding errors and bias from unknown wave ages to the previously mentioned uncertainties.

The third and last part dealt with the effects of an horizontally non-uniform wave field. Three dimensional practical equations for the interactions of waves and current have only recently appeared (McWilliams et al., 2004; Ardhuin et al., 2007*b*). Although these equations will surely give new insights into a lot of fully three-dimensional phenomena, such as rip currents, the macro-vortices or infra-gravity waves, they were studied in the present thesis for their consequences on the steady circulation over the shelf.

Until recently, the circulation over the shelf has never been done in one piece from the surf zone to the mid-shelf. Generally, the Earth rotation was taken into account over the mid-shelf and waves were ignored, and the opposite in the surf zone. That left a large gap in between, and the momentum balance on the inner-shelf zone is still poorly understood (Lentz et al., 1999). It was therefore chosen to use the newly derived equations to attempt to fill this gap.

The approximate GLM2z equations of Ardhuin et al. (2007*b*) have been implemented in a regional ocean circulation model, ROMS, and the results were compared to the existing simpler model of (Newberger and Allen, 2007*a*). One important aspect represented by these equations is the full description of the Lagrangian flow within and immediately outside the surf-zone. Such a model thus gathers the quasi-Eulerian current, related to the Eulerian measurements, and the Lagrangian motion, more important for many applications. Further, the impact of a wave finite-amplitude effect, by modifying the wave pseudo-momentum, was discussed in terms of its impact on the mean flow and on the surface drift.

Through the study of the impact of waves on the ocean circulation, the present thesis helped to take a new insight into the near-surface dynamics, mainly by relating the wave-mixing and the surface drift to the waves. Such better understanding may benefit to many further studies, ranging from costal engineering to remote-sensing applications, air-sea interactions, ocean-atmosphere exchange, oil drift predictions or search and rescue. But what could be a direct application of this thesis ?

As mentioned earlier, the presence of waves allows the presence of both a strong mixing and a large surface drift, which is otherwise impossible. Such a description can significantly modify the trajectory of Lagrangian particles : the vertical distribution can be more homogeneous due to the strong mixing but the drift of surface trapped materials can remain large. This was highlighted off-shore but might also be important in the surf and inner-shelf zones, where the materials, sedimentary or biological, are seldom uniformly distributed along the vertical. A better representation of the vertical mixing and of the vertical shear of the current may then benefit to the modelling of the drift of materials in this key area, link between the continent and the ocean.

Brève conclusion générale en français

Au cours de cette thèse, nous avons abordé l'étude de l'impact des vagues sur l'hydrodynamique littorale et de surface. Cette étude est motivée par les nombreuses applications pratiques auxquelles une meilleure connaissance de ces parties de l'océan peut bénéficier.

Il est apparu en première partie que les vagues constituaient une part dominante de la dérive près de la surface liée au vent. Ainsi, si cette dérive près de la surface peut être bien représentée dans les modèles de circulation océanique ignorant les vagues, c'est alors au détriment du mélange proche de la surface. Les vagues, ou plus précisément la dérive de Stokes qui leur est associée, permettent au contraire de concilier un fort mélange près de la surface et une dérive en surface réaliste. Ce premier résultat a été confronté aux observations. Même si une validation précise n'a pas pu être effectuée, en partie parce que les données de courants "propres" en présence de vagues sont encore rares, les ordres de grandeurs des observations sont en accord avec cette description. Une telle description de la couche de surface peut modifier sensiblement les trajectoires de traceurs lagrangiens : la distribution verticale est ainsi plus homogène, grâce au mélange plus important, alors que la dérive des matériels piégés en surface restera importante.

La deuxième partie évaluait l'impact du mélange lié aux vagues sur la profondeur de la couche de mélange. Si le rôle des circulations de Langmuir n'a pas été abordé, parce que nécessitant une modélisation spécifique (à base de LES par exemple), l'impact du déferlement des vagues est clair sur les couches de mélange de faibles profondeurs, les couches de mélange diurnes par exemple. Il apparaît ainsi que, par états de mer jeunes, la couche de mélange diurne est moins profonde que lorsque les vagues sont développées.

Enfin, une troisième partie regardait les avancées en termes d'hydrodynamique de la zone de déferlement et de la zone infra-littorale. La modélisation cohérente des vagues et des courants, nécessaire dans cette zone, en est à ses premiers pas, les équations théoriques tridimensionnelles étant encore en phase de validation. Une première implémentation dans un modèle de circulation régionale, ROMS, a été effectuée. Les premiers résultats ont été comparés aux modélisations issues de théories

plus simples. Dans la zone littorale et infra-littorale, les transports lagrangiens sont, comme au large, modifiés sous l'effet de la dérive de Stokes. Mais aussi, la non-linéarité des vagues, importante pour les vagues sur le point de déferler, peut sensiblement augmenter la dérive de Stokes associée aux vagues. Une telle description séparée des vagues et du courant de retour, peut, comme au large, concilier fort mélange et fort cisaillement de courant. Les divers matériels, biologiques ou sédimentaires, étant rarement distribués uniformément sur la verticale, une meilleure description des cisaillements de courants et du mélange devrait permettre de mieux modéliser les déplacements de ces matériels dans cette zone clef, interface entre la terre et l'océan.

Annexes

Chapter 8

Annexe A : Equations GLM2z

Explicit wave-averaged primitive equations using a Generalized Lagrangian Mean

Fabrice Ardhuin[(1)], Nicolas Rascle[(1,2)], K. A. Belibassakis[(3)]

Journal of Ocean Modelling, in press
July 2007

[(1)] *Centre Militaire d'Océanographie, Service Hydrographique et Océanographique de la Marine, 29609 Brest, France*
[(2)] *Laboratoire de Physique des Océans, Université de Bretagne Occidentale, 29000 Brest, France*
[(3)] *School of Naval Architecture and Marine Engineering, National Technical University of Athens, Athens, Greece*

Abstract

The generalized Langrangian mean theory provides exact equations for general wave-turbulence-mean flow interactions in three dimensions. For practical applications, these equations must be closed by specifying the wave forcing terms. Here an approximate closure is obtained under the hypotheses of small surface slope, weak horizontal gradients of the water depth and mean current, and weak curvature of the mean current profile. These assumptions yield analytical expressions for the mean momentum and pressure forcing terms that can be expressed in terms of the wave spectrum. A vertical change of coordinate is then applied to obtain $glm2z$-RANS equations (55) and (57) with non-divergent mass transport in cartesian coordinates. To lowest order, agreement is found with Eulerian-mean theories, and the present approximation provides an explicit extension of known wave-averaged equations to short-scale variations of the wave field, and vertically varying currents only limited to weak or localized profile curvatures. Further, the underlying exact equations provide a natural framework for extensions to finite wave amplitudes and any realistic situation. The accuracy of the approximations is discussed using comparisons with exact numerical solutions for linear waves over arbitrary bottom slopes, for which the equations are still exact when properly accounting for partial standing waves. For finite amplitude waves it is found that the approximate solutions are probably accurate for ocean mixed layer modelling and shoaling waves, provided that an adequate turbulent closure is designed. However, for surf zone applications the approximations are expected to give only qualitative results due to the large influence of wave nonlinearity on the vertical profiles of wave forcing terms.

8.1 Introduction

>From wave-induced mixing and enhanced air-sea interactions in deep water, to wave-induced currents and sea level changes on beaches, the effects of waves on ocean currents and turbulence are well documented (e.g. Battjes 1988, Terray et al. 1996). The refraction of waves over horizontally varying currents is also well known, and the modifications of waves by vertical current shears have been the topic of a number of theoretical and laboratory investigations (e.g. Biesel 1950, Peregrine 1976, Kirby and Chen 1989, Swan et al. 2001), and field observations (e.g. Ivonin et al. 2004). In spite of this knowledge and the importance of the topic for engineering and scientific applications, ranging from navigation safety to search and rescue, beach erosion, and de-biasing of remote sensing measurements,

Theory	averaging	momentum variable	main limitations
Phillips (1977)	Eulerian	total (U)	2D, $d\overline{u}/dz = 0$
Garrett (1976)	Eulerian	mean flow ($U - M^w/D$)	2D, $d\overline{u}/dz = 0$, $kh \gg 1$
Smith (2006)	Eulerian	mean flow ($U - M^w/D$)	2D, $d\overline{u}/dz = 0$
GLM (A&M 1978a)	GLM	mean flow ($\overline{\mathbf{u}}^L - \mathbf{P}$)	none (exact theory)
aGLM (A&M 1978a)	GLM	total ($\overline{\mathbf{u}}^L$)	none (exact theory)
Leibovich (1980)	Eulerian	mean flow ($\overline{\mathbf{u}}^L - \mathbf{P}$)	2nd order, ν constant
Jenkins (1987)	GLM	mean flow ($\overline{\mathbf{u}}^L - \mathbf{P}$)	2nd order, horizontal uniformity
Groeneweg (1999)	GLM	total ($\overline{\mathbf{u}}^L$)	2nd order
Mellor (2003)	following ξ_3	total ($\overline{\mathbf{u}}^L$)	2nd order, flat bottom
MRL04	Eulerian	mean flow ($\overline{u}$)	below troughs, $\overline{u} \ll C$, $\nu = 0$
NA07	Eulerian	mean flow ($\overline{u}$)	below troughs, 2nd order, $kH \ll 1$
present paper	GLM	mean flow ($\overline{\mathbf{u}}^L - \mathbf{P}$)	2nd order

Table 8.1: Essential attributes of some general wave-current coupling theories. See list of symbols for details (table 2 at the end of the paper). Although Mellor (2003) derived his wave-averaged equations with spatially varying wave amplitudes, his use of flat-bottom Airy wave kinematics is inconsistent with the presence of bottom slopes (see ARB07). MRL04 stands for McWilliams et al. (2004) and NA2007 stands for Newberger and Allen (2007).

there is no well established and generally practical numerical model for wave-current interactions in three dimensions.

Indeed the problem is made difficult by the difference in time scales between gravity waves and other motions. When motions on the scale of the wave period can be resolved, Boussinesq approximation of nearshore flows has provided remarkable numerical solutions of wave-current interaction processes (e.g. Chen et al. 2003, Terrile et al. 2006). However, such an approach still misses some of the important dynamical effects as it cannot represent real vertical current shears and their mixing effects (Putrevu and Svendsen 1999). This shortcoming has been partly corrected in quasi-three dimensional models (e.g. Haas et al. 2003), or multi-layer Boussinesq models (e.g. Lynnett and Liu 2005).

The alternative is of course to use fully three dimensional (3D) models, based on the primitive equations. These models are extensively used for investigating the global, regional or coastal ocean circulation (e.g. Bleck 2002, Shchepetkin and McWilliams 2003). An average over the wave phase or period is most useful due to practical constraints on the computational resources, allowing larger time steps and avoiding non-hydrostatic mean flows. Wave-averaging also allows an easier interpretation of the model result. A summary of wave-averaged models in 2 or 3 dimensions is provided in table 1.

8.1.1 Air-water separation

In 3D, problems arise due to the presence of both air and water in the region between wave crests and troughs. Various approaches to the phase or time averaging of flow properties are illustrated in figure 8.1 (see also Ardhuin et al. 2007b, hereinafter ARB2007). For small amplitude waves, one may simply take a Taylor expansion of mean flow properties (e.g. McWilliams et al. 2004, hereinafter MRL04). Using a decomposition of the non-linear advection term in the equations of motion $\mathbf{u}\cdot\nabla\mathbf{u} = \nabla u^2 + \mathbf{u}\times\nabla\mathbf{u}$, McWilliams et al. (2004, see also Lane et al. 2007) obtained a relatively simple set of equation for conservative wave motion over sheared currents, for a given choice of small parameters. These parameters include the surface slope $\varepsilon_1 = k_0 a_0$ and the ratio of the wavelength and scale of evolution of the wave amplitucde. Further, these equations were derived with a scaling corresponding to a non-dimensional depth $k_0 h_0$ of order 1, with k_0, a_0 and h_0 typical values of the wavenumber, wave amplitude and water depth, respectively. These authors also assumed that the current velocity was of the same order as the wave orbital velocity, both weaker than the phase speed by a factor ε_1. That latter assumption may generally be relaxed since the equations of motion are invariant by a change of reference frame, so that only the current vertical shear may need to be small compared to the wave radian frequency, provided that the current, water depth and wave amplitudes are slowly varying horizontally.

For waves of finite amplitude, a proper separation of air and water in the averaged equations of motion requires a change of coordinates that maps the moving free surface to a level that is fixed, or at least slowly varying. This is usual practice in air-sea interaction studies, and it has provided approximate solutions to problems such as wind-wave generation or wave-turbulence interactions (e.g. Jenkins 1986, Teixeira and Belcher 2002) but it brings some complications. The most simple change of coordinate was recently proposed by Mellor (2003), but it appears to be impractical in the presence of a bottom slope because its accurate implementation requires the wave kinematics to first order in the wave slope (Ardhuin et al., 2007b, hereinafter ARB07).

8.1.2 Separation of wave and current momentum fluxes

Another approach is to use one of the two sets of exact averaged equations derived by Andrews and McIntyre (1978a). Groeneweg (1999) successfully used the second set, the alternative Generalized Lagragian Mean equations (aGLM), approximated to second order in wave slope, for the investigation of current profile modifications induced by waves (see also Groeneweg and Klopman 1998, Groeneweg and Battjes

2003). This work was also loosely adapted for engineering use in the numerical model Delft3D (Walstra et al. 2001).

However, aGLM equations describe the evolution of the total flow momentum, which includes the wave pseudo-momentum per unit mass $\mathbf{P}$. That vector quantity is generally close to the Lagrangian Stokes drift $\overline{\mathbf{u}}^S$ (see below), and it is not mixed by turbulence[1], unlike the mean flow momentum. Further, $\mathbf{P}$ is carried by the wave field at the group velocity, which is typically one order of magnitude faster than the drift velocity. Thus bundling $\mathbf{P}$ with the rest of the momentum may lead to large errors with the turbulence closure. Other practical problems arise due to the strong surface shear of $\mathbf{P}$ and $\overline{\mathbf{u}}^S$ (e.g. Rascle et al. 2006) whereas the quasi-Eulerian current is relatively uniform in deep water (e.g. Santala and Terray 1992). Thus solving for the total momentum (including $\mathbf{P}$) requires a high resoltion near the surface. Finally, a consistent expression of the aGLM equations with a sloping bottom and wave field gradients is difficult due to the divergence of vertical fluxes of momentum (vertical radiation stresses) that must be expressed to first order in all the small parameters that represent the slow wave field evolution (bottom slope, wave energy gradients, current shears...). This same problem arises with Mellor's (2003) equations and is discussed in ARB07.

The first set of GLM equations describes the evolution of the quasi-Eulerian current only, and, just like the decomposition of $\mathbf{u} \cdot \nabla u$ used by MRL04, it does not require the evaluation of these vertical radiation stresses. These equations were used by Leibovich (1980) to derive the Craik-Leibovich equations that is the basis of theories for Langmuir circulations. However, in that work he did not attempt an explicit integration of the GLM set, and thus did not express the wave forcing terms from wave amplitudes or spectra. The general mathematical structure of the GLM equations and their conservatin properties are also well detailed in Holm (2002) and references therein.

Further, the GLM flow is generally divergent as the averaging operator introduces an implicit change of the vertical coordinate. This question has been largely overlooked by previous users of GLM theory (Leibovich 1980, Groeneweg 1999). Further, in order to be implemented in a numerical model, the wave-induced forcing terms must be made explicit using approximate solutions for wave-induced motions and pressure. We will assume that the slowly varying spectrum is known, typically provided by a wave model. Given the degree of accuracy attained by modelled wave spectra in a wide variety of conditions this is generally appropriate (e.g. Herbers et al. 2000, Ardhuin et al. 2003, 2007, Magne et al. 2007). We note in passing

[1]The Stokes drift is a residual velocity over the wave cycle, its mixing is not possible without a profound modification of the wave kinematics.

that no explicit and theoretically satisfying theory is available for the transport of the wave action spectrum over vertically and horizontally sheared currents. Indeed, the exact theory of Andrews and McIntyre (1978b) is implicit and would require an explicit approximation of the wave action from know wave kinematics, similar to the approximation of the wave pseudo-momentum performed here.

The goal of the present paper is to provide a practical and accurate method for wave-current coupling that is general enough for applications ranging from the ocean mixed layer to, possibly, the surf zone. GLM equations, for the reasons listed above, are a good candidate for this application. Although not as simple as an Eulerian average, the GLM operator is capable of properly separating air and water in the crest to trough region, leading to physically understandable definitions of mean properties on either side of the air-sea interface. The practical use of GLM requires some approximations and transformations. We provide in section 2 a derivation of explicit and approximate $glm2z$-RANS equations. Given the large literature on the subject, we explore in section 3 the relationships between GLM, aGLM and other forms of wave-averaged 3D and depth-integrated 2D equations. A preliminary analysis of the expected errors due to the approximations are provided in section 4, and conclusions follow in section 5. Full numerical solutions using the $glm2z$-RANS equations will be reported elsewhere, in particular in the doctorate thesis of Nicolas Rascle.

8.2 glm2-RANS equations

8.2.1 Generalities on GLM and linear wave kinematics

We first define the Eulerian average $\overline{\phi(\mathbf{x},t)}$ of $\phi(\mathbf{x},t)$, where the average may be an average over phase, realizations, time t or space. We now take this average at displaced positions $\mathbf{x}+\xi$, with $\xi=(\xi_1,\xi_2,\xi_3)$ a displacement vector, and we defining the velocity $\mathbf{v}$ at which the mean position is displaced when the actual position moves at the fluid velocity $\mathbf{u}(\mathbf{x}+\xi)$. One obtains the corresponding GLM of ϕ

$$\overline{\phi(\mathbf{x},t)}^{L}=\overline{\phi(\mathbf{x}+\xi,t)} \tag{8.1}$$

by choosing the displacement field ξ so that

- the mapping $\mathbf{x}\rightarrow\mathbf{x}+\xi$ is invertible
- $\overline{\xi(\mathbf{x},t)}=0$
- $\overline{\mathbf{v}(\mathbf{x},t)}=\mathbf{v}(\mathbf{x},t)$, which gives $\mathbf{v}=\overline{\mathbf{u}(\mathbf{x},t)}^{L}$.

Such a mapping is illustrated in figure 1.c for linear waves. Lagrangian perturbations are logically defined as the field minus its average, i.e.,

$$\overline{\phi(\mathbf{x},t)}^{l} = \phi(\mathbf{x}+\xi,t) - \overline{\phi(\mathbf{x},t)}^{L} = \phi(\mathbf{x}+\xi,t) - \overline{\phi(\mathbf{x}+\xi,t)}. \tag{8.2}$$

Here we shall take our Eulerian average to be a phase average[2]. Given any Eulerian flow field $\mathbf{u}(\mathbf{x},t)$, one may define a first displacement by

$$\xi'(\mathbf{x},t,\Delta t) = \int_t^{t+\Delta t} \mathbf{u}(\mathbf{x}+\xi'(\mathbf{x},t,t'-t),t')\mathrm{d}t'. \tag{8.3}$$

The mean drift velocity is defined as $\mathbf{v}(\mathbf{x},t) = \lim_{\Delta t\to 0} \overline{\xi'(\mathbf{x},t,\Delta t)}/(\Delta t)$. The GLM displacement field is then given by $\xi = \xi' - \mathbf{v}t - \overline{\xi' - \mathbf{v}t}$. This construction of $\mathbf{v}$ and ξ guarantees that the required properties are obtained, provided that the limit $\Delta t \to 0$ commutes with the averaging operator. For periodic motions one may also take $\mathbf{v} = \overline{(\xi'(t+T^L) - \xi'(t))}/(T^L)$, with T^L the Lagrangian wave period (the time taken by a water particle to return to the same wave phase). This definition will be used for Miche waves in section 4.2.

Clearly GLM differs from the Eulerian mean. The difference between the two is given by the Stokes correction (Andrews et McIntyre 1978a). Below the wave troughs, the Stokes correction for the velocity is the Stokes drift, by definition,

$$\overline{\mathbf{u}}^S \equiv \overline{\mathbf{u}}^L - \overline{\mathbf{u}}. \tag{8.4}$$

More generally, for a continuously differentiable field ϕ the Stokes correction is given by (Andrews and McIntyre 1978a, equation 2.27),

$$\overline{\phi}^L \equiv \overline{\phi} + \overline{\phi}^S = \overline{\phi} + \overline{\xi_j \frac{\partial \phi}{\partial x_j}} + \frac{1}{2}\overline{\xi_j \xi_k}\frac{\partial^2 \overline{\phi}}{\partial x_j \partial x_k} + O\left(\max_{i,j,k}\left\{\frac{\partial^3 \overline{\phi}}{\partial x_i \partial x_j \partial x_k}\right\}|\xi|^3\right), \tag{8.5}$$

with an implicit summation over repeated indices.

The GLM average commutes with the Lagrangian derivative, thus the GLM velocity $\overline{\mathbf{u}}^L$ is the average drift velocity of water particles. One should however be careful that the GLM average does not commute with most differential operators, for example the curl operator. Indeed the GLM velocity of irrotational waves is rotational, which is clearly apparent in the vertical shear of the Stokes drift (see also Ardhuin and Jenkins 2006 for a calculation of the lowest order mean shears $\overline{\partial u_\alpha/\partial z}^L$ and $\overline{\partial u_3/\partial x}^L$).

[2]For uncorrelated wave components the phase average is obtained by the sum of the phase averages of each component. In the presence of phase correlations, such as in the case of partially standing waves or nonlinear phase couplings, the sum has to be averaged in a coherent manner.

One of the interesting aspects of GLM theory is that it clearly separates the wave pseudo-momentum $\mathbf{P}$ from the quasi-Eulerian mean momentum $\widehat{\mathbf{u}} = \overline{\mathbf{u}}^L - \mathbf{P}$. This is a key aspect for numerical modelling since $\mathbf{P}$ is transported by the wave field at the group velocity, of the order of 5 m s^{-1} in deep water, while $\widehat{\mathbf{u}}$ is transported at the much slower velocity $\overline{\mathbf{u}}^L$. $\mathbf{P}$ is defined by (Andrews and McIntyre 1978a, eq. 3.1),

$$P_i = -\overline{\xi_{j,i}\left(u^l_j + \epsilon_{jkl} f_k \xi_l/2\right)}, \tag{8.6}$$

where $\epsilon_{ijk}A_jB_k$ is the i-component of the vector product $\mathbf{A}\times\mathbf{B}$, and $f_k/2$ is the k-component of the rotation vector of the reference frame. In the applications considered here the effect of rotation can be neglected in (8.6) due to the much larger rotation period of the Earth compared to the wave period. We will thus take

$$P_i = -\overline{\xi_{j,i}u^l_j}. \tag{8.7}$$

For practical use, the GLM equations have to be closed by specifying the wave-induced forcing terms. In order to give explicit approximations for the wave-induced effects, we will approximate the wave motion as a sum of linear wave modes, each with a local wave phase ψ giving the local wave number $\mathbf{k} = (k_1, k_2) = \nabla\psi$, and radian frequency $\omega = -\partial\psi/\partial t$, and an intrinsic linear wave radian frequency $\sigma = [gk\tanh(kD)]^{1/2} = \omega - \mathbf{k}\cdot\boldsymbol{U}_A$, where $\boldsymbol{U}_A$ is the phase advection velocity, D is the local mean water depth, and g the acceleration due to gravity and Earth rotation. Defining $h(x_1, x_2)$ as the local depth of the bottom and $\zeta(x_1, x_2, t)$ as the free surface elevation, one has $D = \overline{\zeta} + h$. We assume that the wave slope $\varepsilon_1 = \max(|\nabla\zeta|)$ is small compared to unity (this will be our first hypothesis H1), with ∇ denoting the horizontal gradient operator. We also restrict our investigations to cases for which the Ursell number is small $Ur = (a/D)/(kD)^2 < 1$ (this is hypothesis H2). We further restrict our derivations to first order in the slow spatial scale ε_2. That small parameter may be defined as the maximum of the slow spatial scales $|(\partial a/\partial x)/(ka)|$, $|(\partial\overline{u}/\partial x)/(\sigma)|$, $|(\partial D/\partial x)|$, and time scales $|(\partial a/\partial t)/(\sigma a)|$, $|k(\partial\widehat{u}/\partial t)/(\sigma)^2$, and $|(\partial D/\partial t)k/\sigma|$ (hypothesis H3). It will also appear that the current profile may cause some difficulties. Since we have already assumed a small wave steepness we may use Kirby and Chen's (1989) results, giving the dispersion relation

$$\omega = \sigma + k_\alpha \int_{-h}^{\overline{\zeta}} \widehat{u}_\alpha \frac{2k\cosh\left[2k(z+h)\right]}{\sinh(2kD)}\mathrm{d}z + O(\varepsilon_3), \tag{8.8}$$

where α is a dummy index representing any horizontal component 1 or 2, and the summation is implicit over repeated indices. The index 3 will represent the vertical components positive upwards, along the direction $z = x_3$. In particular we shall

assume that their correction to the lowest order stream function (their eq. 23) is relatively small, which may be obtained by requiring that the curvature of the current is weak or concentrated in a thin boundary layer, i.e. $\varepsilon_3 \ll 1$ (hypothesis H4) with

$$\varepsilon_3 = \frac{1}{\omega \sinh(kD)} \int_{-h}^{\zeta} \left| \frac{\partial^2 \overline{u}}{\partial z^2} \right| \sinh\left[2k(z+h)\right] \mathrm{d}z. \tag{8.9}$$

For simplicity we will further require that $a^2 \left[\partial^3 \overline{u}_\alpha / \partial z^3 / (\sigma)\right] \leq \varepsilon_3$ (hypothesis H5), which may be more restrictive than H4. Finally, we will neglect the vertical velocity $\widehat{w}$ in the vertical momentum equation for the mean flow momentum (i.e. we assume the mean flow to be hydrostatic, this is our hypothesis H6).

In the following we take $\varepsilon = \max \varepsilon_i, 1 \leq i \leq 3$. The wave-induced pressure and velocity are given by

$$\widetilde{p} = \rho_w g a \left[F_{CC} \cos\psi + O(\varepsilon)\right] \tag{8.10}$$

$$\widetilde{u}_\alpha = a\sigma \frac{k_\alpha}{k} \left[F_{CS} \cos\psi + O(\varepsilon)\right] \tag{8.11}$$

$$\widetilde{u}_3 = a\sigma \left[F_{SS} \sin\psi + O(\varepsilon)\right], \tag{8.12}$$

where a is the local wave amplitude, ρ_w is the water density, taken constant in the present paper. We have used the short-hand notations $F_{CC} = \cosh(kz + kD)/\cosh(kD)$, $F_{CS} = \cosh(kz+kD)/\sinh(kD)$, and $F_{SS} = \sinh(kz+kD)/\sinh(kD)$.

>From now on, only the lowest order approximations will be given unless explicitly stated otherwise. In order to estimate quantities at displaced positions, the zero-mean displacement field is given by

$$\begin{aligned} u_i^l &\equiv \mathbf{u}(\mathbf{x}+\xi) - \overline{u}_i^L \\ &\simeq \widetilde{u}_i + \xi_j \frac{\partial \overline{u}_i}{\partial x_j} + \left(\xi_j \frac{\partial \widetilde{u}_i}{\partial x_j} - \overline{\xi_j \frac{\partial \widetilde{u}_i}{\partial x_j}} \right) + \frac{1}{2} \left(\xi_j^2 - \overline{\xi_j^2} \right) \frac{\partial^2 \overline{u}_i}{\partial x_j^2}. \end{aligned} \tag{8.13}$$

Thanks to the definition of $\overline{u}^L$, we also have

$$u_i^l = \frac{\partial \xi_i}{\partial t} + \overline{u}_j^L \frac{\partial \xi_i}{\partial x_j} \simeq \frac{\partial \xi_i}{\partial t} + \overline{u}_\alpha^L \frac{\partial \xi_i}{\partial x_\alpha}, \tag{8.14}$$

in which the vertical velocity has been neglected. The greek indices α and β stand for horizontal components only.

To lowest order in the wave amplitude, the displacements ξ_i and Lagrangian velocity perturbations u_i^l are obtained from (8.13) and (8.14),

$$u_3^l = \widetilde{u}_3 \tag{8.15}$$

$$\xi_3 = am\left[F_{SS}\cos\psi\right] \tag{8.16}$$

$$u^l_\alpha = \widetilde{u}_\alpha + \xi_3\frac{\partial\overline{u}_\alpha}{\partial z} + \xi_\beta\frac{\partial\overline{u}_\alpha}{\partial x_\beta} + O\left(\sigma k a^2\right)\cos 2\psi + O\left(a^3\frac{\partial^2\overline{u}_\alpha}{\partial z^3}\right) \tag{8.17}$$

$$\simeq a\left[\sigma\frac{k_\alpha}{k}F_{CS} + mF_{SS}\frac{\partial\overline{u}_\alpha}{\partial z}\right]\cos\psi \tag{8.18}$$

$$\xi_\alpha = -am\left[\frac{k_\alpha}{k}F_{CS} + \frac{m}{\sigma}\frac{\partial\overline{u}_\alpha}{\partial z}F_{SS}\right]\sin\psi + O\left(\frac{a^2}{\sigma}\frac{\partial^2\overline{u}_\alpha}{\partial z^2}\right)\sin 2\psi$$
$$+O\left(\frac{a}{\sigma}\frac{\partial\overline{u}_\alpha}{\partial x_\beta}\right)\cos\psi + O\left(\frac{a^3}{\sigma}\frac{\partial^2\overline{u}_\alpha}{\partial z^3}\right), \tag{8.19}$$

The shear correction parameter m, arising from the time-integration of (8.14), is given by

$$m(\mathbf{x},\mathbf{k},z,t) = \frac{\sigma}{\omega - \mathbf{k}\cdot\overline{\mathbf{u}}^L(\mathbf{x},z,t)}. \tag{8.20}$$

Based on (8.8) m differs from 1 by a quantity of order $\sigma^{-1}\partial\overline{u}/\partial z$.

Using our assumption (H5) the last term in eq. (8.19) may be neglected. The last two term in eq. (8.17) have been neglected because they will give negligible $O(\varepsilon^3)$ terms in $\mathbf{P}$, $\overline{\zeta}^L$ or other wave-related quantities, when multiplied by other zero-mean wave quantities.

Using the approximate wave-induced motions, one may estimate the Stokes drift

$$\overline{\mathbf{u}}^S \equiv \overline{\mathbf{u}}^L - \overline{u} \simeq \overline{\xi\cdot\nabla\widetilde{u}} + \frac{1}{2}\overline{\xi_3^2}\frac{\partial^2\overline{u}_\alpha}{\partial z^2}$$
$$= \frac{ma^2}{4\sinh^2(kD)}\left[2\sigma\mathbf{k}\cosh(2kz+2kh) + \mathbf{k}m\sinh(2kz+2kh)\frac{\mathbf{k}}{k}\cdot\frac{\partial\overline{\mathbf{u}}}{\partial z}\right.$$
$$\left. + \frac{\partial^2\overline{\mathbf{u}}}{\partial z^2}\sinh^2(kz+kh)\right], \tag{8.21}$$

the horizontal wave pseudo-momentum

$$P_\alpha = -\overline{\frac{\partial\xi_\beta}{\partial x_\alpha}u^l_\beta} - \overline{\frac{\partial\xi_3}{\partial x_\alpha}w^l}$$
$$\simeq \frac{ma^2}{4\sinh^2(kD)}\left[2\sigma\mathbf{k}\cosh(2kz+2kh) + 2k_\alpha m\sinh(2kz+2kh)\frac{k_\alpha}{k}\cdot\frac{\partial\overline{\mathbf{u}}}{\partial z}\right.$$
$$\left. +2m\sinh^2(kz+kh)\left(\frac{\partial\overline{\mathbf{u}}}{\partial z}\right)^2\right], \tag{8.22}$$

and the GLM position of the free surface

$$\overline{\zeta}^L = \overline{\zeta} + \overline{\zeta}^S = \overline{\zeta} + \frac{\partial\zeta}{\partial x_\alpha}\xi_\alpha|_{z=\overline{\zeta}} = \overline{\zeta} + \frac{ma^2}{2}\left[\frac{k}{\tanh kD} + \frac{m\mathbf{k}}{\sigma}\cdot\frac{\partial\overline{\mathbf{u}}}{\partial z}|_{z=\overline{\zeta}}\right]. \tag{8.23}$$

Thus the GLM of vertical positions in the water is generally larger than the Eulerian mean of the position of the same particles (see also McIntyre 1988). This is easily understood, given that there are more particles under the crests than under the troughs (figure 8.1.c). As a result, the original GLM equations are divergent ($\nabla \cdot \overline{u}^L \neq 0$) and require a coordinate transformation to yield a non-divergent velocity field. That transformation is small, leading to a relative correction of order ε_1^2. That transformed set of equation is a modified primitive equation that may be implemented in existing ocean circulation models.

The horizontal component of the wave pseudo-momentum P_α differs from the Stokes drift $\overline{u}_\alpha^S$ due to the current vertical shear. Therefore the quasi-Eulerian mean velocity $\widehat{u}_\alpha = \overline{u}_\alpha^L - P_\alpha$ also differs from the Eulerian mean velocity $\overline{u}_\alpha = \overline{u}_\alpha^L - \overline{u}_\alpha^S$

$$\widehat{u}_\alpha = \overline{u}_\alpha + \frac{1}{2}\overline{\xi_3^2}\frac{\partial^2 \overline{u}_\alpha}{\partial z^2} + O(\varepsilon_3). \tag{8.24}$$

The vertical wave pseudo-momentum $P_3 = 0$ is, at most, of order $\sigma\varepsilon^3/k$. Although it may be neglected in the momentum equation, it plays an important role in the mass conservation equation, and will thus be estimated from P_α. In particular, for $m = 1$ and in the limit of small surface slopes, it is straightforward using (8.7) to prove that $\mathbf{P}$ is non-divergent, giving,

$$P_3 = -P_\alpha(-h)\frac{\partial h}{\partial x_\alpha} - \int_{-h}^{z} \frac{\partial P_\alpha(z')}{\partial x_\alpha}\mathrm{d}z'. \tag{8.25}$$

Although this equality is not obvious for $m \neq 1$ and nonlinear waves, corrections to (8.25) are expected to be only of higher order. In particular, once $\mathbf{P}$ is transformed to z coordinates, since, in the absence of a mean flow $\mathbf{P} = \overline{\mathbf{u}}^L$ and it is non-divergent (see section 2.1.1).

*glm*2-RANS equations

The velocity field is assumed to have a unique decomposition in mean, wave and turbulent components $\mathbf{u} = \overline{\mathbf{u}} + \widetilde{\mathbf{u}} + \mathbf{u}'$, with $\langle \mathbf{u}' \rangle = 0$, the average over the flow realizations for prescribed wave phases. The turbulence will be assumed weak enough so that its effect on the sea surface position is negligible. We note $\mathbf{X}$ the divergence of the Reynolds stresses, i.e. $X_i = \partial \left\langle u_i' u_j' \right\rangle / \partial x_j$, and we apply the GLM average to the Reynolds-Average Navier-Stokes equations (RANS). We shall now seek an approximation to the GLM momentum equations by retaining all terms of order $\rho_w g \varepsilon^3$ and larger in the horizontal momentum equation, and all terms of order $\rho_w g \varepsilon^2$ in the vertical momentum equation. The resulting equations, that may be called the "*glm*2-RANS" equations, are thus more limited in terms of wave nonlinearity than

the Eulerian mean equations of MRL04. At the same time, random waves are considered here and that the mean current may be larger than the wave orbital velocity. Indeed we make no hypothesis on the current magnitude, but only on the horizontal current gradients and on the curvature of the current profile. The present derivation differs from that of Groeneweg (1999) by the fact that we use the GLM instead of the aGLM equations (see table 1). The name for these equations is loosely borrowed from Holm (2002) who instead derived an approximate Lagrangian to obtain the momentum equation, and did not include turbulence.

In order to simplify our calculations we shall use the form of the GLM equations given by Dingemans (1997, eq. 2.596) with ρ_w constant, which, among other things, removes terms related to the fluid thermodynamics. The evolution equation for the quasi-Eulerian velocity $\widehat{\mathbf{u}}$ is,

$$\overline{D}^L \widehat{u}_i + \epsilon_{i3j} f_3 \overline{u}_j^L + \frac{\partial}{\partial x_i}\left(\frac{\overline{p}^L}{\rho_w} - \frac{\overline{u_j^l u_j^l}}{2}\right) - \widehat{X}_i + g\delta_{i3} = P_j \frac{\partial \overline{u}_j^L}{\partial x_i}, \tag{8.26}$$

where the Lagrangian derivative D^L is a derivative following the fluid at the Lagrangian mean velocity $\overline{u}^L$, p is the full dynamic pressure, δ is Kronecker's symbol, and the viscous and/or turbulent force $\widehat{\mathbf{X}}$ is defined by

$$\widehat{X}_i = \overline{X}_i^L + \overline{\frac{\partial \xi_j}{\partial x_i}\left(\overline{X}_j^L - X_j\right)}. \tag{8.27}$$

These exact equations will now be approximated using (8.10)-(8.16). We first evaluate the wave forcing terms in (8.26) using monochromatic waves, with a surface elevation variance $E = a^2/2$. The result for random waves follows by summation over the spectrum and replacing E with the spectral density $E(\mathbf{k})$.

We first consider the vertical momentum balance, giving the pressure field. It should be noted that the Lagrangian mean Bernoulli head term $u_j^l u_j^l/2$ differs from its Eulerian counterpart $u_j' u_j'/2$ by a term K_2, which arises from the correlation of the mean current perturbation at the displaced position $\mathbf{x}+\xi$, with the wave-induced velocity, i.e. the second term in (8.17). Eqs. (8.10)–(8.16) give

$$\frac{1}{2}\left(u_j^l u_j^l\right) = \frac{gkE}{2}\left[F_{CC}F_{CS} + F_{SC}F_{SS}\right] + K_2, \tag{8.28}$$

with

$$K_2 = \widetilde{u}_\alpha \xi_3 \frac{\partial \overline{u}_\alpha}{\partial z} + \frac{\xi_3^2}{2}\left|\frac{\partial \overline{\mathbf{u}}}{\partial z}\right|^2 = E\frac{\sigma}{k}\mathbf{k}\cdot\frac{\partial \widehat{\mathbf{u}}}{\partial z} m F_{CS}F_{SS} + \frac{E}{2}\left|\frac{\partial \overline{\mathbf{u}}}{\partial z}\right|^2 m^2 F_{SS}^2. \tag{8.29}$$

The vertical momentum equation (8.26) for $\widehat{w} = \widehat{u}_3$ is,

$$\begin{aligned} \frac{\partial \widehat{w}}{\partial t} &+ \widehat{w}\frac{\partial \widehat{w}}{\partial z} + P_3\frac{\partial \widehat{w}}{\partial z} + (\widehat{u}_\beta + P_\beta)\frac{\partial \widehat{w}}{\partial x_\beta} + \frac{1}{\rho_w}\frac{\partial \overline{p}^L}{\partial z} + g \\ &= \frac{\partial}{\partial z}\left[\left(\overline{\widetilde{u}_\alpha \widetilde{u}_\alpha} + \overline{\widetilde{w}^2}\right)/2 + K_2\right] + P_\beta\frac{\partial}{\partial z}(\widehat{u}_\beta + P_\beta) + P_3\frac{\partial}{\partial z}(\widehat{u}_3 + P_3) \quad (8.30) \end{aligned}$$

For small bottom slopes we may neglect the last term, but we rewrite it in order to compare with other sets of equations. Now using the lowest order wave solution (8.11)–(8.16), eq. (8.30) transforms to

$$\begin{aligned} \frac{1}{\rho_w}\frac{\partial}{\partial z}\left[\overline{p}^L + \rho_w g z - \rho_w \frac{\sigma^2 E}{2}\left(F_{CS}^2 + F_{SS}^2\right) - \rho_w K_2\right] &= -\frac{\partial \widehat{w}}{\partial t} - \widehat{w}\frac{\partial \widehat{w}}{\partial z} \\ - (\widehat{u}_\beta + P_\beta)\frac{\partial \widehat{w}}{\partial x_\beta} + P_\beta\frac{\partial}{\partial z}(\widehat{u}_\beta + P_\beta) &+ P_3\frac{\partial}{\partial z}(\widehat{w} + P_3). \quad (8.31) \end{aligned}$$

We add to both sides the depth-uniform term $-\sigma^2 E\left(F_{CC}^2 - F_{SS}^2\right)/2$, and integrate over z to obtain

$$\frac{\overline{p(z)}^L}{\rho_w} = -g\left[(z - z_s) - kEF_{CC}F_{CS}\right] + K_2 + K_1 - \frac{gkE}{4\sinh(2kD)} \quad (8.32)$$

where the hydrostatic hypothesis (H6, see above) has be made for the mean flow. The depth-integrated vertical component of the vortex-like force K_1 is defined by

$$K_1 = -\int_z^{\overline{\zeta}^L} P_\beta\frac{\partial}{\partial z'}(\widehat{u}_\beta + P_\beta)\,\mathrm{d}z' + \int_z^{\overline{\zeta}^L} P_3\frac{\partial}{\partial x_\beta}(P_\beta)\,\mathrm{d}z', \quad (8.33)$$

where eq. (8.25) has been used. The integration constant z_s is given by the surface boundary condition

$$\overline{p(\zeta)}^L = -\rho_w g\left(\overline{\zeta}^L - z_s - kEF_{CC}F_{CS} - K_2(\overline{\zeta}^L)/g\right) = \overline{p}_a. \quad (8.34)$$

Using (8.23) we find that $z_s = \overline{\zeta} + \overline{p}_a/(\rho_w g) - K_2(\overline{(\zeta)}^L)/g$ and (8.32) becomes

$$\frac{\overline{p}^L}{\rho_w} = \frac{\overline{p}^H}{\rho_w} + gkEF_{CC}F_{CS} + K_1 + K_2 - K_2(\overline{\zeta}^L), \quad (8.35)$$

with p^H the hydrostatic pressure defined equal to the mean atmospheric pressure at the mean sea surface, $p^H = \rho_w g(\overline{\zeta} - z) + \overline{p}_a$.

Below the wave troughs the Stokes correction for the pressure (8.5) gives the

Eulerian-mean pressure

$$\overline{p} = \overline{p}^L - \rho_w g k m E \left(F_{CS} F_{CC} + F_{SS} F_{SC} + \frac{\mathbf{k}}{k\sigma} \cdot \frac{\partial \overline{\mathbf{u}}}{\partial z} m F_{SS} F_{CC} \right). \tag{8.36}$$

Thus equation (8.32) gives the following relationship, valid to order ε_1^2 below the wave troughs, between the Eulerian-mean pressure $\overline{p}$ and $\overline{p}^L$,

$$\begin{aligned} \overline{p} &= p^H - \rho_w g k E F_{SS} F_{SC} + \rho_w \left(K_1 - K_2(\overline{\zeta}^L) + \frac{E}{2} \left| \frac{\partial \overline{\mathbf{u}}}{\partial z} \right|^2 m^2 F_{SS}^2 \right) \\ &\quad + \rho_w g k (1-m) E F_{CC} F_{CS}. \end{aligned} \tag{8.37}$$

For a spectrum of random waves, the modified pressure term that enters the horizontal momentum equation may be written as

$$\widehat{p} \equiv \overline{p}^L - \frac{\rho_w \overline{u_j^l u_j^l}}{2} - P_j \frac{\partial \overline{u}_i^L}{\partial z} = p^H + \rho_w S^{\mathrm{J}} + \rho_w S^{\mathrm{shear}}, \tag{8.38}$$

with the depth-uniform wave-induced kinematic pressure term

$$S^{\mathrm{J}} = g \int_{\mathbf{k}} \frac{k E(\mathbf{k})}{\sinh 2kD} \mathrm{d}\mathbf{k} \tag{8.39}$$

and a shear-induced pressure term, due to the integral of the vertical component of the vortex force K_1, and $K_2(\overline{\zeta}^L)$,

$$\begin{aligned} S^{\mathrm{shear}} &= -\int_{\mathbf{k}} E(\mathbf{k}) \left(\frac{\sigma}{k} k_\beta m \frac{\partial \widehat{u}_\beta(\overline{\zeta}^L)}{\partial z} \tanh(kD) + \frac{m^2}{2} \left| \frac{\partial \widehat{\mathbf{u}}}{\partial z}(\overline{\zeta}^L) \right|^2 \right) \mathrm{d}\mathbf{k} \\ &+ \int_{\mathbf{k}} \int_z^{\overline{\zeta}^L} \left[P_3(\mathbf{k}) \frac{\partial P_\beta(z', \mathbf{k})}{\partial x_\beta} - P_\beta(\mathbf{k}) \frac{\partial \left[\widehat{u}_\beta(z') + P_\beta(\mathbf{k}) \right]}{\partial z'} \right] \mathrm{d}z' \mathrm{d}\mathbf{k}. \end{aligned} \tag{8.40}$$

Now considering the horizontal momentum equations, we rewrite (8.26) for the horizontal velocity,

$$\begin{aligned} \frac{\partial \widehat{u}_\alpha}{\partial t} &+ \left(\widehat{u}_\beta + P_\beta \right) \frac{\partial \widehat{u}_\alpha}{\partial x_\beta} + \widehat{w} \frac{\partial \widehat{u}_\alpha}{\partial z} + \epsilon_{\alpha 3 \beta} f_3 \left(\widehat{u}_\beta + P_\beta \right) + \frac{1}{\rho_w} \frac{\partial p^H}{\partial x_\alpha} \\ &= -\frac{\partial}{\partial x_\alpha} \left(S^{\mathrm{J}} + S^{\mathrm{shear}} \right) + P_\beta \frac{\partial \widehat{u}_\beta}{\partial x_\alpha} - P_3 \frac{\partial \widehat{u}_\alpha}{\partial z} + \widehat{X}_\alpha, \end{aligned} \tag{8.41}$$

Grouping all P_β terms, as in Garrett (1976 eq. 3.10 and 3.11), leads to an expression with the 'vortex force' $\epsilon_{\alpha 3 \beta} \omega_3 P_\beta$. This force is the vector product of the wave pseudo-momentum $\mathbf{P}$ and mean flow vertical vorticity ω_3. Equation (8.41)

transforms to

$$\begin{aligned}\frac{\partial \widehat{u}_\alpha}{\partial t} + \widehat{u}_\beta \frac{\partial \widehat{u}_\alpha}{\partial x_\beta} + \widehat{w}\frac{\partial \widehat{u}_\alpha}{\partial z} \quad &+ \quad \epsilon_{\alpha 3\beta}\left[f_3 \widehat{u}_\beta + (f_3+\omega_3)\, P_\beta\right] + \frac{1}{\rho_w}\frac{\partial p^H}{\partial x_\alpha} \\ &= \quad -\frac{\partial}{\partial x_\alpha}\left(S^{\mathrm{J}} + S^{\mathrm{shear}}\right) - P_3 \frac{\partial \widehat{u}_\alpha}{\partial z} + \widehat{X}_\alpha. \qquad (8.42)\end{aligned}$$

The vortex force is a momentum flux divergence that compensates for the change in wave momentum flux due to wave refraction over varying currents, and includes the flux of momentum resulting from $\widehat{\mathbf{u}}$ momentum advected by the wave motion (Garrett 1976).

The turbulent closure is the topic of ongoing research and will not be explicitly detailed here. We only note that it differs in principle from the closure of the aGLM equations of Groeneweg (1999), which could be extended to include the second term in eq. (8.27). A proper closure involves a full discussion of the distortion of turbulence by the waves when the turbulent mixing time scale is larger than the wave period (e.g. Walmsley and Taylor 1996, Janssen 2004, Teixeira and Belcher 2002). One should consider with caution the rather bold but practical assumptions of Groeneweg (1999) who used a standard turbulence closure to define the viscosity that acts upon the wave-induced velocities, or the assumption of Huang and Mei (2003) who assumed that the eddy viscosity instantaneously adjusts to the passage of waves. These effects may have consequences on the magnitude of wave attenuation through its interaction with turbulence, and the resulting vertical profile of $\widehat{X}_\alpha$. Here we only note that any momentum lost by the wave field should be gained by either the atmosphere, the bottom or the mean flow. Thus a possible parameterization for the diabatic source of momentum is

$$\widehat{X}_\alpha = \frac{\partial R_{\alpha\beta}}{\partial x_\beta} + \frac{\partial}{\partial z}\left(K_z \frac{\partial \widehat{u}_\alpha}{\partial z}\right) - T_\alpha^{\mathrm{wc}} - T_\alpha^{\mathrm{turb}} - T_\alpha^{\mathrm{bfric}}, \qquad (8.43)$$

with $R_{\alpha\beta}$ the horizontal Reynolds stress, and K_z a vertical eddy viscosity, while the last three terms correspond to the dissipative momentum flux from waves to the mean flow, through whitecapping, wave-turbulence interactions, and bottom friction. Although the momentum lost by the waves via bottom friction was shown to eventually end up in the bottom (Longuet-Higgins 2005), the intermediate acceleration of the mean flow, also known as Eulerian streaming, is important for sediment transport, and should be included with a vertical profile of $T_\alpha^{\mathrm{bfric}}$ concentrated near the bottom, provided that the wave boundary layer is actually resolved in the 3D model (e.g. Walstra et al. 2001).

The GLM mass conservation writes

$$\frac{\partial\left(J\right)}{\partial t}+\frac{\partial\left(J\overline{u}_{\alpha}^{L}\right)}{\partial x_{\alpha}}+\frac{\partial\left(J\overline{w}^{L}\right)}{\partial z}=0, \tag{8.44}$$

where the Jacobian J is the determinant of the coordinate transform matrix $(\delta_{ij}+\partial\xi_i/\partial x_j)$ from Cartesian coordinates to GLM. (Andrews and McIntyre 1978a, eq. (4.2)-(4.4) with $\rho^{\xi}=\rho_w$).

8.2.2 *glm*2-RANS equations in z-coordinates

Equations (8.42) and (8.44) hold from $z=-h$ to $z=\overline{\zeta}^{L}$, which covers the entire 'GLM water column'. All terms in (8.42) are defined as GLM averages, except for the hydrostatic pressure p^{H} which does correspond to the Eulerian mean position.

For practical numerical modelling, it is however preferable that the height of the water column does not change with the local wave height. We will thus transform eq. (8.42), except for p^{H}, by correcting for the GLM-induced vertical displacements. This will naturally remove the divergence of the GLM flow related to $J\neq 1$. The GLM vertical displacement $\overline{\xi}_3^{L}$ is a generalization of eq. (8.23)

$$\overline{\xi}_3^{L}(x,z,t)=\int_{\mathbf{k}}E(\mathbf{k})m\left[k\frac{\sinh\left[2k(z+h)\right]}{2\sinh^{2}(kD)}+m\frac{\sinh^{2}\left[k(z+h)\right]}{\sinh^{2}(kD)}\frac{\mathbf{k}}{\sigma}\cdot\frac{\partial\overline{u}_{\alpha}}{\partial z}\right]\mathrm{d}\mathbf{k}. \tag{8.45}$$

and the Jacobian is $J=1+J_2+O(\varepsilon_1^3)$. Because the GLM does not induce horizontal distortions, a vertical distance $\mathrm{d}z'=J\mathrm{d}z$ in GLM corresponds to a Cartesian distance $\mathrm{d}z$, giving,

$$J_2 \;=\; -\frac{\partial\overline{\xi}_3^{L}}{\partial z}. \tag{8.46}$$

One may note that

$$\int_{-h}^{\overline{\zeta}^{L}}J\mathrm{d}z=\overline{\zeta}^{L}+h-\overline{\xi}_3^{L}(0)=D. \tag{8.47}$$

We now implicitly define the vertical coordinate $z^{\star}$ with

$$s=z^{\star}+\overline{\xi}_3^{L} \tag{8.48}$$

Any field $\phi(x_1,x_2,z,t)$ transforms to $\phi^{\star}(x_1^{\star},x_2^{\star},z^{\star},t^{\star})$ with

$$\frac{\partial\phi}{\partial t} \;=\; \frac{\partial\phi^{\star}}{\partial t^{\star}}-\frac{s_t}{s_z}\frac{\partial\phi^{\star}}{\partial z^{\star}} \tag{8.49}$$

$$\frac{\partial \phi}{\partial x_\alpha} = \frac{\partial \phi^\star}{\partial x^\star_\alpha} - \frac{s_\alpha}{s_z}\frac{\partial \phi^\star}{\partial z^\star} \tag{8.50}$$

$$\frac{\partial \phi}{\partial z} = \frac{1}{s_z}\frac{\partial \phi^\star}{\partial z^\star} \tag{8.51}$$

with s_t, s_z and s_α the partial derivatives of s with respect to $t^\star$, $z^\star$ and $x^\star_\alpha$, respectively. The coordinate transform was built to obtain the following identity

$$s_z J = 1 + O\left(\varepsilon_1^3\right). \tag{8.52}$$

Removing the $\star$ superscripts from now on, the mass conservation (8.44) multiplied by s_z may be written as

$$\frac{\partial\left(\overline{u}^L_\alpha\right)}{\partial x_\alpha} + \frac{\partial\left(W\right)}{\partial z} = 0, \tag{8.53}$$

where the vertical velocity,

$$W = J\left[\overline{w}^L - \overline{u}^L_\alpha s_\alpha - s_t\right] = \widehat{w}\frac{1+O(\varepsilon)}{\partial\overline{\xi}^L_3/\partial z}, \tag{8.54}$$

is the Lagrangian mass flux through horizontal planes.

Neglecting terms of order ε_1^3 and higher, the product of (8.42) and $s_z J$ is re-written as,

$$\begin{aligned}\frac{\partial \widehat{u}_\alpha}{\partial t} &+ \widehat{u}_\beta\frac{\partial \widehat{u}_\alpha}{\partial x_\beta} + \widehat{w}\frac{\partial \widehat{u}_\alpha}{\partial z} + \epsilon_{\alpha 3\beta}\left[f_3\widehat{u}_\beta + \left(f_3+\omega_3\right)P_\beta\right] + \frac{\partial p^H}{\partial x_\alpha} \\ &= -\frac{\partial}{\partial x_\alpha}\left(S^{\mathrm{J}} + S^{\mathrm{shear}}\right) - P_3\frac{\partial \widehat{u}_\alpha}{\partial z} + \widehat{X}_\alpha,\end{aligned} \tag{8.55}$$

with

$$\begin{aligned}\widehat{w} &= J\left[\overline{w}^L - \widehat{u}_\alpha s_\alpha - s_t\right] - P_3 = W - P_3 + JP_\alpha s_\alpha \\ &= W - P_3 + O(\sigma\varepsilon_1^4\varepsilon_2/k),\end{aligned} \tag{8.56}$$

the quasi-Eulerian advection velocity through horizontal planes. >From now on we shall use exclusively these $glm2z$-RANS equations in z coordinate, with a non-divergent GLM velocity field $\overline{\mathbf{u}}^L$.

Using eq. (8.25), we may re-write (8.53) as

$$\frac{\partial \widehat{u}_\alpha}{\partial x_\alpha} + \frac{\partial \widehat{w}}{\partial z} = 0. \tag{8.57}$$

Surface boundary conditions

Taking an impermeable boundary, the kinematic boundary condition is given by Andrews and McIntyre (1978a, section 4.2),

$$\frac{\partial \overline{\zeta}^L}{\partial t} + \overline{u}^L_\alpha \frac{\partial \overline{\zeta}^L}{\partial x_\alpha} = \overline{w}^L \quad \text{at} \quad z = \overline{\zeta}^L. \tag{8.58}$$

It is transformed to z coordinates as

$$\frac{\partial \overline{\zeta}}{\partial t} + \overline{u}^L_\alpha \frac{\partial \overline{\zeta}}{\partial x_\alpha} = W = \widehat{w} + P_3 \quad \text{at} \quad z = \overline{\zeta}. \tag{8.59}$$

When the presence of air is considered, it should be noted that the GLM position is discontinuous in the absence of viscosity, because the Stokes corrections for ζ have opposite signs in the air and in the water. This discontinuity arises from the discontinuity of the horizontal displacement ξ_α (air and water wave-induced motions are out of phase). A proper treatment would therefore require to resolve the viscous boundary layer at the free surface. This question is left for further investigation. However, we note that due to the large wind velocities and possibly large surface currents unrelated to wave motions, a good approximation is given by neglecting the Stokes corrections for the horizontal air momentum,

$$\widehat{u}^+_\alpha = \widehat{u}^-_\alpha + P^-_\alpha, \tag{8.60}$$

where the $-$ and $+$ exponents refer to the limits when approaching the boundary from below and above, respectively.

For the mean horizontal stress, we use the results of Xu and Bowen (1994),

$$\tau_\alpha = \overline{S_{nn} n_\alpha} + \overline{S_{ns} n_3} \quad \text{at} \quad z = \overline{\zeta} \tag{8.61}$$

with $\mathbf{S}$ the stress tensor, with normal S_{nn} and shear S_{ns} stresses on the surface, generally defined by

$$S_{ij} = -p\delta_{ij} + \rho_w \nu \left(\frac{\partial u_i}{\partial x_j} + \frac{\partial u_j}{\partial x_i} \right), \tag{8.62}$$

with ν the kinematic viscosity, and the local unit vector normal to the surface, to first order in ε_1,

$$\mathbf{n} = (0, 0, 1) - \left(\frac{\partial \zeta}{\partial x_1}, \frac{\partial \zeta}{\partial x_2}, 0 \right). \tag{8.63}$$

Taking the Lagrangian mean of (8.61), one obtains,

$$\tau_\alpha^a = \overline{\tau_\alpha}^L = \tau_\alpha^w + \rho_w \nu \frac{\partial \widehat{u}_\alpha}{\partial z} + \rho_w \nu \frac{\partial P_\alpha}{\partial z} \quad \text{at} \quad z = \overline{\zeta}, \tag{8.64}$$

where τ_α^a is the total air-sea momentum flux (the wind stress), as can be measured above the wave-perturbed layer (e.g. Drennan et al. 1999). τ_α^w is the α component of the wave-supported stress due to surface-slope pressure correlations,

$$\tau_\alpha^w = \overline{p \frac{\partial \zeta}{\partial x_\alpha}}^L . \tag{8.65}$$

The second viscous term $\rho_w \nu \partial P_\alpha / \partial z$ was estimated using the GLM average of wave orbital shears (Ardhuin and Jenkins 2006), it is the well-known virtual wave stress (e.g. Xu and Bowen 1994, eq. 18). That stress corresponds to wave momentum lost due to viscous dissipation, and it can be absorbed into the boundary conditions because it is concentrated within a few millimeters from the surface (Banner et Peirson 1998). At the base of the viscous layer of thickness δ_s, (8.64) yields, using an eddy viscosity K_z,

$$\tau_\alpha^a - \tau_\alpha^w - \rho_w \nu \frac{\partial P_\alpha}{\partial z} = \rho_w K_z \frac{\partial \widehat{u}_\alpha}{\partial z} \quad \text{at} \quad z = -\delta_s. \tag{8.66}$$

Bottom boundary conditions

The same approach applies to the bottom boundary conditions. The kinematic boundary condition writes

$$\frac{\partial \overline{h}^L}{\partial t} + (\widehat{u}_\alpha + P_\alpha) \frac{\partial \overline{h}^L}{\partial x_\alpha} = (\widehat{w} + P_3) \quad \text{at} \quad z = -\overline{h}^L. \tag{8.67}$$

If an adherence condition is specified at the bottom, which shall be used below, the bottom boundary condition further simplifies as $\overline{h}^L = h$. It may also simplify under the condition that the wave amplitude is not correlated with the small scale variations of h, which is not generally the case (e.g. Ardhuin and Magne 2007). For the dynamic boundary conditions, pressure-slope correlations give rise to a partial reflection of waves, that may be represented by a scattering stress (e.g. Hara and Mei 1987, Ardhuin and Magne 2007). This stress modifies the wave pseudo-momentum without any change of wave action (see also Ardhuin 2006).

The effect of bottom friction is of considerable interest for sediment dynamics and deserves special attention. For the sake of simplicity, we shall here use the conduction solution of Longuet-Higgins for a constant viscosity over a flat sea bed as given in the appendix to the proceedings of Russel and Osorio (1958). We shall

briefly consider waves propagating along the x-axis, and we assume that the mean current in the wave bottom boundary layer (WBBL) is at most of the order of the wave orbital velocity outside of the WBBL. Instead of (8.11)–(8.16) the orbital wave velocity and displacements near the bottom take the form,

$$u_1 = u_0\left[\cos\psi - \mathrm{e}^{-\widehat{z}}\cos(\psi-\widehat{z})\right] \tag{8.68}$$

$$w = \frac{u_0 k\delta_f}{2}\left[2\widehat{z}\sin\psi - \sin(\psi-\widehat{z})\mathrm{e}^{-\widehat{z}} + \sin\psi + \cos(\psi-\widehat{z})\mathrm{e}^{-\widehat{z}} - \cos\psi\right] \tag{8.69}$$

$$\xi_1 = -\frac{u_0}{\omega}\left[\sin\psi - \sin(\psi-\widehat{z})\mathrm{e}^{-\widehat{z}}\right] \tag{8.70}$$

$$\xi_3 = \frac{u_0 k\delta_f}{2\omega}\left[2\widehat{z}\cos\psi - \cos(\psi-\widehat{z})\mathrm{e}^{-\widehat{z}} + \cos\psi + \sin(\psi-\widehat{z})\mathrm{e}^{-\widehat{z}} - \sin\psi\right] \tag{8.71}$$

where $\psi = kx - \omega t$ is the wave phase, $\delta_f = (2\nu/\omega)^{1/2}$ is the depth scale for the boundary layer, $\widehat{z} = (z+h)/\delta_f$ is a non-dimensional vertical coordinate, $u_0 = a\sigma/\sinh(kD)$ is the orbital velocity amplitude outside the boundary layer.

Based on these velocities and displacements, the wave pseudo-momentum P, is

$$P_1 = \overline{-\xi_{1,1}u_1 - \xi_{3,1}w} = \frac{u_0^2}{2C}\left[1 + \mathrm{e}^{-2\widehat{z}}\cos(2\widehat{z}) - 2\cos\widehat{z}\mathrm{e}^{-\widehat{z}}\right]. \tag{8.72}$$

This is equal to the Stokes drift $\overline{u}^S = \overline{u_{1,1}\xi_1 + u_{1,3}\xi_3}$ computed by Longuet-Higgins. Besides, the rate of wave energy dissipation induced by bottom friction is $S_{\mathrm{bfric}} = \rho_w\omega u_0^2/2$ giving a bottom friction stress $\int_{-h}^{\infty} T_\alpha^{\mathrm{bfric}}\mathrm{d}z = k_\alpha S_{\mathrm{bfric}}/(\rho_w\sigma)$.

Generalizing this approach to a turbulent bottom boundary layer (e.g. Longuet-Higgins 2005) one may replace the constant viscosity with a depth-varying eddy viscosity. If the wave bottom boundary layer (WBBL) is resolved, $\overline{\tau}_\alpha^b$ will also include the momentum lost by waves through bottom friction, as given by the depth-integral of $T_\alpha^{\mathrm{bfric}}$. One may estimate P from the vertical profiles of the wave orbital velocities $\widetilde{u}_\alpha$ and $\widetilde{w}$, and the modified pressure (8.38) has to be corrected for the change in wave orbital velocities in the WBBL. Many WBBL models are available for estimating these wave-induced quantities.

If the bottom boundary layer is not resolved, on may take the lowest model level at the top of the wave boundary layer. The bottom stress may then be computed from a parameterization of the bottom roughness $z_{0a'}$ (e.g. Mathisen and Madsen 1996, 1999), which relates the bottom stress

$$\overline{\tau}_\alpha^b = -\rho_w u_{\star c}^2 \frac{\widehat{u}_\alpha}{\widehat{u}}, \tag{8.73}$$

to the current velocity $\widehat{u}_\alpha$ at the lowest model level z,

$$\widehat{u}_\alpha = \kappa u_{\star c} \ln\left[\frac{z+h}{z_{0a'}}\right], \quad \text{for} \quad z+h < \delta_f. \tag{8.74}$$

Then the near-bottom velocity $\widehat{u}_\alpha$ should be taken equal to the Eulerian streaming velocity $\sim 1.5 P_\alpha$ (see e.g. Marin 2004, for turbulent cases with rippled beds). Further, in this case the bottom stress $\overline{\tau}^b_\alpha$ should not include the depth integral of T^{bfric}_α. This latter remark also applies to depth-integrated equations. Indeed, $\tau^{wb}_\alpha = \int_{-h}^{-h+\delta_f} T^{\text{bfric}}_\alpha \mathrm{d}z$ is a flux of momentum into the bottom due to wave bottom friction, τ^{wb}_α does not participate in the momentum balance that gives rise to a sea level set-down and set-up (Longuet-Higgins 2005).

8.3 Relations between the present theory and known equations

8.3.1 Depth-integrated GLM for a constant density ρ_w

Using (8.59) the mass conservation equation in z coordinates (8.53) classically gives (e.g. Phillips 1977)

$$\frac{\partial}{\partial t}\int_{-h}^{\overline{\zeta}} \rho_w \mathrm{d}z = -\frac{\partial}{\partial x_\alpha}\int_{-h}^{\overline{\zeta}} \rho_w \overline{u}^L_\alpha \mathrm{d}z \tag{8.75}$$

which is exactly the classic shallow-water mass conservation for constant density,

$$\frac{\partial D}{\partial t} = -\frac{\partial M_\alpha}{\partial x_\alpha}, \tag{8.76}$$

with the depth-integrated volume flux vector[3] $\mathbf{M}$ defined by

$$\mathbf{M} = \int_{-h}^{\overline{\zeta}} \overline{\mathbf{u}}^L \mathrm{d}z. \tag{8.77}$$

In the momentum equation, the advection terms may be transformed in flux form using mass conservation. However, because some of the original GLM advection terms are included in the vortex force, the remaining terms do not simplify completely. Using (8.57) one has,

$$\rho_w \quad \left[\frac{\partial \widehat{u}_\alpha}{\partial t} + \widehat{u}_\beta \frac{\partial \widehat{u}_\alpha}{\partial x_\beta} + \widehat{w}\frac{\partial \widehat{u}_\alpha}{\partial z}\right] + P_3 \frac{\partial \widehat{u}_\alpha}{\partial z}$$

[3]Phillips (1977) uses the notation $\widetilde{\mathbf{M}}$ instead of $\mathbf{M}$, and $\mathbf{M}$ instead of $\mathbf{M}^w$.

$$= \frac{\partial}{\partial t}\left(\rho_w \widehat{u}_\alpha\right) + \frac{\partial}{\partial x_\beta}\left(\rho_w \widehat{u}_\beta \widehat{u}_\alpha\right) + \frac{\partial}{\partial z}\left[\rho_w\left(\widehat{w}+P_3\right)\widehat{u}_\alpha\right] - \widehat{u}_\alpha \frac{\partial P_3}{\partial z}. \quad (8.78)$$

Using (8.59), (8.67) and (8.25), and after integration by parts, these advection terms integrate to

$$\frac{\partial M^m_\alpha}{\partial t} + \frac{\partial}{\partial x_\beta}\left(\int_{-h}^{\overline{\zeta}} \rho_w \widehat{u}_\alpha \widehat{u}_\beta \mathrm{d}z\right) + u_{A\alpha}\frac{\partial M^w_\beta}{\partial x_\beta} + \frac{\partial u_{A\alpha}}{\partial x_\beta} M^w_\beta - \int_{-h}^{\overline{\zeta}} P_\beta \frac{\partial \widehat{u}_\alpha}{\partial x_\beta}\mathrm{d}z, \quad (8.79)$$

where the zeroth order wave advection velocity $\mathbf{u}_A$ is defined by,

$$u_{A\alpha} M^w_\beta \equiv \int_{-h}^{\overline{\zeta}} \widehat{u}_\alpha P_\beta \mathrm{d}z, \quad (8.80)$$

which is equal, at lowest order, to the second term in (8.8). The wave-induced mass transport is the depth-integrated pseudo-momentum,

$$\mathbf{M}^w = \int_{-h}^{\overline{\zeta}} \mathbf{P}\mathrm{d}z. \quad (8.81)$$

Finally, the quasi-Eulerian volume flux is defined by $\mathbf{M}^m = \mathbf{M} - \mathbf{M}^w$.

For terms uniform over the depth ($\partial p^H/\partial x_\alpha$ and $\partial S^{\mathrm{J}}/\partial x_\alpha$) the integral is simply the integrand times the depth.

It should be noted that the depth-integrated vortex force involves the advection velocity $\mathbf{u}_A$,

$$\int_{-h}^{\overline{\zeta}^L} \epsilon_{\alpha 3\beta}\left(f_3+\omega_3\right) P_\beta \mathrm{d}z = \epsilon_{\alpha 3\beta}\left(f_3+\Omega_3\right) M^w_\beta, \quad (8.82)$$

with

$$\Omega_3 = \epsilon_{3\alpha\beta}\left(\partial u_{A\beta}/\partial x_\alpha - \partial u_{A\alpha}/\partial x_\beta\right). \quad (8.83)$$

The vertical integration of (8.55) thus yields

$$\begin{aligned} \tfrac{\partial M^m_\alpha}{\partial t} & + \frac{\partial}{\partial x_\beta}\left(\int_{-h}^{\overline{\zeta}} \rho_w \widehat{u}_\alpha \widehat{u}_\beta \mathrm{d}z\right) + \epsilon_{\alpha 3\beta} f_3 M^m_\beta + D\frac{\partial}{\partial x_\alpha}\left(\rho_w g\overline{\zeta} + p_a\right) \\ = & -\epsilon_{\alpha 3\beta}\left(f_3+\Omega_3\right) M^w_\beta - u_{A\alpha}\frac{\partial M^w_\beta}{\partial x_\beta} - \frac{\partial u_{A\alpha}}{\partial x_\beta} M^w_\beta + \int_{-h}^{\overline{\zeta}} P_\beta \frac{\partial \widehat{u}_\alpha}{\partial x_\beta}\mathrm{d}z \\ & -D\frac{\partial S^{\mathrm{J}}}{\partial x_\alpha} - \int_{-h}^{\overline{\zeta}} \frac{\partial S^{\mathrm{shear}}}{\partial x_\alpha}\mathrm{d}z - \int_{-h}^{\overline{\zeta}} P_3 \frac{\partial \widehat{u}_\alpha}{\partial z}\mathrm{d}z + X^{\mathrm{int}}. \end{aligned} \quad (8.84)$$

The source of momentum X^{int} is simply the sum of the mean momentum fluxes at the top and bottom, and the source of momentum due to diabatic wave-mean flow interactions (i.e. breaking and wave-turbulence interactions), corresponding to Smith's $k_i D^W$.

These equations are very similar to those of Smith (2006, eq. 2.29), our term

S^{J} is simply termed J in Smith (2006). The only differences are due to the vertical shear in the current. The advection velocity $u_{A\alpha}$ replaces Smith's mean flow velocity. Since $u_{A\alpha}$ is the proper lowest order advection velocity for the wave action (Andrews and McIntyre 1978b), this is a simple extension of Smith's result to depth-varying currents. The term involving S^{shear} is also obviously absent from Smith's equations. The last differences in (8.84) are the last two terms on the second line, but they also cancel for a depth-uniform current $\widehat{u}_\alpha$.

8.3.2 Equations of McWilliams et al. (2004)

The approach of MRL04 is in the line of perturbation theories presented by Mei (1989) for Eulerian variables and monochromatic waves. Although the result of MRL04 corresponds to a particular choice of the relative ordering of small parameters, it is given to a high enough order so that it does cover most situations at a lower order. In particular MRL04 have pushed the expansion to order ε_1^4 for some terms because they assumed a ratio σ/f_3 of order ε_1^4, with ε_1 the wave slope. This ratio, in practice, may only be attained for relatively steep wind waves (developed wind seas and swells generally have slopes of the order of 0.05). They also assumed that $\varepsilon_1^2 \sim \varepsilon_2$ (the wave envelope varies on a scale relatively larger than the wavelength compared to the present theory in which $\varepsilon_1 \sim \varepsilon_2$ is possible). These authors also separated the motion into waves, long waves and mean flow, and considered in detail the rotational part of the wave motion caused by the vertical shear of the current.

MRL04 thus obtained Eulerian-mean equations that only correspond to measurable Eulerian averages under the level of the wave troughs. Because they use an analytic continuation of the velocity profiles across the air-sea interface, the physical interpretation of their average is unclear between the crests and troughs of the waves. We shall neglect here their terms of order ε_1^4 (i.e. terms that involve the wave amplitude to the power of four), which amounts to choosing a slightly different scaling. Since we shall consider here random waves, this avoids cumbersome considerations of the wave bispectrum.

The Eulerian-mean variables of MRL04 should be related to the Lagrangian mean values by the Stokes corrections (8.5), so that their horizontal Eulerian-mean velocity $\mathbf{q}$ corresponds to $\overline{\mathbf{u}}^L - \overline{\mathbf{u}}^S$. Because they have subtracted the hydrostatic pressure with the mean water density ρ_{w0}, their mean pressure $\langle p \rangle$ should be equal to the Eulerian mean pressure $\overline{p} + \rho_{w0} g z$, with $\overline{p}$ related to the GLM pressure via eq. (8.37).

Absorbing the long waves in the mean flow (i.e. allowing the mean flow to vary

on a the wave group scale, see also Ardhuin et al. 2004), MRL04 equations for the 'Eulerian' mean velocity $(q_1, q_2, \overline{w})$ can be written as

$$\frac{\partial q_\alpha}{\partial t} + \left(q_\beta \frac{\partial}{\partial x_\beta} + \overline{w}\frac{\partial}{\partial z} \right) q_\alpha + \epsilon_{\alpha 3\beta} f_3 q_\beta + \frac{1}{\rho_w}\frac{\partial \langle p \rangle}{\partial x_\alpha} = -\frac{\partial}{\partial x_\alpha}\left(\mathcal{K}_1 + \mathcal{K}_2\right) + J_\alpha \tag{8.85}$$

$$\frac{\partial \langle p \rangle}{\partial z} = (\rho_w - \rho_{w0})g - \frac{\partial}{\partial z}\left(\mathcal{K}_1 + \mathcal{K}_2\right) + K \tag{8.86}$$

$$\frac{\partial q_\beta}{\partial x_\beta} + \frac{\partial \overline{w}}{\partial z} = 0 \tag{8.87}$$

$$\langle p \rangle = \rho_w g \left(\overline{\zeta} - kEF_{SC}F_{SS} \right) - \mathcal{P}_0 \quad \text{at} \quad z = 0 \tag{8.88}$$

$$\overline{w} = -w^{St} \quad \text{at} \quad z = 0 \tag{8.89}$$

with

$$\mathcal{K}_1 = \frac{\overline{\widetilde{u}_j \widetilde{u}_j}}{2} = -\frac{1}{2}\left[F_{CC}F_{CS} + F_{SS}F_{SC}\right] gkE \tag{8.90}$$

$$J_\alpha = -\epsilon_{\alpha 3\beta}\left(f_3 + \omega_3\right)\overline{u}^S_\beta - w^{St}\frac{\partial q_\alpha}{\partial z} \tag{8.91}$$

$$K = \overline{u}^S_\beta \frac{\partial q_\beta}{\partial z} \tag{8.92}$$

$$\mathcal{K}_2 = \frac{\sigma k_\beta E}{k}\int_{-h}^{z} \frac{\partial^2 q_\beta(z')}{\partial z^2} F_{CS}(z')F_{SS}(z')\mathrm{d}z' \tag{8.93}$$

$$\mathcal{P}_0 = O(\frac{g}{k}\varepsilon_1^4) \tag{8.94}$$

The original notations of MRL04 (see also Lane et al. 2007) have been translated to the notations used above and order ε_1^4 terms have been neglected.

These equations are clearly analogue to the $glm2z$-RANS equations presented here. In particular the vertical vortex force term K corresponds to our K_1 that gets into S^{shear}, the dynamically relevant kinematic pressure pressure $\langle p \rangle + \mathcal{K}_1 + \mathcal{K}_2$ corresponds to our pressure $\widehat{p}$ defined by (8.38), and the vertical Stokes velocity w^{St} corresponds to our P_3. There are only two differences. One is between the surface boundary conditions for these two pressures, with a difference only due to $\mathcal{K}_2(z = 0) \neq -K_2(\overline{\zeta}^L)$. Integrating by parts to estimate $\mathcal{K}_2(z = 0)$, this difference is found to be of the order of $gkE\varepsilon_3$. Such a difference is of the same order as extra terms that would arise when using wave kinematics to first order in the current curvature (Kirby and Chen 1989), and properly transforming $\widehat{u}$ in $\overline{u}$. The second difference between MRL04 and the present equations is that the wave pseudo-momentum $\mathbf{P}$ differs from the Stokes drift $\overline{\mathbf{u}}^S$ when the current shear is large, and both generally differ from the expression for $\overline{\mathbf{u}}^S$ given by MRL04. Since MRL04 took the current and wave orbital velocity to be of the same order, in that context the difference

$\mathbf{P} - \overline{\mathbf{u}}^S$ is of higher order and thus the two sets of equations are consistent in their common range of validity.

A general comparison of 2D depth-integrated equations is discussed by Lane et al. (2006). The present work therefore brings a further verification of their 3D form of the equations, and an extension to relatively strong currents, possibly as large as the phase velocities. As expected, the Eulerian averages of McWilliams et al. (2004) are identical to the quasi-Eulerian fields in GLM theory, because they obey the same equations, except for current profile curvature effects, which were partly neglected here. The "Eulerian" mean current of MRL04 can thus be physically interpreted as a quasi-Eulerian average, defined as the GLM average minus the wave pseudo-momentum. Except for a Jacobian that introduces relative corrections of second order in the wave slope, this averaging is identical to the procedure used by Swan et al. (2001). Above the trough level, this average should not be confused with a truly Eulerian average, as obtained from in-situ measurements for example. In such measurements the Stokes drift would be recorded in the trough-to-crest region (figure 1.a).

8.4 Limitations of the approximations

The $glm2z$-RANS equations have been obtained from the exact GLM equations, under 6 restricting hypotheses related to the wave slope and Ursell number (H1 and H2), the horizontal scales of variation of the wave amplitude (H3), the current profile (H4 and H5) and the vertical mean velocity (H6). These hypotheses essentially allowed us to use the linear wave-induced quantities given by eqs. (8.11)–(8.19). In practical conditions, these hypotheses may not be verified and the resulting $glm2z$-RANS equations may have to be modified. Here we investigate the importance of H3, H2 and H1, using numerical solutions from an accurate coupled mode model for irrotational wave propagation over any bottom topography, and an accurate analytical solution for incipient breaking waves, respectively.

8.4.1 Bottom slope and standing waves

In absence of dissipation and given proper lateral boundary conditions the flow in wave shoaling over a bottom slope is irrotational and can thus be obtained by a numerical exact solution of Laplace's equation with bottom, surface, and lateral boundary conditions. For waves of small amplitudes this can be provided by a solution to this system of equations to second order in the wave slope. Belibassakis and Athanassoulis (2002) have developed a second order version of the National

Technical University of Athens numerical model (NTUA-nl2) to solve this problem in two dimensions. Here we apply their model to the simple case of monochromatic, unidirectional waves propagating along the x axis, with a topography uniform along the y axis. The topography $h(x)$ varies only for $0 < x < L$ and is constant $h(x) = h_1$ for $x < 0$ and $h(x) = h_2$ for $x > L$. In that case the Eulerian mean current $\nabla\phi_0(\mathbf{x})$ is irrotational, and uniform over the vertical as x approaches $\pm\infty$ (e.g. Belibassakis and Athanassoulis 2002, table 1 and figure 5). We shall further restrict our investigation to the case of a monochromatic wave train of known radian frequency ω and incident amplitude a, giving rise to reflected and transmitted wave trains of amplitudes Ra and Ta. Numerical calculations are given for a bottom profile as given by Roseau (1976) for which the reflection coefficient R is known analytically, thus providing a check on the quality of the numerical solution.

The bottom is defined here by x and z coordinates given by the real and imaginary part of the complex parametric function of the real variable x',

$$Z(x') = x + \mathrm{i}z = \frac{h_1(x' - \mathrm{i}\alpha_0) + (h_2 - h_1)\ln(1 + \mathrm{e}^{x' - \mathrm{i}\alpha_0})}{\alpha_0}. \tag{8.95}$$

We choose $h_1 = 6$ m and $h_2 = 4$ m and a wave frequency of 0.19 Hz ($\omega = 1.2$ rad s^{-1}). For $\alpha_0 = 15\pi/180$ the maximum bottom slope is $\varepsilon_2 = 2.6 \times 10^{-2}$ (figure 1), and the reflection coefficient for wave amplitude is $R = 1.4 \times 10^{-9}$ (Roseau 1976), so that reflected waves may be neglected in the momentum balance. Due to the shoaling of the incident waves, the mass transport induced by the waves increases in shallow water, and thus the mean current must change in the x direction to compensate for the divergence in the wave-induced mass transport. We shall further take a zero-mean surface elevation as $x \to -\infty$. The second order mean elevation is obtained as a result of the model. We also verified that the vertical wave pseudo-momentum compensates for the divergence of the horizontal component so that in this case for linear waves the wave pseudo-momentum is non-divergent (figure 3).

For mild bottom slopes, the reflection coefficient is small as predicted by Roseau (1976). The NTUA-nl2 model used here generally gives accurate reflection coefficients, but it tends to overestimate very weak reflections. In the first case investigated here, the numerical reflection is $R = 1 \times 10^{-3}$, with no significant effect on the wave dynamics. The NTUA-nl2 model is used to provide the Fourier amplitudes of the mean, first and second harmonic components of the velocity potential, over a grid of 401 (horizontal) by 101 (vertical) points. From these discretized potential fields, the mean, first and second harmonic velocity components are obtained using second order centered finite differences. As expected, the numerical solution gives a horizontal mean flow $\overline{u}$ that compensates the divergence of the wave mass

transport and is thus of order $\sigma/k\varepsilon^2$. Further $\overline{u}$ is almost uniform over the vertical and is irrotational (figure 8.2.b). The vertical mean velocity is of higher order. The GLM momentum balance is thus dominated by the hydrostatic and dynamic pressure terms p^H and S^{J}. Although these two terms are individually of the order of 0.01 m^2 s^{-2}, their sum is less than 2×10^{-16} m^2 s^{-2} in the entire domain, at the roundoff error level. It thus appears that this part of the momentum balance is much more accurate than expected from the asymptotic expansion. Indeed, for any bottom slope, in the limit of small surface slopes and for irrotational flow and periodic waves, the Stokes correction (8.5) for the pressure and the time average of the Bernoulli equation give the following expression for the modified kinematic pressure (8.38)

$$\begin{aligned}
\widehat{p} = \frac{\overline{p}^L}{\rho_w} - \frac{\overline{u_j^l u_j^l}}{2} &= \frac{\overline{p}}{\rho_w} + \frac{1}{\rho_w}\overline{\xi_j \frac{\partial \widetilde{p}}{\partial x_j}} - \frac{\overline{\widetilde{u}_j \widetilde{u}_j}}{2} \\
&= -gz + \frac{1}{\rho_w}\overline{\xi_j \frac{\partial \widetilde{p}}{\partial x_j}} - \overline{\widetilde{u}_j \widetilde{u}_j} = -gz - \overline{\xi_j \frac{\partial^2 \widetilde{\phi}}{\partial x_j \partial t}} - \overline{\frac{\partial \widetilde{\xi}_j}{\partial t}\frac{\partial \widetilde{\phi}}{\partial x_j}} \\
&= -gz - \frac{\partial}{\partial t}\overline{\xi_j \widetilde{u}_j} = -gz
\end{aligned} \tag{8.96}$$

where the equalities only hold to second order in the surface slope. Thus the kinematic modified pressure $\widehat{p}$ has no dynamical effect to second order in the wave slope, as already discussed by McWilliams et al. (2004) and Lane et al. (2007). For irrotational flow, this remains true for any bottom topography and even for rapidly varying wave amplitudes, including variations on scales shorter than the wavelength.

Thus the only wave effect is the static change in mean water level (set-up or set-down), and dynamic consequences in the WBBL, where S^{J} goes to zero, leaving the hydrostatic pressure gradient to drive a mean flow that can only be balanced by bottom friction. For slowly varying wave amplitudes the mean sea level is given by Longuet-Higgins (1967, eq. F1)

$$\overline{\zeta}(x) = -\frac{kE}{\sinh(2kD)} + \frac{k_0 E_0}{\sinh(2k_0)} \tag{8.97}$$

where the 0 subscript correspond to quantities evaluated at any fixed horizontal position, the choice of which being irrelevant to the estimation of horizontal gradients of $\overline{\zeta}$.

Equation (8.97) is well verified by the NTUA-nl2 result for the case considered so far (figure 8.4.a). However, this is no longueur true for rapid variations in the wave amplitude $a(x)$, i.e. due to partially standing waves. In that case one should

use Longuet-Higgins' eq. D (op. cit.)

$$\overline{\zeta}(x) = -\left[\frac{\overline{\widetilde{u}_\beta\widetilde{u}_\beta - \widetilde{u}_3^2}}{2g}\right]_{z=0} + \left[\frac{\overline{\widetilde{u}_\beta\widetilde{u}_\beta - \widetilde{u}_3^2}}{2g}\right]_{z=0,x=x_0}, \tag{8.98}$$

with $\widetilde{u}_\beta$ and $\widetilde{u}_3$ given by linear wave theory. Eq. (8.98) is a generalization of Miche's (1944a) mean sea level solution under standing waves. Contrary to propagating wave groups, for which the mean sea level is depressed under large waves, here the depression occurs at the nodes of the standing wave, where the horizontal velocities are largest and amplitudes are smallest (figure 8.4.c).

Eq. (8.98) is well verified in the presence of partially standing waves. To illustrate this, we have modified the bottom topography, adding a sinusoidal bottom perturbation for $x > 180$ m with an amplitude of 5 cm and a bottom wavelength half of the local waves' wavelength, which maximizes wave reflection (Kreisel 1949). This yields a wave amplitude reflection $R = 0.03$, for $\omega = 1.2$ rad s^{-1}, of the order of observed wave reflections over gently sloping beaches (e.g. Elgar et al. 1994). The bottom is shown on figure 8.4.b. Although the standing wave pattern is hardly noticeable in the surface elevation (the amplitude modulation is only 6%, figure 8.4.c), the small pressure modulation occur at much smaller scales, so that the associated gradient can overcome the large scale gradients of the hydrostatic pressure (figure 8.4.d). As a result small partial stading waves can dominating the momentum balance in the WBBL (see Longuet-Higgins 1953, Yu and Mei 2000 for solutions obtained with constant viscosity).

In the presence of such standing waves, and in the absence of strong wave dissipation, the hydrostatic pressure on the scale of the standing waves (e.g. given by Miche 1944a) drives the flow in the WBBL towards the nodes of the standing wave (Longuet-Higgins 1953), and is balanced by bottom friction. This WBBL flow drives an opposite flow above, closing a secondary circulation cell. This secondary circulation is important for nearshore sediment transport just outside of the surf zone (Yu and Mei 2000). If these sub-wavelength circulations are to be modelled, the present $glm2z$-RANS theory should be extended to resolve the momentum balance on the scale of partial standing waves.

This extension is relatively simple as it only introduces additional standing wave terms in all quadratic wave-related quantities, arising from phase-couplings of the incident and reflected waves. This extension provides a generalization of eq. (8.98) in the presence of other processes. For example, eq. (8.39) now becomes

$$S^{\mathrm{J}} = g\int_{\mathbf{k_I}} \frac{kE(\mathbf{k})}{\sinh 2kD}\left[\left(1+R^2\right) - 2R^2(\mathbf{k})\cos(2\psi'(\mathbf{k}))\right]\mathrm{d}\mathbf{k} \tag{8.99}$$

with $R(\mathbf{k})$ the amplitude reflection coefficient and $2\psi'(\mathbf{k})$ is the phase of the partial standing waves defined by $\nabla\psi' = \mathbf{k}$ and $\partial\psi'/\partial t = -\mathbf{k}\cdot\boldsymbol{U}_A t$ such that it is zero at the crest of the incident waves. Note that the integral is over the incident wave numbers only (e.g. for wave propagation directions from 0 to π). Similar expressions are easily derived for the other wave forcing terms.

8.4.2 Effects of wave non-linearity

Deep or intermediate water waves do not break very often in most conditions (e.g. Banner et al. 2000, Babanin et al. 2001), thus the particular kinematics of breaking or very steep waves likely contributes little to the average forcing of the current. However, most of the waves break in the surf zone and deviations from Airy wave kinematics may introduce a systematic bias when the $glm2z$-RANS equations are applied in that context. Many wave theories have been developed that are generally more accurate than the Airy wave theory (e.g. Dean 1970). However, they may lack some realistic features found in breaking waves, such as sharp crests. In order to explore the magnitude of this bias, we shall use the kinematics of two-dimensional incipient breaking waves as given by the approximate theory of Miche (1944b).

Miche's theory is based on the asymptotic expansion of the potential flow from the triangular crest of a steady breaking wave, extending Stokes' 120° corner flow to finite depth. >From this Miche obtained his criterion for the maximum steepness of a steady breaking wave, i.e. $h/\lambda = 0.14\tanh(kh)$ with h the breaking wave height and λ the wavelength, which favorably compares with observations. The Miche wave potential ϕ and streamfunction $\widetilde{\psi}$ are expressed implicitly as a function G of the coordinates $x - x_c + \mathrm{i}(z - z_c)$, with origin on the wave crest (x_c, z_c). The coefficients in the series representing the reciprocal function G' are obtained from the boundary condition at the surface and bottom. Unfortunately, these are imposed only under the wave crest and trough, so that the bottom streamline may not be horizontal away from the crest. This is particularly true for small values of kh. Due to the expansion of G' in powers of $\phi + \mathrm{i}\widetilde{\psi}$, the shape of the wave is nevertheless accurate near the crest, and since the overall drift velocities are dominated by the corner flow near the crest (see also Longuet-Higgins 1979), the approximations of Miche have little consequence on the drift velocities. The function G' was modified here to make the bottom actually flat, and the vertical under the trough an equipotential. This deformation adds a weak rotational component to the motion and the wave streamlines are weakly modified at the bottom under the wave trough[4]. The resulting wave for $kh = 0.58$ (corresponding to $b = 1$ in Miche

[4]This correction leads to negligible differences compared to the exact solution as verified with

1944b) is shown in figure 8.5.a. A numerical evaluation of that solution is obtained at 201 equally spaced values of ψ and 401 equally spaced values of ϕ (figure 8.5.b). The GLM displacement field ξ is computed as described in section 2.1. Since the streamlines are known in the frame of reference of the wave, Lagrangian positions of 201 particles initially placed below the crest at $x_i(0) = 0$, were tracked over four Eulerian wave periods. The positions $(x_i(t), z_i(t))$ are given by the potential $\phi_i(t)$ and streamfunction ψ_i. The Lagrangian period for each particle T_i^L is determined by detecting the first time when the particles pass under the crest again. The Lagrangian mean velocity of each particle is then $x_i(T_i^L)/T_i^L$, and it corresponds to a vertical position $\overline{z}_i = \int_0^{T_i^L} z_i(t)\mathrm{d}t$. This defines the Lagrangian mean velocity $\overline{u}^L(\overline{z}_i)$ in GLM coordinates. Following the coordinate transformation in section 2, we further transform the GLM velocity profile to z coordinate (figure 8.5.c). The resulting profile of $\overline{\mathbf{u}}^L$ has a horizontal tangent at $z = 0$, as discussed by Miche (1944b).

Contrary to Miche (1944b) who defined the phase speed C of his wave by imposing a zero mass transport, we have defined C so that $\mathbf{P} = \overline{\mathbf{u}}^L$ with the pseudo-momentum $\mathbf{P}$ estimated from eq. (7) using finite differences applied to the displacement field. The two profiles of $\mathbf{P}$, estimated from eq. (7), and $\overline{\mathbf{u}}^L$, estimated by time integration of particle positions coincide almost perfectly. Thus the estimation of $\mathbf{P}$ provides a practical method for separating the mean current from the wave motion. Starting from any value of C, the difference between $\overline{\mathbf{u}}^L$ and $\mathbf{P}$ is the mean current velocity $\widehat{\mathbf{u}}$. Here C was corrected to have $\widehat{\mathbf{u}} = 0$.

>From ξ, Bernoulli's equation can be used to obtain the GLM of velocities and pressure. Compared to linear wave theory, the Stokes drift in a Miche wave is much more sheared. It should be noted that in the cnoidal theory investigated by Wiegel (1959) this drift velocity is depth-uniform. Thus cnoidal wave theories may produce inaccurate results for 3D wave-current interactions when extrapolated to breaking waves. This marked difference in the 3D mean flow forcing due to breaking waves compared to linear waves calls for a deeper investigation of this question. Investigating such kinematics, may provide a rationale for the parameterization of nonlinearity in the *glm2z*-RANS equations proposed here. Such a parameterization is proposed by Rascle and Ardhuin (manuscript in preparation for the Journal of Geophysical Research).

streamfunction theory to 60th order.

8.5 Conclusion

We have approximated the exact Generalized Lagrangian Mean (GLM) wave-averaged momentum equations of Andrews and McIntyre (1978a), to second order in the wave slope, allowing for strong and sheared mean currents with limited curvature in the current profile. These approximated equations were then transformed by a change of the vertical coordinate, giving a non-divergent GLM flow in z coordinates. The resulting conservation equations for horizontal momentum (8.55) and mass (8.57), with boundary conditions (8.59)–(8.74) may be solved using slightly modified versions of existing primitive equations models, forced with the results of spectral wave models. Although the Stokes drift introduces a source of mass at the surface for the quasi-Eulerian flow, this is does not pose any particular problem, and such mass source have long been introduced for the simulation of upwellings. The HYCOM model (Bleck 2002) was modified by R. Baraille to solve a simplified set of the present equations, retaining only the wave-induced mass transport in both the mass and momentum equations, and the tracer equation (in which the advection velocity is simply $\overline{\mathbf{u}}^L$, see also MRL04). This work was applied to the a hindcast of the trajectories of sub-surface oil pellets released by the tanker Prestige-Nassau, which sank off Northwest Spain in November 2002 (presentation at the 2004 WMO-JCOMM 'Oceanops' conference held in Toulouse, France). The full equations derived here have also been implemented in the ocean circulation model ROMS (Shchepetkin and McWilliams 2003), and results will be reported elsewhere. The equations presented here have also been applied for the modelling of the ocean mixed layer in horizontally-uniform conditions (Rascle et al. 2006).

Although a general expression for the turbulent closure has been given, it has not been made explicit in terms of the wave and mean flow quantities beyond a heuristic closure that combines an eddy viscosity mixing term with the known sources of momentum due to wave dissipation. A proper turbulent closure is left for further work, possibly extending and combining the approaches of Groeneweg and Klopman (1998), with those of Teixeira and Belcher (2002). Further, some wave forcing quantities have been expressed in terms of the Eulerian mean current $\overline{\mathbf{u}}$ instead of the quasi-Eulerian mean current $\widehat{\mathbf{u}}$. The conversion from one to the other, can be done using eq. (8.24), to the order of approximation used here. However, it would be more appropriate, in particular for large current shears, to start from quasi-Eulerian wave kinematics, instead of Eulerian solutions of the kind given by Kirby and Chen (1989, our eq. 10–12).

Beyond the turbulence closure, there are essentially two practical limitations to the approximate $glm2z$-RANS equations derived here. First, the expansion of wave

quantities to second order in the surface slope is only qualitative in the surf zone. Although this was acceptable in two dimensions (see Bowen 1969 and most of the literature on this subject), it is expected to be insufficient in three dimensions due to a significant difference in the profile of the wave-induced drift velocity $\mathbf{P}$, which exhibits a vertical variation with surface values exceeding bottom values by a factor of 3, even for $kh < 0.2$ in which case linear wave theory predicts a depth-uniform $\mathbf{P}$. This conclusion is based on both the approximate theory of Miche (1944b), and results of the streamfunction theory of Dalrymple (1974) to 80th order. Such numerical results can be used to provide a parameterization of these effects. Further investigations using more realistic depictions of the kinematics of breaking waves will be needed. Second, the vertical profile of the mean current in the surf zone may be such that the wave kinematics are not well described by the approximations used here. A strong nonlinearity combined with a strong current shear and curvature can lead to markedly different wave kinematics (e.g. da Silva and Peregrine 1988).

With these caveats, the equations derived here provide a generalization of existing equations, extending Smith (2006) to three dimensions and vertically sheared currents, or McWilliams et al. (2004) to strong currents. Of course, mean flow equations can be obtained, at least numerically, using any solution for the wave kinematics with the original exact GLM equations, as illustrated in section 8.4.2. The wave-forcing on the mean flow is a vortex force plus a modified pressure, a decomposition that allows a clearer understanding of the wave-current interactions, compared to the more traditional radiation stress form. This is most important for the three-dimensional momentum balance and/or in the presence of strong currents, e.g. when a rip current is widened by opposing waves, as observed by Ismail and Wiegel (1983) in the laboratory. Such a situation was also recently modelled by Shi et al. (2006).

Acknowledgments. The correct interpretation of the vertical wave pseudo-momentum P_3 would not have been possible without the insistent questioning of John Allen. The critiques and comments from Jaak Monbaliu and Rodolfo Bolaños helped correct some misinterpretation of the equations and greatly improved the present paper. N.R. acknowledges the support of a CNRS-DGA doctoral research grant.

Symbol	name	where defined
1 and 2	indices of the horizontal dimensions	after (8.8)
3	index of the vertical dimension	after (8.8)
a	wave amplitude	after (8.12)
$D = h + \overline{\zeta}$	mean water depth	after (8.7)
$\mathbf{f} = (f_1, f_2, f_3)$	Coriolis parameter vector (twice the rotation vector)	after (8.6)
F_{CC}, F_{CS}, F_{SC} and F_{SS}	Vertical profile functions	after (8.12)
g	acceleration due to gravity and Earth rotation	after (8.7)
h	depth of the bottom (bottom elevation is $z = -h$)	before (8.8)
J	Jacobian of GLM average	after (8.44)
$\mathbf{k} = (k_1, k_2)$	wavenumber vector	after (8.7)
K_1	Depth-integrated vertical vortex force	(8.33)
K_2	Shear-induced correction to Bernoulli head	(8.29)
K_z	vertical eddy viscosity	(8.43)
$(\cdot)^l$	Lagrangian perturbation	(8.2)
$\overline{(\cdot)}^L$	Lagrangian mean	(8.1)
m	shear correction parameter	(8.20)
$\mathbf{M}$	depth-integrated momentum vector	(8.77)
$\mathbf{M}^w$	depth-integrated wave pseudo-momentum vector	(8.81)
$\mathbf{M}^m$	depth-integrated mean flow momentum vector	after (8.81)
$\mathbf{n}$	unit normal vector	(8.63)

Table 8.2: Table of symbols

Symbol	name	where defined
p	full dynamic pressure	after (8.26)
$\widetilde{p}$	wave-induced pressure	(8.10)
p^H	hydrostatic pressure	after (8.35)
$\mathbf{P} = (P_1, P_2, P_3)$	wave pseudo-momentum	(8.6)
t	time	before (8.1)
$\mathbf{u} = (u_1, u_2, u_3)$	velocity vector	
$\widetilde{\mathbf{u}}$	wave-induced velocity	(8.11) and (8.68)
$\overline{\mathbf{u}}^L$	Lagrangian mean velocity	after (8.1)
$\mathbf{u}_A$	advection velocity for the wave action	(8.80)
$\widehat{u}_\alpha = \overline{u}^L_\alpha - P_\alpha$	quasi-Eulerian horizontal velocity	before (8.24)
$s = z + \overline{\xi}^L_3$	GLM to z transformation function	(8.48)
$\overline{(\cdot)}^S$	Stokes correction	(8.5)
S_{ij}	stress tensor	(8.62)
S^{J}	wave-induced kinematic pressure	(8.39)
S^{Shear}	shear-induced correction to S^{J}	(8.40)
$w = u_3$	vertical velocity	before (8.30)
$\widehat{w} = \overline{u}^L_3 - P_3$	quasi-Eulerian vertical velocity	before (8.30)
W	GLM vertical velocity in z coordinates	(8.54)
$\mathbf{x} = (x_1, x_2, x_3)$	position vector	before (8.1)

Table 8.2: Table of symbols, continued

Symbol	name	where defined
$\mathbf{X}$	diabatic source of momentum	after (8.24)
$\widehat{\mathbf{X}}$	diabatic source of quasi-Eulerian mean momentum	(8.27)
$z = x_3$	vertical position	after (8.8)
α and β	dummy indices for horizontal dimensions	
δ_{ij}	Kronecker's symbol, zero unless $i = j$	after (8.26)
ε	generic small parameter	after (8.8)
ε_1	maximum wave slope	after (8.7)
ε_2	maximum horizontal gradient parameter	after (8.7)
ε_3	maximum current curvature parameter	(8.9)
$\epsilon_{ijk} A_j B_k$	component i of the vector product $\mathbf{A} \times \mathbf{B}$	after (8.6)
ζ	free surface elevation	before (8.8)
λ	wavelength	section 4.2
ν	kinematic viscosity of water	after (8.62)
$\xi = (\xi_1, \xi_2, \xi_3)$	wave-induced displacement	before (8.1)
ρ_w	density of water (constant)	after (8.12)
σ	relative radian frequency	after (8.7)
τ_{ij}	mean stress tensor	(8.61)
ψ	wave phase	after (8.7)
ω	absolute radian frequency	after (8.7) and (8.8)
Ω_3	depth-weighted vertical vorticity of the mean flow	(8.83)
∇	horizontal gradient operator	after (8.7)

Table 8.2: Table of symbols, continued

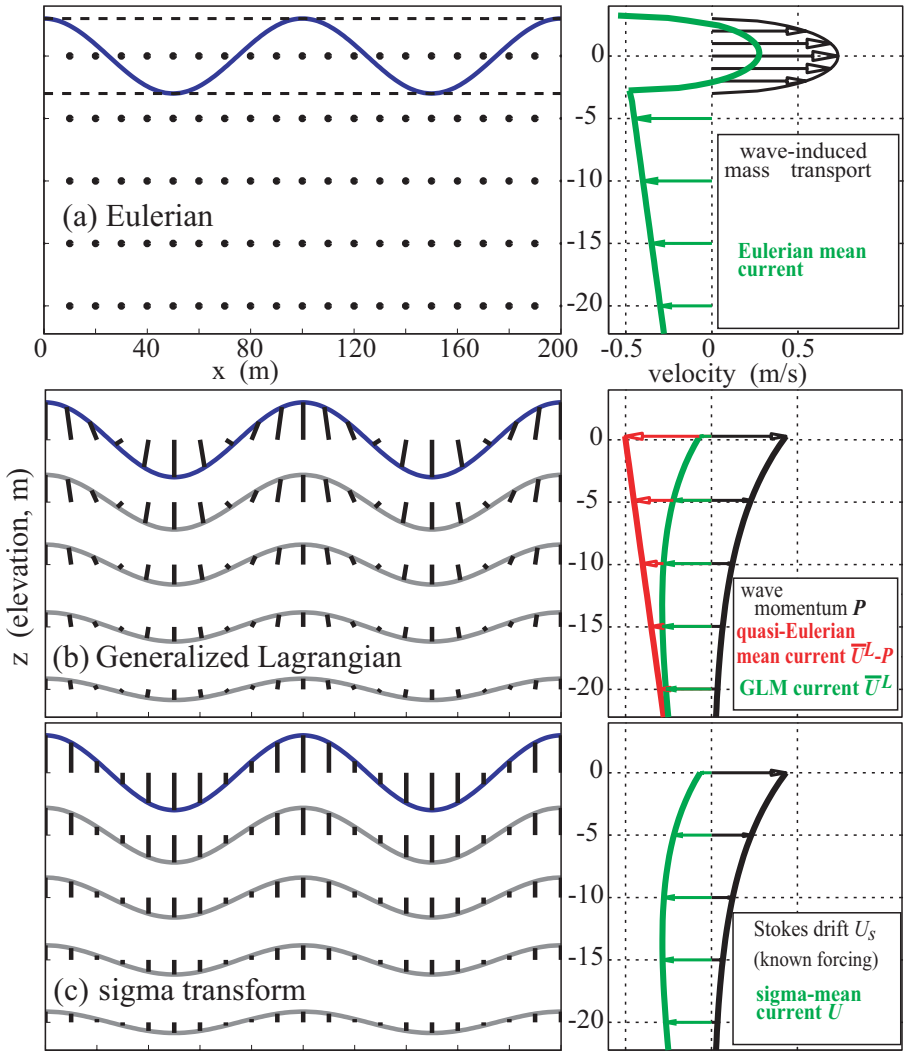

Figure 8.1: Averaging procedures (left) and examples of resulting velocity profiles (right) in the case of (a) Eulerian averages (e.g. Rivero and Sanchez-Arcilla 1995, McWilliams et al. 2004), (b) the Generalized Lagrangian Mean (Andrews and McIntyre 1978a), and (c) sigma transform (Mellor 2003, AJB07). The thick black bars connect the fixed points $\mathbf{x}$ where the average field is evaluated, to the displaced points $\mathbf{x}+\xi$ where the instantaneous field is evaluated. For averages in moving coordinates the points $\mathbf{x}+\xi$ at a given vertical level ξ are along the gray lines. The drift velocity is the sum of the (quasi-Eulerian) current and the wave-induced mass transport. In the present illustration an Airy wave of amplitude 3 m and wavelength 100 m in 30 m depth, is superimposed on a hypothetical current of velocity $u(z) = -0.5 - 0.01z$ m/s for all $z < \zeta(\mathbf{x})$. The current profile is not represented in (c) since it is not directly given in Mellor's theory, although it can obviously be obtained by taking the difference of the other two profiles.

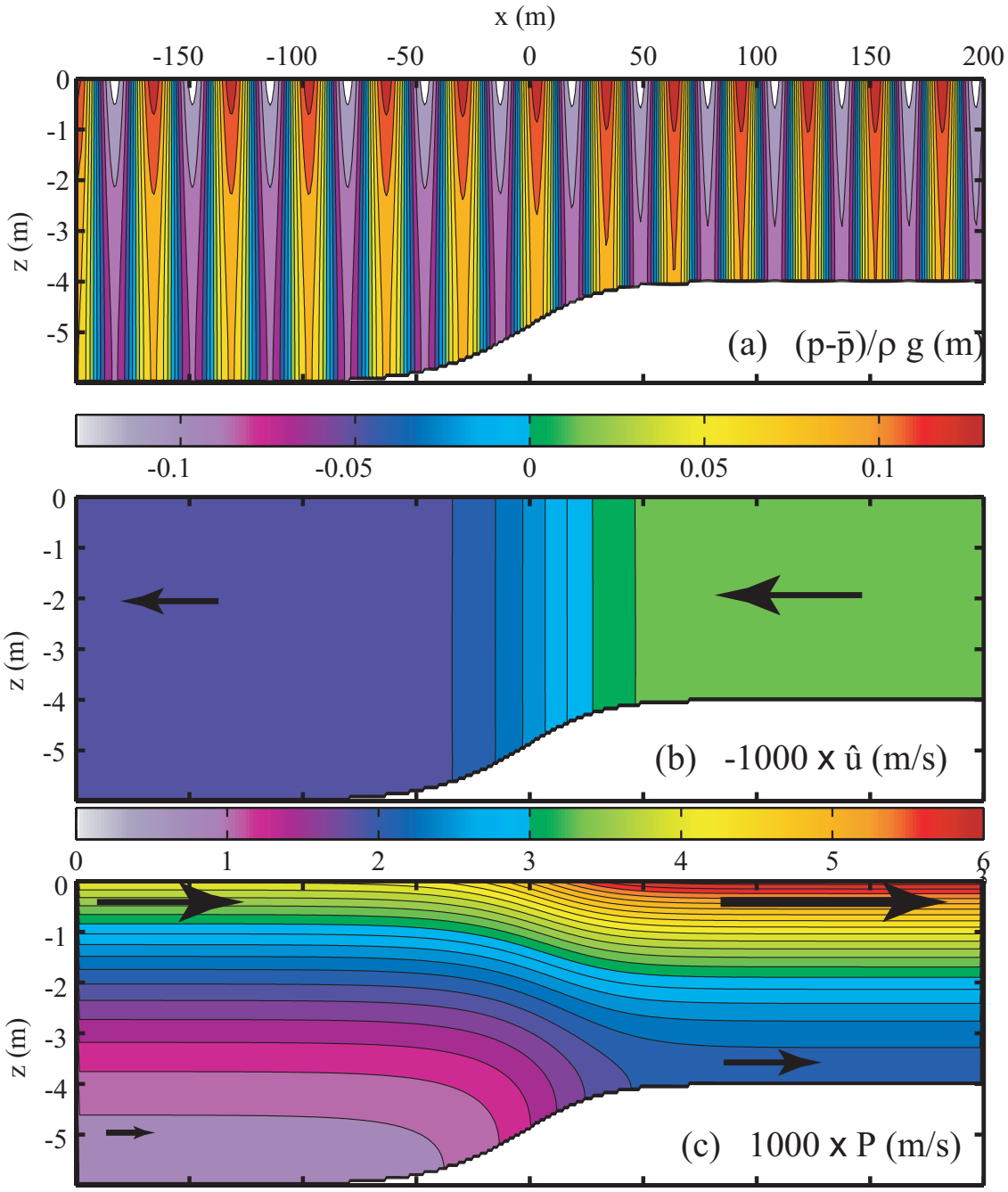

Figure 8.2: (a) Instantaneous pressure perturbation $(p - \overline{p})/(\rho_w g)$ given by the NTUA-nl2 model (Belibassakis and Athanassoulis 2002), including the second order Stokes component in waves with amplitude $a = 0.12$ m, over the bottom given by eq. (8.95). (b) Mean current $-\widehat{u}$, and (c) horizontal wave pseudo-momentum P_1 estimated from eq. (8.7), and verified to be equal to the Stokes drift. Arrows indicate the flow directions.

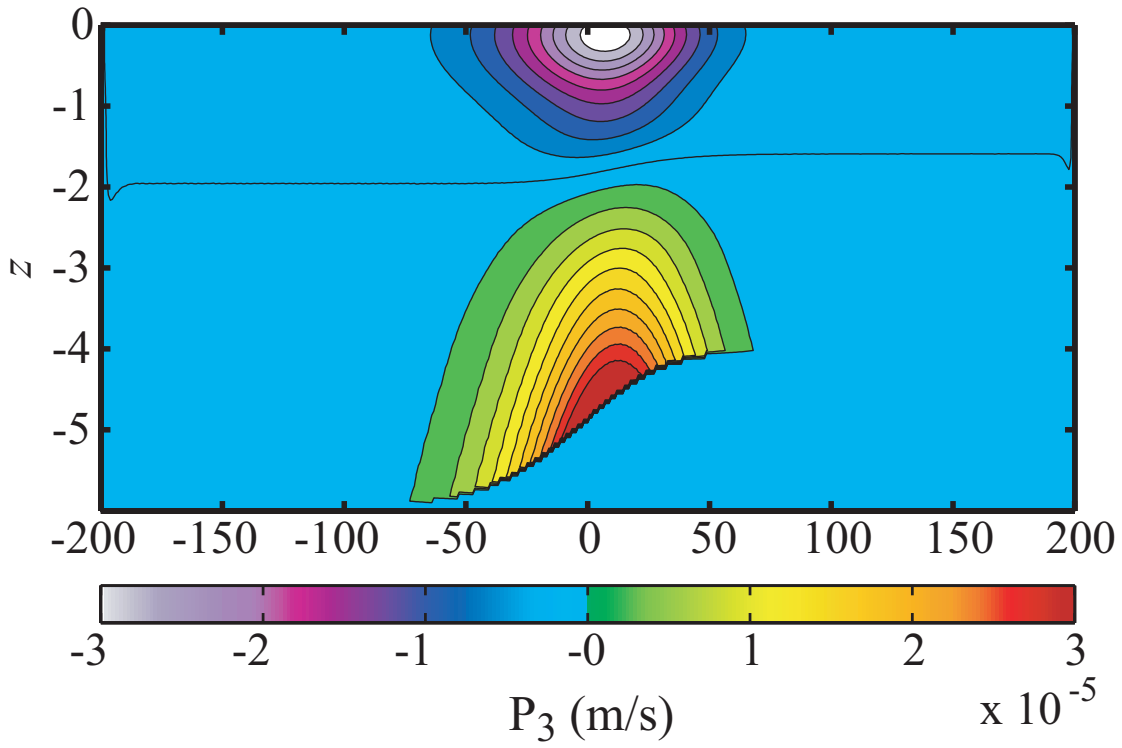

Figure 8.3: Vertical wave pseudo-momentum for the same case as figure 2, estimated from eq. (8.7), and verified to satisfy (8.25).

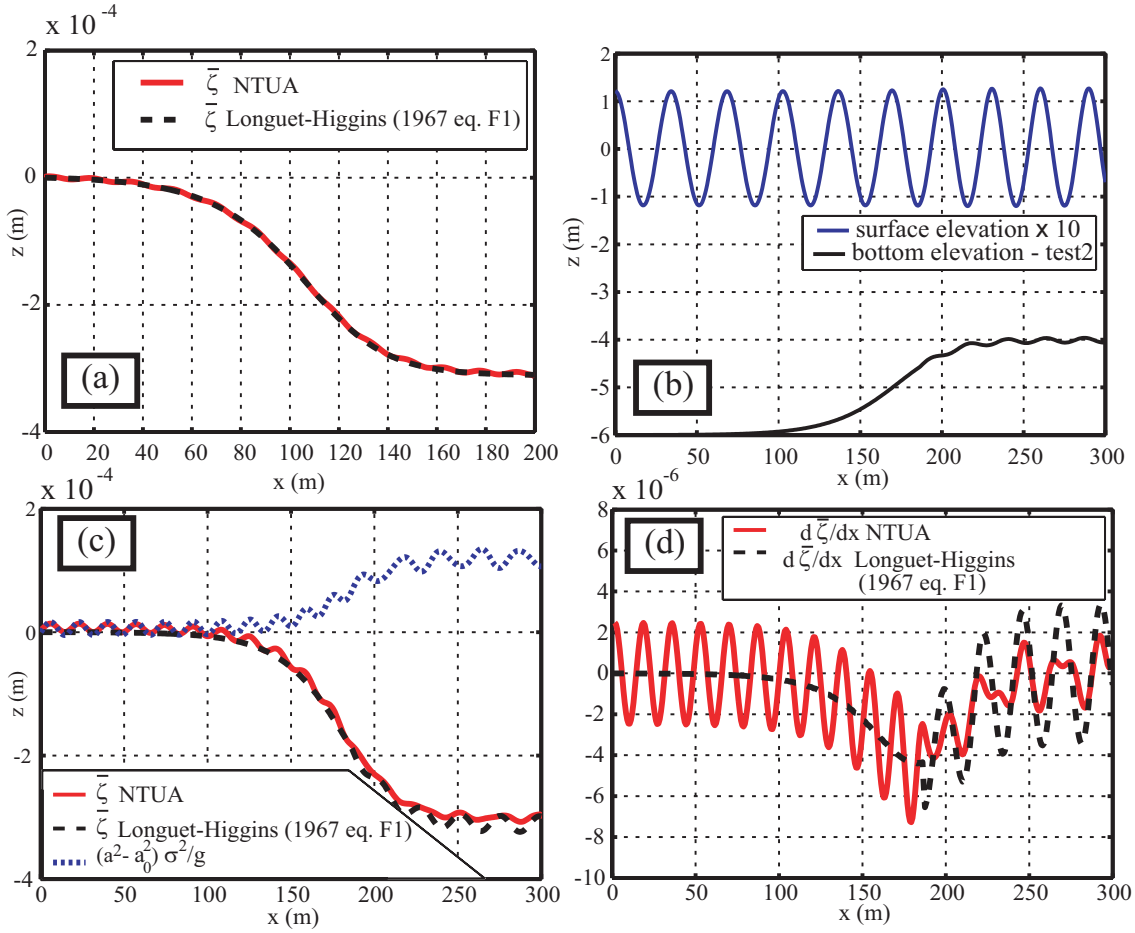

Figure 8.4: (a) Mean sea level obtained with the NTUA-nl2 model (Belibassakis and Athanassoulis 2002) and the theory of Longuet-Higgins (1967 eq. F1: without standing waves) using conservation of the wave energy flux along the profile. (b) modified bottom profile resulting in a 3% amplitude reflection at $\omega = 1.2$ rad s^{-1}, (c) resulting mean sea level and normalized local wave amplitude a, (d) mean sea level gradient (d).

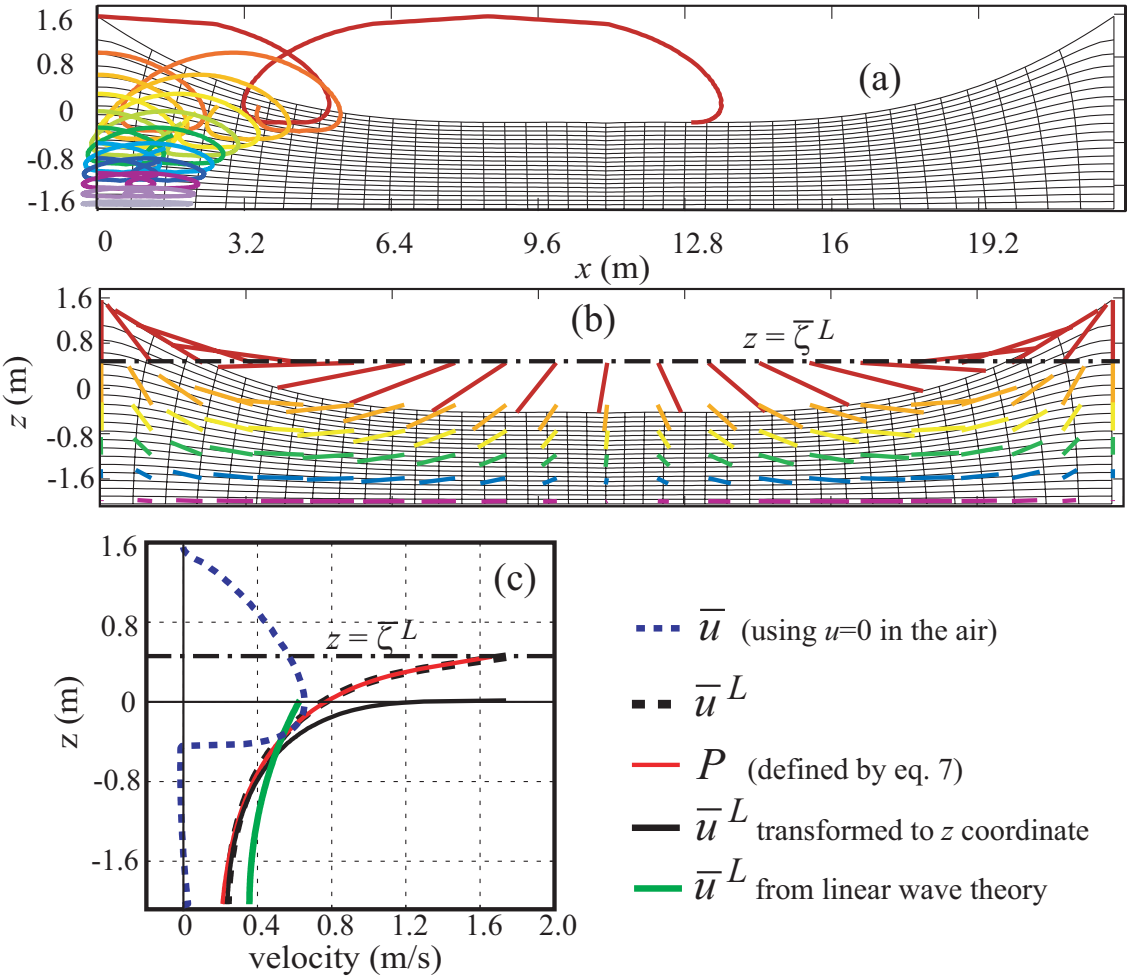

Figure 8.5: (a) Illustration of the drift over 2 Eulerian periods in periodic Miche waves. Trajectories are color-coded with their initial depth, below a wave crest. The thin black lines are the lines of constant potential and streamfunction at $t = 0$. (b) Field of displacements defining the GLM, as in figure 1.c. The dash-dotted line is the GLM position of the free surface $\overline{\zeta}^L$. (c) Profiles of Eulerian and Lagrangian mass transport velocity in a Miche wave compared to a linear wave with the same values of k and h.

Bibliography

Agrawal Y. C., Terray E. A., Donelan M. A., Hwang P. A., Williams A. J., Drennan W., Kahma K., Kitaigorodskii S. 1992: Enhanced dissipation of kinetic energy beneath breaking waves. *Nature*, **359**,219–220

Alves J. H. G. M., Banner M. L. 2003: Performance of a saturation-based dissipation-rate source term in modeling the fetch-limited evolution of wind waves. *J. Phys. Oceanogr.*, **33**,1274–1298

Andrews D. G., McIntyre M. E. 1976: Planetary waves in horizontal and vertical shear: the generalized Eliassen-Palm relation and the mean zonal acceleration. *J. Atmos. Sci.*, **33**(11),2031–2048

Andrews D. G., McIntyre M. E. 1978*a*: An exact theory of nonlinear waves on a Lagrangian-mean flow. *J. Fluid Mech.*, **89**,609–646

Andrews D. G., McIntyre M. E. 1978*b*: On wave action and its relatives. *J. Fluid Mech.*, **89**,647–664 Corrigendum: vol. 95, p. 796

Annika P., George T., George P., Konstantinos N., Costas D., Koutitas C. 2001: The Poseidon operational tool for the prediction of floating pollutant transport. *Marine Pollution Bulletin*, **43**,270–278

Apotsos A., Raubenheimer B., Elgar S., Guza R. T., Smith J. A. 2007: Effects of wave rollers and bottom stress on wave setup. *J. Geophys. Res.*, **112**,C02003

Ardhuin F. (2005) Etat de la mer et dynamique de l'océan superficiel. PhD thesis Université de Bretagne Occidentale Brest, France (mémoire d'habilitation à diriger des recherches), in French, except for appendices

Ardhuin F. 2006: On the momentum balance in shoaling gravity waves: a commentary of Śshoaling surface gravity waves cause a force and a torque on the bottomŠ by K. E. Kenyon. *Journal of Oceanography*, **62**,917–922

Ardhuin F., Chapron B., Elfouhaily T. 2004*a*: Waves and the air-sea momentum budget, implications for ocean circulation modelling. *J. Phys. Oceanogr.*, **34**,1741–1755

Ardhuin F., Herbers T. H. C., Jessen P. F., O'Reilly W. C. 2003: Swell transformation across the continental shelf. part II: validation of a spectral energy balance equation. *J. Phys. Oceanogr.*, **33**,1940–1953

Ardhuin F., Herbers T. H. C., Watts K. P., van Vledder G. P., Jensen R., Graber H. 2007*a*: Swell and slanting fetch effects on wind wave growth. *J. Phys. Oceanogr.*, **37**(4),908–931

Ardhuin F., Jenkins A. D. 2006: On the interaction of surface waves and upper ocean turbulence. *J. Phys. Oceanogr.*, **36**(3),551–557

Ardhuin F., Jenkins A. D., Hauser D., Reniers A., Chapron B. 2005: Waves and operational oceanography: towards a coherent description of the upper ocean for applications. *Eos Trans. AGU*, **86**(4),37–39

Ardhuin F., Le Boyer A. 2006: Numerical modelling of sea states: validation of spectral shapes (in French). *Navigation*, **54**(216),55–71

Ardhuin F., Magne R. 2007: Current effects on scattering of surface gravity waves by bottom topography. *J. Fluid Mech.*, **576**,235–264

Ardhuin F., Martin-Lauzer F.-R., Chapron B., Craneguy P., Girard-Ardhuin F., Elfouhaily T. 2004*b*: Dérive à la surface de l'océan sous l'effet des vagues. *Comptes Rendus Géosciences*, **336**,1121–1130

Ardhuin F., Rascle N., Belibassakis K. A. 2007*b*: Explicit wave-averaged primitive equations using a generalized lagrangian mean. *Ocean Modelling* in press [http://arxiv.org/abs/physics/0702067]

Ardhuin F., Rascle N., Belibassakis K. A. 2007*c*: Explicit wave-averaged primitive equations using a generalized lagrangian mean. *Ocean Modelling* in press. See also [http://arxiv.org/abs/physics/0702067]

Babanin A., Young I., Banner M. 2001: Breaking probabilities for dominant surface waves on water of finite depth. *J. Geophys. Res.*, **106**(C6),11659–11676

Banner M. L., Babanin A. V., Young I. R. 2000: Breaking probability for dominant waves on the sea surface. *J. Phys. Oceanogr.*, **30**,3145–3160

Banner M. L., Peirson W. L. 1998: Tangential stress beneath wind-driven air-water interfaces. *J. Fluid Mech.*, **364**,115–145

Battjes J. A. 1988: Surf-zone dynamics. *Annu. Rev. Fluid Mech.*, **20**,257–293

Battjes J., Stive M. 1985: Calibration and verification of a dissipation model for random breaking waves. *J. Geophys. Res.*, **90**(C5),9159–9167

Belibassakis K. A., Athanassoulis G. A. 2002: Extension of second-order Stokes theory to variable bathymetry. *J. Fluid Mech.*, **464**,35–80

Bidlot J., Abdalla S., Janssen P. (2005) A revised formulation for ocean wave dissipation in CY25R1. Technical Report Memorandum R60.9/JB/0516 Research Department, ECMWF, Reading, U. K.

Biesel F. 1950: Etude théorique de la houle en eau courante. *La houille blanche*, **Numéro spécial A**,279–285

Bleck R. 2002: An oceanic general circulation model framed in hybrid isopicnic-cartesian coordinates. *Ocean Modelling*, **4**,55–88

Bowen A. J. 1969: The generation of longshore currents on a plane beach. *J. Mar. Res.*, **27**,206–215

Brocchini M., Kennedy A. B., Soldini L., Mancinelli A. 2004: Topographically controlled, breaking-wave-induced macrovortices. part 3. the mixing features. *J. Fluid Mech.*, **507**,289–Ű307

Büler O. 2000: On the vorticity transport due to dissipating or breaking waves in shallow-water flow. *J. Fluid Mech.*, **407**,235–263

Charnock H. 1955: Wind stress on a water surface. *Quart. Journ. Roy. Meteorol. Soc.*, **81**,639–640

Chen Q., Kirby J. T., Dalrymple R. A., Shi F., Thornton E. B. 2003: Boussinesq modeling of longshore currents. *J. Geophys. Res.*, **108**(C11),3362 doi:10.1029/2002JC001308

Churchill G. H., Csanady G. T. 1983: Near-surface measurements of quasi-Lagrangian velocities in open water. *J. Phys. Oceanogr.*, **13**,1669–1680

Cokelet E. D. 1977: Steep gravity waves in water of arbitrary uniform depth. *Proc. Roy. Soc. Lond. A*, **286**,183–230

Cox C., Munk W. 1954: Measurement of the roughness of the sea surface from photographs of the sun's glitter. *J. Opt. Soc. Am.*, **44**(11),838–850

Craig P. D., Banner M. L. 1994: Modeling wave-enhanced turbulence in the ocean surface layer. *J. Phys. Oceanogr.*, **24**,2546–2559

Craik A. D. D., Leibovich S. 1976: A rational model for Langmuir circulations. *J. Fluid Mech.*, **73**,401–426

Dalrymple R. A. 1974: A finite amplitude wave on a linear shear current. *J. Geophys. Res.*, **79**,4498–4504

da Silva A. F., Peregrine D. H. 1988: Steep steady surface waves on water of finite depth with constant vorticity. *J. Fluid Mech.*, **195**,281–302

Dean R. G. 1970: Relative validity of water wave theories. *J. Waterways, Harbours Div.*, **96**(WW1),105–119

Denamiel C. (2006) Modélisation hydrodynamique 3D en zone pré-littorale. PhD thesis Universite de Montpellier Montpellier: Université de Montpellier 2, Sciences et Techniques du Languedoc, France in French

Dingemans M. W. (1997) *Water wave propagation over uneven bottoms. Part 1 linear wave propagation*. World Scientific, Singapore 471 p.

Dobson F., Perrie W., Toulany B. 1989: On the deep water fetch laws for wind-generated surface gravity waves. *Atmosphere Ocean*, **27**,210–236

Donelan M. (1990) *The Sea*. Vol 9 B. LeMahaute, D.M. Hanes (Eds), New York Wiley and Sons Ocean Engineering Science

Donelan M. A. (1998) Air-water exchange processes. In: Imberger J. (ed.) Physical Processes in Lakes and Oceans. American Geophysical Union, Washington, D.C. pages 18–36 ISBN 0-87590-268-5

Donelan M. A., Hamilton J., Hui W. H. 1985: Directional spectra of wind-generated waves. *Phil. Trans. Roy. Soc. London A*, **315**,509–562

Donelan M. A., Pierson, Jr. W. J. 1987: Radar scattering and equilibrium ranges in wind-generated waves with application to scatterometry. *J. Geophys. Res.*, **92**(C5),4971–5029

Drennan W. M., Donelan M. A., Terray E. A., Katsaros K. B. 1996: Oceanic turbulence dissipation measurements in SWADE. *J. Phys. Oceanogr.*, **26**,808–815

Drennan W. M., Graber H. C., Hauser D., Quentin C. 2003: On the wave age dependence of wind stress over pure wind seas. *J. Geophys. Res.*, **108**(C3),8062 doi:10.1029/2000JC00715

Drennan W. M., Kahma K., Donelan M. A. 1999: On momentum flux and velocity spectra over waves. *Boundary-Layer Meteorol.*, **92**,489–515

Ekman V. W. 1905: On the influence of the earth's rotation on ocean currents. *Ark. Mat. Astron. Fys.*, **2**,1–53

Elfouhaily T., Chapron B., Katsaros K., Vandemark D. 1997: A unified directional spectrum for long and short wind-driven waves. *J. Geophys. Res.*, **102**(C7),15781–15796

Elgar S., Herbers T. H. C., Guza R. T. 1994: Reflection of ocean surface gravity waves from a natural beach. *J. Phys. Oceanogr.*, **24**(7),1,503–1,511

Garrett C. 1976: Generation of Langmuir circulations by surface waves - a feedback mechanism. *J. Mar. Res.*, **34**,117–130

Gaspar J. P., Grégoris Y., Lefevre J. M. 1990: A simple eddy kinetic energy model for simulations of oceanic vertical mixing : Tests at station papa and long-term upper ocean study site. *J. Geophys. Res.*, **95**(C9),16179–16193

Gelci R., Cazalé H., Vassal J. 1957: Prévision de la houle. La méthode des densités spectroangulaires. *Bulletin d'information du Comité d'Océanographie et d'Etude des Côtes*, **9**,416–435

Gemmrich J. R., Farmer D. M. 1999: Near-surface turbulence and thermal structure in a wind-driven sea. *J. Phys. Oceanogr.*, **29**,480–499

Gemmrich J. R., Farmer D. M. 2004: Near-surface turbulence in the presence of breaking waves. *J. Phys. Oceanogr.*, **34**,1067–1086

Groeneweg J. (1999) Wave-current interactions in a generalized Lagrangian mean formulation. PhD thesis Delft University of Technology, The Netherlands

Groeneweg J., Battjes J. A. 2003: Three-dimensional wave effects on a steady current. *J. Fluid Mech.*, **478**,325–343

Groeneweg J., Klopman G. 1998: Changes in the mean velocity profiles in the combined wave-current motion described in GLM formulation. *J. Fluid Mech.*, **370**,271–296

Haas K. A., Svendsen I. A., Haller M. C., Zhao Q. 2003: Quasi-three-dimensional modeling of rip current systems. *J. Geophys. Res.*, **108**(C7),3217 doi:10.1029/2002JC001355

Hara T., Belcher S. E. 2002: Wind forcing in the equilibrium range of wind-wave spectra. *J. Fluid Mech.*, **470**,223–245

Hara T., Mei C. C. 1987: Bragg scattering of surface waves by periodic bars: theory and experiment. *J. Fluid Mech.*, **178**,221–241

Harcourt R. R., D'Asaro E. A. 2006: Large Eddy Simulation of Langmuir Turbulence in Pure Wind Seas. *AGU Fall Meeting Abstracts*, pp A562+

Hasselmann K. 1970: Wave-driven inertial oscillations. *Geophys. Fluid Dyn.*, **1**,463–502

Hasselmann K. 1971: On the mass and momentum transfer between short gravity waves and larger-scale motions. *J. Fluid Mech.*, **4**,189–205

Hasselmann K., Barnett T. P., Bouws E., Carlson H., Cartwright D. E., Enke K., Ewing J. A., Gienapp H., Hasselmann D. E., Kruseman P., Meerburg A., Müller P., Olbers D. J., Richter K., Sell W., Walden H. 1973: Measurements of wind-wave growth and swell decay during the Joint North Sea Wave Project. *Deut. Hydrogr. Z.*, **8**(12),1–95 Suppl. A

Herbers T. H. C., Russnogle N. R., Elgar S. 2000: Spectral energy balance of breaking waves within the surf zone. *J. Phys. Oceanogr.*, **30**(11),2723–2737

Holm D. D. 2002: Averaged Lagrangians and the mean effects of fluctuations in ideal fluid dynamics. *Physica D*, **179**,253–286

Hristov T., Friehe C., Miller S. 1998: Wave-coherent fields in air flow over ocean waves: identification of cooperative turbulence behavior buried in turbulence. *Phys. Rev. Lett.*, **81**(23),5245–5248

Huang N. E. 1979: On surface drift currents in the ocean. *J. Fluid Mech.*, **91**,191–208

Huang Z., Mei C. C. 2003: Effects of surface waves on a turbulent current over a smooth or rough seabed. *J. Fluid Mech.*, **497**,253–287 DOI : 10.1017/S0022112003006657

Ismail N. M., Wiegel R. L. 1983: Opposing wave effect on momentum jets spreading rate. *J. of Waterway, Port Coast. Ocean Eng.*, **109**,465–483

Ivonin D. V., Broche P., Devenon J.-L., Shrira V. I. 2004: Validation of HF radar probing of the vertical shear of surface currents by acoustic Doppler current profiler measurements. *J. Geophys. Res.*, **101**,C04003 doi:10.1029/2003JC002025

Janssen P. (2004) *The interaction of ocean waves and wind*. Cambridge University Press, Cambridge

Janssen P. A. E. M., Saetra O., Wettre C., Hersbach H. 2004: Impact of the sea state on the atmosphere and ocean. *Annales Hydrographiques*, **6e série, vol. 3**(772),3–1–3–23

Jenkins A. D. 1986: A theory for steady and variable wind- and wave-induced currents. *J. Phys. Oceanogr.*, **16**,1370–1377

Jenkins A. D. 1987: Wind and wave induced currents in a rotating sea with depth-varying eddy viscosity. *J. Phys. Oceanogr.*, **17**,938–951

Jenkins A. D. 1989: The use of a wave prediction model for driving a near-surface current model. *Deut. Hydrogr. Z.*, **42**,133–149

Kantha L. H., Clayson C. A. 2004: On the effect of surface gravity waves on mixing in the oceanic mixed layer. *Ocean Modelling*, **6**,101–124

Kenyon K. E. 1969: Stokes drift for random gravity waves. *J. Geophys. Res.*, **74**,6991–6994

Kirby J. T., Chen T.-M. 1989: Surface waves on vertically sheared flows: approximate dispersion relations. *J. Geophys. Res.*, **94**(C1),1013–1027

Komen G. J., Cavaleri L., Donelan M., Hasselmann K., Hasselmann S., Janssen P. A. E. M. (1994) *Dynamics and modelling of ocean waves*. Cambridge University Press, Cambridge

Kreisel G. 1949: Surface waves. *Quart. Journ. Appl. Math.*, **7**,21–44

Kudryavtsev V., Dulov V., Shira V., Malinovsky V. 2007: On vertical structure of wind-driven sea surface currents. *J. Phys. Oceanogr.* submitted

Kudryavtsev V. N., Makin V. K., Chapron B. 1999: Coupled sea surface–atmosphere model. 2. spectrum of short wind waves. *J. Geophys. Res.*, **104**,7625–7639

Lane E. M., Restrepo J. M., McWilliams J. C. 2007: Wave-current interaction: A comparison of radiation-stress and vortex-force representations. *J. Phys. Oceanogr.*, **37**,1122–1141

Lange B., Johnson H. K., Larsen S., Højtrup J., Kofoed-Hansen H., Yelland M. J. 2004: On detection of a wave age dependency for the sea surface roughness. *J. Phys. Oceanogr.*, **34**,1441–1458

Langmuir I. 1938: Surface motion of water induced by wind. *Science*, **87**,119–123

Large W. G., McWilliams J. C., Doney S. C. 1994: Oceanic vertical mixing: a review and a model with nonlocal boundary layer parameterization. *Rev. of Geophys.*, **32**,363–403

Leibovich S. 1980: On wave-current interaction theory of Langmuir circulations. *J. Fluid Mech.*, **99**,715–724

Lentz S., Guza R. T., Elgar S., Feddersen F., Herbers T. H. C. 1999: Momentum balances on the North Carolina inner shelf. *J. Geophys. Res.*, **104**(C8),18205–18226

Lewis D. M., Belcher S. E. 2004: Time-dependent, coupled, Ekman boundary layer solutions incorporating Stokes drift. *Dyn. Atmos. Oceans*, **37**,313–351

Li M., Zahariev K., Garrett C. 1995: Role of Langmuir circulation in the deepening of the ocean surface mixed layer. *Science*, **25**,1955–1957

Longuet-Higgins M. S. 1953: Mass transport under water waves. *Phil. Trans. Roy. Soc. London A*, **245**,535–581

Longuet-Higgins M. S. 1967: On the wave-induced difference in mean sea level between the two sides of a submerged breakwater. *J. Mar. Res.*, **25**,148–153

Longuet-Higgins M. S. 1969: Action of a variable stress at the surface of water waves. *Phys. of Fluids*, **12**(4),737–740

Longuet-Higgins M. S. 1979: The trajectories of particles in steep, symmetric gravity waves. *J. Fluid Mech.*, **94**,497–517

Longuet-Higgins M. S. 2005: On wave set-up in shoaling water with a rough sea bed. *J. Fluid Mech.*, **527**,217Ũ–234 An audio recording of a conference by Longuet-Higgins on this topic is available at http://av.fields.utoronto.ca:8080/ramgen/03-04/waterwaves/longuet-higgins.rm

Longuet-Higgins M. S., Stewart R. W. 1962: Radiation stresses and mass transport in surface gravity waves with application to 'surf beats'. *J. Fluid Mech.*, **13**,481–504

Lynett P., Liu P. L.-F. 2004: A two-layer approach to wave modelling. *Proc. Roy. Soc. Lond. A*, **460**,2637Ű–2669

Magne R., Belibassakis K., Herbers T. H. C., Ardhuin F., O'Reilly W. C., Rey V. 2007: Evolution of surface gravity waves over a submarine canyon. *J. Geophys. Res.*, **112**,C01002

Makin V. K., Kudryavtsev V. N. 1999: Coupled sea surface–atmosphere model. 1. wind over wave coupling. *J. Geophys. Res.*, **104**(C4),7613–7623

Marin F. 2004: Eddy viscosity and Eulerian drift over rippled beds in waves. *Coastal Eng.*, **50**,139–159

Marmorino G. O., Smith G. B., Lindemann G. J. 2005: Infrared imagery of large-aspect-ratio Langmuir circulation. *Continental Shelf Research*, **25**,1–6

Mathisen P. P., Madsen O. S. 1996: Waves and currents over a fixed rippled bed. 1. bottom roughness experienced by waves in the presence and absence of currents. *J. Geophys. Res.*, **101**(C7),16,533–16,542

Mathisen P. P., Madsen O. S. 1999: Wave and currents over a fixed rippled bed. 3. bottom and apparent roughness for spectral waves and currents. *J. Geophys. Res.*, **104**(C8),18,447–18,461

McIntyre M. E. 1981: On the 'wave momentum' myth. *J. Fluid Mech.*, **106**,331–347

McIntyre M. E. 1988: A note on the divergence effect and the Lagrangian-mean surface elevation in periodic water waves. *J. Fluid Mech.*, **189**,235–242

McWilliams J. C., Huckle E. 2006: Ekman layer rectification. *J. Phys. Oceanogr.*, **36**,1646–1659

McWilliams J. C., Restrepo J. M. 1999: The wave-driven ocean circulation. *J. Phys. Oceanogr.*, **29**,2523–2540

McWilliams J. C., Restrepo J. M., Lane E. M. 2004: An asymptotic theory for the interaction of waves and currents in coastal waters. *J. Fluid Mech.*, **511**,135–178

McWilliams J. C., Sullivan P. P. 2001: Vertical mixing by Langmuir circulations. *Spill science and technology bulletin*, **6**(3/4),225–237

McWilliams J. C., Sullivan P. P., Moeng C.-H. 1997: Langmuir turbulence in the ocean. *J. Fluid Mech.*, **334**,1–30

Mei C. C. (1989) *Applied dynamics of ocean surface waves*. second edn World Scientific, Singapore 740 p.

Mellor G. 2003: The three-dimensional current and surface wave equations. *J. Phys. Oceanogr.*, **33**,1978–1989 Corrigendum, vol. 35, p. 2304, 2005

Mellor G., Blumberg A. 2004: Wave breaking and ocean surface layer thermal response. *J. Phys. Oceanogr.*, **34**,693–698

Mellor G. L. 2001: One-dimensional, ocean surface layer modelling: A problem and a solution. *J. Phys. Oceanogr.*, **31**,790–809

Mellor G. L., Yamada T. 1982: Development of a turbulence closure model for geophysical fluid problems. *Rev. Geophys. Space Phys.*, **20**(C2),851–875

Melsom A., Sæatra Ø. 2004: Effects of wave breaking on the near-surface profiles of velocity and turbulent kinetic energy. *J. Phys. Oceanogr.*, **34**,490–504

Melville W. K., Matusov P. 2002: Distribution of breaking waves at the ocean surface. *Nature*, **417**,58–63

Melville W. K., Verron F., White C. J. 2002: The velocity field under breaking waves: coherent structures and turbulence. *J. Fluid Mech.*, **454**,203–233

Miche A. 1944*a*: Mouvements ondulatoire de la mer en profondeur croissante ou décroissante. forme limite de la houle lors de son déferlement. application aux digues maritimes. deuxième partie. mouvements ondulatoires périodiques en profondeur régulièrement décroissante. *Annales des Ponts et Chaussées*, **Tome 114**,131–164,270–292

Miche A. 1944*b*: Mouvements ondulatoire de la mer en profondeur croissante ou décroissante. forme limite de la houle lors de son déferlement. application aux digues maritimes. troisième partie. forme et propriétés des houles limites lors du déferlement. croissance des vitesses vers la rive. *Annales des Ponts et Chaussées*, **Tome 114**,369–406

Min H. S., Noh Y. 2004: Influence of the surface heating on Langmuir circulation. *J. Phys. Oceanogr.*, **34**,2630–2641

Monismith S. G., Cowen E. A., Nepf H. M., Magnaudet J., Thais L. 2007: Laboratory observations of mean flows under surface gravity waves. *J. Fluid Mech.*, **573**,131Ű–147

Newberger P. A., Allen J. S. 2007*a*: Forcing a three-dimensional, hydrostatic, primitive-equation model for application in the surf zone, Part 2: Application to DUCK94. *J. Geophys. Res.* in press

Newberger P. A., Allen J. S. 2007*b*: Forcing a three-dimensional, hydrostatic, primitive-equation model for application in the surf zone, Part 1: Formulation. *J. Geophys. Res.* in press

Noh Y. 1996: Dynamics of diurnal thermocline formation in the oceanic mixed layer. *J. Geophys. Res.*, **26**,2189–2195

Noh Y., Kang Y. J., Matsuura T., Iizuka S. 2005: Effect of the Prandtl number in the parameterization of vertical mixing in an OGCM of the tropical Pacific. *Geophys. Res. Lett.*, **32**,L23609 doi:10.1029/2005GL024540

Noh Y., Kim H. J. 1999: Simulations of temperature and turbulence structure of the oceanic boundary layer with the improved near-surface process. *J. Geophys. Res.*, **104**(C7),15621–15634

Noh Y., Min H. S., Raasch S. 2004: Large eddy simulation of the ocean mixed layer: the effects if wave breaking and Langmuir circulation. *J. Phys. Oceanogr.*, **34**,720–733

Peregrine D. H. 1976: Interaction of water waves and currents. *Advances in Applied Mechanics*, **16**,9–117

Phillips O. M. (1977) *The dynamics of the upper ocean*. Cambridge University Press, London 336 p.

Pierson, Jr W. J., Moskowitz L. 1964: A proposed spectral form for fully developed wind seas based on the similarity theory of S. A. Kitaigorodskii. *J. Geophys. Res.*, **69**(24),5,181–5,190

Polton J. A., Lewis D. M., Belcher S. E. 2005: The role of wave-induced Coriolis-Stokes forcing on the wind-driven mixed layer. *J. Phys. Oceanogr.*, **35**,444–457

Price J. F., Sundermeyer M. A. 1999: Stratified Ekman layers. *J. Geophys. Res.*, **104**(C9),20467–20494

Price J. F., Weller R. A., Schudlich R. R. 1987: Wind-driven ocean currents and ekman transport. *Science*, **238**,1534–1538

Putrevu U., Svendsen I. A. 1999: Three-dimensional dispersion of momentum in wave-induced nearshore currents. *Eur. J. Mech. B/Fluids*, **18**,410–426

Rascle N., Ardhuin F., Terray E. A. 2006: Drift and mixing under the ocean surface. a coherent one-dimensional description with application to unstrati.ed conditions. *J. Geophys. Res.*, **111**,C03016 doi:10.1029/2005JC003004

Rivero F. J., Arcilla A. S. 1995: On the vertical distribution of $\langle\tilde{u}\tilde{w}\rangle$. *Coastal Eng.*, **25**,135–152

Roseau M. (1976) *Asymptotic wave theory*. Elsevier

Ruessink B. G., Walstra D. J. R., Southgate H. N. 2003: Calibration and verification of a parametric wave model on barred beaches. *Coastal Eng.*, **48**,139–149

Russell R. C. H., Osorio J. D. C. (1958) An experimental investigation of drift profiles in a closed channel. In: Proceedings of the 6th International Conference on Coastal Engineering. ASCE pp 171–193

Santala M. J. (1991) Surface referenced current meter measurements. PhD thesis Woods Hole Oceanographic Institution and the Massachusetts Institute of Technology WHOI-91-35

Santala M. J., Terray E. A. 1992: A technique for making unbiased estimates of current shear from a wave-follower. *Deep Sea Res.*, **39**,607–622

Schudlich R. R., Price J. F. 1998: Observations of seasonal variation in the Ekman layer. *J. Phys. Oceanogr.*, **28**,1187–1204

Semtner A. J. 1995: Modeling ocean circulation. *Science*, **269**,1379–1385

Shchepetkin A. F., McWilliams J. C. 2003: A method for computing horizontal pressure-gradient force in an oceanic model with nonaligned vertical coordinate. *J. Geophys. Res.*, **108**(C3),3090 doi:10.1029/2001JC001047

Shi F., Kirby J. T., Haas K. (2006) Quasi-3d nearshore circulation equations: a cl-vortex force formulation. In: Proceedings of the 30th international conference on coastal engineering, San Diego. ASCE

Smith J. 1998: Evolution of Langmuir circulation during a storm. *J. Geophys. Res.*, **103**(C6),12649–12668

Smith J. A. (1999) Observations of wind, waves, and the mixed layer: the scaling of surface motion. In: Banner M. L. (ed.) The wind-driven air-sea interface. University of New South Wales, Sydney, Australia pages 231–238 ISBN O 7334 0586 X

Smith J. A. 2006*a*: Observed variability of ocean wave Stokes drift, and the Eulerian response to passing groups. *J. Phys. Oceanogr.*, **36**,1381–1402

Smith J. A. 2006*b*: Wave-current interactions in finite-depth. *J. Phys. Oceanogr.*, **36**,1403–1419

Smyth W. D., Skyllingstad E. D., Crawford G., Wijesekera H. 2002: Nonlocal fluxes and Stokes drift effects in the K-profile parameterization. *Ocean Dynamics*, **52**,104–115

Snodgrass F. E., Groves G. W., Hasselmann K., Miller G. R., Munk W. H., Powers W. H. 1966: Propagation of ocean swell across the Pacific. *Phil. Trans. Roy. Soc. London*, **A249**,431–497

Soloviev A., Lukas R. 2003: Observation of wave-enhanced turbulence in the near-surface layer of the ocean during TOGA COARE. *Deep Sea Res.*, **I 50**,371–395

Spaulding M. (1999) Drift current under the action of wind and waves. In: Sajjadi S. G., H.Thomas N., Hunt J. C. R. (eds.) Wind-over-wave couplings. Clarendon Press, Oxford, U. K. pp 243–256

Stacey M. W. 1999: Simulation of the wind-forced near-surface circulation in Knight Inlet: A parameterization of the roughness length. *J. Phys. Oceanogr.*, **29**,1363–1367

Stive M. J. F., Wind H. G. 1986: Cross-shore mean flow in the surf zone. *Coastal Eng.*, **10**,325–340

Stramma L., Cornillon P., Weller R. A., Price J. F., Briscoe M. G. 1986: Large diurnal sea surface temperature variability : Satellite and in situ measurements. *J. Phys. Oceanogr.*, **16**,827–837

Sullivan P. P., McWilliams J. C., Melville W. K. 2004: The oceanic boundary layer driven by wave breaking with stochastic variability. part 1. direct numerical simulation. *J. Fluid Mech.*, **507**,143–174

Swan C., Cummins I. P., James R. L. 2001: An experimental study of two-dimensional surface water waves propagating on depth-varying currents. part 1. regular waves. *J. Fluid Mech.*, **428**,273–304

Teixeira M. A. C., Belcher S. E. 2002: On the distortion of turbulence by a progressive surface wave. *J. Fluid Mech.*, **458**,229–267

Terray E. A., Donelan M. A., Agrawal Y. C., Drennan W. M., Kahma K. K., Williams A. J., Hwang P. A., Kitaigorodskii S. A. 1996: Estimates of kinetic energy dissipation under breaking waves. *J. Phys. Oceanogr.*, **26**,792–807

Terray E. A., Drennan W. M., Donelan M. A. (2000) The vertical structure of shear and dissipation in the ocean surface layer. In: Proc. Symp. on Air-Sea Interaction, Sydney. University of New South Wales pp 239–245

Thornton E. B., Guza R. T. 1983: Transformation of wave height distribution. *J. Geophys. Res.*, **88**(C10),5,925–5,938

Thorpe S. A., Osborn T. R., Farmer D. M., Vagle S. 2003: Bubble clouds and Langmuir circulation: observations and models. *J. Phys. Oceanogr.*, **33**,2013–2031

Tolman H. L. (2002) User manual and system documentation of WAVEWATCH-III version 2.22. Technical Report 222 NOAA/NWS/NCEP/MMAB

Tolman H. L., Balasubramaniyan B., Burroughs L. D., Chalikov D. V., Chao Y. Y., Chen H. S., Gerald V. M. 2002: Development and implementation of wind-generated ocean surface wave models at NCEP. *Weather and Forecasting*, **17**(4),311–333

Ursell F. 1950: On the theoretical form of ocean swell on a rotating earth. *Mon. Not. R. Astron. Soc., Geophys. Suppl.*, **6**,1–8

Walmsley J. L., Taylor P. A. 1996: Boundary-layer flow over topography: impacts of the Askervein study. *Boundary-Layer Meteorol.*, **78**,291–320

Walstra D. J. R., Roelvink J., Groeneweg J. (2001) Calculation of wave-driven currents in a 3D mean flow model. In: Proceedings of the 27th international conference on coastal engineering, Sydney. Vol 2 ASCE pp 1050–1063

WAMDI Group 1988: The WAM model - a third generation ocean wave prediction model. *J. Phys. Oceanogr.*, **18**,1,775–1,810

Warner J., Signell R., Arango H. 2006: Incorporationg nearshore processes into roms. *Eos Trans. AGU, Ocean Sci. Meet. Suppl.*, **87**(36),0S35D–01

Weber J. E. 1981: Ekman currents and mixing due to surface gravity waves. *J. Phys. Oceanogr.*, **11**,1431–1435

White B. S. 1999: Wave action on currents with vorticity. *J. Fluid Mech.*, **386**,329–344

Wiegel R. L. 1959: A presentation of cnoidal wave theory for practical applications. *J. Fluid Mech.*, **7**,273–286

Xu Z., Bowen A. J. 1994: Wave- and wind-driven flow in water of finite depth. *J. Phys. Oceanogr.*, **24**,1850–1866

Youssef M., Spaulding M. (1993) Drift current under the action of wind and waves. In: Proceedings of the Sixteenth Arctic and Marine Oil Spill Program Technical Seminar. Environment Canada, Ottawa, Ontario pp 587–615

Yu J., Mei C. C. 2000: Do longshore bars shelter the shore? *J. Fluid Mech.*, **404**,251–268

Thèse de Doctorat de l'Université de Bretagne Occidentale

Titre : **Impact des vagues sur la circulation océanique**

Auteur : **Nicolas Rascle**

Résumé : L'objectif de cette thèse est d'analyser l'impact des vagues sur la circulation océanique. La partie vagues est séparée du courant moyen et les deux sont décrites différemment. Divers aspects sont abordés. Dans la première partie, la dérive en surface est analysée à l'aide un modèle à 1 dimension, avec l'utilisation d'une paramétrisation du mélange lié au déferlement des vagues. Il apparaît que la dérive de Stokes des vagues domine la dérive d'Ekman en surface. Cette description apparaît cohérente avec les ordres de grandeurs des observations de dissipation d'énergie cinétique turbulente, de courants eulériens et de dérives lagrangiennes. Cependant, plusieurs aspects de cette description, l'effet Stokes-Coriolis par exemple, n'ont pas encore été validés par des observations. Une deuxième partie aborde l'impact des vagues sur le mélange et en particulier sur la profondeur de la couche de mélange. La profondeur de la couche de mélange diurne apparaît très sensible à l'état de mer. Une réanalyse de vagues est utilisée pour évaluer l'ordre de grandeur des paramètres importants pour ce mélange, ainsi que la distribution de ces paramètres à l'échelle globale. Enfin, la séparation des vagues et du courant est étudiée en zone côtière, aux abords de la zone de déferlement, et est comparée aux autres descriptions de la dynamique de la zone littorale et de ses abords immédiats. En particulier, l'impact de la non-linéarité des vagues sur les transports lagrangiens est évaluée.

Mots clés : **interactions vagues/courant, dérive de Stokes, mélange et dérive en surface**

Title: **Impact of waves on the ocean circulation**

Author: **Nicolas Rascle**

Abstract : The purpose of this thesis is to study the impact of waves on the ocean circulation. The wave part is separated from the mean current and both are described differently. Many aspects are investigated. In the first part, the surface drift is analyzed with a one-dimensional model, with the use of a parameterization of the mixing induced by wave breaking. It appears that the Stokes drift of the waves generally dominates the Ekman drift at the surface. This description agrees with the orders of magnitude of the observations of turbulent kinetic energy dissipation, of Eulerian currents and of Lagrangian drifts. However, many aspects of this description, the Stokes-Coriolis effect for instance, have not been validated yet by observations. One reason is that one need a data set fully Eulerian or fully Lagrangian, long enough to allow the filtering out of other processes, with simultaneous observations of waves. A second part deals with the impact of waves on the mixing, and more particularly on the mixed layer depth. The diurnal mixed layer shows much sensitivity to the sea state. A waves reanalysis is used to estimate the parameters important for this mixing, as well as their global scale distributions. Finally, the waves / mean flow separation is studied close to the surf zone, and is compared to the other descriptions of the surf zone and inner-shelf dynamics. In particular, the impact of the waves non-linearity on the Lagrangian transports is evaluated.

Keywords: **waves/current interactions, Stokes drift, surface drift and mixing**